Stellingen

TR 37795

1: De gesuggereerde overeenkomst in fotophysische eigenschappen tussen 5,15-bis{[(5'-10,20-diphenylporphinato)-zinc(II)]ethynyl}[10,20-diphenylporphinato]zinc(II) en de B820 subeenheid van het antenne complex van *Rhodobacter sphaeroides* louter op basis van een matig gelijkend absorptiespectrum[1] is een schromelijke onderschatting van de complexe fotofysica van porphyrine derivaten.

[1]V. S.-Y. Lin, S. G. DiMagno, M. J. Therien: Science 264 (1994), 1105-1111

2a: De opmerking van Schütz en Schmidt[1] dat hun data het eerste bewijs is voor de bezetting van de CT toestand van 9,9'-bianthryl in apolaire oplosmiddelen ontkrachten zij zelf met hun aanval op de "solvent-solute exciplex" interpretatie van Visser et al.[2] in de daarop volgende alinea.

[1]M. Schütz, R. Schmidt: J. Phys. Chem. 100 (1996), 2012-2018.

[2]R.-J. Visser, P. C. M. Weisenborn, P. J. M. van Kan, B. H. Huizer, C. A. G. O. Varma, J. M. Warman, M. P. de Haas: J. Chem. Soc., Faraday Trans. 2 81 (1985), 689-704.

2b: De met "LE state" aangeduide aangeslagen toestand in 9,9'-bianthryl is niet ontaard omdat hij niet locaal is.

2c: Kang et al.[1] gooien zeer waardevolle data weg over het ontstaan van de CT toestand in 9,9'-bianthryl door aan te nemen dat het emissie spectrum in dibutylether karakteristiek is voor de LE emissie.

[1]T. J. Kang, M. A. Kahlow, D. Giser, S. Swallen, V. Nagarajan, W. Jarzeba, P. F. Barbara: *J. Phys. Chem.* **1988**, *92*, 6800-6807.

3: Het vergelijken van de ac en dc mobiliteiten van discotische materialen in de vloeibaar kristallijne fase is vooral een complexe manier om de wanorde te bepalen.

4a: Kuhns beroemde boek: "The structure of scientific revolutions"[1] zegt eigenlijk meer over wetenschappers dan over wetenschap.

[1]T. S. Kuhn: "The structure of scientific revolutions"; 3rd ed., University of Chicago Press, Chicago 1996.

4b: Communicatie tussen wetenschappers onderling is vaak moeizaam omdat zij er ten onrechte vanuitgaan dat de door hun gehanteerde begrippen eenduidig zijn.

4c: De interpretatie van meetgegevens is sterker onderhevig aan slijtage dan de metingen zelf.

5a: De mens is de meest succesvolle exponent van de evolutie omdat hij zich niet aanpast aan zijn omgeving, maar zijn omgeving aan hem.

5b: Het gericht in stand houden van de huidige biodiversiteit is tegennatuurlijk.

6a: Goede verliezers zijn een eerste vereiste voor een functionerende democratie.

6b: Onzorgvuldige positieve discriminatie leidt tot bevestiging van vooroordelen.

6c: Met de schaarste eind jaren '90 op de arbeidsmarkt heeft de Nederlandse overheid een uitgelezen kans voorbij laten gaan om het te zwaar uitgedijde ambtenarenbestand op sociaal verantwoorde wijze te saneren.

7: In de economie wordt welvaart gedefinieerd als de mate waarin men in staat is zijn behoeften te bevredigen. Hieruit volgen twee mogelijkheden: veel geld is veel welvaart, geen behoeften is veel welvaart. De materialistiche mens streeft het eerste na, de spirituele mens kan dus alleen succesvol zijn als hij het tweede nastreeft.

8: Homohaat komt voort uit een overdreven ontkenning van de eigen latent aanwezige homofiele verlangens.

9: Volwassenheid is niet iets om trots op te zijn.

10: Alle moraal ten spijt; uiteindelijk zal Adolf Hitler toch de bekendste persoon van de 20ste eeuw blijken te zijn.

Propositions

1: The suggested similarity in photophysical properties between 5,15-bis{[(5'-10,20-diphenylporphinato)-zinc(II)]ethynyl}[10,20-diphenylporphinato]zinc(II) and the B820 subunit of the *Rhodobacter sphaeroides* ' antenna complex based solely on a weakly resembling absorption spectrum[1] is a gross underestimation of the complex photophysics of porphyrin derivatives.

[1]V. S.-Y. Lin, S. G. DiMagno, M. J. Therien: Science 264 (1994), 1105-1111

2a: The claim by Schütz en Schmidt[1] that the data they present in their paper is the first proof of population of the CT state of 9,9'-bianthryl in apolar solvents is negated by themselves in the next paragraph in their opposition to the "solute-solvent exciplex" interpretation of Visser et al.[2].

[1]M. Schütz, R. Schmidt: J. Phys. Chem. 100 (1996), 2012-2018.

[2]R.-J. Visser, P. C. M. Weisenborn, P. J. M. van Kan, B. H. Huizer, C. A. G. O. Varma, J. M. Warman, M. P. de Haas: J. Chem. Soc., Faraday Trans. 2 81 (1985), 689-704.

2b: The excited state of 9,9'-bianthryl generally denoted with "LE" is not degenerate since it is not local.

2c: Kang et al.[1] discard valuable data on the formation of the CT state in 9,9'-bianthryl by assuming that the emission spectrum in dibutylether is characteristic of the LE emission.

[1]T. J. Kang, M. A. Kahlow, D. Giser, S. Swallen, V. Nagarajan, W. Jarzeba, P. F. Barbara: *J. Phys. Chem.* **1988**, *92*, 6800-6807.

3: Comparing ac and dc mobilities in the liquid crystalline phase of discotic materials is above all a rather complex method to determine the disorder.

4a: Kuhn's famous essay "The structure of scientific revolutions"[1] reveals more about scientists than about science.

[1]T. S. Kuhn: "The structure of scientific revolutions"; 3rd ed., University of Chicago Press, Chicago 1996.

4b: The frequent lack of communication between scientists results from their incorrect assumption that the meaning of the notions they use are unambiguous.

4c: The interpretation of measurements is more liable to revision than the measurements themselves.

5a: Man is evolution's most successful exponent, because he adapts his surroundings to him rather than adapting himself to his surroundings.

5b: The forced preservation of biodiversity is unnatural.

6a: Good losers are a primary requirement for a functioning democracy.

6b: Careless positive discrimination consolidates prejudice.

6c: Given the shortage on the labour market at the end of the 90s, the Dutch government have missed an excellent opportunity to reorganise and reduce the overexpanded civil service in a socially accepted way.

7: In economics welfare is defined as the extent to which one succeeds in fulfilling ones desires. Two possibilities emerge: having a lot of wealth is a lot of welfare, having no desires is a lot of welfare. Material man pursues the former option, spiritual man the latter.

8: Hate towards homosexuals has its source in the overexaggerated denial of one's own suppressed homosexual desires.

9: Adulthood is not something to be proud of.

10: Despite morality, Adolf Hitler will be the best known figure of the 20th century.

EXCITONIC INTERACTIONS

IN

MULTICHROMOPHORIC ARRAYS

Jacob Johan PIET

The research described in this thesis was performed at the Radiation Chemistry department (SC) of the Interfaculty Reactor Institute (IRI), Delft University of Technology, Mekelweg 15, 2629 JB Delft, The Netherlands.

The research described in this thesis has been supported financially by the Nederlandse organisatie voor Wetenschappelijk Onderzoek (NWO), gebied Chemische wetenschappen (CW).

EXCITONIC INTERACTIONS

IN

MULTICHROMOPHORIC ARRAYS

Proefschrift

ter verkrijging van de graad van doctor
aan de Technische Universiteit Delft,
op gezag van de Rector Magnificus prof. ir. K. F. Wakker,
voorzitter van het College voor Promoties,
in het openbaar te verdedigen op dinsdag 20 november 2001 om 16:00 uur

door

Jacob Johan PIET

doctorandus in de scheikunde
geboren te Eindhoven

Dit proefschrift is goedgekeurd door de promotor:
Prof. dr. ir. A. H. M. Verkooijen

Toegevoegd promotor: dr. J. M. Warman

Samenstelling promotiecommissie:

Rector Magnificus,	voorzitter
Prof. dr. ir. A. H. M. Verkooijen,	Technische Universiteit Delft, promotor
Dr. J. M. Warman,	Technische Universiteit Delft, toegevoegd promotor
Prof. dr. ir. R. A. J. Janssen,	Technische Universiteit Eindhoven
Prof. dr. L. W. Jenneskens,	Universiteit Utrecht
Prof. dr. W. Rettig,	Humboldt-Universität Berlin
Prof dr. ir. J. Schoonman,	Technische Universiteit Delft
Dr. H. L. Anderson,	University of Oxford

Published and distibuted by: DUP Science

DUP Science is an imprint of
Delft University Press
P.O. Box 98
2600 MG Delft
The Netherlands
Telephone: +31 15 2785678
Telefax: +31 15 2785706
e-mail: DUP@Library.TUDelft.nl

ISBN 90-407-2252-8

Keywords: microwaves, exciton, symmetric multichromophoric arrays

Printed in The Netherlands.

..., Dus u gelooft me niet, Nee, Waarom niet, als ik vragen mag, Omdat dat wat u zou hebben gedaan niet in mijn werkelijkheid past, en wat niet in mijn werkelijkheid past, bestaat niet, ...

Uit: *Alle namen* (José Saramago; vertaling Maartje de Kort)

Contents

1 EXCITONIC STATES IN MULTICHROMOPHORIC ARRAYS

1.1 INTRODUCTION 1
1.2 THE PHOTOSYNTHETIC MACHINERY 2
1.3 MODEL SYSTEMS 5
1.4 EXCITED STATES. 8
1.4.1 Basic photophysics. 8
1.4.2 Electrostatic interactions between chromophores: Davydov splitting. 11
1.4.3 Electronic interactions between chromophores. 13
1.4.4 Frenkel and Wannier-Mott excitons. 17
1.5 EXPERIMENTAL TECHNIQUES 18
1.6 OUTLINE OF THIS THESIS 21
REFERENCES 22

2 THE FLASH PHOTOLYSIS TIME-RESOLVED MICROWAVE CONDUCTIVITY TECHNIQUE

2.1 A BRIEF HISTORY 25
2.2 BASIC INTRODUCTION 27
2.2.1 Microwaves. 27
2.2.2 Transmission lines. 27
2.2.3 The electrical properties of a medium. 29
2.2.3.1 Static field conditions. 29
2.2.3.2 Alternating field conditions. 32
2.3 PHOTO-INDUCED CHANGES IN THE CONDUCTIVITY AND PERMITTIVITY 36
2.3.1 Photoinduced changes in the complex permittivity. 38
2.3.1.1 The effect of a change in the molecular polarisability. 38
2.3.1.2 The effect of a change in dipole moment. 39
2.3.2 Photoinduced changes in the dc conductivity. 41
2.3.2.1 The effect of mobile charge carriers. 41
2.4 THE FP-TRMC EQUIPMENT 44
2.4.1 Basic overview. 44
2.4.1.1 The excitation source. 45
2.4.1.2 The microwave circuitry. 45
2.4.1.3 The microwave resonant cavity. 47
2.5 THE BASIS OF THE FP-TRMC TECHNIQUE. 48
2.5.1 The cavity resonance. 48
2.5.1.1 The Q-factor. 51
2.5.1.2 The relation between R_0 and Q_l and Q_u. 54
2.5.2 The TRMC sensitivity factors. 57
2.5.2.1 Photo-induced changes in the reflected power. 57
2.5.2.2 The sensitivity at the cavity resonance frequency: the A factors. 64
2.5.2.3 The sensitivity off resonance. 67
2.5.2.3.1 The general dependence of R(f) on changes in $\varepsilon''(\omega)$: derivation of the B factor. 67
2.5.2.3.2 The general dependence of R(f) on changes in $\varepsilon'(\omega)$: derivation of the C factor. 69
2.5.3 Obtaining separate $\Delta\varepsilon'(\omega)$ and $\Delta\varepsilon''(\omega)$ TRMC transients. 71
2.6 QUANTIFICATION OF THE TRMC RESULTS. 74
2.6.1 Short overview of the fitting procedure. 74

2.6.1.1 Non-uniform electric fields and the spatial distribution of excited states. 76
2.6.1.2 The actual number of photons entering the cell: Actinometry. 79
2.6.1.3 The response time of the microwave system: the relation between τ_{rc} and f. 80
2.6.2 The oscillatory contribution to the $\Delta\varepsilon'(\omega)$-related transient: the D-factor. 82
2.6.3 "Cross-talk" contributions. 88
REFERENCES 90

3 TWO FOLD SYMMETRY

3.1 INTRODUCTION 93
3.2 EXPERIMENTAL METHODS 95
3.3 RESULTS AND DISCUSSION 97
3.3.1 Optical measurements. 98
3.3.2 Microwave measurements. 103
3.3.3 General discussion. 111
3.4 SUMMARY 116
ACKNOWLEDGEMENT 116
REFERENCES 117

4 THREE-FOLD SYMMETRY

4.1 INTRODUCTION 119
4.2 EXPERIMENTAL SECTION 121
4.3 RESULTS AND DISCUSSION 122
4.3.1 Photophysical properties of mETP and mEBP. 122
4.3.2 Fluorescence depolarization of mETP and its biphenyl model compound mEBP in propanediol glass. 123
4.3.3 Time-resolved fluorescence depolarization of pEFTP and its biphenyl model compound pEFBP in benzene. 126
4.3.4 Time-resolved microwave conductivity. 126
4.4 CONCLUSION 131
ACKNOWLEDGEMENT 132
REFERENCES 132
APPENDIX A, Supporting Information 134

5 SIX-FOLD SYMMETRY

5.1 INTRODUCTION 137
5.2 EXPERIMENTAL 138
5.3 RESULTS AND DISCUSSION 139
ACKNOWLEDGEMENT 145
REFERENCES 145

6 PORPHYRIN DIMERS

6.1 INTRODUCTION 147
6.2 EXPERIMENTAL 150
6.3 RESULTS AND DISCUSSION 153
6.3.1 Singlet states of P, PP, PBP. 154
6.3.2 Singlet states of P, yPy, yyPyy, yAyPyAy. 156
6.3.3a Singlet state of yPyyPy. 159
6.3.3b Singlet states of the yPyXyPy series. 162
6.3.4 Triplet states. 164
6.4 CONCLUSIONS 165
ACKNOWLEDGEMENT 165
REFERENCES 166

7 PORPHYRIN OLIGOMERS

7.1 INTRODUCTION 169
7.2 EXPERIMENTAL SECTION 171
7.3 RESULTS & DISCUSSION 173
7.3.1 TRMC results. 173
7.3.1.1 $(PB)_n$ series. 174
7.3.1.2 $(yPy)_n$ series. 175
7.3.2 Optical measurements. 178
7.3.2.1 $(PB)_n$ series. 179
7.3.2.2 $(yPy)_n$ series. 182
7.4 CONCLUSION 183
ACKNOWLEDGEMENT 183
REFERENCES 184

8 PORPHYRIN POLYMER

8.1 INTRODUCTION	187
8.2 EXPERIMENTAL	188
8.3 RESULTS AND DISCUSSION	189
ACKNOWLEDGEMENT	192
REFERENCES	192

1

EXCITONIC STATES IN MULTICHROMOPHORIC ARRAYS

1.1 INTRODUCTION

The research reported in this thesis was aimed at providing a better understanding of the nature of photoexcitations within molecular arrays consisting of two or more identical chromophoric units. In particular the interest lay in the electrostatic and electronic interactions between chromophores which lead to "excitonic" states with properties which can differ considerably from those of the isolated chromophore. In addition to conventional optical absorption and emission techniques, the flash-photolysis time-resolved microwave conductivity method has been used to measure the extent of delocalisation of an excitonic state within an array and the degree to which an exciton can undergo heterolytic dissociation into separated charges.

Research on exciton delocalisation and dissociation has been driven in recent years to a large extent by the desire to understand the process of photosynthesis which occurs in green plants and some bacteria. Natural photosynthesis can be considered as one of the keys to life. It sustains life on our planet by using the radiant energy of the sun to generate carbohydrate molecules and oxygen from the degradation products water and carbon dioxide. All other, more complex, biological systems depend for their existence on these carbohydrate molecules and the energy stored within them.

1.2 THE PHOTOSYNTHETIC MACHINERY

In photosynthesis several enzyme systems play a role, with each of them contributing only a part of the total effort. The initial steps in photosynthesis are the absorption of light followed by the transfer of the absorbed energy to the photosynthetic reaction centre where the photon-energy is converted into a potential difference across a membrane (figure 1). The primary steps are performed by "light harvesting" protein complexes, which, like the reaction centre, are incorporated in a membrane, *i.e.* a phospholipid bi-layer. In the case of photosynthetic bacteria, at least two different light-harvesting complexes, denoted LH1 and LH2, have been identified.

The two antenna complexes have in common that their skeletons are built entirely from only two types of protein strands, denoted α and β. The α and β strands of the different antenna complexes are not identical. Both strands consist of *ca.* 50 amino acids and they are combined in a one-to-one fashion to form a single $\alpha\beta$ heterodimer. These $\alpha\beta$ heterodimers are combined with a number of chromophores to form the basic monomeric building blocks, which arrange themselves in circular structures characteristic of the antenna complexes[1-6].

Only two types of chromophores, carotenoids and bacteriochlorophyll a (Bchl-a), could be isolated from the bacterial LH2 complex. Clear differences were observed however in the optical properties of the Bchl-a molecules in the intact complex. On the basis of the position of the maximum of their first absorption bands these two different forms of Bchl-a were denoted B800 and B850. It was quickly realised that the different properties must be determined either by the protein surroundings or by the special arrangements of the chromophores, which allowed excitonic interactions between them[7]. In LH1 B800 is absent and B850 is replaced by B875.

Research on these light harvesting complexes received a large impulse from the elucidation by X-ray diffraction of the 3-dimensional structure of LH2 of the bacterium *Rhodopseudomonas acidophila* with 2.5 Å resolution in 1995[3] and of the bacterium *Rhodospirillum molischianum* with 2.4 Å resolution in 1996[5]. For the first time the true spatial arrangement of the large number of chromophores within an LH2 complex was accurately known. Figure 2 shows the chromophore arrangement of the nonamer of *Rps.*

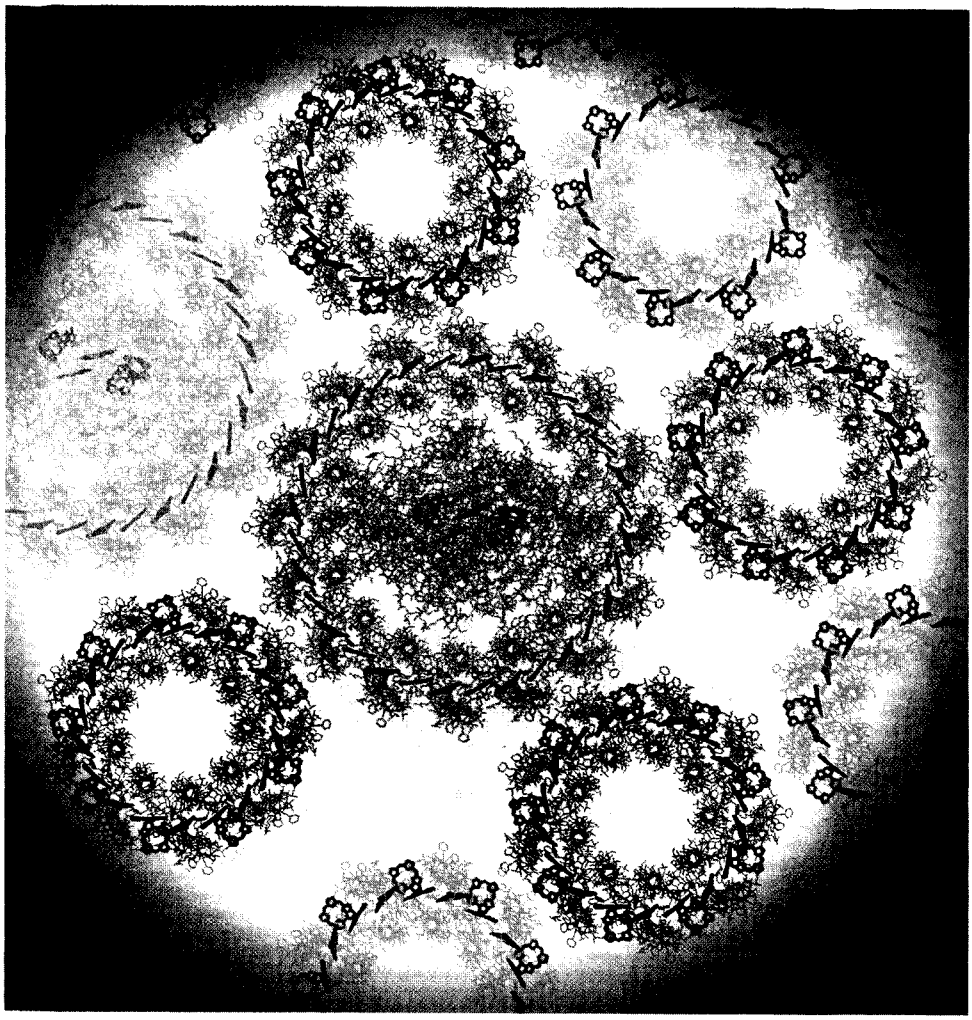

FIGURE 1: Model of the primary photosynthetic machinery of purple bacteria based on the known structural data. The BChl-a molecules of LH2 (B800 and B850), LH1 (B875) and the reaction centre (RC) are blue, green and red, respectively. Polypeptides are light blue. The highlighted five rings (four LH2s and one LH1+RC) correspond to photosynthetic unit (PSU) which in ratio satisfies the approximate 1:2:1 ratio of B800:B850:B875 band intensities in *Rb. sphaeroides*. The boarders of PSUs are tentative and excitation transfer occurs between different PSUs which all together form large domains. The diameter of the yellow background ring is about 230 Å.

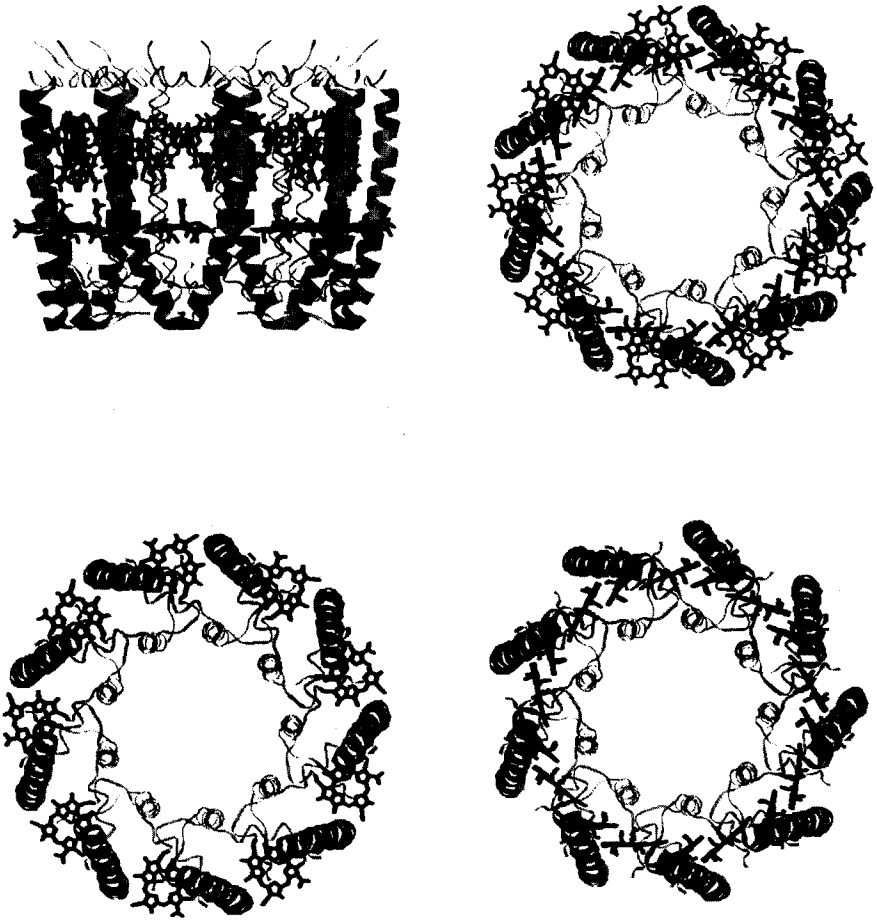

FIGURE 2: Structure of LH2 of *Rps. Acidophila*. The upper two figures display the side and top-view of the complex. The lower figures more clearly show the exact location and orientation of the porphyrin ring of the B800 (left) and (B850) BChl-a chromophores. In all four figures the protein is grey, the B800 Bchl-a's are blue and the B850 BChl-a's are red. The phythyl side chain of BChl-a is omitted for clarity in all four figures. [Markus Wendling of the VU, Amsterdam, The Netherlands is gratefully acknowledge for the preparation of these figures]

acidophila, which has at least 9 carotenoids and 27 Bchl-a molecules (*Rs. molischianum* is an octamer). Two different sites were found for the Bchl-a pigments in agreement with the previous division of the Bchl-a molecules into B800 and B850[6]. The B800 pigment was assigned to the coplanar arrangement of 9 Bchl-a molecules, which are oriented parallel to the membrane surface and are well-separated, hence capable of only weak interactions. The B850 pigment was assigned to the circular arrangement of 18 Bchl-a molecules, which are oriented perpendicular to the membrane-surface in a roof-tile like arrangement so that a considerable part of each chromophore is in van der Waals contact with its two neighbours, allowing therefore strong interactions. The exact structure of LH1 has not yet been elucidated. An 8.5 Å projection map of a 2D crystal however suggested that it is a hexadecamer, *i.e.* 32 Bchl-a chromophores form the B875 ring[4].

Currently LH2 is thought to function as follows[2,8]. Light is initially absorbed by the carotenoids[9,10] and the B800 Bchl-a molecules. This results in the formation of a localised exciton on a single B800 Bchl-a molecule. Within several ps, the excitation energy is transferred *via* Förster transfer from the B800 Bchl-a molecule to a B850 Bchl-a molecule with the loss of a small amount of energy[11,12]. The close-packed arrangement of the B850 Bchl-a molecules allows the energy to migrate rapidly around the ring, which results from the strong excitonic interactions between the chromophores. The exciton most probably does not remain localised on a single B850 chromophore but becomes delocalised over some or possibly even all of the Bchl-a molecules in the ring[12-15]. The excitation energy is eventually transferred from the B850 ring of LH2 to the larger B875 ring of LH1[16]. Finally the excitation energy is transferred from LH1 to the special pair of the photosynthetic reaction centre where it is utilised for multi-step electron-transfer across the membrane.

Sofar, most of the research on the antenna complexes focuses on LH2, in particular on exciton delocalisation and migration in the circular array. A large amount of research has been carried out on the antenna complexes themselves; mainly on isolated complexes in-vitro[17]. Mutants are very useful to investigate the effect of changes in the 3-dimensional arrangement of the chromophores on the photophysics of an antenna complex[8,18,19]. In addition, research has been carried out on many different kinds of model compounds, which allow a more thorough investigation of specific aspects that appear to be relevant for a complete understanding of the photophysics of the antenna-complexes in bacteria and ultimately in green plants.

1.3 MODEL SYSTEMS

In attempts to mimic photosynthesis a large number of model compounds have been synthesised[20-28]. The fundamental interest in photosynthesis focussed initially on the process of trans-membrane electron transfer, which occurs in the reaction centre itself. Therefore, the

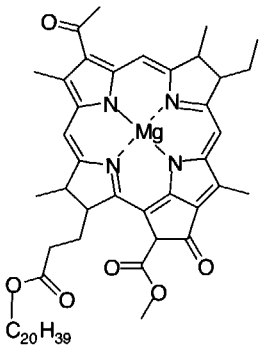

Bacteriochlorophyll a

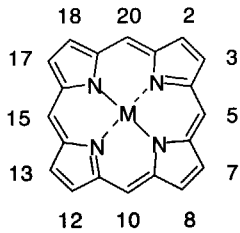

Porphyrin

FIGURE 3: Structure of Bacteriochlorophyll a (top) and that of a metal containing porphyrin (bottom). The numbering in the left figure are the substitution positions. The numbers 5, 10, 15 and 20 correspond to the *meso*-positions.

majority of the model compounds synthesised sofar have been prepared to investigate electron transfer. These model compounds contain different chromophores, which are chosen to function as electron donor or acceptor[20,21]. The extensive knowledge obtained over the last decades on long-range electron transfer has largely increased our understanding of the exact mechanism of trans-membrane electron transfer process in the reaction center. Currently, attention is shifting towards the light harvesting and energy transfer processes occurring in the antenna complexes, such as LH1 and LH2[24,27].

On the assumption that the surrounding protein matrix in antenna complexes mainly plays a passive role as simple scaffolding for the chromophores, model compounds containing chromophores juxtapositioned in a specific geometrical arrangement can be used effectively to study the relation between the mutual positioning and coupling of chromophores and their collective photophysical properties. Multi-chromophoric model compounds can be used therefore to test in more detail hypotheses, which evolve from research on the antenna complexes themselves.

Bacteriochlorophylls are structurally related to the class of porphyrins (see figure 3), which are heterocyclic organic compounds with a conjugated π-system spanning the entire molecule. Unsubstituted porphyrin is planar and has a more or less square shape. Because of their close relation to Bchl, porphyrins and porphyrin derivatives are the primary choice as chromophores in antenna model systems[27]. Examples of model compounds, relevant to this thesis, having porphyrins as chromophores are shown in figure 4. In figure 5 examples of model compounds are shown, which use other types of chromophores. Some of these chromophores have in common with porphyrins that they are planar and have an extensive conjugated π-system. Examples of chromophores which fulfill this description are molecules such as naphthalene, anthracene and carbazole. In model compounds where neither planarity of the chromophore nor an extensive conjugated π-system is a requirement all types of chromophores can be used equally well. In figure 5 the compound with the three triphenyl-amino chromophores is an example of this latter class of model compounds.

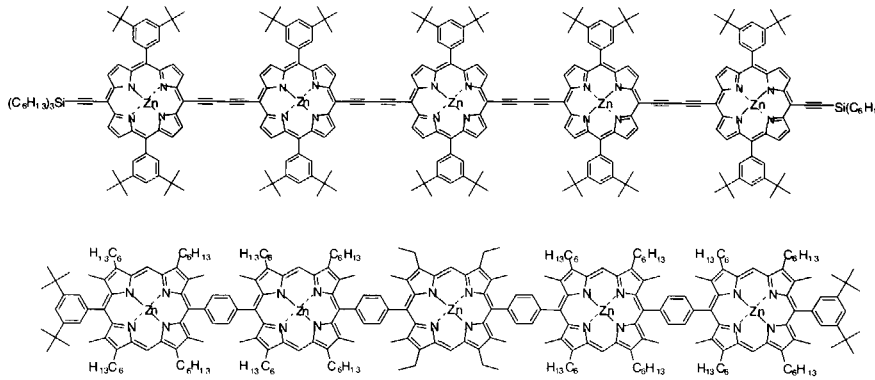

FIGURE 4: Two examples of modelcompounds which have zinc-porphyrins as their main chromophores. Both compounds display translational symmetry.

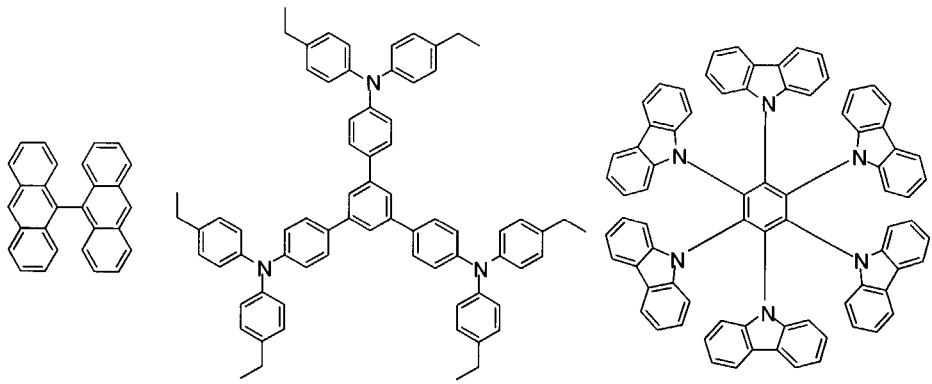

FIGURE 5: Examples of model compounds with two-fold (left), three-fold (middle) and six-fold (right) rotational symmetry.

All model compounds consist of at least two identical chromophores, which are often covalently linked to each other *via* bridges or spacers. These intervening bridges make it possible to position the chromophores in a desired orientation with respect to each other and to keep them at a fixed distance. Using such spacers or bridging units, chromophoric arrays can be constructed with rotational as well as translational symmetry. In figure 5 examples are shown of model compounds having two-, three- and six-fold rotational symmetry. In figure 4 some examples are shown of model compounds with translational symmetry.

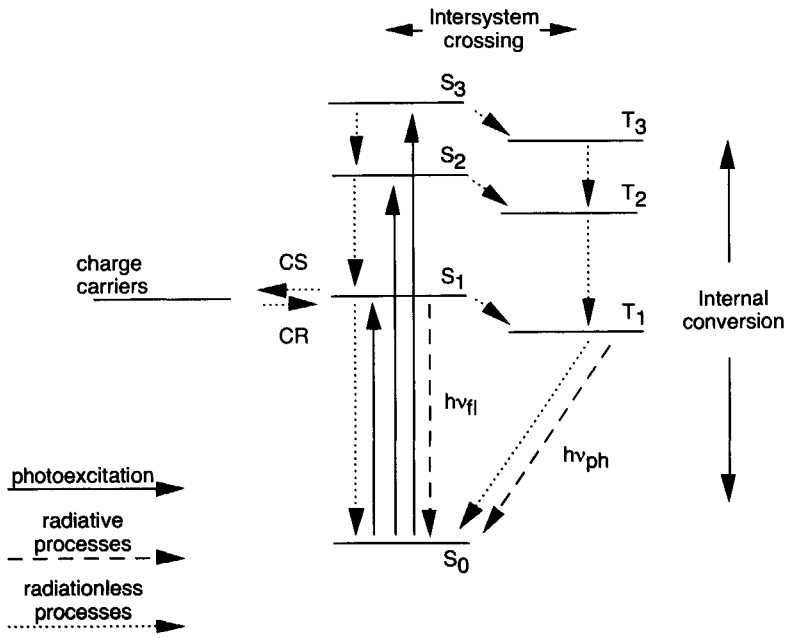

FIGURE 6: Schematic representation showing the ground-state, S_0, and the singlet and triplet excited state manifolds with the transitions between them.

1.4 EXCITED STATES.

1.4.1 Basic photophysics.

In molecules the atomic orbitals are converted into bonding, non-bonding and anti-bonding molecular orbitals, some of which can span the entire molecule. Each orbital can contain two electrons of opposite spin, *i.e.* they are spin-paired. The geometry of a molecule and the distribution of charge over the molecule is determined by which orbitals are occupied. When the electrons occupy the orbitals which are lowest in energy, the molecule is said to be in its ground-state. For the vast majority of molecules all electrons are spin-paired in the ground-state. In this case the ground-state is a singlet state and is usually denoted S_0. An important exception to this is O_2, which has a triplet ground-state, *i.e.* the two electrons highest in energy occupy a pair of degenerate orbitals and are not spin-paired but are spin-parallel. Since the energy required to raise an electron from the highest occupied molecular orbital (HOMO) to the lowest unoccupied molecular orbital (LUMO) is usually much larger than kT, almost all molecules are in their electronic ground-state at room temperature.

Any other distribution of electrons over the available orbitals is higher in energy and is referred to as an excited state. At room-temperature, the additional energy required to form an excited state must be obtained from an external source, for instance photons from a light

source. A photon can be absorbed by a ground-state molecule if its energy is sufficient to transfer an electron from a filled orbital to an empty orbital higher in energy. The initially formed excited state, often referred to as the vertical Franck-Condon excited state, has the electron distribution of the excited state but still has the nuclear geometry of the ground-state. In response to the altered electron distribution the molecule usually relaxes from the Franck-Condon geometry to a new equilibrium geometry by nuclear rearrangement. In this relaxation process part of the energy of the absorbed photon can be released as heat into the molecule's environment. Vibrational relaxation occurs on a (sub)picosecond timescale and the equilibrium state finally reached is referred to as the vibrationally-relaxed excited state.

In a UV-Vis absorption spectrum several absorption bands can be distinguished, which represent the transitions between filled and empty orbitals. Not all transitions have corresponding bands in the absorption spectrum, since not all transitions are optically allowed. For a transition to be optically allowed it is required to have a non-zero transition dipole moment. The cumulative intensity of an absorption band is proportional to the magnitude of this transition dipole moment, M. The lowest energy absorption band represents the transition between the HOMO and the LUMO, unless it happens to be a forbidden transition, *i.e.* $M = 0$. The other absorption bands are related to transitions to higher excited states within the singlet manifold, S_n ($n \geq 1$). Apart from a few exceptions, these higher excited states relax within a few picoseconds to the lowest excited singlet state, S_1, by radiationless internal conversion. In this process the excess energy is released *via* a series of vibrational relaxations into the surroundings as heat (Figure 6).

Even though in an excited state electrons will singly occupy an orbital, their spin-pairing is initially retained. However, the spin of an electron in a singly occupied orbital can be reversed *via* coupling with the orbital electronic motion or the spin of nuclei. This process result in intersystem crossing (Figure 6) and the formation of a triplet state, denoted T_n with the lowest triplet state T_1. Usually, a triplet state is lower in energy than the corresponding singlet state.

Eventually the energy stored in either the S_1 or T_1 excited state is released when the molecule returns to the ground-state, S_0. The pathways available for depopulation of an excited state to the ground-state can be either radiative or non-radiative (figure 6). To what extent each pathway is used depends on the probability for the process which can be expressed as a rate, $k_{i \rightarrow j}$. The sum of all pathways available determines the overall rate of depopulation of that state. This overall rate of depopulation does not depend only on the probability of the two types of transitions to the ground-state but will also depend on the probabilities of the transitions to other excited states, *e.g.* intersystem crossing.

For example, we can focus on the S_1 state and its decay pathways, which are shown in figure 4. S_1 can be depopulated by intersystem crossing to T_1:

$$S_1 \xrightarrow{k_{S_1 \to T_1}} T_1 \qquad \text{(A)}$$

and by internal conversion to S_0:

$$S_1 \xrightarrow{k_{S_1 \to S_0}} S_0 \qquad \text{(B)}$$

Hence the lifetime of the S_1 state, which is the inverse of the sum of the decay rates, is given by:

$$\tau_{S_1} = \frac{1}{\left(k_{S_1 \to S_0} + k_{S_1 \to T_1}\right)} \qquad (1)$$

As mentioned above, internal conversion can be either radiative or non-radiative. The sum of the rates of these two processes, k_r and k_{nr} respectively, is equal to the overall rate of internal conversion, *i.e.*:

$$k_{S_1 \to S_0} = k_r + k_{nr} \qquad (2)$$

Radiative internal conversion is observed as fluorescence. The probability of excited states to decay by emitting light is called the fluorescence quantum yield, ϕ_{fl}, which is given by:

$$\phi_{fl} = \frac{k_r}{k_r + k_{nr} + k_{S_1 \to T_1}} = \frac{k_r}{k_{S_1 \to S_0} + k_{S_1 \to T_1}} = k_r . \tau_{S_1} \qquad (3)$$

The probability for intersystem crossing, ϕ_{isc}, is given by:

$$\phi_{isc} = \frac{k_{S_1 \to T_1}}{k_r + k_{nr} + k_{S_1 \to T_1}} = \frac{k_{S_1 \to T_1}}{k_{S_1 \to S_0} + k_{S_1 \to T_1}} = k_{S_1 \to T_1} . \tau_{S_1} \qquad (4)$$

Finally we will briefly focus on the T_1 state. Hypothetically, depopulation of the T_1 state could occur by intersystem crossing back to the S_1 state. This is very rare since the T_1 state is normally considerably lower in energy than the S_1 state. Hence, intersystem crossing to S_0 is normally the only available pathway for depopulation. Intersystem crossing from T_1 to S_0 can occur either radiatively or non-radiatively. Of these two possibilities radiationless intersystem crossing to S_0 is usually the major decay pathway of the T_1 state at room

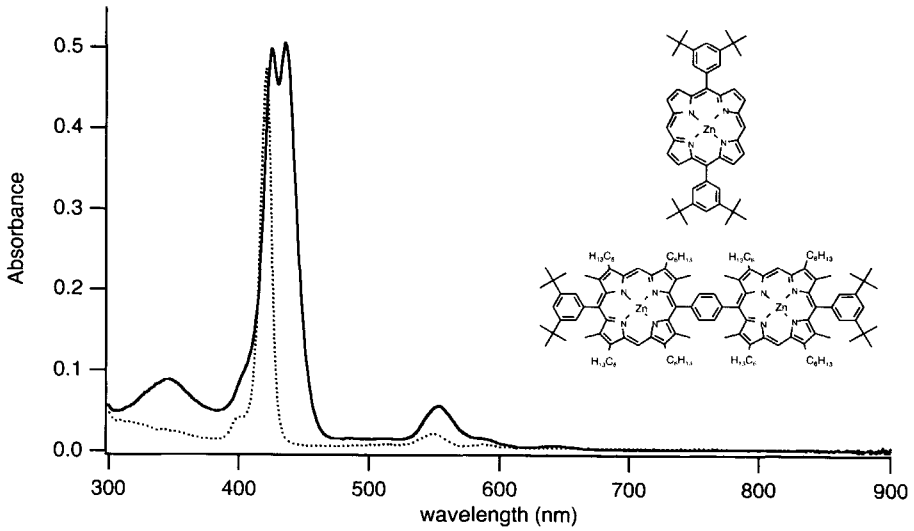

FIGURE 7: The spectra of a single porphyrin (dotted line) and a related bis-porphyrinic compound (full line). The difference in the B-band region (400-500 nm) can be attributed to Davydov splitting, which is characteristic for electrostatic interactions between chromophores. The molecular structures of both compounds are given at the right.

temperature. In this process, the energy stored in the T_1 state is released as heat into the surroundings *via* vibrational motion of the molecule. At low temperatures or in a rigid matrix the radiationless pathways can be impaired and depopulation can occur *via* the radiative pathway. Light observed from radiative intersytem crossing is known as phosphorescence. In general, intersystem crossing is spin-forbidden and is therefore a slow process. The rate for intersystem crossing from T_1 to S_0, $k_{T_1 \rightarrow S_0}$, is usually orders of magnitude slower than the overall decay rate of S_1.

1.4.2 Electrostatic interactions between chromophores: Davydov splitting.

Excitonic interactions were originally introduced to explain the differences between the optical absorption spectra of molecular crystals and the absorption spectra of the isolated molecules. In the original theory, Davydov[29] attributed the observed shifts of the absorption bands in the spectra of a molecular crystal to the electrostatic interaction between the transition dipole moments of neighbouring chromophores. Kasha utilised the theory of Davydov to explain the spectra of isolated bis- and multi-chromophoric molecules[30,31].

The occurrence of Davydov splitting is illustrated in figure 7 in the case of a linear bis-chromophoric molecule, having porphyrins as chromophores separated by a 1,4-phenylene bridge. As can be seen in this figure two peaks are observed in the spectrum of the

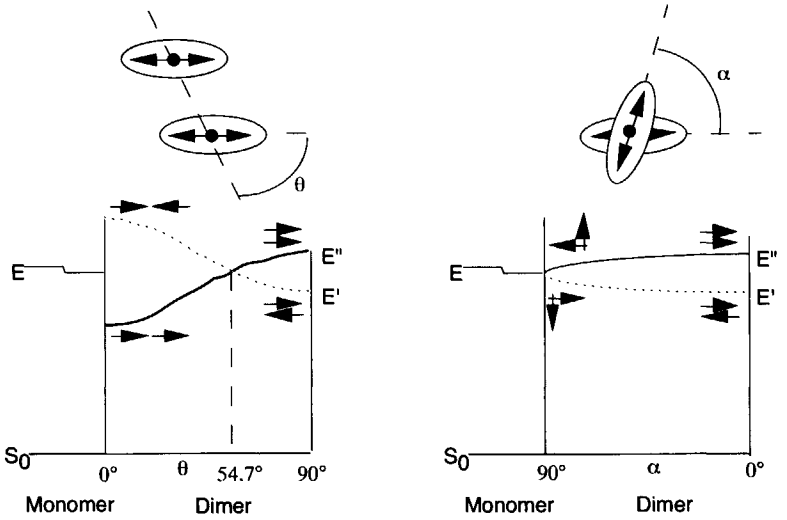

FIGURE 8: The magnitude of Davydov splitting, 2ΔE=E"-E', results from the interaction between the transition dipole moments of two chromophores and depends on the angle of inclination, θ, and torsion angle, α.

bis-chromophore, whereas only a single peak is observed in the spectrum of the isolated chromophore. The effect results from the electrostatic interaction between *iso*-energetic transition dipole moments located on the two chromophores. The mutual orientation, determined by the torsion angle, α, and the angle of inclination, θ (see figure 8) and the centre-to-centre distance between the two chromophores, R_c, determine the magnitude of the splitting, $2\Delta E$[31]:

$$\Delta E = \frac{|M|^2}{R_c^3}\left(\cos\alpha - 3\cos^2\theta\right) \qquad (5)$$

In equation (5), M is the magnitude of the transition dipole moment of the unperturbed chromophore. The important role of M is illustrated in figure 7: no splitting is observed for the S_0-S_1 transition (in porphyrins referred to as the Q-band), whose M is small, while a clear splitting is observed for the S_0-S_2 transition (in porphyrins referred to as the B-band), whose M is extremely large.

If the transitions from the ground-state to both of these new excited states are equally allowed, then instead of the original single absorption band, two new bands, one at lower and one at higher energy and both half the height of the original peak, will be observed in the absorption spectrum of a bis-chromophore. This is however almost never the case, because the transition dipole moments of the two new transitions will not be identical. The magnitude of the new transition dipole moments is the sum of the two original transition dipole

moments. If these are oppositely oriented they will cancel and the transition will be forbidden and thus absent in the absorption spectrum. In that case, only a hypsochromic or a bathochromic shift of the absorption band of the involved transition is observed.

The fact that in figure 7 two peaks are observed for the dimer is because the degeneracy of the two orthogonal transitions responsible for the B-band of a monomeric porphyrin is lifted in the dimer as a result of the different inter-chromophoric interactions. The two degenerate transition dipole moments of the B-band of a porphyrin are orientated along the line through the 5 and 15 and through the 10 and 20 carbon atoms respectively. Thus, the lowest energy peak in figure 7 results from the interaction between the two transition dipole moments in the direction parallel to the bridge ($\theta = 0°$ in figure 8), the other peak results from the two transition dipole moments in the direction perpendicular to the line through the bridging unit ($\theta \approx 90°$ in figure 8).

On going from a bis-chromophoric to a multi-chromophoric array, equation (5) has to be modified to incorporate the effect of multiple interactions. Two equations have been developed to describe the increased splitting, $2\Delta E(N)$, for an absorption band in the case of a linear multi-chromophoric array of N chromophores[32,33]:

$$\Delta E(N) = 2\left[\frac{N-1}{N}\right]\frac{|M|^2}{R_c^3}\left(\cos\alpha - 3\cos^2\theta\right) \qquad (6)$$

and[23,32]:

$$\Delta E(N) = 2\cos\left(\frac{\pi}{N+1}\right)\frac{|M|^2}{R_c^3}\left(\cos\alpha - 3\cos^2\theta\right) \qquad (7)$$

For small N the values of ΔE calculated using equation (6) or equation (7) differ only slightly. If N is very large both equations converge and give $\Delta E(N)=2\Delta E(2)$.

The Kasha model works well qualitatively. However, the point-dipole approach, which is the basis of equations (5), (6) and (7), limits the reliability of the quantitative results. This is particularly the case when R_c becomes small[34]. Attempts have been made to replace the point-dipole approach by a more sophisticated model[35]. However, these models lack the simplicity and therefore the ready applicability of the original treatment.

1.4.3 Electronic interactions between chromophores.

An electronic interaction between two chromophores requires overlap of the wavefunctions of orbitals localised on the two chromophores. Overlap can occur either directly or can be mediated *via* the orbitals of an intervening bridge: "through-bond coupling"

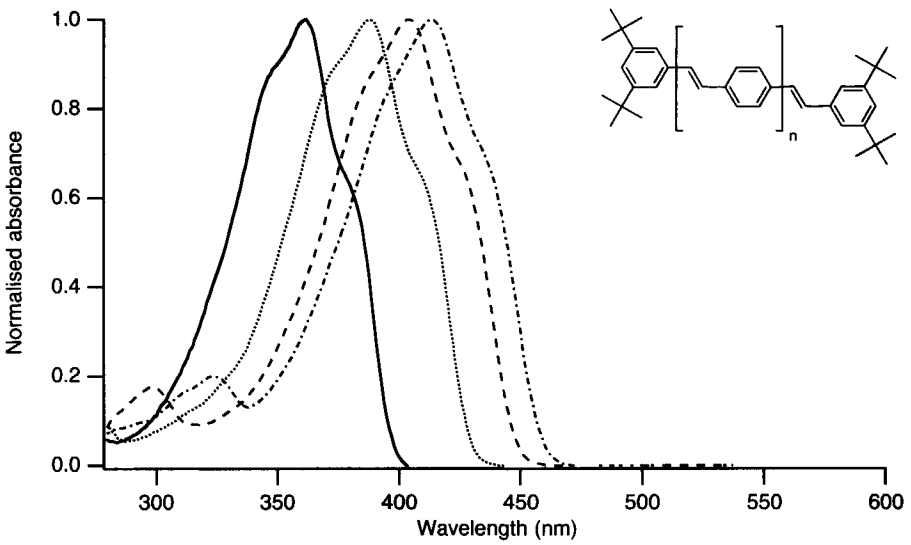

FIGURE 9: The spectra of a series of *para*-phenylenevinylene oligomers (OPV's), showing the lowest absorption band corresponding to the HOMO-LUMO transition. The general molecular structure of these oligomers is shown in the upper right corner. The full line corresponds to n=1, the dotted line to n=2, the dashed line to n=3 and the dotted-dashed line to n=4. The bathochromic shift can be attributed to electronic interactions between the monomeric PV units.

or "superexchange"[36-40]. The primary result of interchromophoric electronic interaction is a set of orbitals which are delocalised over all chromophores involved. In the simplest case when just two *iso*-energetic orbitals on two neighbouring chromophores interact, two delocalised orbitals are formed: one at lower energy, the bonding combination, and one at higher energy, the anti-bonding combination. The energy difference between the bonding and anti-bonding combination depends on the magnitude of the electronic interaction. Since the energy of the resulting orbitals differ from the energy of the original orbitals, all electronic transitions related to these orbitals are changed as well. For instance, the UV-Vis absorption spectrum of any multi-chromophoric array in which the chromophores interact strongly electronically is distinctly different from the absorption spectrum of the related single chromophore. In general the most readily distinguishable feature is a bathochromic shift of the lowest energy transition (figure 9). In contrast to an electrostatic interaction, the shift is independent of the oscillator strength of the related transition in the parent chromophore.

In certain cases the electronic coupling between the chromophores is extremely weak in the ground-state geometry and the absorption spectrum resembles closely that of the isolated monomer. In the excited state however, geometrical relaxation can occur leading to an increase in the electronic coupling. This is observed as a change in shape and a bathochromic shift of the emission spectrum compared with the monomer. A classical example of this phenomenon is found for 9,9'-bianthryl, whose absorption spectrum is very

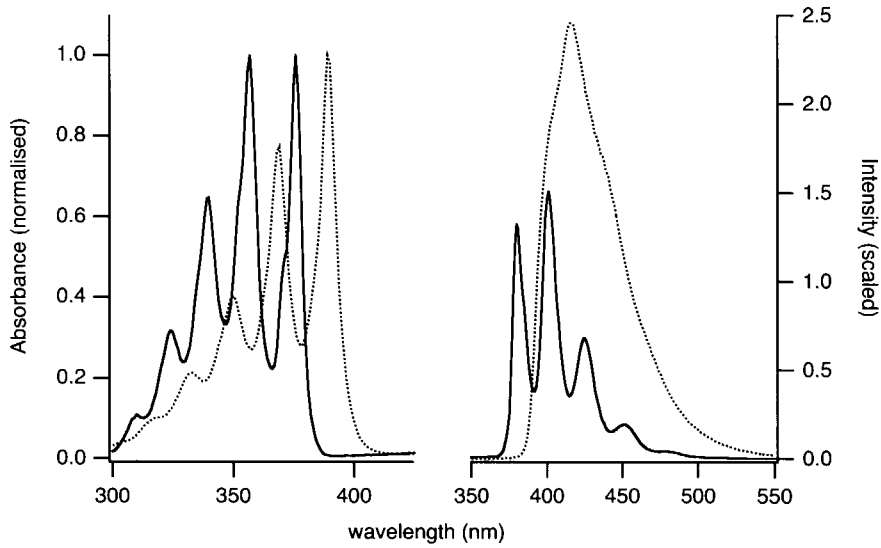

FIGURE 10: The absorption (left) and emission (right) spectra of a single anthracene (full line) and 9,9'-bianthryl (dotted line) in di-*n*-butylether. Apart from the bathochromic shift, the absorption spectra of the two compounds are very similar. The emission spectra differ considerably, which is evidence for the formation of an excitonic state spanning both anthracene moieties in 9,9'-bianthryl.

similar to that of anthracene but whose fluorescence spectrum differs greatly. This is illustrated in figure 10.

If the chromophores are not identical, which can be either an intrinsic property or caused by the environment or the geometry, the ability of the charge to migrate as a consequence of electronic interaction between the chromophores will result in a charge separated excited state. The chromophore with the lowest ionization potential will function as electron donor, while the chromophore with the highest electron affinity will be the electron acceptor. Usually in organic molecules thermodynamics do not favour electron transfer in the ground-state. In the excited state more energy is available, which has been supplied by excitation of one of the chromophores. This additional energy can shift the balance in favour of electron transfer. The free energy for electron transfer, ΔG_{et}, can be estimated using the Weller equation[41,42]:

$$\Delta G_{et} = e\left(E_{ox} - E_{red}\right) - \frac{hc}{\lambda_a} - \frac{1}{4\pi\varepsilon_0}\frac{e^2}{\varepsilon_r R_c} - \frac{e^2}{8\pi\varepsilon_0}\left[\left(\frac{1}{r_{d+}} + \frac{1}{r_{a-}}\right)\left(\frac{1}{35.94} - \frac{1}{\varepsilon_r}\right)\right] \qquad (8)$$

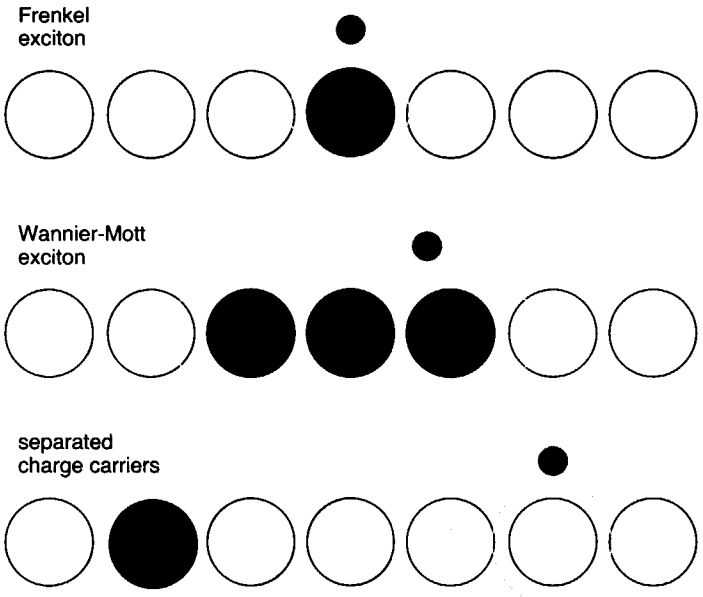

FIGURE 11: Schematic representation of a Frenkel exciton (top), a Wannier-Mott exciton (middle) and a pair of charge carriers (bottom) on a 1-dimensional chain of identical chromophoric units.

In equation (8), h is Planck's constant, c is the speed of light, e is the elementary charge, ε_r is the dielectric constant of the solvent and ε_0 is the permittivity of vacuum. Further, λ_a is the wavelength of the (0,0) transition of the excited chromophore, R_c is the centre-to-centre distance between the two chromophores and r_{d+} and r_{a-} are the radii of the donor radical cation and the acceptor radical anion. The ionization potential and the electron affinity are replaced by the more readily measureable oxidation potential of the donor, E_{ox}, and the reduction potential of the acceptor, E_{red}, respectively. E_{ox} and E_{red} are usually measured in acetonitrile (ε_r = 35.94) using cyclic voltammetry. For solvents with a different ε_r the last term of equation (8) corrects for the difference in solvent reorganisation around the charged chromophores in these solvents compared to acetonitrile.

When ΔG_{et} is negative, electron transfer is thermodynamically feasible. Whether or not it actually occurs, depends on the rate for electron transfer, k_{et}. This rate is given by the Golden Rule relationship[43]:

$$k_{et} = \frac{4\pi^2}{h} H_{da}^2 F_{da} \qquad (9)$$

The term related to the electronic interaction between the chromophores involved is H_{da}, which is the electronic coupling matrix element. The term F_{da} in equation (9) is the Franck

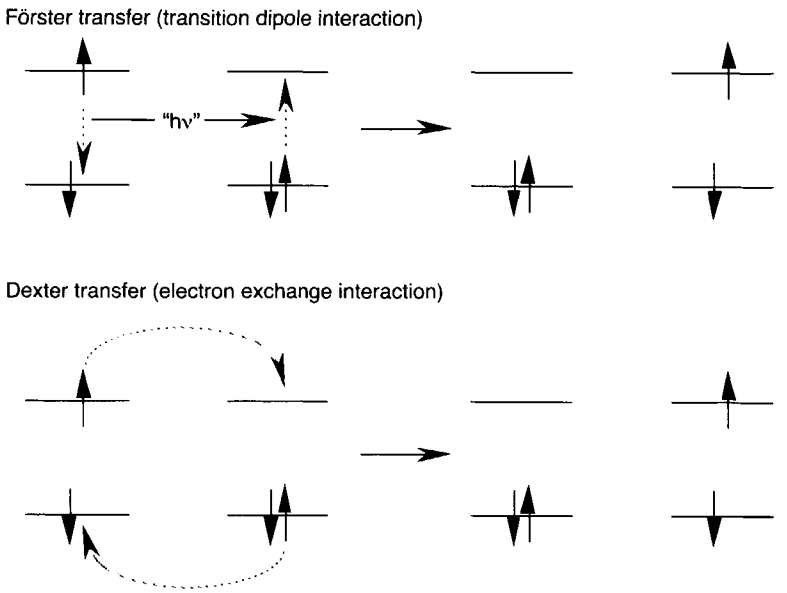

FIGURE 12: A schematic representation showing the difference between Förster- and Dexter-type exciton migration. Förster transfers occurs by the exchange of a virtual photon and requires an electrostatic interaction between the transition dipole moments of the two chromophores involved. Dexter transfer occurs by electron exchange between the two chromophores involved and depends on the electronic coupling between both chromophores.

Condon factor[44,45], which corresponds to the number of vibrational states on the acceptor capable of coupling with the initial state on the donor, of which one is localised on the acceptor and the other on the donor.

1.4.4 Frenkel and Wannier-Mott excitons.

The term exciton was originally introduced in solid-state physics to describe electronic excitations in crystalline materials. Excitons differ from the excited states of isolated molecules in their ability to migrate between the identical chromophoric units of a crystal or any other type of multichromophoric array. Excitons are frequently discussed in terms of an "electron-hole pair" consisting of the photoexcited electron and the positively charged electron vacancy remaining after removal of the electron from the highest occupied ground-state orbital. Two different types of excitons are distinguished: Frenkel excitons and Wannier-Mott excitons[46]. The distinction between these two is based on the type of interaction between the chromophores: electrostatic or electronic.

In a Frenkel exciton[46-48], electron exchange between chromophores is negligible, so that at any given moment in time both the hole and electron are localised on the same

chromophore (figure 11). Migration of Frenkel excitons occurs exclusively by Förster transfer[49]: *i.e.* electrostatic interactions between the transition dipole moments of the chromophores involved results in energy transfer by a concerted emission-excitation mechanism (figure 12). As a result of this process, the tightly bound electron-hole pair making up the exciton appears to migrate as a single entity. In fact, only the energy migrates through the array. The energy of a Frenkel exciton will be close to the energy of the lowest electronic transition of the isolated chromophore.

In a Wannier-Mott exciton[46,47,50,51] the electron-hole pair is only weakly bound and the electron and hole need not to be localised on the same chromophore at a fixed instant in time; the exciton is delocalised over two or more chromophores (figure 11). Electronic interaction between the chromophores is required to allow electron exchange to occur. The process of exchange of the electron and hole between chromophoric units offers an additional pathway for exciton migration which is not available to Frenkel excitons. This additional pathway bears a strong resemblance to Dexter transfer[52], the difference is that the hole and the electron do not have to move simultaneously as is assumed to be the case in Dexter transfer process (figure 12). In contrast to a Frenkel exciton, the energy of a Wannier-Mott exciton is always lower that the energy of the lowest electronic transition of the corresponding single chromophore. If thermal energy suffices to overcome the weak electrostatic attraction between the electron-hole pair of a Wannier-Mott exciton, it can dissociate into separate mobile charge carriers[46,47] (figure 11).

1.5 EXPERIMENTAL TECHNIQUES

Most of the information on the photophysical properties of antenna complexes and model compounds has been obtained using optical detection techniques[8,17]. However, the term optical technique is rather broad and comprises a number of rather distinct techniques. These techniques can either be steady-state or time-resolved and they probe either the absorptive or the emissive properties of one or more states of a system under investigation. The information obtained with one technique is often complementary to that obtained with an other.

Steady-state UV-Vis absorption and emission spectroscopy yield direct information on the energy of allowed transitions. If the HOMO-LUMO transition is observed in both absorption and emission spectra the energy difference between their maxima, referred to as the Stokes shift, can be determined. The Stokes shift is a measure of the difference between the HOMO-LUMO gap for the ground-state nuclear configuration and for the equilibrium nuclear configuration reached after relaxation from the Franck-Condon state. It is therefore indicative of the extent to which the geometry of the molecule changes in response to the change in the electron distribution.

An emissive transition between two states can be accompanied by a change in dipole moment, for instance the initial excited state is dipolar the final ground-state is not. The energy of the dipolar state is lowered by solvent reorganisation in polar solvents. The energy difference between the two states, and thus the energy of the transition, will therefore decrease with increasing solvent polarity. This bathochromic shift of the emission band with increasing solvent polarity is referred to as the solvatochromic shift. It is possible to determine the difference in magnitude of the dipole moment of the ground-state and excited state, $\Delta\mu(S_1)$, from the observed shift using the Lippert-Mataga equation[53-56]:

$$\left(\nu_a - \nu_{fl}\right) = \frac{2\Delta\mu(S_1)^2}{3h\varepsilon_0 c V_c}\left[\frac{(\varepsilon_r - 1)}{(2\varepsilon_r + 1)} - \frac{\left(n^2 - 1\right)}{\left(2n^2 + 1\right)}\right] + Const. \qquad (10)$$

or the equation derived by Beens, Knibbe and Weller[57]:

$$\nu_{fl} = \nu_{fl}^0 - \frac{2\Delta\mu(S_1)^2}{3h\varepsilon_0 c V_c}\left[\frac{(\varepsilon_r - 1)}{(2\varepsilon_r + 1)} - \frac{1}{2}\frac{\left(n^2 - 1\right)}{\left(2n^2 + 1\right)}\right] \qquad (11)$$

In equations (10) and (11) the term in square brackets is a solvent parameter, which depends on the refractive index, n, and the dielectric constant of the solvent, ε_r, and V_c the molecular volume of the dipolar solute molecule. In the original Lippert-Mataga plot the Stokes shift, *i.e.* difference between the absorption and emission maximum, ν_a and ν_f respectively (both in cm^{-1}), is plotted *versus* a solvent parameter. From the slope of the plot $\Delta\mu(S_1)$ is determined; the y-axis cut-off is a constant which has no special meaning. In the Beens, Knibbe and Weller approach ν_f (in cm^{-1}) is plotted *versus* a slightly modified solvent parameter. Again $\Delta\mu(S_1)$ is determined from the slope of the plot, while the y-axis cut-off gives ν_f^0 (in cm^{-1}), which should be the wavelength of the emission maximum in vacuum.

Time-resolved measurements are used to obtain detailed information on the spectra and formation and decay kinetics of short-lived excited states. Time-resolved emission measurements by definition can only be used to determine the lifetime of states which are emissive. Transient absorption is in principle a more versatile but experimentally more difficult technique; detection of an excited state requires that an allowed transition between that state and a higher excited state occurs in the spectral range available for detection. Therefore transient absorption techniques can be used to monitor the kinetics of excited states which do not have an allowed radiative transition to the ground-state. Femto- and pico-second pump-probe transient absorption experiments are fast enough to be able to distinguish between the different vibrational levels of an excited state and can thus be used to monitor the

relaxation processes from the primarily formed Franck-Condon excited state to the vibrationally relaxed excited states eventually attained.

An optical technique which is particularly relevant in the context of excitons and charge separation is Stark or electrooptical spectroscopy. Stark spectroscopy is a steady-state technique which measures the change induced in the shape and position of an absorption or an emission spectrum when an external electric field is applied. By an extensive analysis of the observed changes, the difference in polarisability and in dipole moment between the ground-state and an excited state can be determined[58,59]. However, the results from Stark spectroscopy are not the actual difference between the geometrically relaxed ground-state and the geometrically relaxed excited state, since the information is obtained from the vertical transition. This means that the difference is determined between the ground-state and the excited state either for the case that the nuclei are in a ground-state geometry, electroabsorption, or that they are in an excited state geometry, electroemission. Therefore, different results can be obtained when applying Stark spectroscopy to the absorption band or the emission band of the same transition.

In the research described in this thesis microwave conductivity is used as the detection technique. This can provide information on the nature of excited states, which is not obtainable using optical detection techniques. The flash-photolysis time-resolved microwave conductivity (FP-TRMC) technique measures the photo-induced change in the complex conductivity of a solution containing the molecule of interest with nanosecond time-resolution[60,61]. The FP-TRMC measurements are conducted at room temperature. Under these conditions nuclear relaxation is usually complete well within a nanosecond and the observed transient changes can be assigned to differences in the properties of the excited state populated and the ground-state, both having their energetically favoured nuclear geometry, *i.e.* they are vibrationally-relaxed states. An advantage of the TRMC technique is that it does not depend on optically allowed transitions, therefore the properties of singlet and triplet excited states can be probed equally well. A drawback is that the solutions that can be investigated with the TRMC technique are limited to those in non-dipolar solvents.

Until recently, the FP-TRMC technique has been applied mainly to study photoinduced intra-molecular charge separation and subsequent recombination in molecules containing an electron donating moiety and an electron accepting moiety[62]. In such studies the FP-TRMC technique has been used to monitor the change in dipole moment on photoexcitation *via* the change in the real component of the conductivity (the imaginary component of the permittivity, often referred to as dielectric loss). In this thesis more attention will be focused on changes in the imaginary component of the conductivity, which provides information on the excess polarisability. A large excess polarisability of an excited state in a multichromophoric array is indicative of exciton delocalisation over several chromophores or,

as in the case of some of the molecules studied, a rapid intramolecular dipole relaxation process.

If mobile charge carriers are formed by exciton dissociation they are also observed with the FP-TRMC technique *via* their contribution to the real component of the conductivity.

1.6 OUTLINE OF THIS THESIS

Except for chapters 1 and 2, the contents of all other chapters in this thesis have been accepted for publication by various international journals[63-68]. The common thread connecting these papers is the application of the flash-photolysis time-resolved microwave conductivity (FP-TRMC) technique to study the electronic properties of the vibrationally relaxed excited state of multichromophoric molecular arrays. Chapter 2 explains the background of the FP-TRMC technique and the quantitative determination of the real and imaginary conductivity from the FP-TRMC transients. The molecules investigated in the chapters 3 to 8 are multichromophoric arrays and can be considered to be model compounds for the study of exciton migration, delocalisation and dissociation.

In chapters 3, 4 and 5 model compounds with non-porphyrinic chromophores are considered whose symmetry increases from two-fold, *via* three-fold to six-fold rotational symmetry. 9,9'-Bianthryl in chapter 3 is an example of a directly linked bischromophore, which has two-fold rotational symmetry. It is shown that the torsional angle between the two anthracene moieties determines the electronic overlap and thus the kind of exciton formed. The highly dipolar character of the excited state of 9,9'-bianthryl indicates that the delocalised exciton can temporarily dissociate into a charge separated state. Small perturbations in the molecule's surroundings are thought to be responsible for this behaviour. Chapter 4 considers a number of molecules with three-fold rotational symmetry all of which have a central 1,3,5-triphenylbenzene core. Although the rotational symmetry is identical their excited state behaviour is different and is shown to depend on the interaction between the chromophores. In Chapter 5 results are shown for a six-fold rotational symmetric molecule: hexacarbazolylbenzene. The carbazole substituents are in a propeller-like arrangement so that overlap can occur with both neighbours. The optical behaviour of this circular array is completely different to that of N-phenyl-carbazole and can be explained by assuming that exciton delocalisation occurs over at least two carbazole chromophores and that the exciton rapidly migrates around the molecule.

In chapter 6, 7 and 8 linear compounds are considered which all contain zinc-porphyrins as the chromophores. Chapter 6 focuses on a number of *meso,meso*-bridged bisporphyrins. The distinct properties of these bichromophores can be related to the type of coupling between them, which is determined by the intervening bridge. In chapter 7 two oligomer series are investigated whose dimers were shown in chapter six to have very distinct

excitonic properties. These two series illustrate the differences between Frenkel and Wannier-Mott excitons on multichromophoric chains. Chapter 8 contains experimental evidence for the occurrence of the dissociation of Wannier-Mott type excitons into mobile charge carriers on a polymeric zinc-porphyrin chain.

REFERENCES

[1] W. Kühlbrandt, D. N. Wang, Y. Fujiyoshi: Nature 367 (1994), 614-621.
[2] W. Kühlbrandt: Nature 374 (1995), 497-498.
[3] G. McDermott, S. M. Prince, A. A. Freer, A. M. Hawthornthwaite-Lawless, M. Z. Papiz, R. J. Cogdell, N. W. Isaacs: Nature 374 (1995), 517-521.
[4] S. Karrasch, P. A. Bullough, R. Ghosh: The EMBO J. 14 (1995), 631-638.
[5] J. Koepke, X. Hu, C. Muenke, K. Schulten, H. Michel: Structure 4 (1996), 581-597.
[6] K. Sauer, R. J. Cogdell, S. M. Prince, A. Freer, N. W. Isaacs, H. Scheer: Photochem. Photobiol. 64 (1996), 564-576.
[7] A. Scherz, W. W. Parson: Photosynth. Res. 9 (1986), 21-32.
[8] V. Sundström, T. Pullerits, R. van Grondelle: J. Phys. Chem. B 103 (1999), 2327-2346.
[9] G. D. Scholes, R. D. Harcourt, G. R. Fleming: J. Phys. Chem. B 101 (1997), 7302-7312.
[10] B. P. Krueger, G. D. Scholes, R. Jimenez, G. R. Fleming: J. Phys. Chem. B 102 (1998), 2284-2292.
[11] R. Jimenez, S. N. Dikshit, S. E. Bradforth, G. R. Fleming: J. Phys. Chem. 100 (1996), 6825-6834.
[12] J. T. M. Kennis, A. M. Streltsov, H. Permentier, T. J. Aartsma, J. Amesz: J. Phys. Chem. B 101 (1997), 8369-8374.
[13] T. Pullerits, M. Chachivilis, V. Sundström: J. Phys. Chem. 100 (1996), 10787-10792.
[14] M. Chachisvilis, O. Kühn, T. Pullerits, V. Sundström: J. Phys. Chem. B 101 (1997), 7275-7283.
[15] A. M. van Oijen, M. Ketelaars, J. Köhler, T. J. Aartsma, J. Schmidt: Science 285 (1999), 400-402.
[16] V. Nagarajan, W. W. Parson: Biochemistry 36 (1997), 2300-2306.
[17] *J. Phys. Chem. B.* (Special issue on Light-Harvesting Physics Workshop) 101 (1997), 7197-7359.
[18] L. M. P. Beekman, R. N. Frese, G. J. S. Fowler, R. Picorel, R. J. Cogdell, I. H. M. van Stokkum, C. N. Hunter, R. van Grondelle: J. Phys. Chem. B 101 (1997), 7293-7301.
[19] M. H. C. Koolhaas, R. N. Frese, G. J. S. Fowler, T. S. Bibby, S. Georgakopoulou, G. van de Zwam, C. N. Hunter, R. van Grondelle: Biochem. 37 (1998), 4693-4698.
[20] V. Balzani, F. Scandola:"Supramolecular Photochemistry", Ellis Horwood: New York 1991, ISBN 0-13-877531-1.
[21] M. R. Wasielewski: Chem. Rev. 92 (1992), 435-461.
[22] A. A. Bothner-By, J. Dadok, T. E. Johnson, J. S. Lindsey: J. Phys. Chem. 100 (1996), 17551-17557.
[23] T. Nagata, A. Osuka, K. Maruyama: J. Am. Chem. Soc. 112 (1990), 3054-3059.
[24] V. S.-Y. Lin, M. J. Therien: Chem. Eur. J. 1 (1995), 645-651.
[25] J. M. Tour: Chem. Rev. 96 (1996), 537-553.
[26] R. W. Wagner, T. E. Johnson, J. S. Lindsey: J. Am. Chem. Soc.: 118 (1996), 11166-11180.
[27] T. S. Balaban. A. Eichenhöfer, J.-M. Lehn: Eur. J. Org. Chem. (2000), 4047-4057.
[28] N. Aratani, A. Osuka, Y. H. Kim, D. Hong Jeong, D. Kim: Angew. Chem. Int. Ed. 39 (2000), 1458-1462.
[29] A. S. Davydov:"Theory of Molecular Excitons", McGraw-Hill: New York 1962.
[30] M. Kasha: Rad. Res. 20 (1963), 55-71.
[31] M. Kasha, H. R. Rawls, M. A. El-Bayoumi: Pure Appl. Chem. 11 (1965), 371-392.
[32] E. S. Emerson, M. A. Conlin, A. E. Rosenoff, K. S. Norland, H. Rodriguez, D. Chin, G. R. Bird: J. Phys. Chem. 71 (1967), 2396-2403.
[33] E. G. McRae, M. Kasha: J. Chem. Phys. 28 (1958), 721-722.
[34] C. A. Hunter, J. K. M. Sanders, A. J. Stone: Chem. Phys. 133 (1989), 395-404.
[35] J. C. Chang: J. Chem. Phys. 67 (1977), 3901-3909.
[36] R. Hoffmann, A. Imamura, J. Hehre: J. Am. Chem. Soc. 90 (1968), 1499-1509.
[37] R. Hoffmann: Acc. Chem. Res. 4 (1971), 1-9.
[38] R. Gleiter: Angew. Chem. Int. Ed. 13 (1974), 696-701.
[39] T. K. Brunck, F. Weinhold: J. Am. Chem. Soc. 98 (1976), 4392-4393.
[40] M. N. Paddon-Row: Acc. Chem. Res. 15 (1982), 245-251.

[41] A. Weller: Z. Phys. Chem. (Neue Folge) 133 (1982), 93-98.
[42] H. Oevering, M. N. Paddon-Row, M. Heppener, A. M. Oliver, E. Cotsaris, J. W. Verhoeven, N. S. Hush: J. Am. Chem. Soc. 109 (1987), 3258-3269.
[43] M. Bixon, J. Jortner: Adv. Chem. Phys. 106 (1999), 35-202.
[44] J. J. Hopfield: Proc. Natl. Acad. Sci. USA 171 (1974), 3640-3644.
[45] M. Redi, J. J. Hopfield: J. Chem. Phys. 72 (1980), 6651-6660.
[46] M. A. Pope, C. E. Swenberg:" Electronic Processes in Organic Crystals and Polymers", Oxford University Press: New York 1999.
[47] A. S. Davydov:"Theory of Molecular Excitons", Plenum: New York 1971.
[48] J. Frenkel: Phys. Rev. 37 (1931), 1276-1294.
[49] Th. Förster: Ann. Phys. 2 (1948), 55-75.
[50] G. H. Wannier: Phys. Rev. 52 (1937), 191-197.
[51] N. F. Mott: Trans. Faraday Soc. 34 (1938), 500-506.
[52] D. L. Dexter: J. Chem. Phys. 21 (1953), 836-850.
[53] E. Lippert: Z. Naturforsch. 10a (1955), 541-545.
[54] N. Mataga, Y. Kaifu, M. Koizumi: Bull. Chem. Soc. Jpn 28 (1955), 690-691.
[55] N. Mataga, Y. Kaifu, M. Koizumi: Bull. Chem. Soc. Jpn 29 (1955), 465-471.
[56] E. Lippert: Ber. Bunsenges. Physik. Chem. 61 (1957), 962-975.
[57] H. Beens, H. Knibbe, A. Weller: J. Chem. Phys. 47 (1967), 1183-1184.
[58] W. Liptay, G. Walz, W. Baumann, H.-J. Schlosser, H. Deckers, N. Detzer: Z. Naturforsch. 26a (1971), 2020-2038.
[59] W. Baumann, E. Spohr, H. Bischof, W. Liptay: J. Luminesc. 37 (1987), 227-233.
[60] M. P. de Haas, J. M. Warman: Chem. Phys. 73 (1982), 35-53.
[61] W. Schuddeboom: "Photophysical Properties of Opto-Electric Molecules studied by Time-Resolved Microwave Conductivity.". Ph.D. Thesis, Delft 1994, ISBN 90-73861-21-7.
[62] J. M. Warman, M. P. de Haas, J. W. Verhoeven, M. N. Paddon-Row: Adv. Chem. Phys. 106 (1999), 571-601.
[63] J. J. Piet, J. M. Warman, H. L. Anderson: Chem. Phys. Lett. 266 (1997), 70-74.
[64] W. Verbouwe, M. van der Auweraer, F. C. De Schryver, J. J. Piet, J. M. Warman: J. Am. Chem. Soc. 120 (1998), 1319-1324.
[65] J. J. Piet, H. A. M. Biemans, J. M. Warman, E. W. Meijer: Chem. Phys. Lett. 287 (1998), 13-18.
[66] J. J. Piet, P. N. Taylor, H. L. Anderson, A. Osuka, J. M. Warman: J. Am. Chem. Soc. 122 (2000), 1749-1757.
[67] J. J. Piet, P. N. Taylor, B. R. Wegewijs, H. L. Anderson, A. Osuka, J. M. Warman: J. Phys. Chem. B. 105 (2001), 97-104.
[68] J. J. Piet, W. Schuddeboom, B. R. Wegewijs, F. C. Grozema, J. M. Warman: J. Am. Chem. Soc. 123 (2001), 5337-5347.

2

THE FLASH PHOTOLYSIS TIME-RESOLVED MICROWAVE CONDUCTIVITY TECHNIQUE

2.1 A BRIEF HISTORY

The first steady-state microwave experiments were performed already in the mid 1930's[1]. The radar technology developed during the second world war stimulated the development of time-resolved microwave conductivity (TRMC) techniques in the period directly after the war[2,3]. In these early time-resolved experiments both pure and mixed gases were pulse-ionised and microwaves were used to probe the dielectric properties of the ionised gases as a function of time following the pulse. The aim of these measurements was to determine the mobility of electrons and their rates of attachment and charge recombination[4,5,6]. Because of its proven merits in the investigation of the properties of charge carriers in gaseous systems, the applicability of the TRMC technique was expanded to

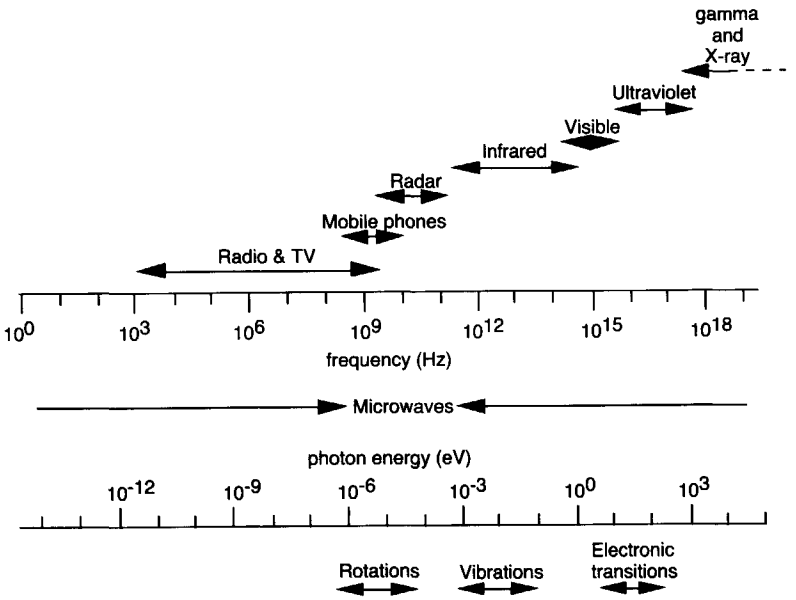

FIGURE 1: The various regions of the electromagnetic spectrum in terms of frequency and photon energy.

solid samples in the 1960's with the rapidly growing interest in semiconductors such as silicon and germanium[7,8,9]. An increase in sensitivity and time-response allowed a further extension of the TRMC technique in the 1970's to the study of the relatively low mobility charge carriers formed in molecular liquids[10-16].

Fessenden and co-workers were the first to realise that the increased sensitivity would allow the determination of the dipole moment of photogenerated radicals[17]. This discovery initiated the development of a time-resolved version using a pulsed laser as excitation source[18,19]. This flash photolysis time-resolved microwave conductivity (FP-TRMC) technique has nanosecond time-resolution. Both singlet and triplet excited states can be monitored, as long as the dipole moment or polarisibility of the excited state differs from that of the ground-state. In addition to changes in dipole moment and polarisability, the decay kinetics of the excited states formed can be determined from the measured transients. Over the last two decades the FP-TRMC technique has been applied mainly to dilute solutions and in particular to the study of photoinduced intra-molecular charge separation and subsequent charge recombination[20]. It has been shown recently however that the method can also be applied to the study of photoinduced charge separation in solid films of organic materials[21,22].

2.2 BASIC INTRODUCTION

2.2.1 Microwaves.

Figure 1 displays the electromagnetic spectrum, which ranges from low energy radiowaves, *via* infrared (IR), visible (Vis) and ultra-violet (UV) light to high energy radiation such as X- and γ-rays. The term microwave is used for electromagnetic radiation with a frequency, f, between 300 MHz and 300 GHz. In contrast to what the name microwaves might suggest, the free space wavelength is not on the order of microns but is at least three orders of magnitude larger and ranges from 1 m to 1 mm. The X-band microwaves used in our FP-TRMC set-up are cm-waves with frequencies from 8.2 to 12.4 GHz corresponding to photon energies from 34 to 51 μeV. Therefore, absorption of a microwave photon can only cause a transition between rotational or spin quantum states, since a vibrational transition requires a photon-energy of at least a few meV's, *i.e.* in the infrared, while an electronic transition requires a photon-energy of a few eV's, which corresponds to the region of visible and UV light.

2.2.2 Transmission lines.

Microwaves, which are characterized by a rapidly oscillating electromagnetic field, can be considered to behave like a high frequency alternating electric current (ac). In order to transmit the microwave energy over long distances in a preferred direction, suitable transmission lines have been devised. The ac properties of a piece of transmission line can be visualised by the lumped equivalent circuit given in Figure 2. An ideal transmission line should have certain specific properties: the resistance along the line (R_1 in figure 2) should be as low as possible, while the resistance of the medium separating the two lines (R_2 in figure 2) should be as high as possible. In addition, the opposite phase shifts caused by the inductive and capacitive elements, L and C respectively in figure 2, should balance to give a negligible overal phase shift.

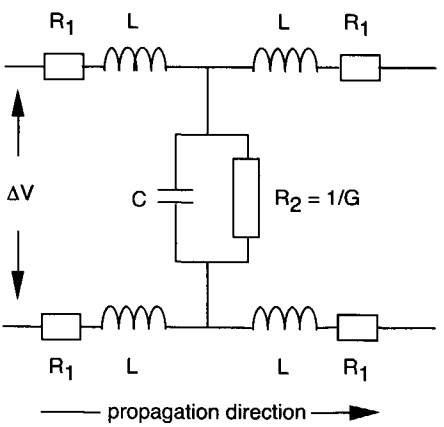

FIGURE 2: Lumped circuit representing the properties of a transmission line such as a waveguide: L and R_1 depend on the properties of the walls of the waveguide and R_2 (= 1/G) and C depend on the dielectric properties of the medium inside the waveguide.

Waveguides are ideally suited as low-loss, high power transmission lines for microwaves. A microwave waveguide consists of a hollow tube of a conducting material, often with a rectangular cross-section. The internal dimensions of the waveguide determine the frequency range of the microwaves that can propagate in its interior. For X-band microwaves (8.2-12.4 GHz) rectangular waveguides are used with inner dimensions of 2.28 by 1.01 cm (corresponds to outer dimensions of 1 by 1/2 inch). The dominant propagation mode in rectangular waveguides is the so-called TE_{10} mode, in which the electric field lines are perpendicular to the propagation direction. The electric and magnetic field lines of the TE_{10} mode are shown in figure 3. The field lines of the rapidly alternating electric field are parallel to the narrow-wall sides of the waveguide.

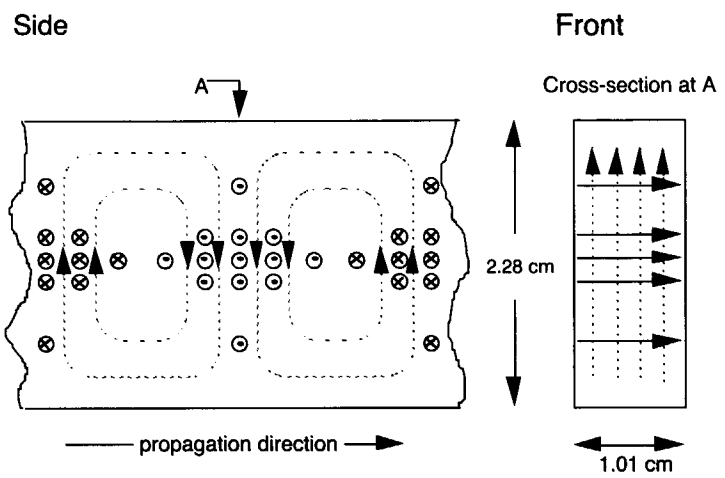

FIGURE 3: The dimensions and electric (full line and circular symbols) and magnetic (dotted lines) field lines inside an X-band waveguide for the TE_{10} mode.

During propagation of a microwave through a waveguide the amount of power transmitted decreases continuously. A significant contribution to this attenuation originates from the resistance of the walls of the waveguide, corresponding to R_1 in figure 2. This contribution can be minimised by using low resistivity metals such as copper to form the waveguide and hence keep R_1 as low as possible. Due to the skin-effect, characteristic for high frequency AC currents, coating the inside of a waveguide with a layer only a few microns thick of a material with a low electrical resistivity is usually sufficient. The other important contribution to the attenuation of microwaves travelling through a waveguide results from the complex conductivity of the medium inside. The lower the conductivity, the smaller the attenuation per unit length of the waveguide. It is this dependence of the attenuation of microwaves on the complex conductivity (or permittivity) of the medium inside the waveguide that is the basis of the TRMC technique. In waveguides used for transmission the medium is usually air, which, when dry, has a conductivity close to zero and a relative permittivity close to unity.

2.2.3 The electrical properties of a medium.

2.2.3.1 Static field conditions.

The dielectric constant, ε, and the conductivity, σ_{dc}, are intrinsic properties of a medium, which characterise that medium's macroscopic response to an externally applied electric field. The characteristic features of this response are best illustrated using a simple example: a net excess of charge, Q, on one side of a medium of cross-sectional area A and thickness d. The resulting potential difference, V, across the medium is accompanied by an electric field, E = V/d. If the medium is vacuum, the excess energy, which is proportional to the potential difference, is stored entirely in the electric field. Under static conditions, the following relation exists between the excess charge and the potential difference:

$$Q = \varepsilon \frac{A}{d} V = \varepsilon_0 \varepsilon_r \frac{A}{d} V \qquad (1)$$

In equation (1) ε_0 is the permittivity of vacuum (8.85419×10^{-12} F.m^{-1}) and ε_r is the relative dielectric constant of the medium. Subsequently in this thesis, where "dielectric constant" is used the "relative dielectric constant" is meant.

For vacuum $\varepsilon_r = 1$ and V has its maximum value for a given Q. In all media other than vacuum ε_r will be greater than unity. A change of intervening medium does not affect Q, therefore according to equation (1) the potential difference and thus also the field strength must decrease as ε_r increases. As the magnitude of the field strength is lowered the energy contained by the electric field decreases proportionally. To conserve energy, the apparent missing amount of energy must have been transferred from the electric field to the medium. The energy transferred is stored in the medium in the form of an induced electric field which opposes the external electric field. Partial cancellation inside the medium of the external field by the opposing induced field yields a resulting electric field inside the medium whose field strength, V/d, is in agreement with equation (1).

The generation of an induced electric field within a medium requires that the average charge distributions of the negatively charged electrons and the positively charged nuclei no longer completely coincide, *i.e.* the medium is polarised. These field-induced changes of the charge distributions within the medium are attributed to the occurrence of displacement currents. The macroscopic concept of displacement currents is comprised of three distinct microscopic processes: electronic polarisation, distortional polarisation and dipole orientational polarisation. These are illustrated separately in figure 4.

Electronic polarisation plays a role in all media. Monatomic gases, *e.g.* the noble gases, are the simplest example to explain the electronic polarisation. In the absence of an external field the electron density distribution of a noble gas atom is symmetrical about the

nucleus or, alternatively stated, the centre of gravity of the electron density distribution coincides with the nucleus. The magnitude of the coulombic attraction between the nucleus and the bound electrons determines how easily an external field can perturb this symmetry. As a result of this perturbation the centre of the electron density distribution is displaced. Since it no longer coincides with the oppositely charged nucleus a dipole moment is induced by the external field. The ratio between the induced dipole moment, p_e, and the external field, E, is known as the electronic polarisability, α_e, which is a characteristic property of an atom or molecule.

Distortion polarisation can only occur in media which consist of either oppositely charged ions in a crystal lattice or molecules with oppositely charged moieties. The distance between the opposite charges is determined by the balance between the attractive and repulsive forces experienced within the crystal or molecule. An external electric field can perturb this balance and alter the distances between the charged moieties, as shown in figure 4. As a result the overlap between the two opposite charge distributions is altered. The extent to which this occurs depends on the distortional polarisability, α_v, of the molecules of the medium.

For certain molecules a non-uniform charge distribution results in the molecules having a net dipole moment, p, which will interact with an external electric field. In low viscosity liquid or gaseous media, dipolar molecules are able to reorient the axis of their dipole moment preferentially in the direction of the external field by rotational motion. As a result, the net zero dipole moment of a molecular ensemble resulting from the random orientation of the molecules inside the medium is replaced by an ensemble having a net dipole moment in the direction of the external electric field (figure 4). In line with the other contributions to polarisation the process of dipole orientation can also be characterised by a polarisability: α_p. However in contrast to α_e and α_v, α_p is not an intrinsic property of a molecule alone, since the surroundings of the molecule influence its ability to reorient.

Thus, the observed macroscopic polarisation of a medium is the collective result of the different polarisation processes which occur at a molecular level. All three processes have in common that the zero-field equilibrium within the medium is replaced by a new equilibrium under influence of the external electric field. The energy needed to attain this new equilibrium has been obtained from the external field and is stored in the polarised medium. This energy is released again when the polarised medium returns to the zero-field situation.

If a medium does not attain a new equilibrium in response to an external potential difference, equation (1) is no longer valid. In such a medium, instead of microscopic displacement currents, a macroscopic current, I, is observed, which is proportional to the potential difference, V, according to:

$$I = \sigma_{dc} \frac{A}{d} V \qquad (2)$$

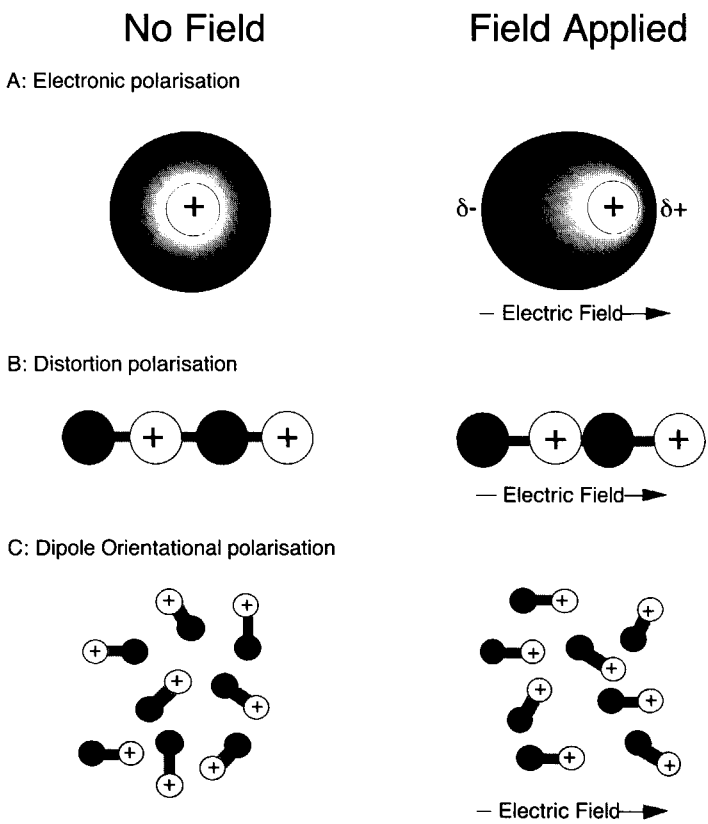

FIGURE 4: Pictorial illustration of the three major contributions to the polarisability of a medium in the absence (left) and the presence (right) of an electric field.

The magnitude of the current through a medium is directly proportional to that medium's conductivity, σ_{dc}. The higher the value of σ_{dc} the larger the amount of charge that will flow through the medium per unit time. The reduction of the potential difference across the medium is the driving force for this flow of charge. Just as in the case of a dielectric medium, energy is absorbed from the electric field by a conducting medium. In contrast to a purely dielectric medium, this energy is not stored in a polarisation of the medium but is dissipated as heat due to the friction experienced by the charges as they move through the medium. Therefore, to sustain the continuous flow of charge, a continuous flow of energy into the medium is required, which must be provided by the potential difference.

Without going into detail as to the actual mechanism of conduction, the following general expression applies which is just the sum of all the individual contributions of the

different types of charge carriers present:

$$\sigma_{dc} = e.\sum_i N_i.z_i.\mu_i \qquad (3)$$

In this equation e is the elementary charge, while N_i, z_i and μ_i are the number per unit volume, the multiplicity and the mobility of one type of charge carrier, which is identified by the index i. Examples of charge carriers in different types of media are the conduction band electrons in semi-conductors, ions in liquids and solid electrolytes, and polarons on conjugated polymer chains.

2.2.3.2 Alternating field conditions.

Under alternating field or ac conditions, the static or dc dielectric constant, ε_r, and conductivity, σ_{dc}, fail to describe the response of the medium. Therefore, both ε_r and σ_{dc} have to be replaced by their frequency dependent counterparts, $\varepsilon(\omega)$ and $\sigma(\omega)$[23,24]:

$$\varepsilon(\omega) = 1 + \chi(\omega) \qquad (4)$$
$$\sigma(\omega) = \sigma_{dc} + j\omega\varepsilon_0\chi(\omega) = \sigma_{dc} + \sigma_{ac}(\omega) \qquad (5)$$

In equation (5) $j = \sqrt{-1}$. The parameter $\chi(\omega)$ in the equations (4) and (5) is known as the dielectric susceptibility. Both of these equations can be seen to consist of a fixed contribution, which determines the lower limit of either $\varepsilon(\omega)$ or $\sigma(\omega)$, and a variable contribution, $\chi(\omega)$ and $\sigma_{ac}(\omega)$ respectively, which are both a function of the radian frequency of the alternating electric field, ω (= $2\pi f$). Both $\chi(\omega)$ and $\sigma_{ac}(\omega)$ (= $j\omega\varepsilon_0\chi(\omega)$) are complex and can be written in terms of a real and an imaginary part:

$$\chi(\omega) = \chi'(\omega) - j\chi''(\omega) \qquad (6)$$
$$\sigma_{ac}(\omega) = \sigma_{ac,re}(\omega) + j\sigma_{ac,im}(\omega) \qquad (7)$$

All the different contributions to the polarisability, which have been identified in the previous section, will contribute independently to $\chi(\omega)$ which can therefore be written as[23]:

$$\chi(\omega) = \sum_i \chi_i(\omega) = \chi_e(\omega) + \chi_v(\omega) + \chi_p(\omega) \qquad (8)$$

Changes in both $\varepsilon(\omega)$ and $\sigma_{ac}(\omega)$, $\Delta\varepsilon(\omega)$ and $\Delta\sigma_{ac}(\omega)$, result from changes in $\chi(\omega)$ and are

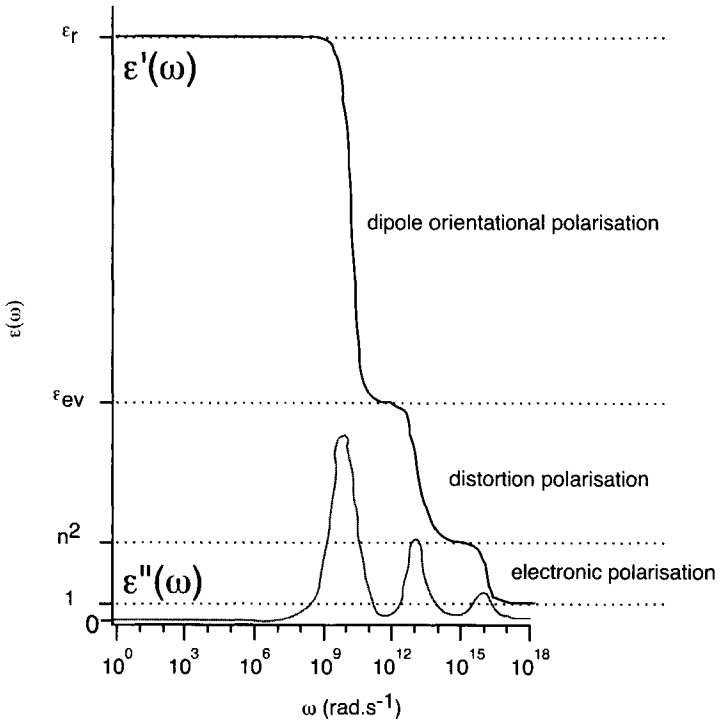

FIGURE 5: The dependence of the real, $\varepsilon'(\omega)$, and imaginary, $\varepsilon''(\omega)$, part of the complex permittivity of a medium on the radian frequency, ω, of an alternating electric field for a medium in which all three contributions to the polarisability shown in figure 4 are operative.

related to each other *via*:

$$\Delta\sigma_{ac}(\omega) = j\omega\varepsilon_0\Delta\varepsilon(\omega) \qquad (9)$$

This relationship can result in confusion since the real component of $\Delta\varepsilon(\omega)$ corresponds to the imaginary component of $\Delta\sigma_{ac}(\omega)$ and *vice-versa*[24]:

$$\Delta\sigma_{ac,re}(\omega) = \omega\varepsilon_0\Delta\varepsilon''(\omega) \qquad (10)$$

$$\Delta\sigma_{ac,im}(\omega) = \omega\varepsilon_0\Delta\varepsilon'(\omega) \qquad (11)$$

In the case that $\Delta\sigma_{dc} = 0$ the subscript ac can be dropped in the equations (9), (10) and (11).

The frequency dependences of both $\varepsilon'(\omega)$ (= 1 + $\chi'(\omega)$) and $\varepsilon''(\omega)$ (= $\chi''(\omega)$) of an arbitrary non-conducting polar liquid ($\sigma_{dc} = 0$) are shown in figure 5. The value of $\varepsilon'(\omega)$ at low frequencies is identical to the static dielectric constant, $\varepsilon'(0) = \varepsilon_r$, while at optical frequencies ($\omega \approx 10^{15}$-10^{16} rad.s^{-1}) the value of $\varepsilon'(\omega)$ is equal to the square of the refractive

index, n, which is conventionally determined at the D-line of the sodium spectrum (λ_D = 589 nm, $\omega = 3.2\times10^{15}$ rad.s^{-1}). In a polar solvent the difference between ε_r and n^2 can be large; in water at 25° C for instance $\varepsilon_r = 78.5$ and $n^2 = 1.78$.

In figure 5 it can be seen that $\varepsilon'(\omega)$ decreases in three steps from a high value at low frequencies to a low value at optical frequencies. The steps in $\varepsilon'(\omega)$ occur in the microwave, the infrared and the UV-Vis range of the electromagnetic spectrum. The three separate contributions to the polarisability shown in figure 4 become in succession negligible beyond these three frequency ranges. Hence, the value of $\chi'(\omega)$ in the regions just beyond a step will be equal to the remaining contributions, which will still have their maximum value. As can be seen in figure 5, in the same frequency range where $\varepsilon'(\omega)$ strongly decreases with increasing frequency, $\varepsilon''(\omega)$ rises to a maximum and subsequently decays.

In the next paragraphs we will focus on the changes in $\varepsilon(\omega)$, and $\sigma(\omega)$, which occur in the microwave frequency range. Because of this, it is useful to define a dielectric constant ε_{ev} which corresponds to the low frequency limit resulting from the combined contributions from the electronic and distortion polarisation, *i.e.*

$$\varepsilon_{ev} = 1 + \chi_e(0) + \chi_v(0) \tag{12}$$

The significance of this parameter is indicated in figure 5. For frequencies upto the microwave range, *i.e.* $\omega << \omega_v$ (= $2\pi\nu_v$ with ν_v the characteristic (infrared) frequency of molecular vibrations), the frequency dependence of $\varepsilon(\omega)$ will be given by:

$$\begin{aligned}\varepsilon(\omega' \omega_v) &= \varepsilon_{ev} + \chi_p(\omega) \\ &= \varepsilon_{ev} + \chi'_p(\omega) - j\chi''_p(\omega)\end{aligned} \tag{13}$$

For a medium devoid of dipolar interactions ε_{ev} will be equal to ε_r and if distortion polarisation plays no role ε_{ev} will be equal to n^2.

The energy of a microwave photon, between 1 μeV and 1 meV, is of the same order as the energy difference between the rotational levels of molecules. The rotational motion of a molecule in a liquid depends on the thermal energy, the moment of inertia of the molecule and the interactions with its surroundings. The rotational motion of a molecule can be characterised by its rotational relaxation time, Θ, which is the mean time required for rerandomisation of an externally induced preferential orientation. As an example, Θ is *ca.* 15 ps for a small molecule such as water in a liquid of viscosity 1 cP.

According to Debye[25], for a single-exponential dipole relaxation, the frequency dependence of $\chi_p(\omega)$ is given by:

$$\chi_p(\omega) = \frac{1}{1 + j\omega\Theta}\chi_p(0)$$

$$= \frac{1 - j\omega\Theta}{1 + (\omega\Theta)^2}\chi_p(0) \qquad (14)$$

The real and imaginary parts of $\chi_p(\omega)$ are therefore:

$$\chi'_p(\omega) = \frac{1}{1 + \omega^2\Theta^2}\chi_p(0) \qquad (15)$$

and

$$\chi''_p(\omega) = \frac{\omega\Theta}{1 + \omega^2\Theta^2}\chi_p(0) \qquad (16)$$

In the equations (14), (15) and (16) $\chi_p(0)$ is equal to the difference between ε_r and ε_{ev}. The exact value of ε_{ev} to be used to calculate $\varepsilon(\omega)$ for frequencies up to the microwave region is often taken to be equal to n^2, *i.e.* the distortion polarisation contribution to ε_{ev} is taken to be negligible compared to the contribution from electronic polarisation. The value of $\chi_p(0)$ is then given by $\varepsilon_r - n^2$.

Using the values of Θ, ε_r and $\varepsilon_{ev} = n^2$ for water given above, $\chi_p'(\omega)$ and $\chi_p''(\omega)$ can be calculated. The values of $\varepsilon'(\omega)$ ($= n^2 + \chi_p'(\omega)$) and $\varepsilon''(\omega)$ ($= \chi_p''(\omega)$) resulting from equation (13) are plotted in figure 6A. This figure shows the type of frequency dependence expected for a dipole relaxation contribution to the real and imaginary component of $\varepsilon(\omega)$ in the microwave frequency range. The corresponding values of $\sigma_{ac,re}(\omega)$ and $\sigma_{ac,im}(\omega)$ are shown in figure 6B.

The frequency dependent relation between permittivity and conductivity can be understood from the plots in figure 6. As long as the radian frequency of the microwaves, ω, is considerably smaller than $1/\Theta$ the molecules can reorient much faster than the field changes direction and the contribution to the polarisability will be as high as under static field conditions, *i.e.* $\varepsilon(\omega) \approx \varepsilon_r$. Under these conditions energy is exchanged efficiently between the external electric field and the medium, *i.e.* $\sigma_{ac}(\omega)$ will be negligible. In the other extreme, when ω well exceeds $1/\Theta$ the rate of rotation is so slow that hardly any preferential orientation will occur. The amount of energy of the alternating electric field temporarily stored in a preferential orientation of the dipolar molecules will then be negligible. Hence, the dipolar contribution to $\varepsilon(\omega)$ will no longer be significant, *i.e.* $\chi_p'(\omega)$ will approach zero.

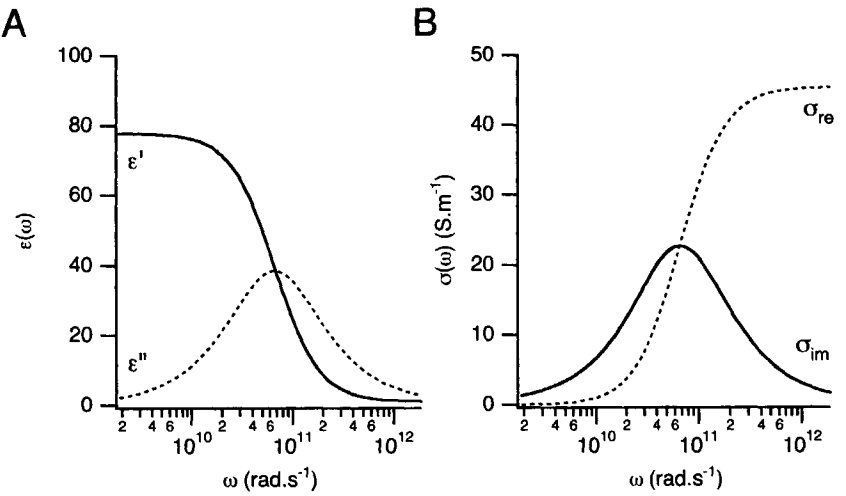

FIGURE 6: The contribution to $\varepsilon(\omega)$ (A) and $\sigma(\omega)$ (B) of dipole orientation of water molecules as function of ω in the microwave frequency range according to the Debye dispersion relation as given in equation (14).

However, at these high frequencies the two charged moieties of the dipole still move under influence of the rapidly alternating electric field, but only over very short distances. This motion will be in-phase with the alternating electric field and as a result the displacement current resulting from the motion of the two charged moieties will become indistinguishable from a true current. The energy absorbed from the alternating electric field is dissipated in the medium as heat in this process of continuous in-phase motion of charges. Therefore, when ω is much larger than $1/\Theta$ the dipolar motion will contribute exclusively to the real component of the conductivity *via* $\sigma_{ac,re}(\omega)$.

In the frequency range centered around $\omega = 1/\Theta$ rotational motion of the dipolar molecules will contribute to both $\varepsilon'(\omega)$ ($= \sigma_{ac,im}(\omega)/\omega\varepsilon_0$) and $\varepsilon''(\omega)$ ($= \sigma_{ac,re}(\omega)/\omega\varepsilon_0$). With increasing frequency the latter increases at the expense of the former. The difference in shape between $\varepsilon'(\omega)$ and $\varepsilon''(\omega)$ in figure 6A and $\sigma_{im}(\omega)$ and $\sigma_{re}(\omega)$ in figure 6B can be understood when one realises that $\varepsilon(\omega)$ is proportional to the amount of charge displacement, while $\sigma(\omega)$ is proportional to the amount of charge displacement per unit time.

2.3 PHOTO-INDUCED CHANGES IN THE CONDUCTIVITY AND PERMITTIVITY

The FP-TRMC technique measures the change in the complex conductivity which occurs on flash-photolysis as a function of time during and after the light pulse, $\Delta\sigma(\omega,t)$. The observed $\Delta\sigma(\omega,t)$ results from the photoexcitation of solute molecules. For small changes, $\Delta\sigma(\omega,t)$ will be proportional to the concentration of excited molecules present at a given time

t after excitation, $N_*(t)$. In some cases more than one excited state can be formed. Each of these states will make a contribution to $\Delta\sigma(\omega,t)$ proportional to its concentration, $N_i(t)$:

$$\Delta\sigma(\omega,t) = \sum_i N_i(t)\left[\frac{\partial\sigma(\omega)}{\partial N}\right]_i \tag{17}$$

According to equation (5) $\sigma(\omega)$ consists of a frequency dependent and a frequency independent part: σ_{dc} and $\sigma_{ac}(\omega)$ respectively. Hence, $\partial\sigma(\omega)$ can be written as:

$$\partial\sigma(\omega) = \partial\sigma_{dc} + \partial\sigma_{ac}(\omega) \tag{18}$$

According to equation (9), $\partial\sigma_{ac}(\omega)$ can equally well be expressed as $j\omega\varepsilon_0\partial\varepsilon(\omega)$. Both $\partial\sigma_{dc}$ or $\partial\sigma_{ac}(\omega)$ must find its origin in a change in one or more of the relevant properties of the solute molecule. The photoinduced formation of charge carriers with a mobility, μ, affects $\partial\sigma_{dc}$, while $\partial\sigma_{ac}(\omega)$ is related to changes in the solute molecule's electronic polarisability, α_e, its distortional polarisability, α_v, or its dipole moment, p:

$$\left[\frac{\partial\sigma(\omega)}{\partial N}\right]_i = \left[\frac{\partial\sigma_\mu(\omega)}{\partial N}\right]_i + \left[\frac{\partial\sigma_{\alpha_e}(\omega) + \partial\sigma_{\alpha_v}(\omega) + \partial\sigma_p(\omega)}{\partial N}\right]_i$$

$$= \left[\frac{\partial\sigma_\mu(\omega)}{\partial N}\right]_i + \left[\frac{\partial\sigma_{\alpha_e}(\omega)}{\partial N}\right]_i + \left[\frac{\partial\sigma_{\alpha_v}(\omega)}{\partial N}\right]_i + \left[\frac{\partial\sigma_p(\omega)}{\partial N}\right]_i \tag{19}$$

Since FP-TRMC measurements are performed in the microwave frequency domain no distinction can be made between changes in the distortion and the electronic polarisability. These can therefore be combined in a single term, α_{ev} ($=\alpha_e+\alpha_v$). Thus, equation (19) can be written as:

$$\left[\frac{\partial\sigma(\omega)}{\partial N}\right]_i = \left[\frac{\partial\sigma_\mu(\omega)}{\partial N}\right]_i + \left[\frac{\partial\sigma_{ev}(\omega)}{\partial N}\right]_i + \left[\frac{\partial\sigma_p(\omega)}{\partial N}\right]_i \tag{20}$$

Recalling equation (18), the first contribution on the right hand side of equation (20) is related to $\partial\sigma_{dc}$ while the other two contributions are related to $\partial\sigma_{ac}(\omega)$. Considering the origin of $\partial\sigma_{ev}(\omega)$ and $\partial\sigma_p(\omega)$ it is more convenient to discuss these changes in terms of changes in permittivity, $\partial\varepsilon_{ev}(\omega)$ and $\partial\varepsilon_p(\omega)$ respectively, than in terms of changes in the conductivity.

2.3.1 Photoinduced changes in the complex permittivity.

As mentioned above, at microwave frequencies both $\chi_e(\omega)$ and $\chi_v(\omega)$ are frequency independent and contribute only to the real part of $\varepsilon(\omega)$ since their imaginary part is negligibly small at these frequencies (see equation (13) and figure 5). Only $\chi_p(\omega)$ consists of a real and imaginary part, both of which can have a significant value in the microwave frequency range depending on the value of ω (and the dipole relaxation time Θ). From the equations (13), (14), (15) and (16) the complex permittivity for frequencies in the microwave region and lower is given by:

$$\varepsilon(\omega << \omega_v) = \varepsilon_{ev} + \chi_p(\omega) = \varepsilon_{ev} + \frac{1 - j\omega\Theta}{1 + (\omega\Theta)^2}\chi_p(0)$$

$$= \varepsilon_{ev} + \frac{1}{1 + (\omega\Theta)^2}\chi_p(0) - j\frac{\omega\Theta}{1 + (\omega\Theta)^2}\chi_p(0) \qquad (21)$$

The desired relations $\partial\varepsilon_{ev}(\omega)/\partial N$ and $\partial\varepsilon_p(\omega)/\partial N$ are related to photoinduced changes in the molecular polarisability, α_{ev}, and the dipole moment, p, respectively. The former is related to the frequency independent part ε_{ev}, while the latter is related to the frequency dependent part $\chi_p(\omega)$ in equation (21).

2.3.1.1 The effect of a change in the molecular polarisability.

In analogy to a non-polar solvent in which $\varepsilon_{ev} = \varepsilon_r$ and $\alpha_{ev} = \alpha$, ε_{ev} can be given by the Clausius-Mossotti equation:

$$\frac{\varepsilon_{ev} - 1}{\varepsilon_{ev} + 2} = \frac{N\alpha}{3\varepsilon_0} \qquad (22)$$

Equation (22) can be rewritten to give the following expression for $\varepsilon_{ev}(\omega)$:

$$\varepsilon_{ev}(\omega) = \frac{3\varepsilon_0 + 2N\alpha}{3\varepsilon_0 - N\alpha} \qquad (23)$$

In an FP-TRMC experiment a very small concentration of the molecules of the medium, *ca.* 1 ppm, are photoexcited and may undergo a change in their polarisability, $\Delta\alpha$ ($=\alpha^*-\alpha_0$). This corresponds therefore to a small change in the product $N\alpha$ in (23), *i.e.* $\partial(N\alpha)=N^*\Delta\alpha$. The resulting change in ε_{ev} can therefore be obtained simply by

differentiating (23) with respect to Nα, which leads to:

$$\partial\varepsilon_{ev}(\omega) = \frac{[\varepsilon_{ev}+2]^2}{9\varepsilon_0}\partial(N\alpha)$$

$$= \frac{[\varepsilon_{ev}+2]^2 N_*}{9\varepsilon_0}\Delta\alpha = \frac{[\varepsilon_{ev}+2]^2 N_*}{9\varepsilon_0}(\alpha_* - \alpha_0) \qquad (24)$$

The concentration of solute molecules in an FP-TRMC experiment is in the μM to mM range so that their effect on ε will be less then 1%. Therefore it is safe to approximate ε_{ev} in the right-hand side of equation (24) by ε_r of the non-polar solvent, which leads to:

$$\partial\varepsilon_{ev}(\omega) = \frac{[\varepsilon_r+2]^2 N_*}{9\varepsilon_0}\Delta\alpha = \frac{[\varepsilon_r+2]^2 N_*}{9\varepsilon_0}(\alpha_* - \alpha_0) \qquad (25)$$

Equation (25) needs to be combined with equation (9) and slightly rewritten to give the relation between $\Delta\sigma_{ac}(\omega)$ and α required in equation (20):

$$\left[\frac{\partial\sigma_{ev}(\omega)}{\partial N}\right]_i = j\omega\varepsilon_0\frac{[\varepsilon_r+2]^2}{9\varepsilon_0}\Delta\alpha_i$$

$$= j\omega\varepsilon_0\frac{[\varepsilon_r+2]^2}{9\varepsilon_0}(\alpha_* - \alpha_0)_i \qquad (26)$$

2.3.1.2 The effect of a change in dipole moment.

The frequency dependent part in equation (21), $\chi_p(\omega)$, depends on the orientational relaxation of the molecule's dipole moment p and is taken into account by the Debye approach[25] which was already given in equation (14):

$$\chi_p(\omega) = \frac{1}{1+j\omega\Theta}\chi_p(0) \qquad (27)$$

The next step in this approach, is to relate $\chi_p(0)$ to p. The difficulty lies in the estimation of the local field experienced by the dipolar solute molecule. Different formulations for the local field have been suggested by Lorentz and Onsager[26-30], which result in the following

relationships:

$$\chi_p(0)_L = [\varepsilon_r + 2][\varepsilon_{ev} + 2]\frac{Np^2}{27\varepsilon_0 k_b T} \tag{28}$$

$$\chi_p(0)_O = \frac{\varepsilon_r[\varepsilon_{ev} + 2]^2}{[2\varepsilon_r + \varepsilon_{ev}]}\frac{Np^2}{9\varepsilon_0 k_b T} \tag{29}$$

For dilute solutions of dipolar molecules in the non-polar solvents used in the FP-TRMC measurements ε_r and ε_{ev} should be identical up to the infrared frequency range. The concentration of solute molecules in an FP-TRMC experiment is in the μM to mM range so that their effect on ε will be less than 1%. Therefore it is safe to approximate ε_{ev} by ε_r in the right-hand side of equations (28) and (29). Substitution of $\varepsilon_{ev} = \varepsilon_r$ in equation (28) and equation (29) yields in both cases the same result:

$$\chi_p(0) = \frac{[\varepsilon_r + 2]^2}{27\varepsilon_0 k_b T} Np^2 \tag{30}$$

Substitution of equation (30) into equation (27) gives:

$$\chi_p(\omega) = \frac{[\varepsilon_r + 2]^2}{27\varepsilon_0 k_b T}\frac{Np^2}{1 + j\omega\Theta} \tag{31}$$

The change in ε(ω) caused by a photo-induced change in p, $\partial\varepsilon_p(\omega)$, is equal to the difference in susceptibility of the ground-state, $\chi_{p_0}(\omega)$, and excited state, $\chi_{p_*}(\omega)$:

$$\partial\varepsilon_p(\omega) = \chi_{p_*}(\omega) - \chi_{p_0}(\omega) \tag{32}$$

According to equation (32), if N* is the number of excited molecules, $\partial\varepsilon_p(\omega)$ should be given by:

$$\partial\varepsilon_p(\omega) = \frac{[\varepsilon_r + 2]^2}{27\varepsilon_0 k_b T}\frac{N_* p_*^2}{1 + j\omega\Theta_*} - \frac{[\varepsilon_r + 2]^2}{27\varepsilon_0 k_b T}\frac{N_* p_0^2}{1 + j\omega\Theta_0}$$

$$= \frac{[\varepsilon_r + 2]^2}{27\varepsilon_0 k_b T} N_* \left[\frac{p_*^2}{1 + j\omega\Theta_*} - \frac{p_0^2}{1 + j\omega\Theta_0}\right] \tag{33}$$

Equation (33) can be separated into a real part,

$$\partial\varepsilon'_p(\omega) = \frac{[\varepsilon_r + 2]^2}{27\varepsilon_0 k_b T} N_* \left[\frac{1}{1+\omega^2\Theta_*^2} p_*^2 - \frac{1}{1+\omega\Theta_0^2} p_0^2 \right] \tag{34}$$

and an imaginary part,

$$\partial\varepsilon''_p(\omega) = \frac{[\varepsilon_r + 2]^2}{27\varepsilon_0 k_b T} N_* \left[\frac{\omega\Theta_*}{1+\omega^2\Theta_*^2} p_*^2 - \frac{\omega\Theta_0}{1+\omega\Theta_0^2} p_0^2 \right] \tag{35}$$

Equation (33) needs to be combined with equation (9) and slightly rewritten to give the relation between $\Delta\sigma_{ac}(\omega)$ and p required in equation (20):

$$\left[\frac{\partial\sigma_p(\omega)}{\partial N} \right]_i = j\omega \frac{[\varepsilon_r + 2]^2}{27 k_b T} \left[\frac{p_*^2}{1 - j\omega\Theta_*} - \frac{p_0^2}{1 - j\omega\Theta_0} \right]_i \tag{36}$$

As for equation (33), equation (36) can be separated into a real part,

$$\left[\frac{\partial\sigma_p(\omega)}{\partial N} \right]_{i,re} = \frac{[\varepsilon_r + 2]^2}{27 k_b T} \left[\frac{\omega^2\Theta_*}{1+\omega^2\Theta_*^2} p_*^2 - \frac{\omega^2\Theta_0}{1+\omega^2\Theta_0^2} p_0^2 \right]_i \tag{37}$$

and an imaginary part,

$$\left[\frac{\partial\sigma_p(\omega)}{\partial N} \right]_{i,im} = \frac{[\varepsilon_r + 2]^2}{27 k_b T} \left[\frac{\omega}{1+\omega^2\Theta_*^2} p_*^2 - \frac{\omega}{1+\omega^2\Theta_0^2} p_0^2 \right]_i \tag{38}$$

2.3.2 Photoinduced changes in the dc conductivity

2.3.2.1 The effect of mobile charge carriers.

The previous sections have been devoted to changes in $\varepsilon(\omega)$, which are directly related to changes in $\sigma_{ac}(\omega)$ *via* equation (9). The photo-induced generation of mobile charge carriers will result in a change in $\Delta\sigma_{dc}$. If the number of photo-generated charge carrier pairs is given by N_p, then in accordance with equation (3), $\partial\sigma_{dc}(\omega)$ is given by:

$$\partial\sigma_{dc}(\omega) = N_p e[\mu_- + \mu_+] = N_p e[\Sigma\mu] \tag{39}$$

From equation (39) the relation between $\Delta\sigma(\omega)$ and μ required in equation (20) is:

$$\left[\frac{\partial\sigma_{\mu}(\omega)}{\partial N}\right]_i = e\left[\Sigma\mu\right]_i \tag{40}$$

Only the sum of the mobilities can be determined from an TRMC experiment, since it is not possible to discriminate with this technique between the contributions from positively and negatively charged charge carriers.

In the above it was assumed that the value of $\Sigma\mu$ is independent of ω. However, this is not necessarily the case. Therefore it is more correct to write equation (40) as:

$$\left[\frac{\partial\sigma_{\mu}(\omega)}{\partial N}\right]_i = e\left[\mu_{-}(\omega)+\mu_{+}(\omega)\right]_i = e\left[\Sigma\mu(\omega)\right]_i \tag{41}$$

Two completely different theoretical relations between $\mu(\omega)$ and ω exist, depending on the model used to describe the mechanism of charge transport in a material: the hopping model and the band model[31,32]. Which model is applicable in a particular medium depends on the nature of the charge carriers, *i.e.* whether they are localised or quasi-free.

In the hopping model the charge carriers are considered to be localised on a molecular scale at any instant in time. The charge carriers migrate by hopping between these localised sites, which can be considered to be local minima on the potential energy surface of the medium. In a perfectly ordered medium all minima are equally low in depth and all barriers between them are equal in height. The frequency dependence in the hopping model results from disorder in the medium[33], which results in a distribution in the depths of the minima or the heights of the barriers or both[34,35]. Hence, various regions in which the charge carrier mobility differs significantly can be distinguished in a disordered medium.

The net dc mobility, μ_{dc} (= $\mu(0)$), in a disordered medium is equal to the time-weighted average of all the mobilities in the regions successively encountered by a migrating charge carrier crossing the entire medium[36]. As a result, μ_{dc} in a disordered medium is determined mainly by the regions with low mobility since the transit time for these regions is largest. Under high frequency ac conditions the average displacement of charge carriers is small and a charge carrier is only able to probe a small region around its own position. The ac mobility, μ_{ac} (= $\mu(\omega)$), of a disordered medium is just the average of all the different mobilities experienced by all the charge carriers at an instant in time[36]. In contrast to μ_{dc}, μ_{ac} will be very sensitive to regions of high mobility. The increase of the mobility with frequency in a disordered material can be approximated by the following empirical relation, in which s

has a value between 0 and 1[23,24,31,37]:

$$\mu(\omega) \propto \omega^{s} \tag{42}$$

In the case of the band model, the charge carriers are quasi-free, *i.e.* they are not bound to a certain region, but move most of the time unhindered through the medium and suffer only infrequently scattering events. This bears considerable resemblance to the motion of charged particles in a gas. Hence the frequency dependence of the mobility is expected to be similar to that derived from the Drude model[31,38]:

$$\mu(\omega) = \frac{1}{1 + j\omega\tau_m}\mu(0) = \frac{1}{1 + (\omega\tau_m)^2}\mu(0) - j\frac{\omega\tau_m}{1 + (\omega\tau_m)^2}\mu(0) \tag{43}$$

In this equation τ_m is the momentum relaxation time. In classical terms τ_m is the average time within which the net momentum of a charge carrier is rerandomised. Equation (43) is a dispersion relation similar to the one used in the Debye approach for dipole relaxation (see previous sections). Therefore it can be assumed that as long as $\omega \ll 1/\tau_m$ the value of $\mu(\omega)$ will remain close to the dc value, $\mu(0)$ ($= \mu_{dc}$).

In crystalline semiconductor materials such as silicon $\mu(0)$ is on the order of 10^3 $cm^2V^{-1}s^{-1}$ which corresponds to a value of τ_m of *ca.* 10^{-12} s^{-1}. The value of $\mu(\omega)$ will differ significantly from $\mu(0)$ only for frequencies in excess of 50 GHz. Hence, the frequency dependence of $\mu(\omega)$ will become of importance in the higher frequency range of the microwave spectrum, but should be negligible around the 10 GHz frequency range used in the FP-TRMC technique. This is particularly the case in the materials investigated since the mobilities are expected to be much smaller than the value given above for crystalline silicon. As a result the imaginary part in equation (43) will still be negligible at the microwave frequencies used.

Since FP-TRMC experiments in the present work are performed on dilute solutions, any mobile charge carriers formed on the solute molecules after excitation can only move within a limited domain determined by the dimensions of the solute molecule itself. Therefore, under static field conditions σ_{dc} would not be altered by the formation of these charge carriers. Actually under static field conditions these mobile charge carriers can be considered to be space-limited mobile charges and will contribute to the dielectic constant instead. Under ac condition the average displacement of these space-limited mobile charges decreases with increasing frequency. When the average displacement becomes smaller than the domain size, their contribution to $\Delta\varepsilon'(\omega)$ will decrease rapidly in favour of a contribution to $\Delta\varepsilon''(\omega)$ ($=\Delta\sigma_{ac,re}(\omega)/\omega\varepsilon_0$).

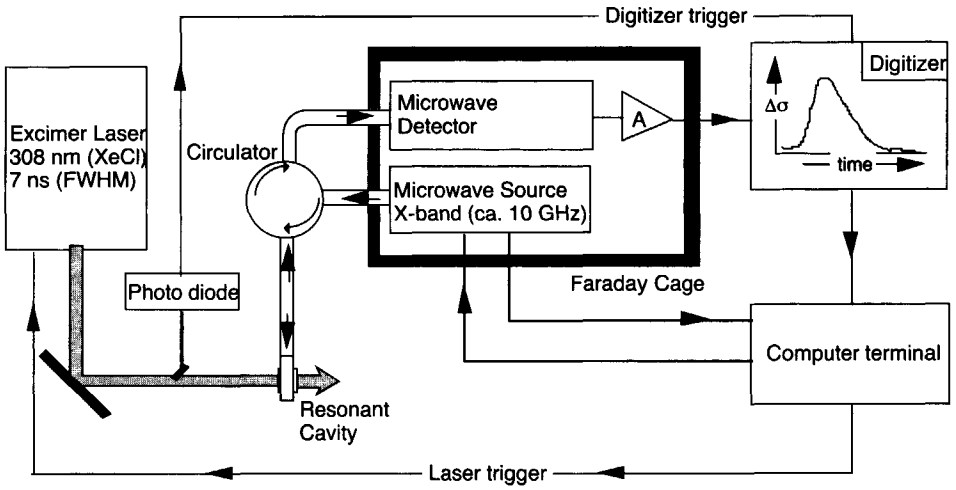

FIGURE 7: A schematic representation of the FP-TRMC set-up.

2.4 THE FP-TRMC EQUIPMENT

2.4.1 Basic overview.

In Figure 7 a schematic drawing is shown of the FP-TRMC set-up used. The computer terminal is the primary user-interface from which the two major functionalities are controlled: the laser, which is used as the excitation source to generate the excited states, and the microwave circuitry, which is used to measure the resulting change in the complex conductivity of the photo-excited solution. The measuring cell, a microwave resonant cavity, is where these two functionalities interact with the sample. The excitation source, the detection system and the resonant cavity will be described in more detail in the next sections.

The sample in the resonant cavity is continuously probed by microwaves of a single frequency. An actual measuring sequence starts with a trigger pulse from the computer which fires a single shot from the laser. The emitted light travels through the measuring cell depositing a part of its energy in the sample. Just before the light enters the measuring cell, a trigger signal is picked-off by a photodiode (FND 100Q) positioned along the path of the laser beam. On receiving this trigger the digitizer starts to record the output of the microwave detector over a pre-specified time window. Finally, this measured transient is transferred to the computer, where it can be manipulated and stored. If enhancement of the signal-to-noise ratio is required, several single-shot transients are combined and averaged. This can be done automatically by the digitizer or immediately afterwards by the computer.

In the original set-up a Tektronix 7912 transient digitizer was used in combination with a Tektronix 604 monitor. The experiment was controlled from an Atari mega ST2

computer and a data-acquisition programme written in BASIC was used. Currently a Tektronix TDS 680B digital oscilloscope is used in combination with an Apple Macintosh G3 computer. For the data-acquisition a programme called REACH is used, which is written in LabView.

2.4.1.1 The excitation source.

A Lumonics HyperEX 400 (HE 420) excimer laser is used as the excitation source. The heart of this laser is a gas-filled discharge tube in which the required population inversion is created by a *ca.* 40 kV electric discharge through a gas mixture with a total pressure of *ca.* 1600 torr (*ca.* 0.21 MPa). The composition of the gas mixture determines the wavelength of the laser light. Using a mixture of Xe and HCl in He the emitted light has a wavelength of 308 nm, *i.e.* a photon energy of 4.0 eV. The emitted laserbeam is non-coherent and only weakly polarized. After leaving the chamber through a semi-transparent mirror, a system of lenses is used to produce a broad non-focussed beam to ensure a close to uniform illumination of an area of *ca.* 1 × 2.5 cm^2 on the measuring cell.

The output power of the laser is measured using a Scientec 365 power meter. For this purpose the laser is set to deliver pulses with a repetition rate of 10 Hz. The energy emitted by the laser is monitored continuously on the power meter until a plateau is reached. From the power level at the plateau the energy per pulse is calculated taking into account the 10 Hz repetition rate. The power output of the laser with a new gas mixture is *ca.* 70 mJ per pulse. Due to gradual exhaustion of the gas mixture the power output decreases with time. Measurements are performed as long as the power output is greater than 40 mJ per pulse. Over a single measuring day only a minor decrease in power output is observed.

The shape of the laser pulse is determined with the same photodiode (FND 100Q, risetime *ca.* 1 ns) as that used to trigger a TRMC measurement. The laser pulse consists of a high main pulse followed by a weak after-pulse and has a full width at half maximum (FWHM) of *ca.* 7 ns.

2.4.1.2 The microwave circuitry.

A more detailed scheme of the microwave section of the set-up is given in figure 8. The aim of the detection system is to determine, with a time resolution of no more than several nanoseconds, the transient changes in the microwave power reflected by the resonant cavity.

The microwave source is a Gunn diode (Midcentury MC16/34B) mounted in a resonant cavity. With a moveable plunger the inner dimensions of the resonant cavity can be adjusted so that the microwave frequency can be tuned over a range from 8.2 to 12.4 GHz.

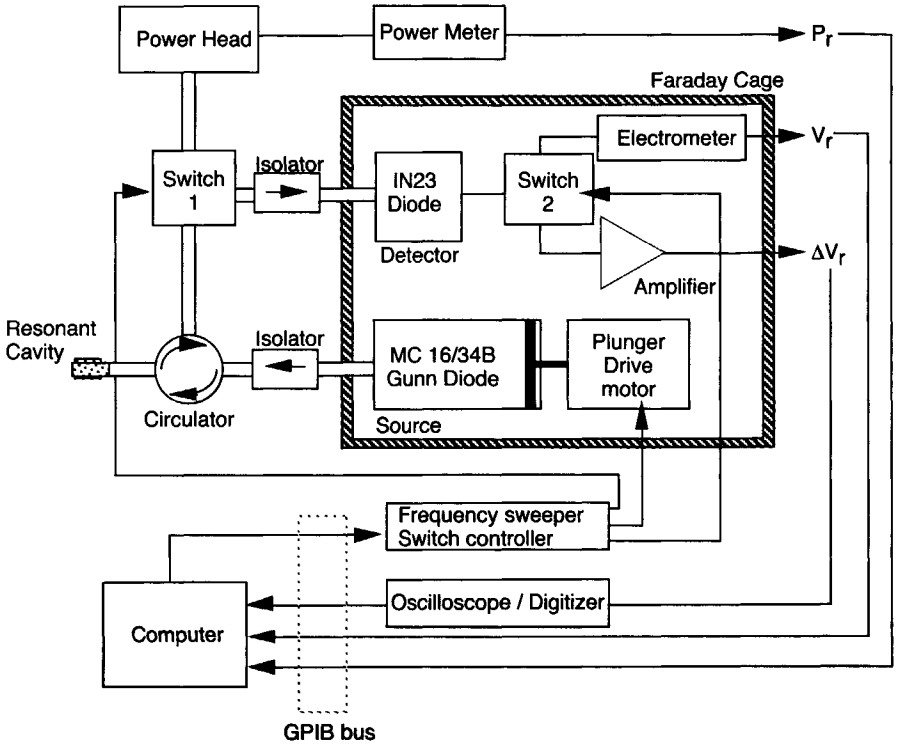

FIGURE 8: A detailed picture of the microwave part of the FP-TRMC set-up.

The power output has a maximum of *ca.* 100 mW at 9.0 GHz. The maximum electric field strength in the sample resonant cavity obtainable with this source is limited to *ca.* 10 $kV.m^{-1}$.

On leaving the source the microwaves enter the circuitry *via* an isolator, which is a device which has a low loss in the forward direction and a high loss in the reverse direction, *i.e.* it functions as a diode for microwaves. After passing the isolator the microwaves travel to a circulator which directs them to the resonant cavity containing the solution of interest. Microwaves that are not absorbed in the resonant cavity are reflected back to the circulator which directs them to the microwave detection side of the system. For steady-state measurements, the power level, P_r, is measured using a slow-response power meter (Marconi instruments tft 6425). For time-resolved measurements a IN23 Schottky barrier diode is used. The Schottky barrier diode converts the incident microwave power into a DC voltage, V_r. The transient change in this voltage is amplified 100 times using either a Hewlett-packard 8447A (risetime 1 ns) or a Hewlett-packard 462A (risetime: 4 ns) amplifier and is then fed into the digitizer.

At the power levels used, *ca.* 100 mW, the voltage output of the detector diode does not vary linearly with the incident power of the microwaves. Small fractional changes in the

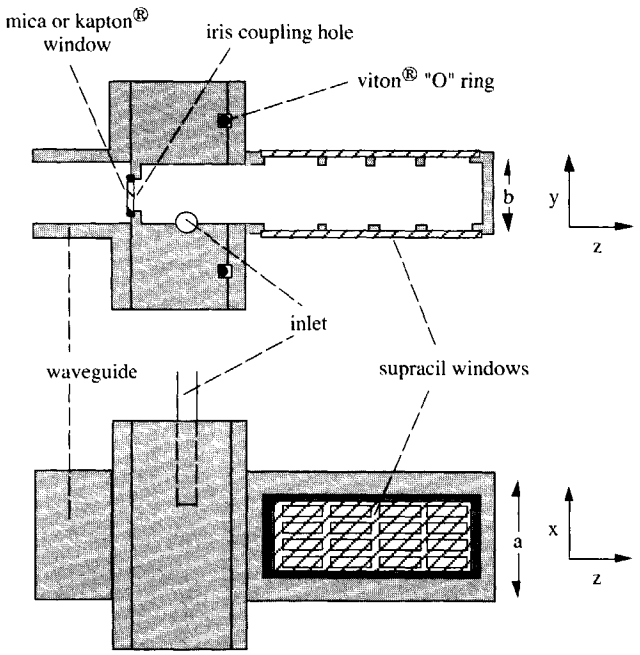

FIGURE 9: Top view (top) and side view (bottom) of the resonant cavity used in the FP-TRMC experiments. The dimensions a (= 2.28 cm) and b (= 1.01 cm) are characteristic for an X-band waveguide.

microwave power at the detector, $\Delta P_r/P_r$, are related to the change in detector output, $\Delta V_r/V_r$, according to:

$$\frac{\Delta P_r}{P_r} = n\frac{\Delta V_r}{V_r} \tag{44}$$

In the current experiments the value of n varies between 1.65 and 2.00 and is routinely checked after each measured set of transients. For this purpose a variable attenuator is used to vary the power output of the microwave source. Both P_r and V_r are measured at the full power setting and at an attenuated power setting. From these two related data pairs ΔP_r and ΔV_r are calculated and the n-factor is then calculated using equation (44).

2.4.1.3 The microwave resonant cavity.

In the FP-TRMC experiments the liquid samples are contained in a microwave resonant cavity, which is designed to operate in the "cavity reflection" mode. In Figure 9 the important features of this measuring cell are shown. The resonant cavity is constructed out of copper and brass, which are gold-plated. The purpose of the gold plating is to have a surface

inside the cavity which combines low resistivity with high chemical inertness. The different pieces are bolted together and a viton® O-ring is used to ensure that the sample compartment is solvent tight.

Both broadwall sides contain 4 rows of 4 holes each of 1.5 × 5.0 mm^2. Together these holes make up an area of 1.2 cm^2, through which the laser beam can enter the measuring cell. The holes are distributed over an area of 1.0 × 2.4 cm^2, which is covered by a supracil quartz window.

The resonant cavity has a width and height of 1.01 and 2.28 cm respectively, which are the typical inner dimensions of X-band waveguides, and has a length of 4.7 cm. The cell is short-circuited by a metal plate at one end and coupled to the microwave circuitry *via* an iris at the other end. The iris consists of a circular hole at the centre of a 0.5 mm thick metal plate. The iris hole can have a diameter of 8.0, 8.2 or 8.3 mm, depending on the solvent used. The size of the iris hole determines the reflection conditions at the iris plate, which determine the fraction of the incident microwave power that is transmitted through the iris-plate and the fraction that is reflected. To retain the solution in the resonant cavity the iris hole is covered by a thin sheet of mica. The mica has been replaced by a more robust kapton® foil in the currently used cells.

2.5 THE BASIS OF THE FP-TRMC TECHNIQUE.

2.5.1 The cavity resonance.

In a waveguide, which is bounded by conducting walls in the two directions parallel to the propagation direction, the inner dimensions between the walls determine the range of microwave frequencies that can be transmitted efficiently by that waveguide. In a cavity, which is bounded by conducting surfaces in all three directions, an additional boundary condition must be satisfied. This additional boundary condition limits the microwaves allowed inside the cavity to those with wavelengths such that they have a node at both the iris plate and the endplate. This condition is only fulfilled for specific frequencies of the microwaves, which are referred to as the resonance frequencies of the resonant cavity. Only close to these frequencies can an electric field exist inside the cavity, which is a necessity in order to be able to probe the dielectric properties of a medium contained in the resonant cavity. The resonance frequencies for a resonant cavity of length d and rectangular cross section a × b which is filled with a uniform dielectric are given by[39]:

$$f_0 = \frac{c}{\sqrt{\varepsilon_r K_r}} \frac{\sqrt{\left(\left(\frac{q}{a}\right)^2 + \left(\frac{r}{b}\right)^2 + \left(\frac{s}{d}\right)^2\right)}}{2} \qquad (45)$$

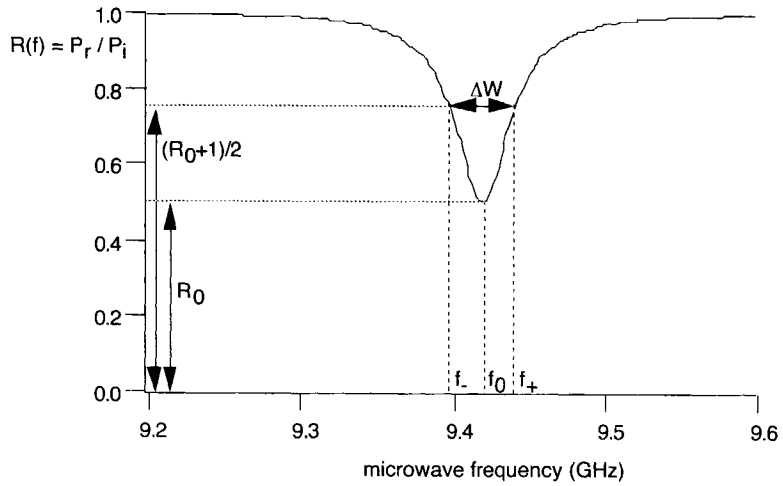

FIGURE 10: Resonance curve of the cavity displayed in figure 9 filled with a benzene solution (ε_r = 2.28). The resonance curve has the shape of a Lorentzian, whose width is determined by ΔW and depth by R_0. The minimum occurs at the resonance frequency, f_0, while f- and f+ are the half-power frequencies.

In equation (45) the first part ($c/\sqrt{\varepsilon_r \kappa_r}$) is the velocity of the microwave in the medium which is determined by the velocity of light in vacuum, c, and the relative dielectric constant, ε_r, and the relative magnetic permeability, κ_r, of the medium. Since the medium in the resonant cavity is a solution and thus non-ferromagnetic, κ_r is close to unity and can therefore be neglected.

The second part in equation (45) contains the three boundary conditions. Resonance occurs at any combination where q, r and s are integers and the corresponding resonance mode is denoted as TE_{qrs}. In a waveguide with the same a to b ratio as the resonant cavity the dominant TE_{qr} mode for microwave propagation is the TE_{10} mode. Therefore, from all cavity modes that fulfill equation (45), the TE_{10s} modes will be dominant and equation (45) can be reduced to:

$$f_0 = \frac{c}{\sqrt{\varepsilon_r}} \frac{\sqrt{\left(\left(\frac{s}{d}\right)^2 + \left(\frac{1}{a}\right)^2\right)}}{2} \qquad (46)$$

According to equation (46), the wavelength at which resonance occurs is related to the length of the cavity and width of of the broadwall. For an apolar solvent with an ε_r of *ca.* 2 and the cell dimensions d=47 mm and a=23 mm, we can calculate from equation (46) that the resonant frequency, f_0, is approximately 10 GHz for the TE_{104} mode (s=4).

Power is dissipated in the cavity as a result of the interaction of the electric field component with the medium and the cavity walls. At frequencies far from f_0 the reflected power, P_r, is equal to the incident power, P_i. Hence the ratio of the reflected to the incident power, $R(f) = P_r/P_i$, is close to unity. The cavity resonance curve at close to resonance frequencies can be described by a Lorentzian function, which can be written as:

$$R(f) = \frac{R_0 + \left(\frac{2(f - f_0)}{\Delta W}\right)^2}{1 + \left(\frac{2(f - f_0)}{\Delta W}\right)^2} \tag{47}$$

A plot of R(f) as a function of frequency, f, in the vicinity of f_0 is given in figure 10. According to equation (47), the cavity resonance curve can be fully characterised by three parameters: f_0, R_0 and ΔW. The first two parameters are related to the minimum in the resonance curve. The position of the minimum corresponds to f_0, the resonance frequency of the cavity, while R_0 is the magnitude of R(f) at resonance. The value of R_0 depends on the design of the cell and the solvent used and will be the subject of a later section. The third parameter, ΔW, is the full width of the resonance curve between the two half power frequencies, f_- and f_+ ($R(f) = (1+R_0) / 2$). Often it is more convenient to write equation (47) as:

$$R(f) = \frac{R_0 + \left(2Q_l(\frac{f}{f_0} - 1)\right)^2}{1 + \left(2Q_l(\frac{f}{f_0} - 1)\right)^2} = \frac{R_0 + \zeta^2}{1 + \zeta^2} \tag{48}$$

In equation (48) Q_l is the "loaded" quality factor of the cavity which is related to the width of the resonance curve *via*:

$$Q_l = \frac{f_0}{\Delta W} = \frac{f_0}{f_+ - f_-} \tag{49}$$

The "loaded" quality factor can be considered to express the sharpness of the resonance curve, *i.e.* the larger the Q the sharper the resonance. The origin and the actual meaning of Q_l will be the subject of a later section.

A resonant cavity has a characteristic response time, τ_{rc}, which corresponds to the mean time for the exponential decay of the electric field within the cavity after removal of the incident power. The response time of the resonant cavity at f_0 is directly proportional to Q_l

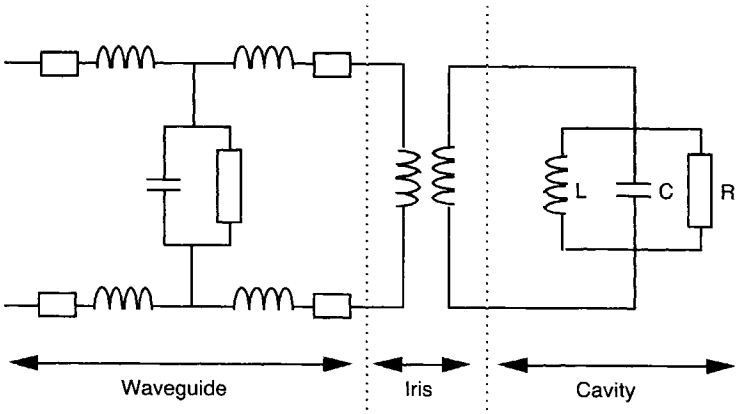

FIGURE 11: Lumped equivalent circuit, which from left to right corresponds to one length of waveguide, the iris coupling hole and the resonant cavity itself.

and is given by the following relation:

$$\tau_{rc} = n\frac{Q_l}{2\pi f_0} \approx \frac{Q_l}{\pi f_0} \tag{50}$$

This equation is only valid at f_0. In a later section, equation (50) is extended to yield an expression for τ_{rc} which is valid over the entire frequency range covered by the resonance curve.

2.5.1.1 The Q-factor.

Any type of resonant system can be characterised by a Q factor. The Q factor is proportional to the ratio of energy stored in the resonant system to the energy dissipated per cycle:

$$Q = 2\pi.\frac{U_{stored}}{U_{dissipated}} \tag{51}$$

This equation can be simplified by replacing the energy dissipated per cycle by the power dissipated divided by the resonance frequency:

$$Q = 2\pi f_0.\frac{U_{stored}}{P_{dissipated}} = \omega_0.\frac{U_{stored}}{P_{dissipated}} \tag{52}$$

The lumped equivalent circuit for a waveguide in figure 2 can be developed into a lumped equivalent circuit for an iris coupled resonant cavity[40], which is given in figure 11. The Q-factor of the entire iris coupled resonant cavity, Q_l, can be divided into a contribution from the cavity itself, Q_u, and a contribution from the coupling *via* the iris, Q_c:

$$\frac{1}{Q_l} = \frac{1}{Q_u} + \frac{1}{Q_c} \tag{53}$$

The contribution from the cavity can be derived from the equivalent circuit assuming that the iris functions as a source of electromotive force. In this simplified circuit the energy is stored in the inductor L and the capacitor C. When V reaches its maximum value all energy in the resonant circuit is stored in C, while all energy is stored in L when I reaches its maximum. This can be used to calculate the total amount of energy that can be stored. The maximum amount of energy that can be stored when $V = V_{max}$ is determined by the circuit's capacitance C and can be calculated from:

$$U_{stored} = \frac{1}{2} C V_{max}^2 \tag{54}$$

The power dissipated in the circuit of figure 11 is determined by the impedance Z of the system:

$$P_{dissipated} = \frac{V_{eff}^2}{Z} \tag{55}$$

For a parallel RLC circuit, which represents the cavity in figure 11 with the iris excluded, Z is given by:

$$\frac{1}{Z} = \sqrt{\frac{1}{R^2} + \left(\omega C - \frac{1}{\omega L}\right)^2} \tag{56}$$

At resonance ($\omega = \omega_0 = (\sqrt{LC})^{-1}$) the contributions from L and C cancel and Z is determined exclusively by the resistance R of the system, *i.e.* $Z = R$. For an alternating sinusoidal potential difference $V_{eff} = V_{max}/\sqrt{2}$, which allows $P_{u,dissipated}$ to be expressed in terms of V_{max}:

$$P_{u,dissipated} = \frac{V_{max}^2}{2R} \tag{57}$$

Combining (52), (54) and (57) yields for Q_u:

$$Q_u = 2\pi f_0 RC = \omega_0 RC \tag{58}$$

The "unloaded" Q, Q_u, contains the contribution of most interest for the FP-TRMC technique: that of the medium in the resonant cavity. Recalling the equivalent circuit for a piece of waveguide (figure 2), the capacitance C was determined entirely by the dielectric properties of the medium inside, while the resistance R depended on the resistivity of the walls, R_w, of the waveguide and on the conductivity of the medium ($G_m = 1/R_m$). Taking into account that the two contributions to R are parallel, equation (58) can be rewritten as:

$$\frac{1}{Q_u} = \frac{1}{\omega_0 C}\cdot\frac{1}{R} = \frac{1}{\omega_0 C_m}\cdot\left(\frac{1}{R_m}+\frac{1}{R_w}\right) = \frac{1}{\omega_0 C_m R_m}+\frac{1}{\omega_0 C_m R_w} \tag{59}$$

At resonance the amount of energy that can be stored in the capacitance of the medium should be identical to the amount of energy that can be stored in the inductance of the walls. Therefore when $\omega = \omega_0$, the following relation should hold:

$$C_m = \frac{1}{\omega_0^2 L_w} \tag{60}$$

Combining equation (59) and (60) then yields:

$$\frac{1}{Q_u} = \frac{1}{\omega_0 C_m R_m}+\frac{\omega_0 L_w}{R_w} = \frac{1}{Q_m}+\frac{1}{Q_w} \tag{61}$$

In this equation Q_w is a contribution which is determined by the cell walls only, while Q_m depends exclusively on the dielectric properties of the medium. In line with equation (1) and (2), for a medium with area A and depth d the capacitance of the medium, C_m, is given by:

$$C_m = \varepsilon_0 \varepsilon'(\omega)\frac{A}{d} \tag{62}$$

and its resistance, R_m, is given by:

$$R_m = \frac{1}{\sigma_{re}(\omega)}\cdot\frac{d}{A} = \frac{1}{\omega_0 \varepsilon_0 \varepsilon''(\omega)}\cdot\frac{d}{A} \tag{63}$$

According to equation (5) the latter step is only true for a purely dielectric medium, *i.e.*

$\sigma_{dc} \approx 0$. Using equation (62) and (63) yields for Q_m:

$$Q_m = \omega_0 R_m C_m = \omega_0 \frac{\varepsilon_0 \varepsilon'(\omega)}{\sigma_{re}(\omega)} = \frac{\varepsilon'(\omega)}{\varepsilon''(\omega)} \tag{64}$$

This outcome is not surprising when it is realised that $\varepsilon'(\omega)$ is proportional to the amount of energy stored in the medium and $\sigma_{re}(\omega)$ ($= \omega_0 \varepsilon_0 \varepsilon''(\omega)$ in the case of a non-conducting dielectric) is proportional to the amount of energy dissipated.

To expand Q_u into Q_l the iris has to be taken into account, which has an impedance Z_i. Therefore incorporation of the contribution of the iris will only affect the amount of power dissipated, which will increase by:

$$P_{c,dissipated} = \frac{V_{max}^2}{2Z_i} \tag{65}$$

Then, the total amount of power dissipated is the sum of equation (57) and (65):

$$P_{dissipated} = P_{u,dissipated} + P_{c,dissipated}$$

$$= \frac{V_{max}^2}{2R} + \frac{V_{max}^2}{2Z_i} = \frac{V_{max}^2}{2}\left(\frac{1}{R} + \frac{1}{Z_i}\right) = \frac{V_{max}^2}{2R}\left(1 + \frac{R}{Z_i}\right) \tag{66}$$

The ratio R/Z_i can be defined as the coupling parameter, β. Depending on the value of β a cavity is said to be undercoupled ($\beta<1$), critically coupled ($\beta=1$) or overcoupled ($\beta>1$). Combining equation (66), (54) and (52) yields for Q_l:

$$Q_l = \frac{2\pi f_0 RC}{(1+\beta)} = \frac{\omega_0 RC}{(1+\beta)} \tag{67}$$

The response time, τ_{rc}, is defined as the product of R and C, therefore the experimentally derived equation (50) and the theoretically derived equation (67) must be very similar. This is only the case when β does not deviate substantially from unity.

2.5.1.2 The relation between R_0 and Q_l and Q_u.

R_0 is defined as the ratio between the reflected power, P_r, and the incident power, P_i, at the resonance frequency. The amount of power reflected at the interface between the

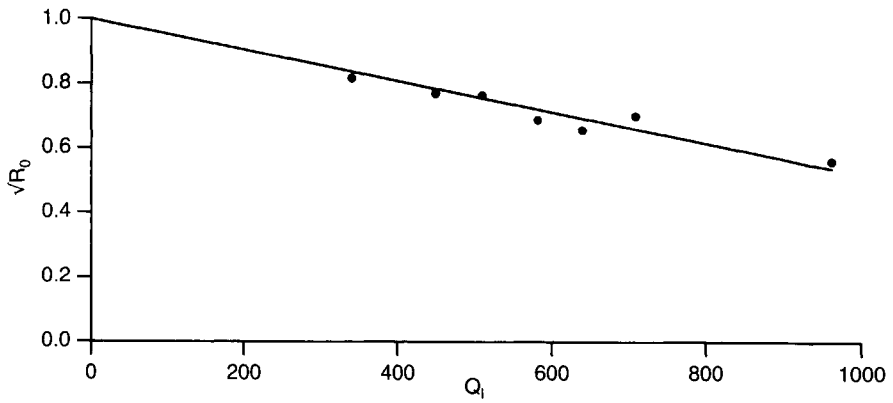

FIGURE 12: The relation between $\sqrt{R_0}$ and Q_l determined with a series of FP-TRMC resonant cavities which only differ in the diameter of the iris coupling hole. The straight line confirms the validity of equation (72). The medium inside the resonant cavity is air.

waveguide and the cavity is determined by the reflection coefficient, Γ, of this interface:

$$P_r = V_r.I_r = V_i\Gamma.I_i\Gamma = P_i\Gamma^2 \tag{68}$$

When Γ is complex, Γ^2 in equation (68) has to be replaced by the product of Γ and its complex conjugate. In its general form Γ is given by:

$$\Gamma = \frac{Z - Z_i}{Z + Z_i} \tag{69}$$

In equation (69) Z_i is the impedance of the microwave transmission line and Z is the impedance of the cavity. Recalling the equivalent circuit of the resonant cavity in figure 11, Z is given by equation (56). At resonance Z=R and equation (69) can be written as:

$$\Gamma = \frac{(R - Z_i)}{(R + Z_i)} = \frac{\left(1 - \frac{Z_i}{R}\right)}{\left(1 + \frac{Z_i}{R}\right)} = \frac{\left(1 - \frac{1}{\beta}\right)}{\left(1 + \frac{1}{\beta}\right)} = \frac{(\beta - 1)}{(\beta + 1)} \tag{70}$$

Using equation (58) and (67) β can be expressed in Q's:

$$\beta = \frac{Q_u}{Q_l} - 1 \tag{71}$$

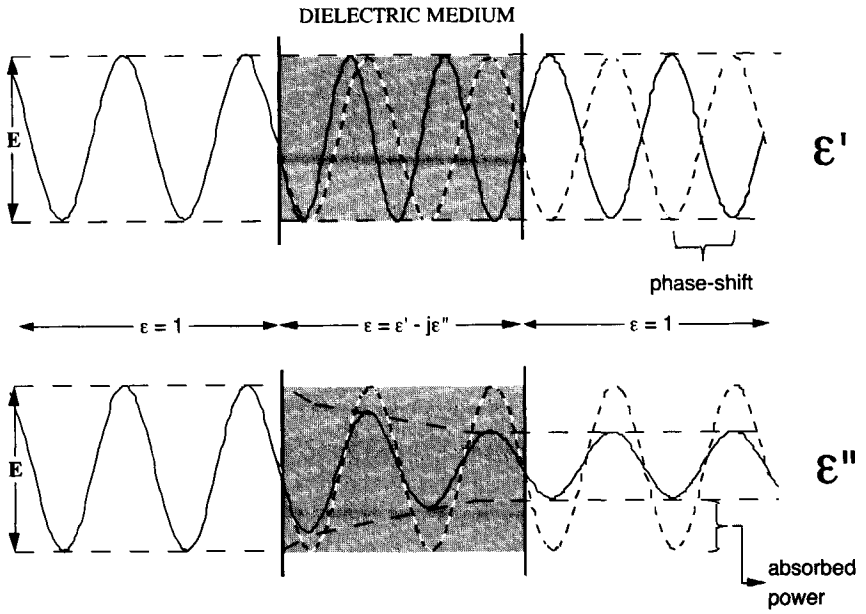

FIGURE 13: The interaction between an electromagnetic wave, such as a microwave, and a dielectric medium. (Top) a non-zero real part, ε', of the complex permittivity results in a phase-shift of the microwave. (Bottom) a non-zero imaginary part, ε", of the complex permittivity results in the decrease of the amplitude of the microwave.

Combining equations (68), (70) and (71) then yields:

$$R_0 = \frac{P_r}{P_i} = \Gamma^2 = \left(\frac{(\beta-1)}{(\beta+1)}\right)^2 = \left(1 - 2\frac{Q_l}{Q_u}\right)^2 \qquad (72)$$

The validity of equation (72) was confirmed by the observed linear dependence of $\sqrt{R_0}$ on Q_l, which is shown in figure 12. The data in figure 12 was obtained experimentally for a series of resonant cavities which are identical except for the diameter of the iris-hole, *i.e.* β is varied. The medium inside the resonant cavity is air. Using figure 12, a value of 4.2×10^3 is estimated for Q_u. This value is much larger than the value of Q_l, which ranges from 300-1000. Substituting these values of Q_u and Q_l in equation (71) shows that $\beta > 1$. Therefore, it can be concluded that in low-loss media the measuring cells used in the FP-TRMC experiments are overcoupled resonant cavities.

2.5.2 The TRMC sensitivity factors.

2.5.2.1 Photo-induced changes in the reflected power.

A change in the power reflected by a resonant cavity can result from a change in $\sigma(\omega)$ as well as $\varepsilon(\omega)$. In the case of the dilute solutions used in the FP-TRMC measurements both σ_{dc} and $\Delta\sigma_{dc}$ are expected to be negligibly small, in which case the photoinduced changes can be fully explained in terms of changes in $\varepsilon(\omega)$ ($= \varepsilon'(\omega) - j\varepsilon''(\omega)$). Figure 13 illustrates the different effects of a medium's $\varepsilon'(\omega)$ and $\varepsilon''(\omega)$ on microwaves propagating through that medium. In the case of $\varepsilon'(\omega)$ energy is absorbed from the electric field when the field increases and returned when the field decreases. However since this process is not instantaneous the energy exchange causes a retardation of the propagating electric field. This results in a decrease in the wavelength of the microwave inside the dielectric medium, which is observed as a phase-shift in the transmitted wave. In the case of $\varepsilon''(\omega)$ energy is absorbed from the microwaves and dissipated as heat in the medium. Therefore the amplitude of a microwave decreases on propagation through a medium with a non-zero $\varepsilon''(\omega)$, which is observed as a reduction of the power of the microwave.

On excitation of the solution contained in the resonant cavity, photons are absorbed by the solute molecules. The absorbed energy raises an electron to a higher energy molecular orbital. This can lead to a change in the molecular polarisability and/or dipole moment and a resulting change in the permittivity of the solution. When the permittivity is altered, the propagation conditions for the microwaves in the cavity are altered and the amount of power reflected by the cavity, P_r, is changed. Hence, the ratio between incident power and reflected power, R(f) is changed in proportion:

$$\left[\frac{\Delta P_r}{P_r}\right]_f = \frac{\Delta R(f)}{R(f)} \qquad (73)$$

Changes in either $\varepsilon'(\omega)$ or $\varepsilon''(\omega)$ have distinctly different effects on the resonance curve. An increase in $\varepsilon'(\omega)$ results in a decrease in the wavelength of the microwaves within the resonant cavity. Therefore, resonance will occur at a lower frequency and the entire resonance curve will shift to lower frequencies (figure 14A). Since the amount of power dissipated in the medium is proportional to $\varepsilon''(\omega)$, an increase in $\varepsilon''(\omega)$ results in a decrease in the value of R_0 and thus a deepening of the resonance curve (figure 14B) without changing f_0. Often both $\varepsilon'(\omega)$ and $\varepsilon''(\omega)$ are changed at the same time and both effects, a deepening and a shift, will occur simultaneously but to different extents (figure 14C)[41-44]. An important difference between the combined effects at the two half-power frequencies is that at f_- the contributions from changes in $\varepsilon'(\omega)$ and $\varepsilon''(\omega)$ are additive while at f_+ they partially cancel.

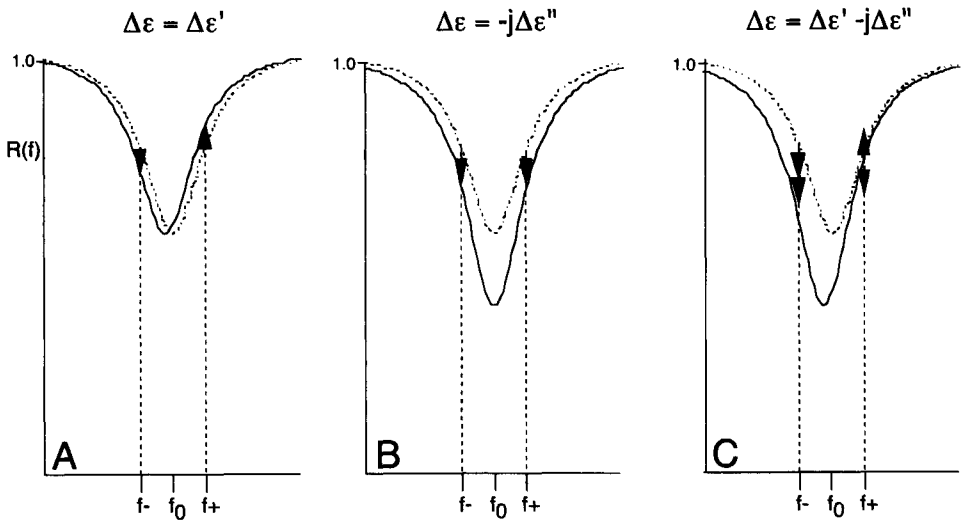

FIGURE 14: The effect on the position and depth of the resonance curve caused by an increase of the real part of the permittivity (A) or imaginary part of the permittivity (B) and the more general case (C) when both occur simultaneously. The dashed curves represent the situation prior to a change in ε.

The different effects can be clearly seen at the half-power frequencies of the resonance, f+ and f-, as shown in figure 14. Thus, an increase in $\varepsilon'(\omega)$ results in an increase in R(f) at f+ and a decrease at f-, *i.e.* the changes are of equal magnitude but of opposite sign. An increase in $\varepsilon''(\omega)$, on the other hand, results in a decrease in reflected power, R(f), at both f+ and f-, *i.e.* the changes at the two frequencies are of equal magnitude and of the same sign. In figure 15 are shown actual experimental results which illustrate this difference. In figure 15A the results are shown for a molecule which yields a highly delocalised (highly polarisable) excited state which results in a change mainly in $\varepsilon'(\omega)$. In this case the transients at f+ and f- are seen to be of similar magnitude but of different sign. In figure 15B the transient changes in R(f) at the half-power frequencies are for a molecule which on excitation gives a highly dipolar excited state and a resulting large change in $\varepsilon''(\omega)$. The transients are seen to be almost equal in magnitude and of the same sign. In figure 15C the results are shown for a molecule in which both $\varepsilon'(\omega)$ and $\varepsilon''(\omega)$ are changed on excitation. The lack of decay observed in this example indicates that besides the optically accessible singlet state, S_1, the lowest excited triplet state, T_1, becomes populated from the S_1 state by intersystem crossing.

These different effects are illustrated in more detail for the same three compounds by the contour plots shown in figures 16, 17 and 18 which are constructed from transients taken at many different frequencies over the entire width of the resonance curve. The change in R(f) shown in figure 16 is anti-symmetric around the steady-state resonance frequency, f_0: A negative going signal (from green *via* yellow to red) is observed at all $f < f_0$, while a positive going signal (from green to blue) is observed for all $f \geq f_0$. This can be attributed to a shift of

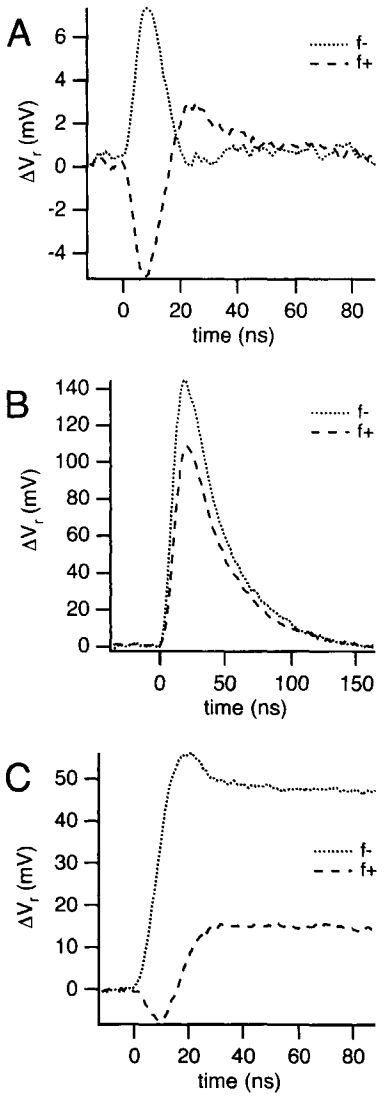

FIGURE 15: FP-TRMC transients measured at both half-power frequencies, f- and f+, for three different solutes in benzene. The three pairs of transients are, from top to bottom, examples of the three situations given in the figure 14A, 14B and 14C respectively. A positive signal corresponds to a decrease in R(f), *i.e.* a deepening of the resonance curve.

the resonance curve to lower frequencies. The excitation of the solute molecules in this case caused almost exclusively a change in $\varepsilon'(\omega)$ of the solution. In contrast, the change in R(f) in figure 17 is almost symmetrical around the steady-state resonance frequency: At all frequencies a negative going (green to red) signal is observed. This can be attributed to a deepening of the resonance curve on excitation. In this case excitation of the solute molecules caused exclusively a change in $\varepsilon''(\omega)$ of the solution. Figure 18 is an example which illustrates what happens when both $\varepsilon'(\omega)$ and $\varepsilon''(\omega)$ change on excitation.

The contour plots clearly illustrate that the FP-TRMC technique is most sensitive to changes in $\varepsilon''(\omega)$ at f_0, while changes in $\varepsilon'(\omega)$ hardly affect the microwave transmission at this frequency. In contrast the FP-TRMC technique is most sensitive to changes in $\varepsilon'(\omega)$ near f_- and f_+, where the resonance curve is very steep. Unfortunately, at these frequencies the system is also sensitive to changes to $\varepsilon''(\omega)$ albeit less than at f_0.

Legends for the FIGURES 16, 17 and 18 on the pages 61, 62 and 63.

FIGURE 16 (see page 61): Contour plot constructed from a series of FP-TRMC transients measured over the entire width of the resonance curve on the same dilute solution in benzene. The molecular structure of the solute molecule (referred to as OPV3) is shown in the upper right corner. The colours indicate a decrease (from green *via* yellow to red) or an increase (from green *via* blue to purple) of the reflected microwave power on excitation. The green contours at times before t = 0 are indicative of the magnitude of the background noise. The resonance frequency, f_0, (full black line) and both half-power frequencies, f- and f+ (dashed black lines), are also shown. The two transients shown in figure 15A correspond to the frequencies marked with the dashed black lines. The observed changes are anti-symmetric about f_0 which corresponds to the case shown in figure 14A: a change in the real part of the permittivity, $\varepsilon'(\omega)$.

FIGURE 17 (see page 62): Contour plot constructed from a series of FP-TRMC transients measured over the entire width of the resonance curve on the same dilute solution in benzene. The molecular structure of the solute molecule (referred to as PR-8b) is shown in the upper right corner. The colours indicate a decrease (from green *via* yellow to red) of the reflected microwave power on excitation. The green contours at times before t = 0 are indicative of the magnitude of the background noise. The resonance frequency, f_0, (full black line) and both half-power frequencies, f- and f+ (dashed black lines), are also shown. The two transients shown in figure 15B correspond to the frequencies marked with the dashed black lines. The observed changes are symmetric about f_0 which corresponds to the case shown in figure 14B: a change in the imaginary part of the permittivity, $\varepsilon''(\omega)$.

FIGURE 18 (see page 63): Contour plot constructed from a series of FP-TRMC transients measured over the entire width of the resonance curve on the same dilute solution in benzene. The molecular structure of the solute molecule (referred to as MiKe) is shown in the lower right corner. The colours indicate a decrease (from green *via* yellow to red) or an increase (from green *via* blue to purple) of the reflected microwave power on excitation. The green contours at times before t = 0 are indicative of the magnitude of the background noise. The resonance frequency, f_0, (full black line) and both half-power frequencies, f- and f+ (dashed black lines), are also shown. The two transients shown in figure 15C correspond to the frequencies marked with the dashed black lines. The observed changes are neither symmetric nor anti-symmetric about f_0 which corresponds to the case shown in figure 14C: a change in both the real, $\varepsilon'(\omega)$, and the imaginary, $\varepsilon''(\omega)$, parts of the permittivity.

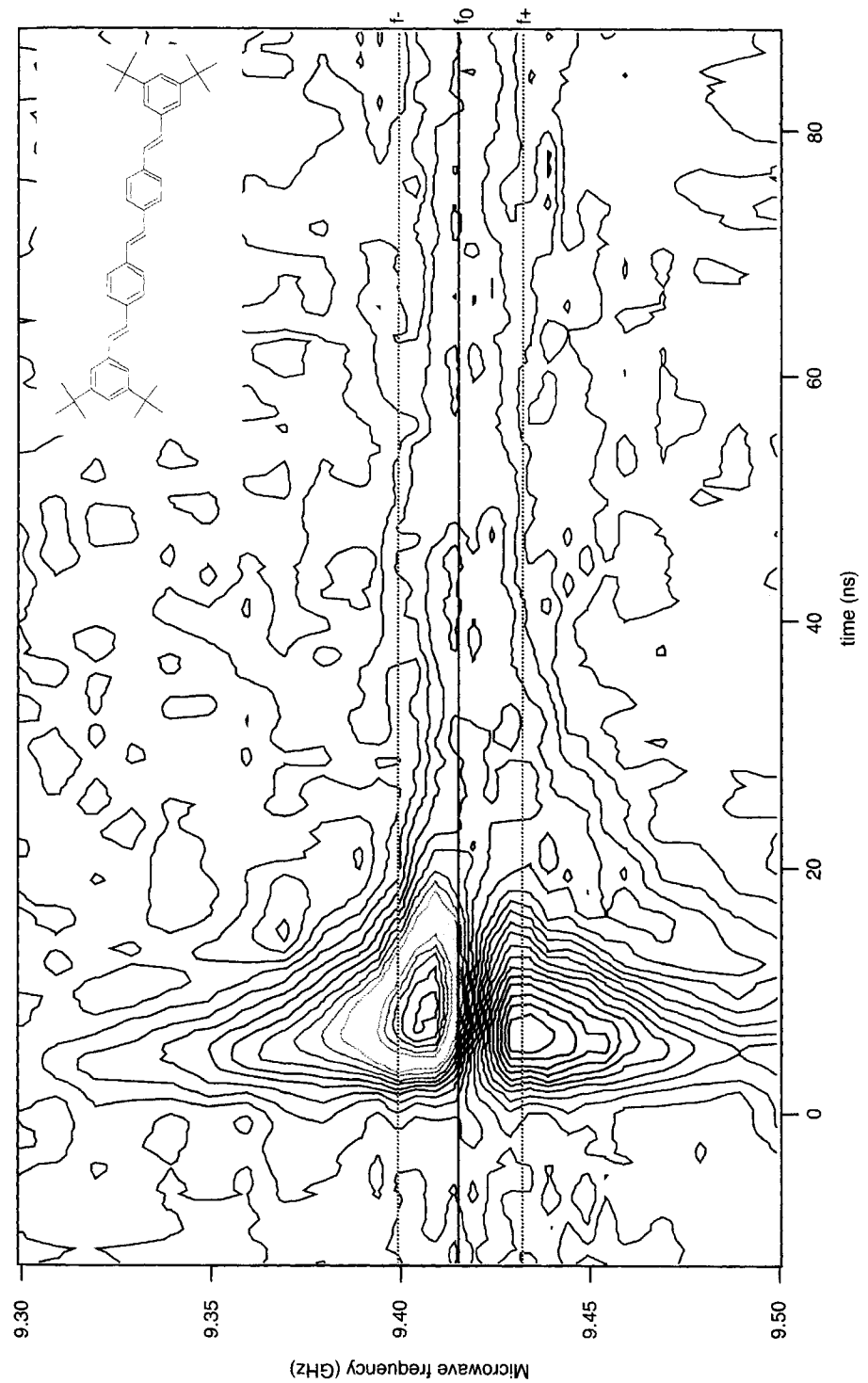
f-
f0
f+
9.30
9.35
9.40
9.45
9.50
Microwave frequency (GHz)
0
20
40
60
80
time (ns)

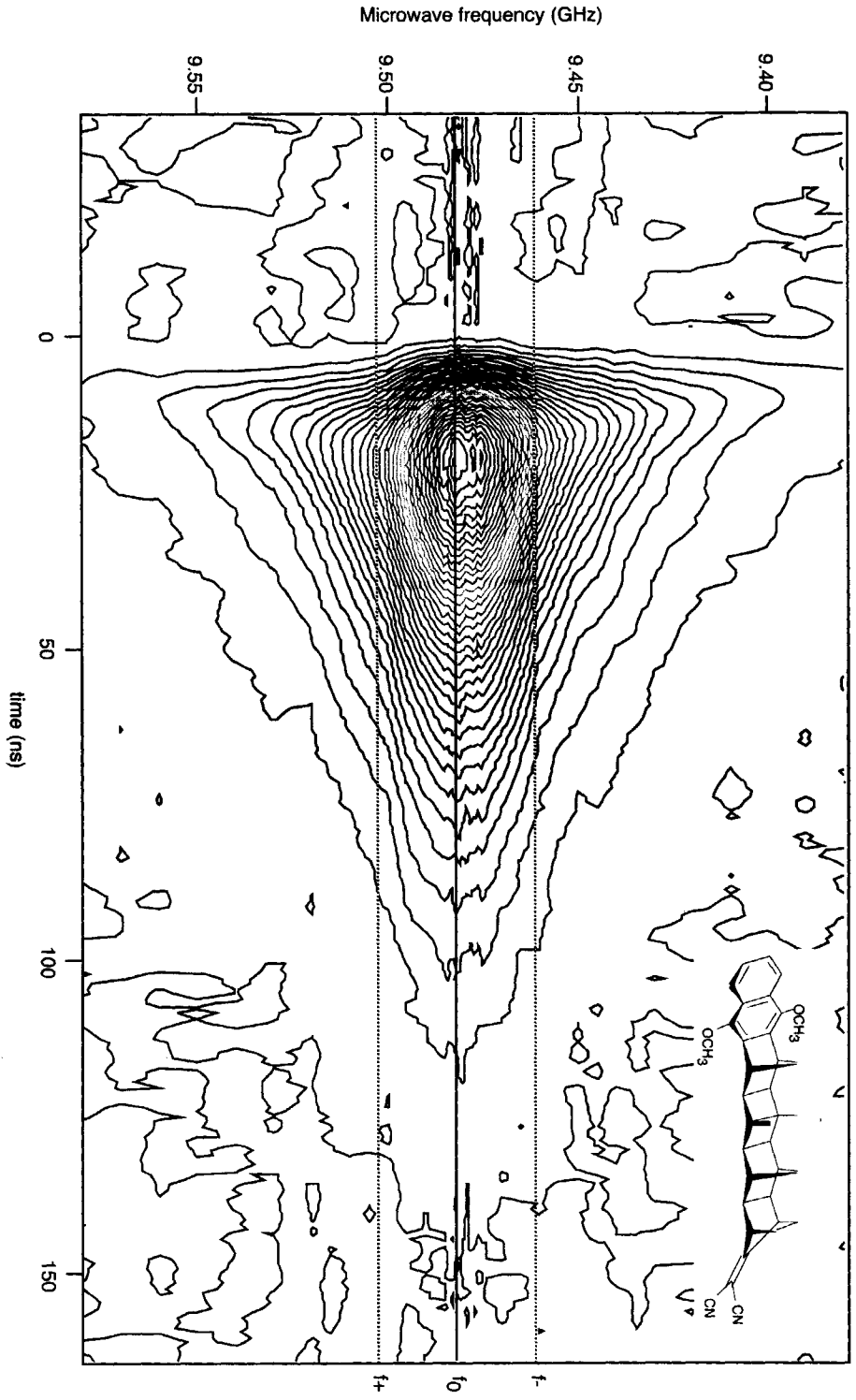
Microwave frequency (GHz)
9.55
9.50
9.45
9.40
0
50
100
150
time (ns)
f+
f0
f-
OCH3
OCH3
CN
CN

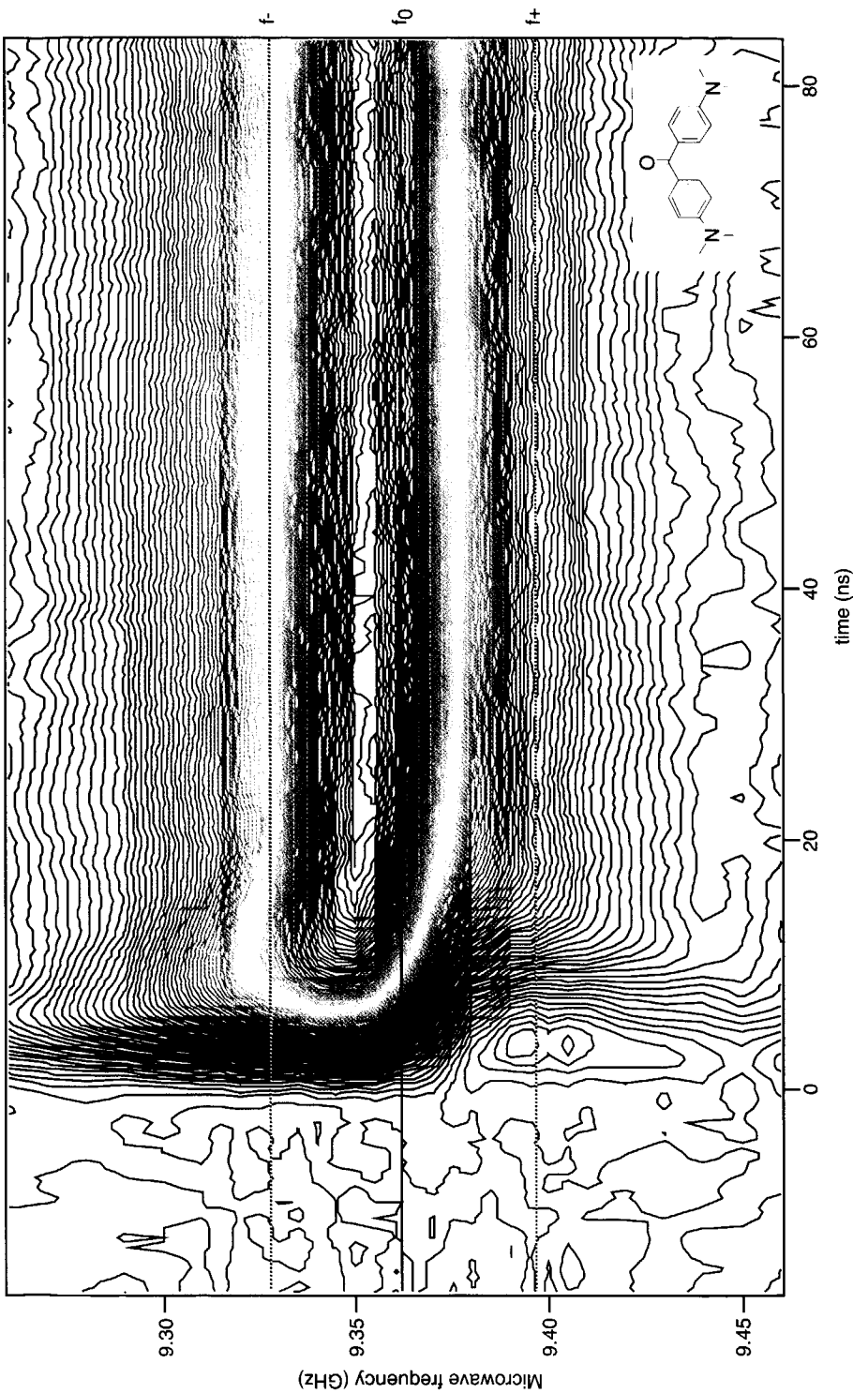
f-
f0
f+
9.30
9.35
9.40
9.45
Microwave frequency (GHz)
0
20
40
60
80
time (ns)

2.5.2.2 The sensitivity at the cavity resonance frequency: the A factors.

A photo-induced change in the permittivity of the medium contained within the resonant cavity can be observed at the resonance frequency as a change in R_0. For small changes in $\varepsilon(\omega)$, the magnitude of the resulting change in R_0 is determined by the sensitivity factor A, which is defined by

$$\frac{\Delta R_0}{R_0} = -A\Delta\varepsilon(\omega) \tag{74}$$

The derivation of the A parameter in terms of the cavity characteristics is presented below.

As shown previously, R_0 is related to the loaded and unloaded quality factors, Q_l and Q_u, by equation (72):

$$\sqrt{R_0} = \left(1 - 2\frac{Q_l}{Q_u}\right) \tag{75}$$

According to equation (53) Q_u can be written in terms of Q_l and the quality factor associated with the coupling *via* the iris, Q_c,

$$\frac{1}{Q_u} = \frac{1}{Q_l} - \frac{1}{Q_c} = \frac{Q_c - Q_l}{Q_l Q_c} \tag{76}$$

Substitution for Q_u from (76) in (75) results in:

$$\sqrt{R_0} = 1 - 2\frac{Q_c - Q_l}{Q_c} = 2\frac{Q_l}{Q_c} - 1 \tag{77}$$

Differentiating equation (77) with respect to $\varepsilon(\omega)$ will give the relation between a change in R_0 and a small change in ε.

Since Q_c depends only on the properties of the iris, it is insensitive to changes in the dielectric properties of the medium, *i.e.*

$$\frac{\partial Q_c}{\partial\varepsilon(\omega)} = 0 \tag{78}$$

Therefore differentiating equation (77) with respect to ε(ω), yields the following relation:

$$\frac{\partial\sqrt{R_0}}{\partial\varepsilon(\omega)} = \frac{1}{2\sqrt{R_0}}\frac{\partial R_0}{\partial\varepsilon(\omega)} = \frac{2}{Q_c}\frac{\partial Q_l}{\partial\varepsilon(\omega)} \tag{79}$$

This can be expressed as:

$$\frac{\partial R_0}{\partial\varepsilon(\omega)} = \frac{4\sqrt{R_0}}{Q_c}\frac{\partial Q_l}{\partial\varepsilon(\omega)} \tag{80}$$

According to equation (77) Q_c is given by:

$$Q_c = \frac{2Q_l}{(1+\sqrt{R_0})} \tag{81}$$

Combining this with equation (80) yields:

$$\frac{\partial R_0}{\partial\varepsilon(\omega)} = \frac{2\left(1+\sqrt{R_0}\right)\sqrt{R_0}}{Q_l}\frac{\partial Q_l}{\partial\varepsilon(\omega)} = \frac{2R_0\left(1+\frac{1}{\sqrt{R_0}}\right)}{Q_l}\frac{\partial Q_l}{\partial\varepsilon(\omega)} \tag{82}$$

From equations (53), (61) and (64) it follows that Q_l is given by:

$$\frac{1}{Q_l} = \frac{1}{Q_m} + \frac{1}{Q_w} + \frac{1}{Q_c} = \frac{\varepsilon''(\omega)}{\varepsilon'(\omega)} + \frac{1}{Q_w} + \frac{1}{Q_c} \tag{83}$$

Since Q_w depends only on the properties of the walls of the resonant cavity it is insensitive to changes in the dielectric properties of the medium as was also the case for Q_c:

$$\frac{\partial Q_w}{\partial\varepsilon(\omega)} = 0 \tag{84}$$

Differentiation of equation (83) with respect to ε(ω) yields therefore:

$$\frac{\partial\left(\frac{1}{Q_l}\right)}{\partial\varepsilon(\omega)} = -\frac{1}{Q_l^2}\frac{\partial Q_l}{\partial\varepsilon(\omega)} = \frac{\partial\left(\frac{\varepsilon''(\omega)}{\varepsilon'(\omega)}\right)}{\partial\varepsilon(\omega)} \tag{85}$$

From this equation the following relationships can be derived for the dependence of Q_l on changes in the real and imaginary part of the permittivity:

$$\frac{\partial Q_l}{\partial \varepsilon'(\omega)} = Q_l^2 \frac{\varepsilon''(\omega)}{\varepsilon'(\omega)^2} \tag{86}$$

$$\frac{\partial Q_l}{\partial \varepsilon''(\omega)} = -Q_l^2 \frac{1}{\varepsilon'(\omega)} \tag{87}$$

Substitution in (82) yields the expressions relating the change in R_0 to a change in $\varepsilon'(\omega)$ or $\varepsilon''(\omega)$:

$$\frac{\partial R_0}{\partial \varepsilon'(\omega)} = 2Q_l R_0 \left(1 + \frac{1}{\sqrt{R_0}}\right) \frac{\varepsilon''(\omega)}{\varepsilon'(\omega)^2} \tag{88}$$

$$\frac{\partial R_0}{\partial \varepsilon''(\omega)} = -2Q_l R_0 \left(1 + \frac{1}{\sqrt{R_0}}\right) \frac{1}{\varepsilon'(\omega)} \tag{89}$$

These relationships can be rearranged to give the relative change in the reflected power, $\partial R_0/R_0$, in terms of $\partial\varepsilon'$ and $\partial\varepsilon''$:

$$\frac{\partial R_0}{R_0} = 2Q_l \left(1 + \frac{1}{\sqrt{R_0}}\right) \frac{\varepsilon''(\omega)}{\varepsilon'(\omega)^2} \partial\varepsilon'(\omega) = A_{\varepsilon'} . \partial\varepsilon'(\omega) \tag{90}$$

$$\frac{\partial R_0}{R_0} = -2Q_l \left(1 + \frac{1}{\sqrt{R_0}}\right) \frac{1}{\varepsilon'(\omega)} \partial\varepsilon''(\omega) = -A_{\varepsilon''} . \partial\varepsilon''(\omega) \tag{91}$$

The ratio between the sensitivity factors for changes in the real and imaginary components of the permittivity is seen to be given by,

$$\frac{A_{\varepsilon'}}{A_{\varepsilon''}} = \frac{\varepsilon''(\omega)}{\varepsilon'(\omega)} = \frac{1}{Q_m} \tag{92}$$

For the low dielectric loss, non-polar solvents used in the present studies, the value of Q_m is very large and always larger than the value of Q_l (see equation (83)), which is usually between 100 and 300. The sensitivity of detection of changes in $\varepsilon'(\omega)$ will therefore be orders of magnitude less than for changes in $\varepsilon''(\omega)$ for measurements carried out at the resonance frequency of the cavity.

2.5.2.3 The sensitivity off resonance.

The general expression for the frequency dependence of the fractional power reflected by a cavity at close to a resonance, R(f), is

$$R(f) = \frac{R_0 + \zeta^2}{1 + \zeta^2} \tag{93}$$

with:

$$\zeta = 2Q_l\left(\frac{f}{f_0} - 1\right) \tag{94}$$

Differentiation of (93) with respect to $\varepsilon(\omega)$ results in the following expression:

$$\frac{\partial R(f)}{\partial \varepsilon(\omega)} = \frac{\left(1+\zeta^2\right)\left(\frac{\partial R_0}{\partial \varepsilon(\omega)} + 2\zeta\frac{\partial \zeta}{\partial \varepsilon(\omega)}\right) - \left(R_0 + \zeta^2\right)2\zeta\frac{\partial \zeta}{\partial \varepsilon(\omega)}}{\left(1+\zeta^2\right)^2} \tag{95}$$

which yields after rearrangement:

$$\frac{\partial R(f)}{\partial \varepsilon(\omega)} = \frac{1}{\left(1+\zeta^2\right)}\frac{\partial R_0}{\partial \varepsilon(\omega)} + \frac{\left(1-R_0\right)}{\left(1+\zeta^2\right)^2}2\zeta\frac{\partial \zeta}{\partial \varepsilon(\omega)} \tag{96}$$

The expression for $\partial R_0/\partial\varepsilon(\omega)$ is given by equation (89) or (88) in the case of changes in $\varepsilon''(\omega)$ or $\varepsilon'(\omega)$ respectively. The expression for $\partial\zeta/\partial\varepsilon(\omega)$ in case of changes in $\varepsilon''(\omega)$ or $\varepsilon'(\omega)$ can be derived by differentiating equation (94) and are given below.

The general dependence of R(f) on changes in $\varepsilon''(\omega)$: derivation of the B factor.

Since the resonance frequency should be independent of changes in the dielectric loss, $\varepsilon''(\omega)$, differentiation of (94) with respect to $\varepsilon''(\omega)$ yields:

$$\frac{\partial \zeta}{\partial \varepsilon''(\omega)} = \frac{\partial\left[2Q_l\left(\frac{f}{f_0} - 1\right)\right]}{\partial \varepsilon''(\omega)} = 2\left(\frac{f}{f_0} - 1\right)\frac{\partial Q_l}{\partial \varepsilon''(\omega)} = \frac{\zeta}{Q_l}\frac{\partial Q_l}{\partial \varepsilon''(\omega)} \tag{97}$$

and substitution of $\partial Q_l/\partial\varepsilon''(\omega)$ from equation (87) leads to:

$$\frac{\partial\zeta}{\partial\varepsilon''(\omega)} = -Q_l\frac{\zeta}{\varepsilon'(\omega)} \tag{98}$$

Substitution of $\partial R_0/\partial\varepsilon''(\omega)$ from equation (89) and $\partial\zeta/\partial\varepsilon''(\omega)$ from (98) in (96) gives:

$$\frac{\partial R(f)}{\partial\varepsilon''(\omega)} = -\frac{1}{\left(1+\zeta^2\right)}2Q_lR_0\left(1+\frac{1}{\sqrt{R_0}}\right)\frac{1}{\varepsilon'(\omega)} - \frac{\left(1-R_0\right)}{\left(1+\zeta^2\right)^2}2\zeta^2Q_l\frac{1}{\varepsilon'(\omega)} \tag{99}$$

which can be rearranged *via*:

$$\frac{\partial R(f)}{\partial\varepsilon''(\omega)} = -2Q_l\frac{\left(\zeta^2\sqrt{R_0}+R_0+\zeta^2+\sqrt{R_0}\right)}{\left(1+\zeta^2\right)^2}\frac{1}{\varepsilon'(\omega)} \tag{100}$$

to give:

$$\frac{\partial R(f)}{\partial\varepsilon''(\omega)} = -2Q_l\frac{\left(1+\sqrt{R_0}\right)\left(\zeta^2+\sqrt{R_0}\right)}{\left(1+\zeta^2\right)^2}\frac{1}{\varepsilon'(\omega)} \tag{101}$$

Dividing equation (101) by equation (93) gives the relation between the relative change in the reflected power, $\partial R(f)/R(f)$, and $\partial\varepsilon''(\omega)$:

$$\frac{\partial R(f)}{R(f)} = -2Q_l\frac{\left(1+\sqrt{R_0}\right)\left(\zeta^2+\sqrt{R_0}\right)}{\left(1+\zeta^2\right)\left(R_0+\zeta^2\right)}\frac{1}{\varepsilon'(\omega)}\partial\varepsilon''(\omega) \tag{102}$$

At the half-power frequencies, f- (= f_0 - f_0 / $2Q_l$) and f+ (= f_0 + f_0 / $2Q_l$), $\zeta^2 = 1$ and (102) reduces to:

$$\left[\frac{\partial R}{R}\right]_{\pm} = -Q_l\frac{\left(1+\sqrt{R_0}\right)^2}{\left(1+R_0\right)}\frac{1}{\varepsilon'(\omega)}\partial\varepsilon''(\omega)$$

$$= -B\partial\varepsilon''(\omega) \tag{103}$$

The B factor is therefore given by:

$$B = Q_l \frac{\left(1+\sqrt{R_0}\right)^2}{\left(1+R_0\right)} \frac{1}{\varepsilon'(\omega)} \tag{104}$$

2.5.2.3.2 The general dependence of R(f) on changes in ε'(ω): derivation of the C factor.

On differentiation of (94) with respect to ε'(ω) account must be taken of the fact that both Q_l and f_0 depend on ε'(ω). This results in

$$\frac{\partial \zeta}{\partial \varepsilon'(\omega)} = \frac{\partial\left[2Q_l\left(\frac{f}{f_0}-1\right)\right]}{\partial \varepsilon'(\omega)} = \frac{2ff_0 \frac{\partial Q_l}{\partial \varepsilon'(\omega)} - 2Q_l f \frac{\partial f_0}{\partial \varepsilon'(\omega)}}{f_0^2} - 2\frac{\partial Q_l}{\partial \varepsilon'(\omega)}$$

$$= 2\left(\frac{f}{f_0}-1\right)\frac{\partial Q_l}{\partial \varepsilon'(\omega)} - 2Q_l \frac{f}{f_0^2}\frac{\partial f_0}{\partial \varepsilon'(\omega)} \tag{105}$$

The expression for $\partial Q_l/\partial \varepsilon'(\omega)$ is given by equation (86). The expression for $\partial f_0/\partial \varepsilon'(\omega)$ can be derived by differentiating equation (46):

$$\frac{\partial f_0}{\partial \varepsilon'(\omega)} = -\frac{1}{2\varepsilon'(\omega)} \cdot \frac{c}{\sqrt{\varepsilon'(\omega)}} \frac{\sqrt{\left(\left(\frac{s}{d}\right)^2 + \left(\frac{1}{a}\right)^2\right)}}{2} = -\frac{1}{2\varepsilon'(\omega)} \cdot f_0 \tag{106}$$

Substitution of equations (86) and (106) in (105) results in:

$$\frac{\partial \zeta}{\partial \varepsilon'(\omega)} = 2\left(\frac{f}{f_0}-1\right)Q_l^2 \frac{\varepsilon''(\omega)}{\varepsilon'(\omega)^2} + Q_l \frac{f}{f_0}\frac{1}{\varepsilon'(\omega)}$$

$$= \zeta Q_l \frac{\varepsilon''(\omega)}{\varepsilon'(\omega)^2} + Q_l \frac{f}{f_0}\frac{1}{\varepsilon'(\omega)} = \left[\zeta \frac{\varepsilon''(\omega)}{\varepsilon'(\omega)} + \frac{f}{f_0}\right]\frac{Q_l}{\varepsilon'(\omega)} \tag{107}$$

According to equation (94), f/f_0 can be given in terms of ζ and Q_l. This yields for equation (107):

$$\frac{\partial \zeta}{\partial \varepsilon'(\omega)} = \left[\zeta \frac{\varepsilon''(\omega)}{\varepsilon'(\omega)} + \left(\frac{\zeta}{2Q_l}+1\right)\right]\frac{Q_l}{\varepsilon'(\omega)} \tag{108}$$

The full expression for the effect on R(f) of a change in $\varepsilon'(\omega)$ can now be obtained by substituting for $\partial R_0/\partial\varepsilon'(\omega)$ from equation (88) and $\partial\zeta/\partial\varepsilon'(\omega)$ from equation (108) in equation (96):

$$\frac{\partial R(f)}{\partial\varepsilon'(\omega)} = \frac{1}{\left(1+\zeta^2\right)} 2Q_l R_0 \left(1+\frac{1}{\sqrt{R_0}}\right)\frac{\varepsilon''(\omega)}{\varepsilon'(\omega)^2} +$$

$$+\frac{\left(1-R_0\right)}{\left(1+\zeta^2\right)^2} 2\zeta\left[\zeta\frac{\varepsilon''(\omega)}{\varepsilon'(\omega)}+\left(\frac{\zeta}{2Q_l}+1\right)\right]\frac{Q_l}{\varepsilon'(\omega)} \qquad (109)$$

This can be rearranged to give:

$$\frac{\partial R(f)}{\partial\varepsilon'(\omega)} = \frac{2Q_l}{\left(1+\zeta^2\right)^2}\frac{1}{\varepsilon'(\omega)}\left[\left(1+\zeta^2\right)\left(R_0+\sqrt{R_0}\right)\frac{\varepsilon''(\omega)}{\varepsilon'(\omega)}+\left(1-R_0\right)\zeta^2\frac{\varepsilon''(\omega)}{\varepsilon'(\omega)}+\right.$$

$$\left.+\left(1-R_0\right)\frac{\zeta^2}{2Q_l}+\left(1-R_0\right)\zeta\right] \qquad (110)$$

This rather complex expression can be considerably simplified by taking into account that all terms within the square brackets which are divided by $\varepsilon'(\omega)/\varepsilon''(\omega)$ (= Q_m) or Q_l will not contribute significantly because of the large Q values operative. Equation (110) can therefore be replaced to a good approximation by:

$$\frac{\partial R(f)}{\partial\varepsilon'(\omega)} = 2\zeta Q_l\frac{\left(1-R_0\right)}{\left(1+\zeta^2\right)^2}\frac{1}{\varepsilon'(\omega)} \qquad (111)$$

The general expression for the relative change in reflected power, $\partial R(f)/R(f)$, resulting from a small change in $\varepsilon'(\omega)$ is obtained by dividing equation (111) by equation (93):

$$\frac{\partial R(f)}{R(f)} = 2\zeta Q_l\frac{\left(1-R_0\right)}{\left(1+\zeta^2\right)\left(R_0+\zeta^2\right)}\frac{1}{\varepsilon'(\omega)}\partial\varepsilon'(\omega) \qquad (112)$$

As can be seen from (94), the expression on the right-hand sides of (111) and (112) will be positive for frequencies higher than f_0 and negative for frequencies lower than f_0. At the half-power frequencies, f- (= f_0 - f_0 / $2Q_l$) and f+ (= f_0 + f_0 / $2Q_l$), ζ will be -1 and 1

respectively. Hence, the sensitivity at f- will be given by:

$$\left[\frac{\partial R}{R}\right]_{-} = -Q_l \frac{(1-R_0)}{(1+R_0)} \frac{1}{\varepsilon'(\omega)} \partial\varepsilon'(\omega)$$

$$= -C\partial\varepsilon'(\omega) \qquad (113)$$

and at f+ by:

$$\left[\frac{\partial R}{R}\right]_{+} = Q_l \frac{(1-R_0)}{(1+R_0)} \frac{1}{\varepsilon'(\omega)} \partial\varepsilon'(\omega)$$

$$= +C\partial\varepsilon'(\omega) \qquad (114)$$

Hence, the C parameter is given by the following expression:

$$C = Q_l \frac{(1-R_0)}{(1+R_0)} \frac{1}{\varepsilon'(\omega)} \qquad (115)$$

2.5.3 Obtaining separate $\Delta\varepsilon'(\omega)$ and $\Delta\varepsilon''(\omega)$ TRMC transients.

The frequency dependences of the sensitivity to $\Delta\varepsilon''(\omega)$ and to $\Delta\varepsilon'(\omega)$ are plotted in figure 19 using equations (102) and (112) respectively for the same cavity parameters and medium. This shows that the sensitivity towards changes in $\Delta\varepsilon''(\omega)$ reaches a maximum at f_0 and decreases as Δf (= $|f-f_0|$) increases. In contrast, the sensitivity for $\Delta\varepsilon'(\omega)$ is highest at frequencies close to f_- and f_+. Since the sensitivity for $\Delta\varepsilon'(\omega)$ can be considered to be negligible at f_0, measurements at f_0 will provide almost exclusively information on $\Delta\varepsilon''(\omega)$. The sensitivity for $\Delta\varepsilon''(\omega)$ however never becomes negligible at a frequency where the sensitivity for $\Delta\varepsilon'(\omega)$ still has a significant value.

As a result of the symmetry around f_0 of the sensitivity to $\Delta\varepsilon''(\omega)$ the contribution of $\Delta\varepsilon''(\omega)$ to a transient measured at f_- and f_+ will be equal in sign and magnitude. Because of the anti-symmetry around f_0 of the sensitivity to $\Delta\varepsilon'(\omega)$ the contribution of $\Delta\varepsilon'(\omega)$ will be equal in magnitude at f_- and f_+ but opposite in sign (see figure 19). The overall result of changes in both $\varepsilon'(\omega)$ and $\varepsilon''(\omega)$ on the fractional change in reflected power at the upper and lower half-power frequencies is the following:

$$\left[\frac{\Delta R}{R}\right]_{+} = -B\Delta\varepsilon''(\omega) + C\Delta\varepsilon'(\omega) \qquad (116)$$

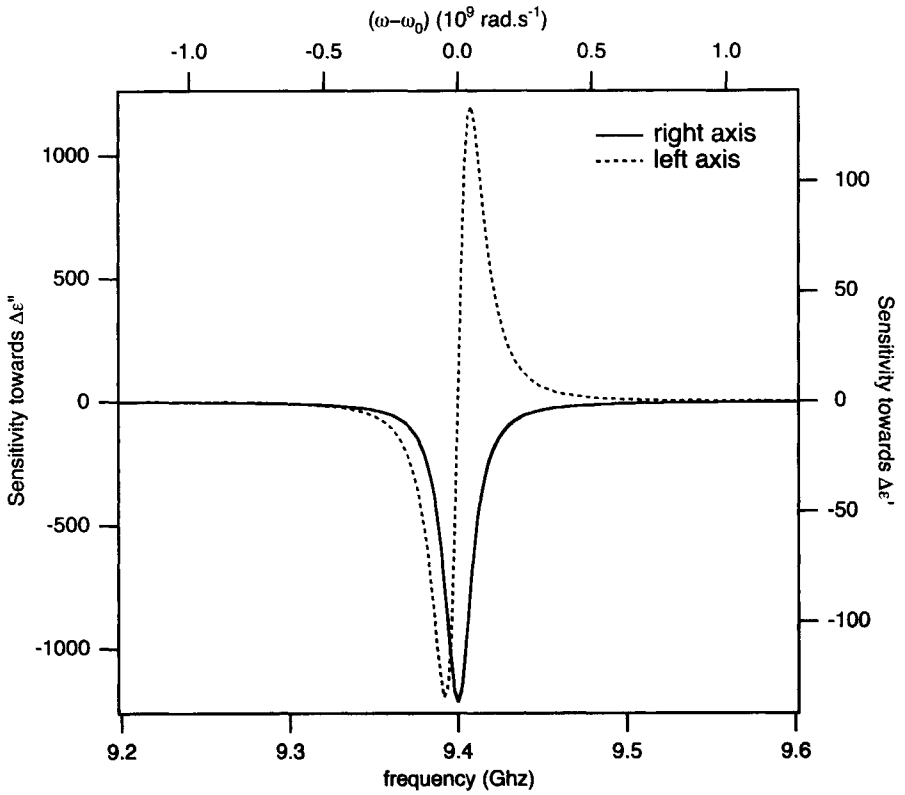

FIGURE 19: The sensitivity of the FP-TRMC technique to changes in the imaginary part (full line, left axis) and the real part (dashed line, right axis) of the complex permittivty as determined using the equations (102) and (112) respectively with $R_0 = 0.5$, $Q_l = 300$ and $f_0 = 9.400$ GHz.

$$\left[\frac{\Delta R}{R}\right]_- = -B\Delta\varepsilon''(\omega) - C\Delta\varepsilon'(\omega) \tag{117}$$

Therefore, on addition of a transient measured at f_- to a transient measured at f_+ the $\Delta\varepsilon'(\omega)$ contributions cancel and a transient related exclusively to $\Delta\varepsilon''(\omega)$ will be obtained:

$$\Sigma_\pm = \left[\frac{\Delta R}{R}\right]_- + \left[\frac{\Delta R}{R}\right]_+ = -2B\Delta\varepsilon''(\omega) \tag{118}$$

On the other hand, subtraction of a transient measured at f_+ from a transient measured at f_- will yield a transient exclusively related to $\Delta\varepsilon'(\omega)$:

$$\Delta_\pm = \left[\frac{\Delta R}{R}\right]_- - \left[\frac{\Delta R}{R}\right]_+ = -2C\Delta\varepsilon'(\omega) \tag{119}$$

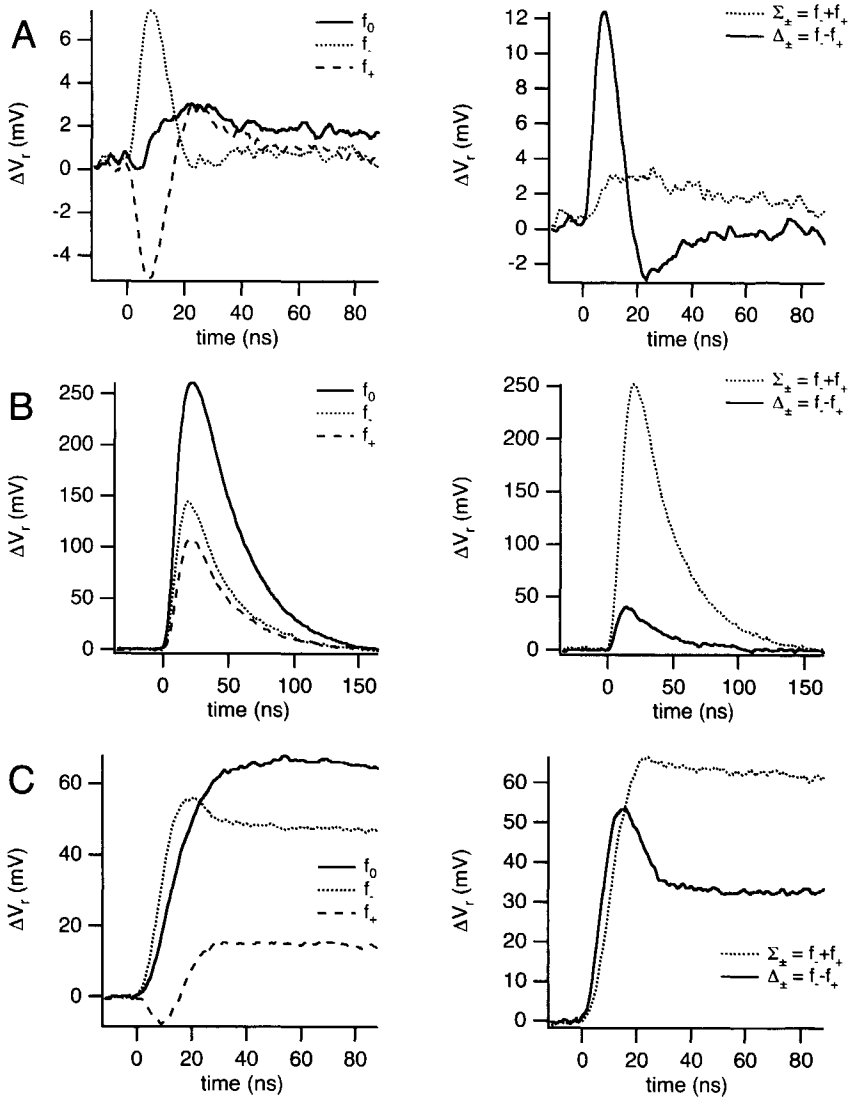

FIGURE 20: Left column: The FP-TRMC transients measured at the resonance frequency, f_0 (full line), and both half-power frequencies, f- (dotted line) and f+ (dashed line). Right column: the sum (dotted line) and difference (full line) transients determined from the f- and f+ transient. The transients were obtained from the contour plots shown in figure 16 (top, A), 17 (middle, B) and 18 (bottom, C) respectively.

The application of this approach is illustrated in figure 20 for the same three examples shown in figure 15. Figure 20A shows a readily observable $\Delta\varepsilon'(\omega)$-related transient and a weak $\Delta\varepsilon''(\omega)$-related transient. Figure 20B shows exactly the opposite: a large $\Delta\varepsilon''(\omega)$-related and a weak $\Delta\varepsilon'(\omega)$-related transient. Figure 20C shows an example of a case for which both contributions are significant.

2.6 QUANTIFICATION OF THE TRMC RESULTS.

2.6.1 Short overview of the fitting procedure.

To obtain quantitative data on the absolute magnitude of the change in polarisability, dipole moment or charge carrier mobility, which are the molecular origins of the observed photoinduced changes in $\sigma_{im}(\omega)$ (= $\omega\varepsilon_0\varepsilon'(\omega)$) and $\sigma_{re}(\omega)$ (= $\omega\varepsilon_0\varepsilon''(\omega)$ when $\sigma_{dc} = 0$), the measured FP-TRMC transients have to be fitted. The currently used fitting procedure is an extension of the fitting procedure used to fit the f_0 transients, which already has been described in considerable detail[18,45]. Therefore, only the main features of the fitting procedure will be outlined in this section. In general, the FP-TRMC transients are fitted using a Runge-Kutta convolution method and three major steps can be distinguished in the fitting procedure.

In the first step the time dependence is calculated of the concentration of the ground-state, S_0, and all of the excited states formed. Relaxation from higher excited singlet states, S_n ($n > 1$), to the lowest excited singlet state, S_1, is expected to occur on a (sub)picosecond time-scale. Since the time-resolution of the FP-TRMC technique is nanoseconds, the excited states that can be observed are therefore limited to the lowest singlet, S_1, and triplet, T_1, states. The relevant processes occurring during an FP-TRMC experiments can be represented by:

$$S_0 \xrightarrow{h\nu} S_1 \qquad \text{(A)}$$

$$S_1 \xrightarrow{k_{S_1 \to S_0}} S_0 \qquad \text{(B)}$$

$$S_1 \xrightarrow{k_{S_1 \to T_1}} T_1 \qquad \text{(C)}$$

$$T_1 \xrightarrow{k_{T_1 \to S_0}} S_0 \qquad \text{(D)}$$

If necessary, additional states, *e.g.* charge transfer states, can be taken into account as well in the reaction mechanism by including additional steps.

The concentrations of the states involved at time t, $[X_i]_t$, can be calculated by solving the following set of differential equations derived from the processes shown in schemes (A) to (D):

$$\frac{\partial[S_0]_t}{\partial t} = -\Xi_{S_0,\lambda}.\Phi_\lambda(t)[S_0]_t + k_{T_1 \to S_0}[T_1]_t + k_{S_1 \to S_0}[S_1]_t \qquad (120)$$

$$\frac{\partial[S_1]_t}{\partial t} = \Xi_{S_0,\lambda}.\Phi_\lambda(t)[S_0]_t - \left(k_{S_1\rightarrow S_0} + k_{S_1\rightarrow T_1}\right)[S_1]_t \quad (121)$$

$$\frac{\partial[T_1]_t}{\partial t} = k_{S_1\rightarrow T_1}[S_1]_t - k_{T_1\rightarrow S_0}[T_1]_t \quad (122)$$

In these equations $\Phi_\lambda(t)$ is the photon flux of the excitation light of wavelength λ at time t (in photons.cm^{-2}.s^{-1}) and $\Xi_{S_0\lambda}$ is the cross section for exciting the ground-state with photons of wavelength λ (in cm^2.photon^{-1}). Furthermore, $k_{i\rightarrow j}$ is the rate constant of a transition from state i to state j as shown in the schemes (B) to (D). The lifetime of a given state, τ_i, is inversely proportional to the sum of all of the decay rate constants for that state, *e.g.*

$$\tau_{S_1} = \frac{1}{\left(k_{S_1\rightarrow S_0} + k_{S_1\rightarrow T_1}\right)} \quad (123)$$

and

$$\tau_{T_1} = \frac{1}{k_{T_1\rightarrow S_0}} \quad (124)$$

The intersystem crossing efficiency for the formation of the T_1 state from the S_1 state is given by:

$$\phi_{isc} = \frac{k_{S_1\rightarrow T_1}}{\left(k_{S_1\rightarrow S_0} + k_{S_1\rightarrow T_1}\right)} = \left(k_{S_1\rightarrow T_1}\right)\tau_{S_1} \quad (125)$$

Both τ_{S_1} and τ_{T_1} can be determined accurately from the decay of the TRMC transients as long as they are comparable to, or longer than, the *ca.* 5 ns response time of the resonant cavity. This is generally the case for τ_{T_1} but not always for τ_{S_1}. If the lifetime of the S_1 state is too short, it has to be measured separately using an other time-resolved technique with a faster time response. This value is then used in the fitting procedure.

The actual shape of the excitation function $\Phi_\lambda(t)$ is identical to the intensity of the laser pulse as a function of time, which is measured using a fast photodiode detector. The absolute value of $\Phi_\lambda(t)$ incident on the sample is obtained by setting the total area under the transient of the laser pulse equal to the number of photons entering the sample through the transparent area of the measuring cell:

$$\int \Phi_\lambda(t)dt = F_{act}\frac{E_{laser}}{E_{h\nu}} \quad (126)$$

In equation (126) E_{hv} is the energy per photon (= 4.0 eV.photon^{-1} = 6.4×10^{-16} mJ.photon^{-1} at 308nm) E_{laser} is the average energy per laser pulse (in mJ) as determined with the power meter and F_{act} is the actinometry factor (in cm^{-2}), that will be the subject of a later section.

The second step in the fitting procedure takes the overall response time, τ_{rc}, of the detection system into account. In the present experiments the main contribution to τ_{rc} arises from the response time of the cavity, which at f_0 can be calculated using equation (50). The response time causes a transient change, which occurs at time t_i, $\Lambda_{i,0}$, to contribute to the observed signal at times longer than t_i, according to:

$$\Lambda_i(t) = \begin{cases} 0 & t < t_i \\ \Lambda_{i,0} e^{-\frac{(t-t_i)}{\tau_{rc}}} & t \geq t_i \end{cases} \qquad (127)$$

In the fitting procedure $\Lambda_{i,0}$ is taken to be equal to the average concentration of an excited state formed within a time domain ∂t ranging from t_i to $t_{(i+1)}$ (= t + ∂t). For each $\Lambda_{i,0}$, the corresponding $\Lambda_i(t)$ is constructed using equation (127). The "response-time-convoluted" contribution of an excited state is subsequently determined by summing all the individual contributions, $\Lambda_i(t)$, related to the same excited state over the time domain of interest.

Finally, in the third and last step, the "response-time-convoluted" contributions from the S_1 and T_1 excited states are added with their relative contributions varied until the shape of the measured transient is best matched. The actual amplitude of each contribution is directly related to the change in the molecular properties of interest, as given by the equations (17), (19) and (20).

2.6.1.1 Non-uniform electric fields and the spatial distribution of excited states.

The formula given in equation (17) is valid only in the case of a uniform distribution of excited solute molecules throughout the whole sample volume. This is however never the case in any practical cell design. Therefore the value of $\Delta\sigma(\omega)$ derived from an FP-TRMC experiment is an average value $\langle\Delta\sigma(\omega)\rangle_{xyz}$[18,45]. Two main contributions causing this averaging can be distinguished. Firstly, the laser light is attenuated as it penetrates the solution resulting in a concentration gradient across the cell, in the y direction. Secondly, in the present case excitation of the sample occurs only in the volume elements exposed to the excitation light by the 16 small openings in the broadwall side of the cell (see figure 9). For the dominant TE_{10s} cavity modes, the field strength inside the cavity is only constant in the y-direction, but strongly varies in the x and z direction. Therefore, the contribution from the different volume elements to the observed change in $\Delta\sigma(\omega)$ strongly depends on its x,z position. How both these contributions can be taken into account will be shown in the next few paragraphs.

As the laser beam travels through the sample volume in the y-direction, it is attenuated along its path and the concentration of excited states will therefore decrease with the penetration depth of the light, y. Since the field strength in the y direction is constant no field weighing is required and the relevant concentration is simply the average over the length b of the irradiated region in the cell:

$$\langle N \rangle_y = \frac{1}{b}\int_0^b N(y)dy \qquad (128)$$

The number of solute molecules initially excited should be identical to the number of photons absorbed, which in turn is directly proportional to the difference in the intensity between the incident light, I_0, and the transmitted light, I_T. For low light intensities, the relation between I_0 and I_T is given by the Lambert-Beer equation:

$$\frac{I_T}{I_0} = 10^{-y\varepsilon_\lambda[N_a]} = 10^{-OD_{\lambda,y}} \qquad (129)$$

In this equation $OD_{\lambda,y}$ is the optical density of the solution measured at wavelength λ and a pathlength of y (in cm). As can be seen in equation (129) the optical density of a solution is directly proportional to the concentration of the molecules that absorb the light, $[N_a]$, and the distance traveled by the light through the solution in the y-direction. The proportionality constant, ε_λ is called the extinction coefficient (in $M^{-1}.cm^{-1}$) and is a characteristic property of a specific electronic transition of a molecule. Using the linear dependence of the optical density on the distance traveled (see equation (129)) the number of photons absorbed could in principle be calculated as a function of the penetration depth y. From this distribution of absorbed photons the number of initially formed excited states as a function of penetration depth, N(y), could in principle be calculated.

However, because of the use of the short and intense light pulse of a laser as the excitation source, the occurrence of depletion of ground-state molecules has to be taken into account. This effect is most relevant for solute molecules with a high extinction coefficient at the excitation wavelength, *i.e.* $\varepsilon_{308nm} > 5\times10^4\ M^{-1}.cm^{-1}$. From the initially generated excited state the lowest singlet and triplet excited states monitored with the FP-TRMC technique are formed subsequently. From the initially obtained distribution of excited states the concentration of molecules in the i^{th} excited state, $N_i(y,t)$, at a depth y and a fixed moment in time t can be determined[45]. Hence, equation (17) is slightly modified according to equation (128) to relate the molecular properties of the equations (19) and (20) to the concentration

averaged change in conductivity, $\langle\Delta\sigma(\omega,t)\rangle_y$:

$$\langle\Delta\sigma(\omega,t)\rangle_y = \frac{1}{b}\int_0^b \left(\sum_i N_i(y,t)\left[\frac{\partial\sigma(\omega)}{\partial N}\right]_i \right) dy$$

$$= \sum_i \langle N_i(t)\rangle_y \left[\frac{\partial\sigma(\omega)}{\partial N}\right]_i \qquad (130)$$

The conductivity given by equation (130) is only corrected for non-uniformity of the concentration in the y-direction. In the x and z directions, account has to be taken of the fact that the electric field strength is not uniform. For the TE_{10s} cavity modes there is a $\sin[\pi x/a]$ dependence of the field strength in the x direction. In the z-direction the standing wave pattern of a TE_{10s} cavity mode has s maxima and (s+1) nodes over the length of the cell, corresponding to a field strength dependence of $\sin[s\pi z/d]$. Since the contribution to $\langle\Delta\sigma(\omega)\rangle_{xyz}$ resulting from a change in permitivity within a small volume element $\Delta x\Delta y\Delta z$ is proportional to the square of the field strength at that position, a field weighted correction factor, W(x,z), is necessary to take into account this non-uniform field strength distribution. This parameter is calculated from the sum of the individual contributions, $\Delta W(x,z)$, from each opening in the broadwall side of the cell using:

$$\Delta W(x,z) = \frac{1}{4ad}\iint \sin^2\left(\frac{\pi x}{a}\right)\sin^2\left(\frac{s\pi z}{d}\right)dxdz \qquad (131)$$

For the cell design shown in figure 9 W(x,z) ($= \Sigma\, \Delta W(x,z)$) is found to be 0.185 for s=4. This value is considerably higher than the value of 0.107, which is just the ratio of the sum of areas of the openings to the total broadwall area of the cell.

The overall effective average value of the change in conductivity, $\langle\Delta\sigma(\omega,t)\rangle_{xyz}$, which should be comparable to the measured $\Delta\sigma(\omega)$ is given by

$$\langle\Delta\sigma(\omega,t)\rangle_{xyz} = W(x,z).\langle\Delta\sigma(\omega,t)\rangle_y \qquad (132)$$

The corrections given in equation (130) and (132) work well as long as the optical density of the solution is close to or larger than unity. As figure 21 shows, deviation of the optical density from unity results in an overestimation of $\Delta\varepsilon'$ at lower optical densities. Therefore if the optical density of a sample is considerably lower than unity, the results have to be corrected according to the magnitude of the deviation shown in figure 21.

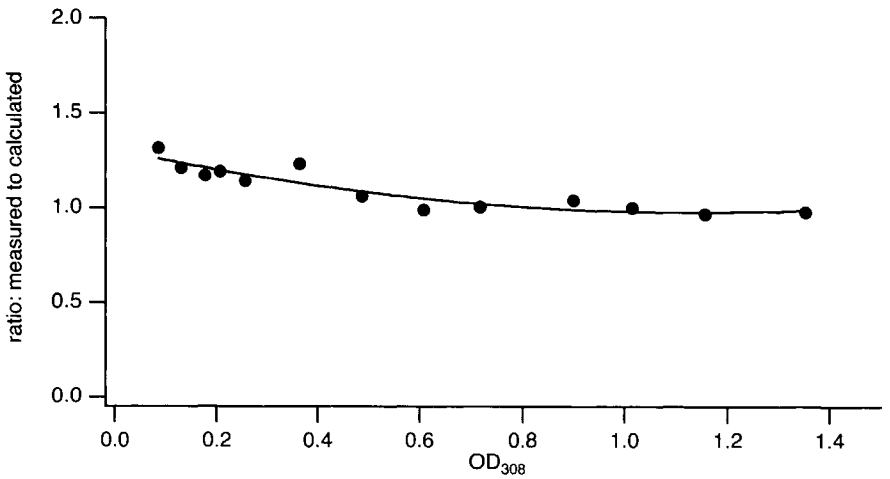

FIGURE 21: The overestimation of the conductivity or permittivity per excited state occurring at optical densities below unity as determined for a series of dilute solutions of DMANS in benzene.

2.6.1.2 The actual number of photons entering the cell: Actinometry.

From equation (130) in the previous section it is clear that in order to be able to derive quantitative data on $\Delta\sigma_{re}(\omega)$ (= $\omega\varepsilon_0\Delta\varepsilon''(\omega)$) and $\Delta\sigma_{im}(\omega)$ (= $\omega\varepsilon_0\Delta\varepsilon'(\omega)$) from the FP-TRMC transients, the number of photons absorbed by the solute molecules, N_*, must be known accurately. In the previous section a simple method was outlined to determine N_* starting from the optical density and using a modified version of Lambert-Beer's law to account for bleaching. However this approach requires a good estimate of the intensity of the laser beam incident on the solution within the cell, *i.e.* I_0 in equation (129).

The intensity of the laser beam itself is measured routinely during experiments using a power meter. From the output of the power meter the amount of photons incident on the measuring cell can be calculated. Unfortunately the irradiated area is not fully transparent but is covered by 4 x 4 windows, see figure 9. Therefore only a fraction of the incident photons enters the cell. To determine the magnitude of the fraction of incident photons that is available for exciting the sample an internal actinometer is used.

The internal actinometer used over the years for calibrating the FP-TRMC set-up is a solution of 4'-(N,N-dimethylamino)-4-nitrostilbene (DMANS) in benzene with an optical density of close to unity at 308 nm. From the FP-TRMC transient measured by photoexcitation of this solution $\langle\Delta\sigma_{re}(\omega)\rangle_{xyz}$ is determined, from which $\langle\Delta\sigma_{re}(\omega)\rangle_y$ is calculated *via* equation (132). This change can be attributed exclusively to a change in the dipole moment of the solute molecule, *i.e.* $[\partial\sigma_p(\omega)/\partial N]$, of its singlet and triplet excited states on excitation. Equation (33) shows that the magnitude of $[\partial\sigma_p(\omega)/\partial N]$ is proportional to

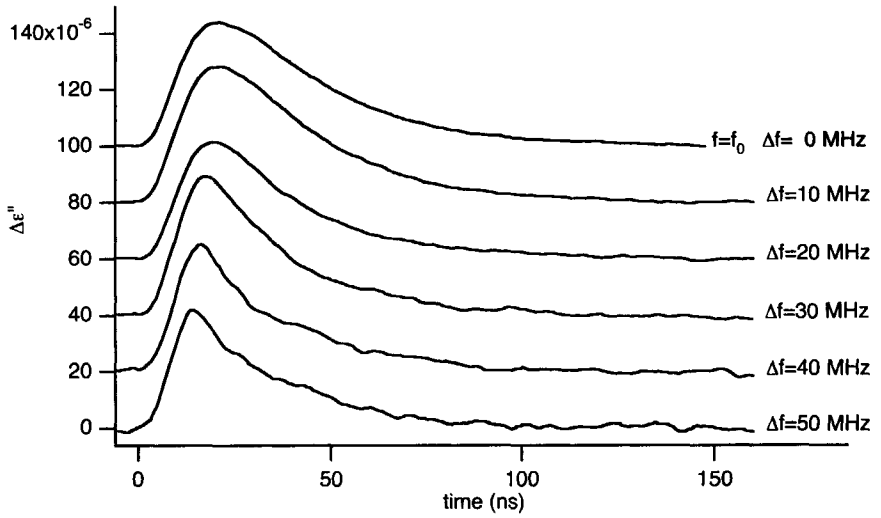

FIGURE 22: Transients measured for the compound shown in figure 17 at a series of frequencies deviating from f_0. For clarity the transients are offset with decreasing Δf. The transients have been corrected for differences in the sensitivity at the measuring frequencies, using equation (102). The decrease in response time, τ_{rc}, with increasing Δf is apparent.

$[p^{*2}-p_0^2]$. Thus, $[\partial\sigma_p(\omega)/\partial N]$ can be calculated from the values given in the literature, p_0 = 7.3 D and p^* = 24.5 D[46,47], and taking for the rotational relaxation time, Θ, a value of 196 ps for all states involved[48]. The value of $[\partial\sigma_p(\omega)/\partial N]$ calculated for the singlet dipole contribution is taken to be the same for the triplet dipole contribution.

According to equation (130), to describe accurately the measured transient $\langle N_{S_1}(t)\rangle_y$ and $\langle N_{T_1}(t)\rangle_y$ have to be calculated as well. These two parameters can be determined by solving the set of differential equations given by the equations (120)-(122). Taking the experimentally derived values of 3.1 ns for τ_{S_1}, 1400 ns for τ_{T_1} and 0.029 for ϕ_{isc} the only remaining unknown is the incident photon-flux, $\Phi_\lambda(t)$. This parameter is then determined from the best fit to the measured transient. From Φ_λ the intensity of the laser beam which has entered the measuring cell is calculated (= $E_{h\nu}\int\Phi_\lambda(t)dt$); compare equation (126)). The ratio between the calculated incident intensity of the laser beam within the cell ($J.cm^{-2}$) and the power per pulse (J) measured with the power meter is the actinometry conversion factor, F_{act}. For the current cell design F_{act} has a value between 0.10 and 0.15 cm^{-2}.

2.6.1.3 The response time of the microwave system: the relation between τ_{rc} and f.

Figure 20B and figure 20C show that the $\Delta\varepsilon''(\omega)$ transient, which results from the summation of an f_- and an f_+ transient, only slightly differs in shape from the transient obtained at f_0. This confirms the validity of equation (118). The minor difference is attributed

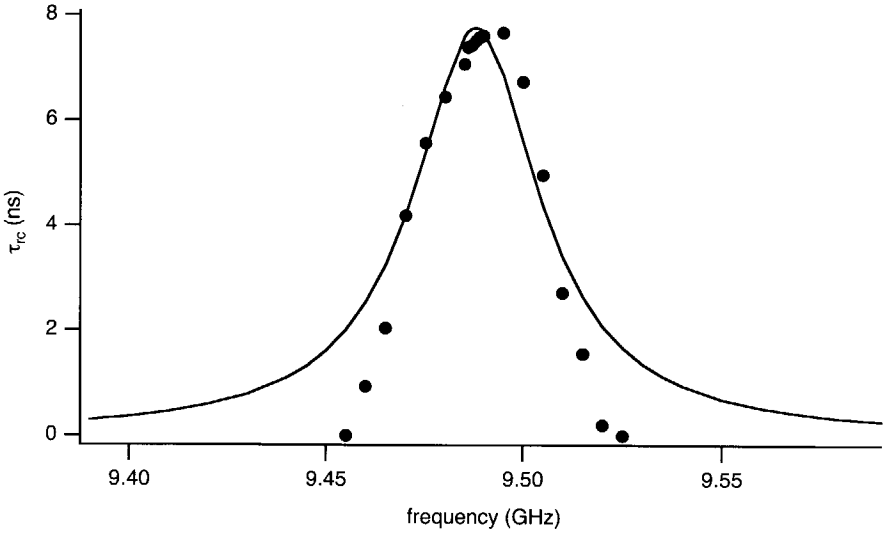

FIGURE 23: The frequency dependence of the experimentally determined response time, τ_{rc} (markers). The full line was calculated using equation (133) together with experimental parameters: n = 1.90, Q_l = 243.75 and f_0 = 9.488 GHz.

to the difference in the FP-TRMC set-up's response time, τ_{rc}, which is expected to be faster at f_- and f_+ then at f_0. The transients, which have been used to construct the contour plot of figure 17, are ideally suited to determine the relation between τ_{rc} and f experimentally, since the change in $\varepsilon'(\omega)$ is negligible for this solute and the measured transients can be attributed entirely to a photo-induced $\Delta\varepsilon''(\omega)$. The difference in height of the transients is the direct result of the different sensitivity factor for $\Delta\varepsilon''(\omega)$ at the different measuring frequencies. The relation between the sensitivity factor and f is known (see figure 19) and given by equation (102), which is used to correct the data. Figure 22 shows that the remaining difference is that the rise and decay appear to be faster as Δf (= $|f-f_0|$) increases. Since the decay kinetics of an excited state are independent of f this effect must be attributed to a decreasing τ_{rc} with increasing Δf. Therefore, using the same solution for the set of differential equations given in the equations (120)-(122) for all transients, the fitting of this collection of transients yields the experimental relation between τ_{rc} and f which is displayed in figure 23. The plot can be described by the following relation:

$$\tau_{rc} = n\frac{Q_l}{2\pi f_0}\frac{1-R(f)}{1-R_0} = n\frac{Q_l}{2\pi f_0}\frac{1}{\left(1+\zeta^2\right)} \qquad (133)$$

The discrepancies at the wings between the experimental data and equation (133) can be understood when one realises that the laser pulse has a width of 7 ns (FWHM), which prevents τ_{rc} from being determined accurately when its value becomes smaller than *ca.* 2 ns.

The fitting procedure of the $\Delta\varepsilon'(\omega)$ and $\Delta\varepsilon''(\omega)$ transients requires an accurate value of τ_{rc} at f_- and f_+. Since R(f) at the half-power frequencies equals $(R_0+1)/2$ (see figure 10) equation (133) will yield a value of τ_{rc} at f_- and f_+ which is half the value found at f_0.

2.6.2 The oscillatory contribution to the $\Delta\varepsilon'(\omega)$-related transient: the D-factor.

As is most clearly illustrated in figure 20A but also in figure 20C, the $\Delta\varepsilon'(\omega)$ transient contains an oscillatory contribution absent in the $\Delta\varepsilon''(\omega)$ transients. As figure 20C most clearly shows, the oscillatory contribution is significant during and shortly after excitation, but becomes negligible at longer times. Thus, equation (119), (116) and (117) are only valid for times much longer than the laser pulse. In order to be generally valid, equation (119) has to be expanded with an oscillatory term:

$$\Delta_{\pm}(t) = -2C\left[\Delta\varepsilon'(\omega,t) + D.g\left(\Delta\varepsilon'(\omega,t),t\right)\right] \qquad (134)$$

In equation (134) the D factor gives the ratio between the oscillatory contribution and the normal signal. The magnitude of the D-factor will depend on the exact formulation of $g(\Delta\varepsilon'(\omega,t),t)$.

The contribution of the oscillatory function, $g(\Delta\varepsilon'(\omega,t),t)$, is most clearly observed when the rate of change of $\varepsilon'(\omega)$ is largest, *i.e.* during the excitation. The most obvious expression for $g(\Delta\varepsilon'(\omega,t),t)$ would therefore appear to be the first derivative of $\Delta\varepsilon'(\omega,t)$ with respect to time:

$$g(\Delta\varepsilon'(\omega,t),t) = \frac{\partial\Delta\varepsilon'(\omega,t)}{\partial t} \qquad (135)$$

However substituting equation (135) into equation (134) does not yield the desired shape to describe a $\Delta_{\pm}$ transient exactly. The major shortcoming is that the width of the signals is to small when the height is correct. This problem can be circumvented by using a gaussian function to broaden the differential:

$$h_{t_i}(t) = H_{t_i} e^{-\left(\frac{t-t_i}{\sqrt{\text{var}}}\right)^2} \qquad -\infty < t < \infty \qquad (136)$$

In this equation H_i is the height of the calculated transient at time t_i, *i.e.* $g(\Delta\varepsilon'(\omega,t_i),t_i)$, and $\sqrt{(\text{var})}$ is a parameter which determines the broadness of the gaussian curve. The new

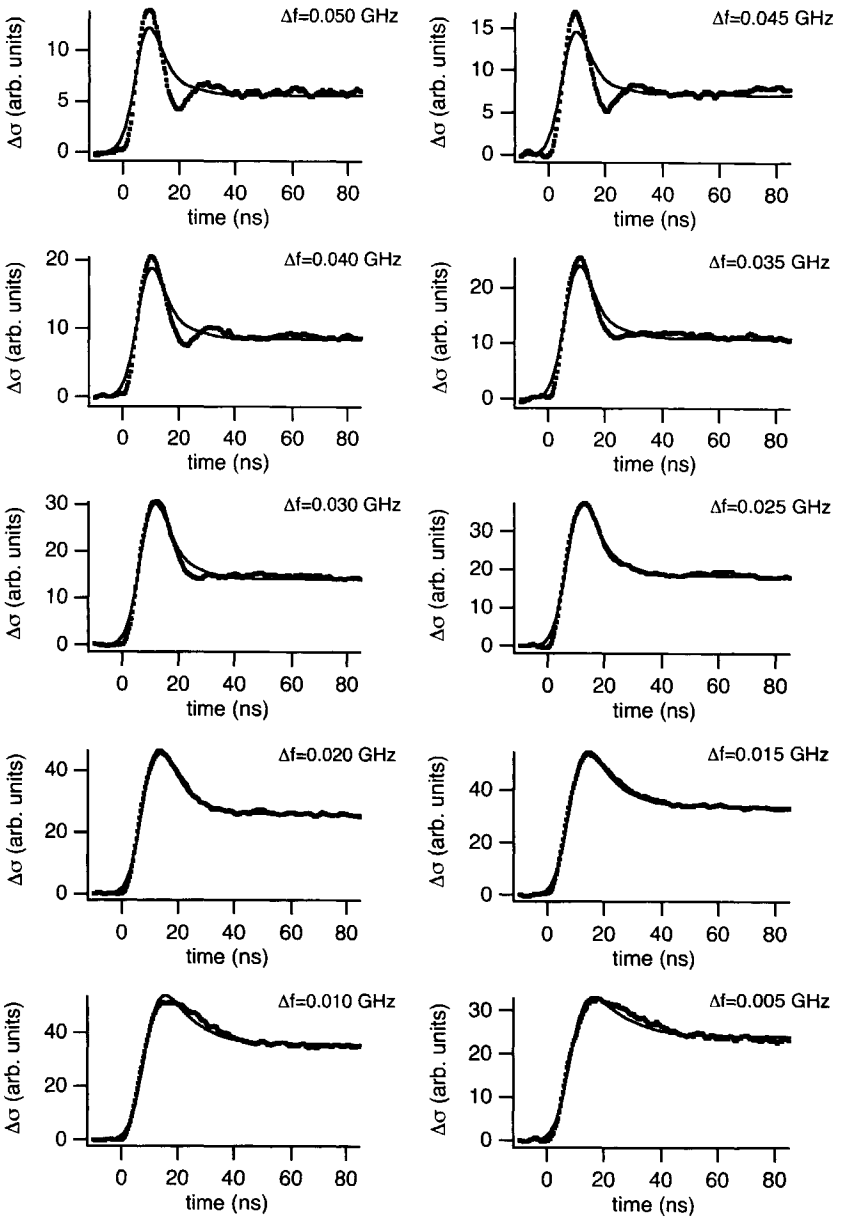

FIGURE 24: Calculated fits (solid lines) to the difference transients (black dots) using the approach with the differential and the Gaussian broadening, see equations (134), (135) and (136). The difference transients are obtained by subtracting a pair of transients measured at a frequency Δf lower and higher than f_0 for the compound shown in figure 18.

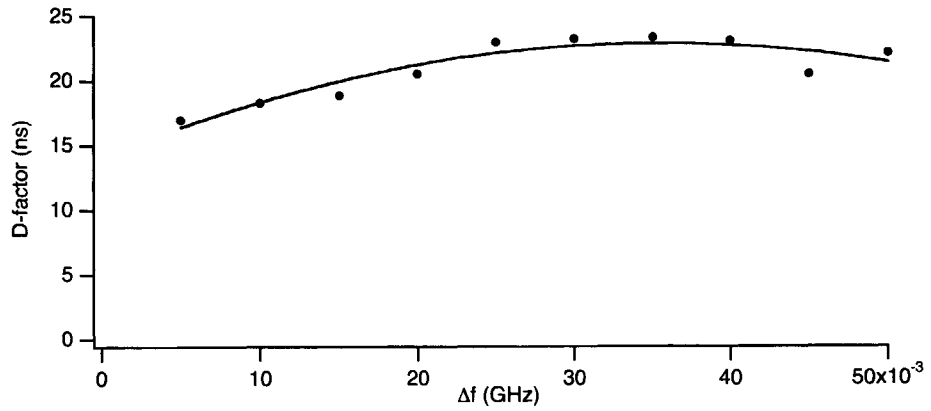

FIGURE 25: The D-factor in equation (134) obtained from the fits displayed in figure 24 as a function of the deviation from the resonance frequency, Δf.

gaussian-broadened differential, which replaces the differential obtained from equation (135), is constructed by applying equation (129) to all points of the previous differential and subsequently sum all the functions $h_{t_i}(t)$ obtained. The result is illustrated in figure 24 for a set of $\Delta\varepsilon'(\omega)$-related transient of Michler's ketone, MiKe (figure 18 and figure 20C). In all fits a value of 12 ns is used for $\sqrt{(var)}$, independent of Δf. As figure 24 shows, this approach yields good fits to the $\Delta\varepsilon'(\omega)$ transients when Δf is smaller than or equal to (1/2)ΔW, but the quality of the fits decreases when Δf is larger than (1/2)ΔW. Changing the broadness of the gaussian function with increasing Δf is ineffective in solving this problem.

The value of the D-factor in equation (134) for the approach described above, has been determined from the fits to the $\Delta\varepsilon'(\omega)$ transient of MiKe. For this purpose the apparent overshoot at the start of the $\Delta\varepsilon'(\omega)$ transient, which is absent in the $\Delta\varepsilon''(\omega)$ transient, is attributed exclusively to the oscillatory contribution. As shown in figure 25, the D-factor increases only slightly with increasing Δf. At the half-power frequencies a value of *ca.* 16 ns was determined for the D-factor.

The major inconvenience of the "gaussian broadening" approach is that $g(\Delta\varepsilon'(\omega,t),t)$ can no longer be expressed as a simple mathematical function of time. In the remaining part of this section an attempt is made to derive a mathematical expression in time for $g(\Delta\varepsilon'(\omega,t),t)$ using an alternative approach. Since equation (135) did not suffice, but the oscillatory contribution is largest when the changes in $\Delta\varepsilon'$ are largest, $g(\Delta\varepsilon'(\omega,t),t)$ is expected to be described instead by an expression of the form:

$$g\left(\Delta\varepsilon'(\omega,t),t\right) = \sum_{t_s=(t_0+\partial t)}^{t} \frac{\Delta\varepsilon'\left(\omega,t_s\right) - \Delta\varepsilon'\left(\omega,t_s-\partial t\right)}{\partial t}.G(t-t_s) \qquad (137)$$

Clearly, this equation does not solve the problem with $g(\Delta\varepsilon'(\omega,t),t)$ in equation (134), but only shifts the problem to that of finding a suitable expression for $G(t-t_s)$ in equation (137). For this purpose it would be helpful to obtain some idea of what actually occurs inside the measuring cell that is responsible for the oscillatory component.

Electrical resonance, as for instance in a resonant cavity, can be described as a forced harmonic oscillator with damping[49]. Before excitation the system is at equilibrium at a radian microwave frequency ω (= $2\pi f$). The energy stored in the cavity is oscillating forward and backward between the inductive, L, and the capacative, C, elements of the resonance cavity (see figure 11) with the frequency of the external microwave source. The amount of energy that is continuously exchanged is highest when the microwave frequency equals the system's own resonance frequency, $\omega = \omega_0$, and decreases with increasing deviation of ω from ω_0. The relation between ω and the amount of oscillating energy is the true origin of the sensitivity for $\Delta\varepsilon'(\omega)$ and an example of the ω-dependence of the amount of oscillating energy has actually been displayed already in figure 19. During the exchange some of the energy is dissipated as heat by the resistive elements, R, of the cavity. The dissipative process would damp the oscillation, which does not occur since the amount of energy lost in the damping process is matched by the amount of energy supplied by the external microwave source.

On excitation of the solution, both $\varepsilon'(\omega)$ and $\varepsilon''(\omega)$ can change. A change in $\varepsilon''(\omega)$ only affects the resistance R of the resonant cavity. A decrease in R reduces the damping of the oscillation inside the cavity. The damping process only indirectly affects the amount of energy that is stored in the cavity. An increase in $\varepsilon'(\omega)$ results in an increase of the capacitance, C, of the system. A change in the capacitance does directly affect the amount of energy that can be stored in the cavity. Since $\omega_0 = (\sqrt{LC})^{-1}$, any change in the capacitance of the system will alter ω_0 and thus $(\omega - \omega_0)$. This change in $(\omega - \omega_0)$ disrupts the pre-excitation equilibrium situation by changing the amount of microwave energy oscillating between the capacitive and inductive elements of the microwave cavity. The observed damped oscillation on the $\Delta\varepsilon'(\omega)$ transients can then be attributed to the system overshooting the new equilibrium in an attempt to adjust the amount of oscillating microwave energy to the changed capacitive properties of the cavity. If this is the case $G(t-t_s)$ in equation (130) should be expressed as a damped oscillation:

$$G(t-t_s) = \cos(\varphi(t-t_s)).e^{-\gamma(t-t_s)} \qquad (138)$$

In equation (138), φ is the radian frequency of the oscillation and γ the damping constant.

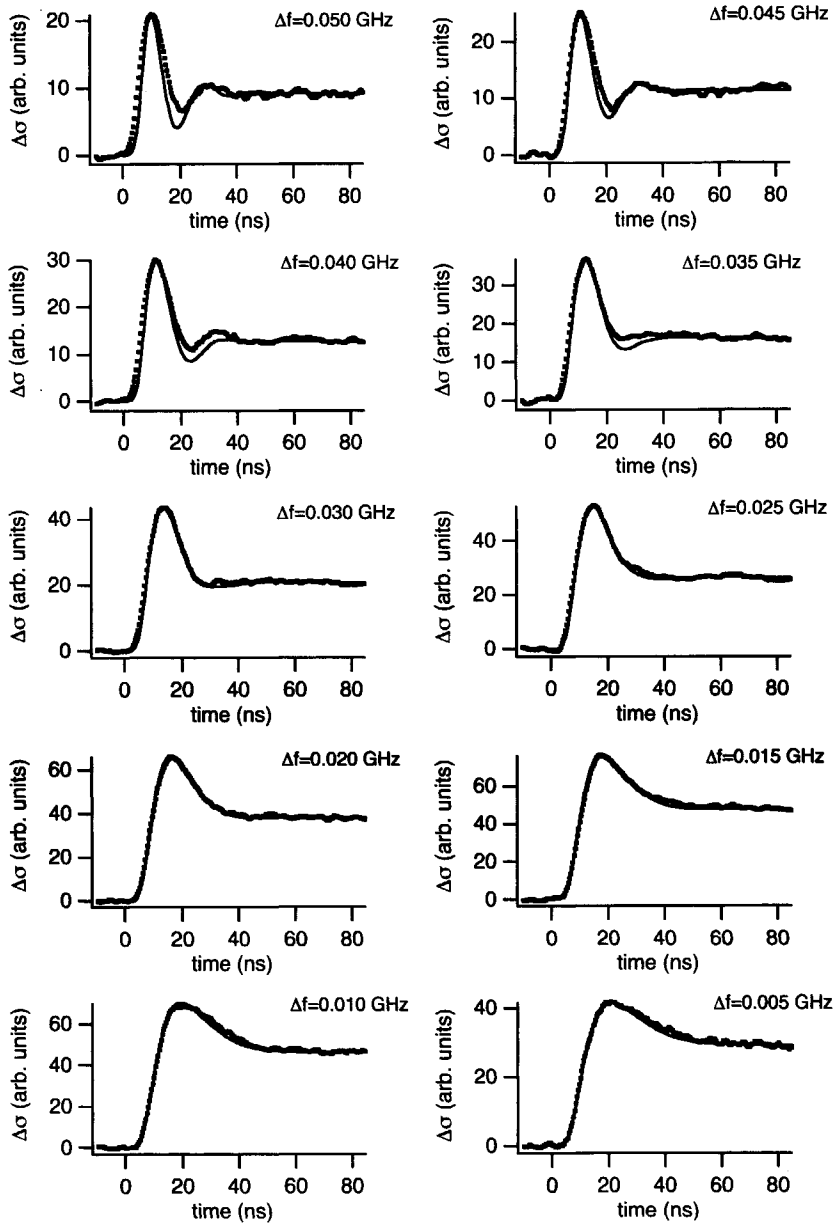

FIGURE 26: Calculated fits (solid lines) to the difference transients (black dots) using the approach with the differential and the damped oscillation, see equations (134) and (139). The difference transients are obtained by subtracting a pair of transients measured at a frequency Δf lower and higher than f_0 for the compound shown in figure 18.

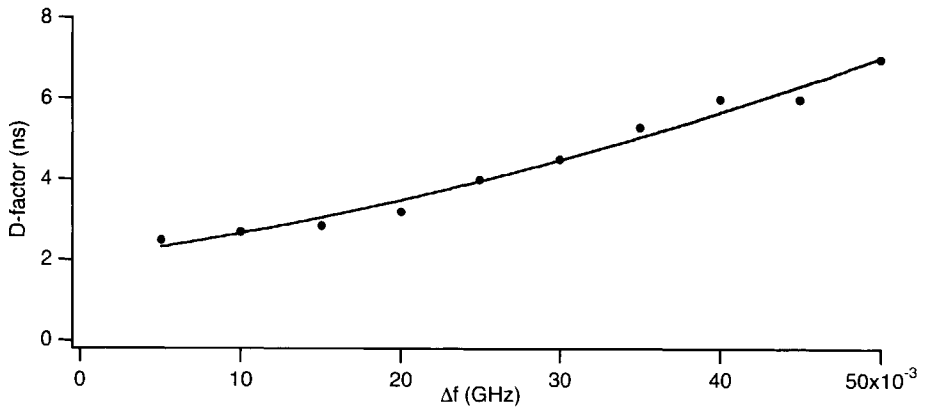

FIGURE 27: The D-factor in equation (134) obtained from the fits displayed in figure 26 as a function of the deviation from the resonance frequency, Δf.

Substituting equation (138) in (137) yields for g(Δε'(ω,t),t):

$$g\left(\Delta\varepsilon'(\omega,t),t\right) =$$

$$\sum_{t_s=(t_0+\partial t)}^{t} \frac{\Delta\varepsilon'(\omega,t_s)-\Delta\varepsilon'(\omega,t_s-\partial t)}{\partial t}.\cos\left(\varphi\left(t-t_s\right)\right).e^{-\gamma\left(t-t_s\right)} \qquad (139)$$

The series of Δε'(ω) transients shown in figure 24 has also been fitted using equation (134) in which g(Δε'(ω,t),t) is substituted by equation (139). These fits are shown in figure 26 and they succeed in reproducing the shape of the Δε'(ω)-related transients over the entire Δf range, although the fits are better at small Δf than at large Δf. For all fits, independent of Δf, a value of 0.15 ns^{-1} was used for γ, while φ cannot be taken independent of Δf but is best approximated by:

$$\varphi = \frac{0.35}{\tau_{rc}} \qquad (140)$$

Assuming that the response time of the system, τ_{rc}, is given by equation (133).

The value of the D-factor in equation (134) for this alternative approach is determined experimentally in the same way as was done for the "gaussian broadening" approach. In figure 27 the D-factor is plotted as a function of Δf. This plot shows that the D-factor increases with increasing Δf and a value of *ca.* 3 ns was determined for the D-factor at the half-power frequencies.

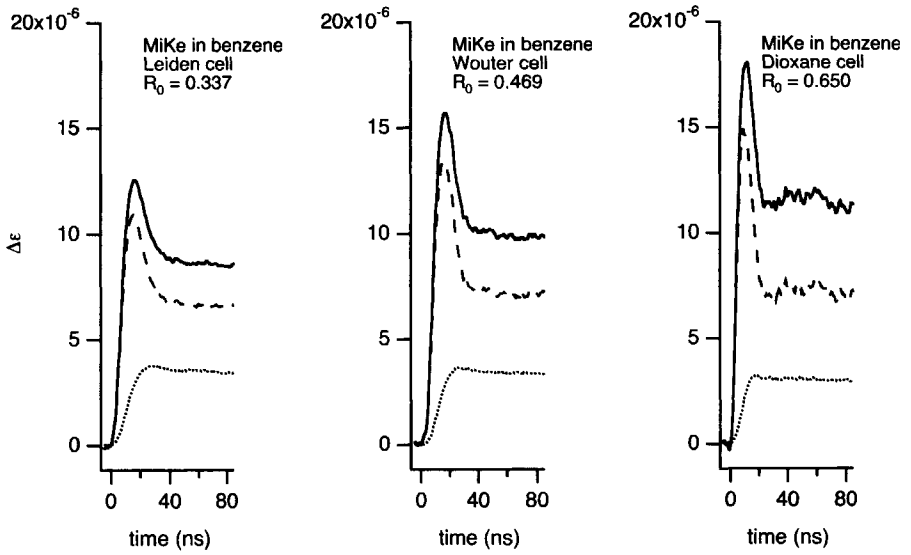

FIGURE 28: The $\Sigma_{\pm}$ (solid line) and $\Delta_{\pm}$ (dotted line) transients of the same sample (MiKe in benzene; see figure 18) measured in three different FP-TRMC cells. The cells only differ in the diameter of their iris-coupling hole which results in a different R_0. "Cross-talk" correction using equation (142) yields the dashed lines.

2.6.3 "Cross-talk" contributions.

The method of addition and subtraction of a pair of transients with the same Δf to separate the complex transient change in permittivity into a $\Delta\varepsilon'(\omega)$ and $\Delta\varepsilon''(\omega)$ transient assumes a perfect symmetry of the sensitivity towards $\Delta\varepsilon''(\omega)$ or perfect anti-symmetry of the sensitivity towards $\Delta\varepsilon'(\omega)$ around the resonance frequency. Small discrepancies in the magnitude of the sensitivity for $\Delta\varepsilon''(\omega)$ at $-\Delta f$ and $+\Delta f$ will result in "cross-talk", *i.e.* an apparent change in $\varepsilon'(\omega)$ which actually results from a change in $\varepsilon''(\omega)$. The ratio between the sensitivity factor for $\Delta\varepsilon''(\omega)$ and $\Delta\varepsilon'(\omega)$ at Δf determines the relative magnitude of the "cross-talk" contribution. Thus, for measurements at the half-power frequencies the magnitude of the "cross-talk" contribution to a $\Delta\varepsilon'(\omega)$ transient is proportional to the ratio of B over C, which according to the equations (104) and (115) should be equal to:

$$\frac{B}{C} = \frac{1+\sqrt{R_0}}{1-\sqrt{R_0}} \qquad (141)$$

According to this equation, the "cross-talk" contribution to a $\Delta\varepsilon'(\omega)$ transient increases in magnitude with decreasing depth of the resonance curve, *i.e.* increasing R_0, and a significant error could result from neglecting this contribution.

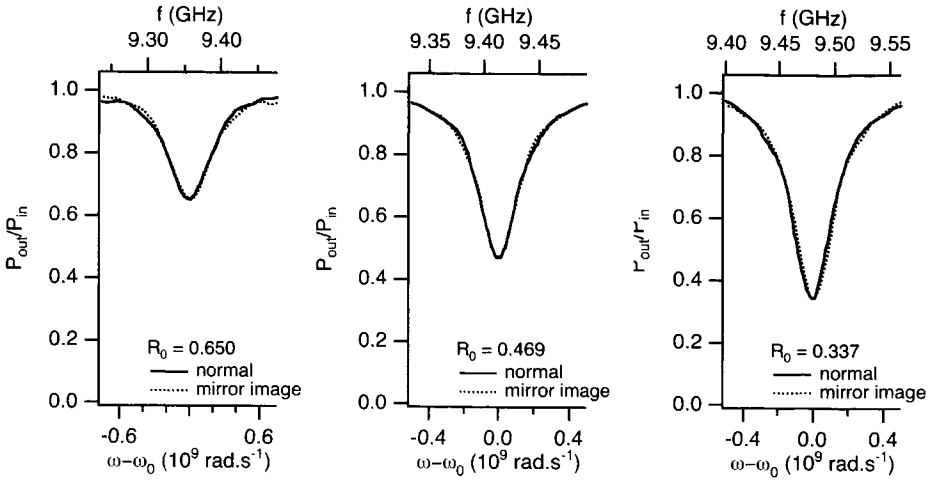

FIGURE 29: The measured resonance curves (solid line) and their mirror image obtained by inversion at f_0 (dotted line) shown in the same figure for the samples whose transients are displayed in figure 28.

The opposite case of "cross-talk" will in principle also occur, *i.e.* a contribution to the $\Delta\varepsilon''(\omega)$ transient which originates from a change in $\varepsilon'(\omega)$. Since its magnitude is proportional to the reciprocal of equation (141), the "cross-talk" contribution to the $\Delta\varepsilon''(\omega)$ transient decreases to zero with decreasing R_0. Therefore this contribution can be neglected without causing a significant error in $\Delta\varepsilon''(\omega)$.

The dependence of the magnitude of the "cross-talk" contribution to the $\Delta\varepsilon''(\omega)$ and $\Delta\varepsilon'(\omega)$ transients on R_0 is illustrated in Figure 28. This figure displays three sets of three transients, a $\Sigma_\pm$, a $\Delta_\pm$ and a corrected $\Delta_\pm$ transient. The $\Sigma_\pm$ and $\Delta_\pm$ are measured on identical solutions of MiKe in benzene, but in different TRMC cells. Between the three cells the value of their R_0 is changed by increasing the diameter of the iris hole of the cell. The $\Sigma_\pm$ transients are seen to be hardly affected by the increase in R_0, which confirms that the "cross-talk" contribution to the $\Delta\varepsilon''(\omega)$ transient is indeed negligible. The amplitude of the $\Delta_\pm$ transients on the other hand can be seen to increase significantly with increasing R_0, which shows that the "cross-talk" contribution can be even of the same order of magnitude as the signal resulting from $\Delta\varepsilon'(\omega)$.

Since $\Delta\varepsilon'(\omega)$ should be independent of R_0, the three $\Delta_\pm$ transients must be identical in height when the oscillatory contribution is no longer significant. The lifetime of at least several μs of the observed excited state of MiKe ensures that the change in $\Delta\varepsilon'(\omega)$ and thus the magnitude of the oscillatory contribution becomes negligible at times well beyond the duration of the laser pulse. Therefore the height of the three transients must be identical after t = 40 ns and onwards. This would be the case if they were corrected for "cross-talk" in the

following way:

$$\Delta_{\pm}(t)_{corr.} = \Delta_{\pm}(t) - 0.15.\frac{B}{C}.\Sigma_{\pm}(t) \qquad (142)$$

This is illustrated in Figure 28, which shows, besides the $\Delta_{\pm}(t)$ and $\Sigma_{\pm}(t)$ transients, the corrected transients, $\Delta_{\pm}(t)_{corr.}$, obtained by applying equation (142).

In equation (142) the value of 0.15 has been determined empirically. This indicates that "cross-talk" in the example shown in figure 28 will result from a mismatch of *ca.* 15% in sensitivity to $\Delta\varepsilon''(\omega)$ at f- and f+. However as figure 29 shows, no indication of a substantial asymmetry in the resonance curve can be found, that could explain a *ca.* 15% higher sensitivity for $\Delta\varepsilon''(\omega)$ at f- than at f+. A mismatch between the measuring frequencies and the actual halfpower frequencies can also be discarded as an explanation for the occurrence of "cross-talk", since the effect is structural: in all samples investigated sofar the f- transient is always higher than the f+ transient.

A change in f_0 will also affect the sensitivities at both half-power frequencies: one will increase, the other will decrease. Interestingly, an increase in $\varepsilon'(\omega)$ will be accompanied by a shift of f_0 to lower frequencies. If this occurs the sensitivity for $\Delta\varepsilon''(\omega)$ will increase at f- and decrease at f+, which is in agreement with observation. However this would imply that the value of 0.15 in equation (142) is not universally valid, but must be related to the magnitude of the shift in f_0 and thus to the magnitude of $\Delta\varepsilon'(\omega)$.

REFERENCES

[1] C. E. Cleeton, N. H. Williams: Phys. Rev. 45 (1934), 234-237.
[2] H. Margenau, F. L. McMillan, I. H. Dearnley, C. S. Pearsall, C. G. Montgomery: Phys. Rev. 70 (1946), 349-357.
[3] M. A. Biondi, S. C. Brown: Phys. Rev. 75 (1949), 1700-1705.
[4] S. C. Brown, D. J. Rose: J. Appl. Phys. 23 (1952), 711-718.
[5] S. C. Brown, D. J. Rose: J. Appl. Phys. 23 (1952), 719-722.
[6] S. C. Brown, D. J. Rose: J. Appl. Phys. 23 (1952), 1028-1032.
[7] A.F. Gibson, J.W.Granville, E.G.S.Paige: J.Phys.Chem.Solids 19 (1961), 198-217.
[8] J. A. Naber, D. P. Snowden: Rev. Sci. Instr. 40 (1969), 1137-1141.
[9] M. Brousseau, R. Schuttler: Solid-State. Elec. 12 (1969), 417-423.
[10] J. M. Warman, M. P. de Haas, A. Hummel: Chem. Phys. Lett. 22 (1973), 480-483.
[11] M. P. de Haas, J. M. Warman, P. P. Infelta, A. Hummel: Chem. Phys. Lett. 31 (1975), 382-386.
[12] J. M. Warman, P.P. Infelta, M. P. de Haas, A. Hummel: Chem. Phys. Lett. 43, (1976), 321-325.
[13] M. P. de Haas, A. Hummel, P. P. Infelta, J. M. Warman: J. Chem. Phys. 65 (1976), 5019-5020.
[14] J. M. Warman, P. P. Infelta, M. P. de Haas, A. Hummel: Can. J. Chem. 55 (1977), 2249-2257.
[15] P. P. Infelta, M. P. de Haas, J. M. Warman: Radiat. Phys. Chem. 10 (1977), 353-365.
[16] M. P. de Haas: "The measurement of electric conductance in irradiated dielectric liquids with nanosecond time resolution.", Ph.D. Thesis, University of Leiden 1977.
[17] R. W. Fessenden, P. M. Carton, H. Paul, H. Shimamori: J. Phys. Chem. 83 (1979), 1676-1677.
[18] M. P. de Haas, J. M. Warman: Chem. Phys. 73 (1982), 35-53.
[19] R. W. Fessenden, P. M. Carton, H. Shimamori, J. C. Scaiano: J. Phys. Chem. 86 (1982), 3803-3811.
[20] J. M. Warman, M. P. de Haas, J. W. Verhoeven, M. N. Paddon-Row: Adv. Chem. Phys. 106 (1999), 571-601.

[21] T. J. Savenije, J. M. Warman, H. M. Barentsen, M. van Dijk, H. Zuilhof, E. J. R. Sudhölter: Macromolecules 33 (2000), 60-66.
[22] B. R. Wegewijs, G. Dicker, J. Piris, A. Alba García, M. P. de Haas, J. M. Warman: Chem. Phys. Lett. 332 (2000), 79-84.
[23] A. K. Jonscher: Nature 267 (1977), 673-679.
[24] S. R. Elliott: Adv. Phys. 36 (1987), 135-218.
[25] P. Debye: "Polar Molecules.", Dover: New York 1945.
[26] R. Coehlo: "Physics of Dielectrics.", Elsevier: Amsterdam 1979, p 38-47.
[27] R. Pethig: "Dielectric and Electronic Properties of Biological Materials.", John Wiley, New York 1979, p 15-23.
[28] C. J. F. Böttcher: "Theory of Electric Polarisation.", Elsevier, Amsterdam 1973, vol. I.
[29] C. J. F. Böttcher, P. Borderwijk: "Theory of Electric Polarisation.", Elsevier: Amsterdam 1978, vol. II.
[30] H. Fröhlich: "Theory of Dielectrics.", Oxford University Press: London 1958, 2nd ed.
[31] N. F. Mott, E. A. Davis: "Electronic processes in non-crystalline materials.", Oxford University Press: Oxford 1979, 2nd ed, p 223-235.
[32] P. Bernier, S. Lefrant, G. Bidan: "Advances in synthetic metals.", Elsevier: Amsterdam 1999, p 354-360.
[33] J. C. Dyre, T. B. Schrøder: Rev. Mod. Phys. 72 (2000), 873-892.
[34] O. Hilt, L. D. A. Siebbeles: Chem. Phys. Lett. 269 (1997), 257-262.
[35] A. M. van de Craats, L. D. A. Siebbeles, I. Bleyl, D. Haarer, Y. A. Berlin, A. A. Zharikov, J. M. Warman: J. Phys. Chem. B 102 (1998), 9625-9634.
[36] G. P. van der Laan: "Charge Transport in π- and σ-Conjugated Polymers.", Ph.D. Thesis, Delft 1996, ISBN 90-73861-41-1, p 38-40.
[37] L. J. Adriaanse, J. A. Reedijk, P. A. A. Teunissen, H. B. Brom, M. A. J. Michels, J. C. M. Brokken-Zijp: Phys. Rev. Lett. 78 (1997), 1755-1758.
[38] O. Hilt, H. B. Brom, M. Ahlskog: Phys. Rev. B 61 (2000), R5129-R5132.
[39] E. R. Dobbs: "Basic Electromagnetism", Chapman & Hall, London 1993, 206.
[40] M. Sucher in "Handbook of Microwave Measurements", M. Sucher, J. Fox, Eds., John Wiley & Sons Inc., New York 1963, 3rd ed. vol. II, p 417-431.
[41] J. Kawamura, Y. Oyama: Solid State Ionics 35 (1989), 311-315.
[42] J. Kawamura, N. Kuwata, Y. Nakamura: Solid State Ionics 113-115 (1998), 703-709.
[43] S. Y. Grabtchak, M. Cocivera: Phys. Rev. B 50 (1994), 18219-18225.
[44] S. Y. Grabtchak, M. Cocivera: J. Appl. Phys. 79 (1996), 786-793.
[45] W. Schuddeboom: "Photophysical Properties of Opto-Electric Molecules studied by Time-Resolved Microwave Conductivity.", Ph.D. Thesis, Delft 1994, ISBN 90-73861-21-7, p 60-66.
[46] A. L. McLellan: "Tables of Experimental Dipole Moments", Rahara enterprises: El Cerrito 1974, vol. 2.
[47] A. L. McLellan: "Tables of Experimental Dipole Moments", Rahara enterprises: El Cerrito 1974, vol. 3.
[48] ibid [45], 69-70.
[49] R. P. Feynman, R. B. Leighton, M. Sands: "The Feynman lectures on Physics", Addison-Wesley publishing company, Reading 1996, vol. 1, p 23-5.

3

TWO-FOLD SYMMETRY[‡]

3.1 INTRODUCTION

9,9'-Bianthryl (AA), with its D_{2d} symmetry in the ground-state, has become the classic example of the occurrence of symmetry breaking on photoexcitation. The initial evidence that the relaxed S_1 state of bianthryl could be highly dipolar was presented in 1968 by Schneider and Lippert[1,2] in the form of the pronounced bathochromic shift of its fluorescence in polar solvents. The photophysical processes leading to charge separation after photoexcitation were described in considerable detail by the original authors. The absolute value of the dipole moment of the S_1 state of AA in polar solvents of close to 20 D estimated in the initial study

[‡] Chapter 3 has appeared previously as an article: J. J. Piet, W. Schuddeboom, B. R. Wegewijs, F. C. Grozema, J. M. Warman:"Symmetry breaking in the relaxed S_1 excited state of bianthryl derivatives in weakly polar solvents", J. Am. Chem. Soc. 123 (2001), 5337-5347.

from the solvatochromic shift has been reproduced in subsequent studies[3-6]. Most of the discussion and the large body of experiments carried out in more recent years have focused on the precise mechanism and the dynamics of the conversion from the initially formed, locally excited state, A^*A, to the eventual charge-separated state, A^+A^-. A full understanding is complicated by the fact that both torsional motion around the central σ-bond and solvent reorganization can be invoked as reaction coordinates[7].

While there is reasonable agreement at present concerning the photophysics of bianthryl in polar solvents for which solvation is considered to play the major role, the processes occurring in non-polar (saturated hydrocarbon) and weakly polar solvents (*e.g.* benzene, dioxane, dialkylethers) remain contentious. In the region of effective dielectric constant less than *ca.* 6, Schneider and Lippert, and subsequent workers, found only a very weak dependence of the fluorescence on the solvent polarity (as defined for example by the $E_T(30)$ value)[1-6]. Liptay *et al.*[8,9] showed that the temperature-dependent fluorescence spectra of bianthryl in an alkane solvent and benzene could be adequately explained in terms of a single, neutral excitonic state whose potential energy surface has a shallow double minimum at torsional angles of *ca.* 60° and 120° in contrast to the ground-state whose potential energy surface has only a single minimum at a torsional angle of 90° between the anthracene units. While this excitonic state is considered to contain an admixture of charge resonance states at the torsional minima, the degeneracy of these states, resulting from the D_2 symmetry, should result in no net dipole moment of the molecule. Further evidence for the lack of charge transfer character in weakly polar solvents has been provided by transient optical absorption measurements which display no spectral features characteristic of the known radical ion spectra of anthracene; features which are however observed for bianthryl in polar solvents such as acetonitrile[5,6].

Despite the above evidence to the contrary, time-resolved microwave conductivity (TRMC)[10,11] and electro-optical emission (EOEM)[12] measurements have clearly demonstrated that the relaxed S_1 state of AA does have an appreciable dipole moment within the low polarity regime, even in saturated hydrocarbon solvents. In addition, several groups[4,5,13-18] have suggested that the spectral form and picosecond-time scale relaxation of the fluorescence of AA in weakly polar media can best be explained in terms of an equilibrium between a neutral, excitonic state, E (frequently denoted as LE), and a zwitterionic, charge transfer state, CT. From spectral and kinetic analysis of the experimental data values of the equilibrium constant, $K_{ECT} = [CT]_{eq}/[E]_{eq}$, have been derived.

Evidence for an equilibrium between a neutral and a dipolar state in weakly polar solvents was also provided by the TRMC study of Fessenden *et al.*[11], who measured the change in both the real (dielectric constant) and imaginary (dielectric loss) components of the permittivity of AA solutions on photo-excitation. From these measurements the dipole relaxation time could be measured and was found to be *ca.* 10 ps in benzene and dioxane.

Since this was too fast to be explained by rotational diffusion of the molecules, it was attributed to intramolecular dipole reversal, possibly via an intermediate, neutral excitonic state. The dipole moments of the individual dipolar states calculated from the TRMC data using the equilibrium constants determined in the fluorescence measurements were however much lower than the *ca.* 20 D found in polar solvents: a value which is close to that expected for full charge separation over the center-to-center distance of 4.3 Å between the anthryl units.

It is apparent from the above that considerable uncertainty still exists as to the nature of the relaxed S_1 state of AA in weakly polar media. The possibility that the molecular symmetry could be broken even in completely non-polar hydrocarbon solvents is of particular relevance for a full understanding of the mechanism of intramolecular charge separation in general, not just for bianthryl itself. Since, in our opinion, TRMC experiments should provide the most clear-cut evidence for a dipolar character of the relaxed S_1 state, we have repeated the measurements of Visser *et al.*[10] and Fessenden *et al.*[11] using a somewhat different approach to measure the photo-induced changes in the real and imaginary components of the permittivity. In addition to solutions of AA in benzene and dioxane, we have carried out measurements on the symmetric 10,10'-dicyano-substituted derivative (CAAC) and the asymmetric 10-cyano derivative (CAA). Measurements have also been made on alkane solutions which could not be studied by Fessenden *et al.*[11]. The results confirm the dipolar nature of the S_1 states of the symmetrical molecules even in alkane solvents and show that flip-flop dipole reversal occurs on a time scale of *ca.* 10 picoseconds in benzene and dioxane, and *ca.* 2 ps in the alkanes. The TRMC results are complemented by optical absorption and emission measurements in a variety of solvents.

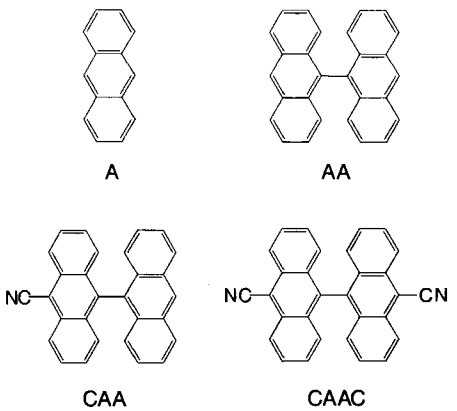

FIGURE 1: The molecular structures of the compounds studied together with their pseudonyms used in the text.

3.2 EXPERIMENTAL METHODS

The molecular structures of the four solute molecules investigated together with their pseudonyms used throughout the text are shown in figure 1. The solvents *n*-hexane (NHX; Merck Uvasol), cyclohexane (CHX; Merck Uvasol), benzene (BEN; Fluka, for spectroscopy),

tetrahydrofuran (THF; Aldrich, spectrograde), ethylacetate (Fluka, for spectroscopy), N,N-dimethylformamide (DMF; Aldrich, spectrograde) and acetonitrile (Aldrich, spectrograde) were used without further purification. The ethers dibutylether (Aldrich, anhydrous), diisopropylether (Aldrich, anhydrous) and diethylether (Aldrich, spectrograde) were dried on potassium hydroxide pellets, while 1,4-dioxane (DOX; Fluka, for spectroscopy) was dried over activated silica gel prior to use.

The optical density of the solutions at 308 nm (TRMC) or 337 nm (fluorescence) were monitored using a Kontron Uvikon 940 UV-Vis spectrophotometer. For TRMC measurements an optical density of close to unity is usually preferred, but due to an extremely low extinction coefficient at 308 nm for all bianthryls investigated the optical density was less than 0.3 in all cases. All solutions used for fluorescence measurements had an optical density between 0.05 and 0.15 at 337 nm.

Steady state emission spectra were measured on a PTI "quantamaster 1" spectrofluorometer equipped with a double excitation and a single emission monochromator. All solutions were degassed by bubbling for at least 15 minutes with Ar prior to use and excited at 337 nm. One slit setting was used for all samples investigated. All spectra were corrected for any spurious emission originating from impurities in the solvent. The quantum yield of the observed emission, ϕ_{fl}, was calculated from the integrated intensity under the emission band, A, using[19]:

$$\phi_{fl} = \frac{OD_{ref} . A_{fl} . n_{fl}^2}{OD_{fl} . A_{ref} . n_{ref}^2} \phi_{ref} \qquad (1)$$

In equation (1) OD is the optical density of the solution at the excitation wavelength and n is the refractive index of the solvent. 9,10-Diphenylanthracene (DPA) in cyclohexane was used as reference ($\phi_{ref} = 0.90$)[19].

The fluorescence decay transients were measured after photoexcitation of the Ar degassed solutions using a 0.8-ns pulse of 337-nm light from a PRA LN1000 N_2 laser. The light emitted from the sample perpendicular to the laser beam is passed through a Jobin-Yvon monochromator and was detected using a Photek PMT-113-UHF channel-plate photomultiplier with a risetime of 150 ps. Lifetimes were obtained from convolution fits to the transients taking into account the separately recorded shape of the laser pulse.

The TRMC solutions were contained in a resonant cavity and irradiated with the 7-ns pulse of a Lumonics HyperEx 400 excimer laser (XeCl: 308 nm). Oxygen was removed from the solutions by bubbling with CO_2, which is also a good scavenger for mobile electrons that might be formed in low-yield multi-photon ionisation events. The power output of the laser was monitored routinely using a Scientec 365 power meter and the actual fraction of photons entering the TRMC-cell, was determined using a solution of 4-(N,N-dimethylamino)-4'-

nitrostilbene (DMANS) in benzene as an internal actinometer. Averaging up to 64 single-shot transients was used to improve the signal-to-noise ratio. A full description of the microwave circuitry has been given elsewhere[20,21].

The transient change in the reflected microwave power, ΔR, was not only monitored at the resonance frequency, f_0, but also at both half power frequencies, f- and f+. In contrast to measurements at f_0, which allow only the determination of the changes in the dielectric loss of the solution, $\Delta\varepsilon''$, measurements at f- and f+ allow the determination of both $\Delta\varepsilon''$ and the change in the dielectric constant of the solution, $\Delta\varepsilon'$. By addition and subtraction of a pair of f- and f+ transients, separate transients can be obtained which are related to changes in $\Delta\varepsilon''$ and $\Delta\varepsilon'$ respectively:

$$\Sigma_{\pm} = \left(\Delta R_{-} + \Delta R_{+}\right) = B\Delta\varepsilon'' \tag{2}$$

$$\Delta_{\pm} = \left(\Delta R_{-} - \Delta R_{+}\right) = C\Delta\varepsilon' + D\frac{d\Delta\varepsilon'}{dt} \tag{3}$$

The values of B and C in equations (2) and (3) can be calculated from the characteristics of the resonant cavity[21]. The differential term in equation (3) results from a non-dissipative change in the energy stored within the cavity as a result of the fluctuation in ε'. This leads to an oscillatory component in the $\Delta_{\pm}$ transients. The value of D was determined by fitting transients for the formation of the highly polarizable triplet state of Michler's ketone[22]. Knowing B, C, and D, the absolute magnitude of $\Delta\varepsilon'$ and $\Delta\varepsilon''$ on flash-photolysis can be determined.

A slight difference in the sensitivity for $\Delta\varepsilon''$ at f+ and f- will result in a contribution to the $\Delta_{\pm}$ transient. This "cross-talk" contribution will become appreciable when $\Delta\varepsilon''$ is large. The proportionality between the "cross-talk" contribution and the magnitude of $\Delta\varepsilon''$ has been determined experimentally. This allows the correction of all $\Delta_{\pm}$ transients for the apparent change in ε' resulting from "cross-talk".

3.3 RESULTS AND DISCUSSION

The optical absorption and emission spectra of bianthryl and its derivatives have been studied extensively[1-6,8,9]. However, no single report has appeared in which data are provided on all of the solute/solvent combinations studied in the present TRMC investigation. We have therefore carried out a comprehensive study of the solvatochromic properties of AA, CAAC and CAA in order to have a consistent set of optical data which can be related to the microwave results.

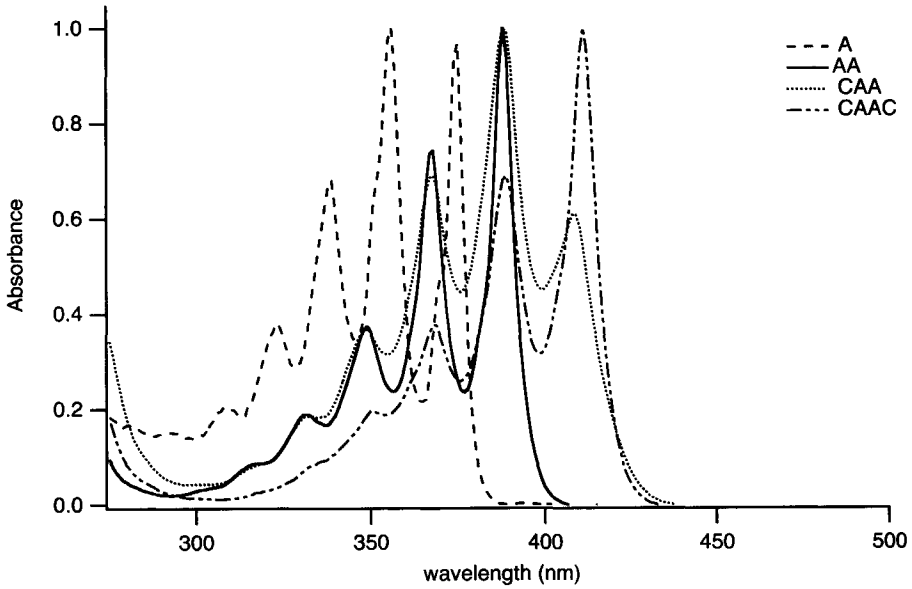

FIGURE 2: The absorption spectra of n-hexane solutions of anthracene (A), 9,9'-bianthryl (AA), 10-cyano-9,9'-bianthryl (CAA), and 10,10'-dicyano-9,9'-bianthryl (CAAC).

3.3.1 Optical measurements.

The absorption spectra of the present bianthryl derivatives are almost independent of solvent polarity from saturated hydrocarbons to acetonitrile, in agreement with previous studies. Only the spectra in *n*-hexane are therefore shown in Figure 2. All of the solutes display equally sharp, vibrationally structured absorption bands. A red shift of the 0,0 band of 13 nm (0.11 eV) occurs in going from monomeric anthracene to bianthryl, and a further red shift of 22 nm (0.18 eV) occurs on going from AA to CAAC. The great similarity of the form of the spectra of the dimeric compounds to that of anthracene alone indicates that absorption of a photon results initially in the excitation of a single anthryl unit and the formation of a locally excited state, A*A. The absorption spectrum of CAA is seen to be close to an equally-weighted sum of the spectra for AA and CAAC, indicating that photoexcitation of this asymmetric compound also involves initially the separate, vertical excitation of the individual A and CA chromophoric units, with the ratio CAA*/CA*A being dependent on the excitation wavelength. Therefore, in the initial state formed for all three bianthryl derivatives in all solvents the excitation energy resides on a single anthryl moiety and the two anthryl units are almost completely electronically decoupled as a result of their mutual orthogonal orientation.

The emission spectra in selected solvents are shown in Figure 3. They illustrate the dramatic difference between the relaxed S_1 state of all three bianthryl derivatives and that of

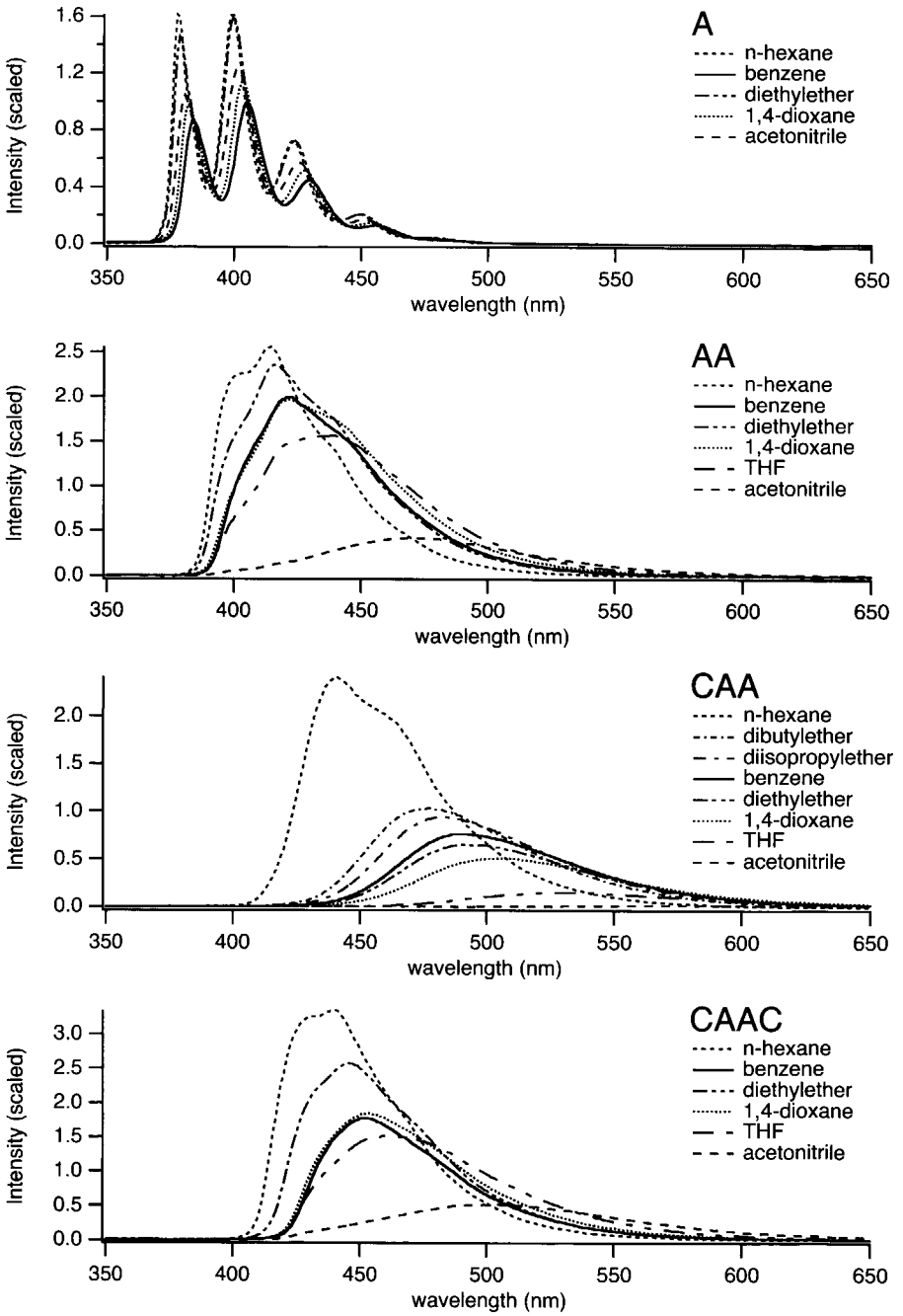

FIGURE 3: The fluorescence spectra of A, AA, CAA, and CAAC in selected solvents. For a complete compilation of fluorescence maxima, decay times and quantum yields see Table I.

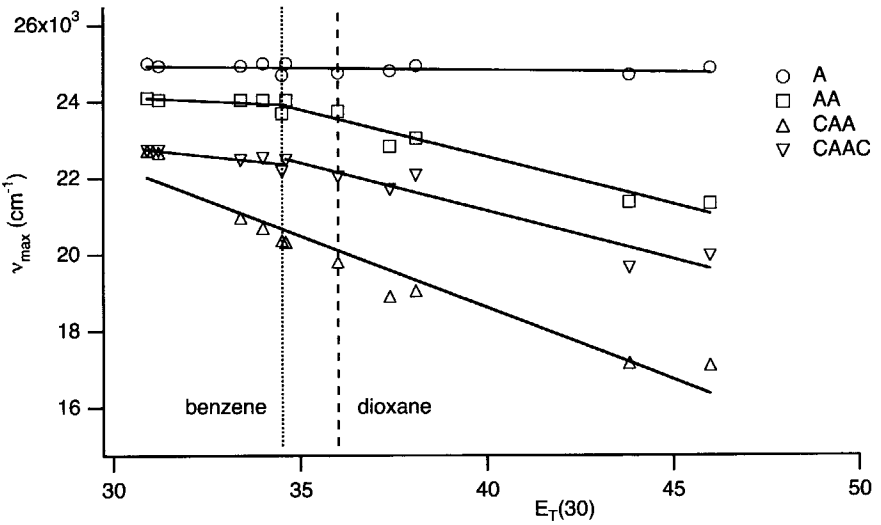

FIGURE 4: The dependence of the fluorescence maxima on the solvent polarity parameter $E_T(30)$.

anthracene alone. The sharply structured, almost solvent-independent anthracene fluorescence is replaced by spectra which are much broader, less structured and display pronounced bathochromic shifts with increasing polarity of the solvent. Even the emission spectra in *n*-hexane are significantly different to that found for anthracene itself.

Also illustrated by the data in Figure 3 is the difference between the symmetrical compounds, AA and CAAC, and the asymmetric derivative, CAA. Thus, while the latter displays a continuous red-shift in emission maximum with increasing solvent polarity, even for low polarity solvents, the former show a substantial shift only for solvents of intermediate to high polarity. This difference is illustrated more clearly in Figure 4 where the emission maxima, $h\nu_{fl}$, are plotted against the solvent polarity parameter $E_T(30)$ for all of the solute/solvent combinations studied. The very weak initial dependence of $h\nu_{fl}$ on increasing polarity for AA and CAAC gives way to a pronounced, close-to-linear dependence for $E_T(30)$ values in excess of *ca.* 35, as was found in the initial work of Schneider and Lippert[1,2]. The CAA compound, on the other hand, shows a continuous, close-to-linear decrease from the lowest polarity (alkane) solvents. In the intermediate- to high-polarity regime the solvent dependence is seen to be quite similar for all three solutes. A complete compilation of the data obtained from the fluorescence measurements is given in Table I.

TABLE I: Fluorescence maximum, λ_{max}, quantum yield, ϕ_f, and decay time, τ_f, for compounds investigated in the solvents shown.

solvent	$E_T(30)$[a]	Δf[b]	A			AA			CAA			CAAC		
			λ_{max} (nm)	ϕ_f	τ_f (ns)	λ_{max} (nm)	ϕ_f	τ_f (ns)	λ_{max} (nm)	ϕ_f	τ_f (ns)	λ_{max} (nm)	ϕ_f	τ_f (ns)
cyclohexane	30.9	0.100	401	0.35	5.9	416	0.84	8.0	441	0.83	14.5	440	-[c]	7.3
n-hexane	31.0	0.093	400	0.40	5.9	415	0.94	7.3	440	0.89	13.8	440	-[c]	8.0
dibutylether	33.0	0.192	401	0.38	5.9	416	0.94	10.3	477	0.43	29.7	445	0.98	9.3
diisopropylether	34.1	0.237	400	0.40	5.9	416	0.84	9.9	483	0.40	33.0	444	0.94	9.8
benzene	34.3	0.116	405	0.27	4.3	422	0.82	11.7	491	0.32	33.8	451	0.65	9.2
diethylether	34.5	0.256	400	0.40	6.2	416	0.96	12.2	492	0.28	31.7	445	0.97	11.4
1,4-dioxane	36.0	0.122	404	0.30	5.1	421	0.88	16.5	505	0.23	30.1	454	0.73	12.3
THF	37.4	0.309	403	0.33	5.5	438	0.78	21.3	529	0.07	15.8	461	0.70	17.0
ethylacetate	38.1	0.292	401	0.35	5.9	434	0.78	20.0	525	0.07	15.6	453	0.78	17.5
DMF	43.2	0.377	405	0.26	4.1	468	0.38	37.8	583	0.01	6.2	509	0.30	28.0
Acetonitrile	45.6	0.392	402	0.33	5.4	469	0.22	25.8	585	0.01	5.6	501	0.29	24.2

a) Solvent polarity parameter from ref 23.
b) Solvent polarity parameter calculated using equation (5).
c) Solubility to low.

Plots of the $h\nu_{fl}$ data have also been made against the polarity parameter Δf which should obey the linear relationship[24-26]:

$$h\nu_{fl} = h\nu_{fl}^{0} - \frac{2[\mu(S_1)]^2}{3\varepsilon_0 c V_c}\Delta f \qquad (4)$$

with:

$$\Delta f = \frac{(\varepsilon_s - 1)}{(2\varepsilon_s + 1)} - \frac{1}{2}\frac{(n^2 - 1)}{(2n^2 + 1)} \qquad (5)$$

In equations (4) and (5), $\mu(S_1)$ is the dipole moment of the relaxed S_1 state, ε_0 is the permittivity of vacuum, c is the velocity of light in vacuum, V_c is the cavity volume of the solute, and ε_s and n are the static dielectric constant and refractive index of the solvent respectively. Excited state dipole moments were calculated from best linear fits to the data in the intermediate- to high-polarity regime using cavity volumes calculated on the basis of a sphere with a radius of 6 Å for AA (as used in the original work of Schneider and Lippert[2]) and increased in proportion to the molecular weight for CAA and CAAC. The values of $\mu(S_1)$ found are 21, 23 and 21 D for AA, CAAC, and CAA respectively. These values are in good agreement with previously determined estimates.

In connection with the subsequent TRMC measurements we emphasise that the red shift in the fluorescence maxima of AA and CAAC on going from *n*-hexane to benzene or dioxane is considerably less than 0.1 eV and is similar for both of the latter solvents. This is to be compared with shifts for CAA of 0.29 eV for benzene and 0.36 eV for dioxane; values which approach those of 0.40 eV and 0.55 eV respectively, which have been determined for the completely charge separated state (dipole moment *ca.* 25 D) of the 3 σ-bond-bridged donor-acceptor compound Fluoroprobe[27]. The fluorescence results therefore clearly show that the dipolar character of S_1 and the accompanying solvent reorganization energy are very much smaller for AA and CAAC in benzene and dioxane than for CAA. The question is whether S_1 has in fact any net dipolar character at all in weakly polar solvents. As pointed out in the introduction, the answer derived from the fluorescence measurements depends on the model used to interpret the spectral data.

As mentioned above, while the emission maxima of AA and CAAC are not strongly red-shifted in weakly polar media, the spectral shapes do differ considerably from that of the monomer and display a pronounced temperature dependence even in alkane solvents[10]. Liptay *et al.*[8,9] have shown that the fluorescence spectra of AA and CAAC in alkanes and benzene can be described very well in terms of a single, neutral excitonic S_1 state by taking into account the large amplitude torsional motion about the central bond. From their analysis

of the fluorescence data, it was concluded that the double-minimum potential of the S_1 state of AA occurs at angles of 62°/118° and 58°/122° in isopentane and benzene with barriers to rotation at the orthogonal conformation of 0.035 eV and 0.058 eV respectively. These values are to be compared with energy minima at 71°/109° and a barrier height of 0.015 eV determined for AA in the gas phase[28-30]. The position of the minima and the central barrier height were found to be very similar for AA and CAAC in isopentane[31]. For CAA in isopentane a considerably higher barrier of 0.084 eV was estimated compared with 0.036 eV for CAAC. Even in the case of the asymmetric compound, however, it was concluded that there was no evidence in the spectral data for a charge transfer nature of S_1.

A completely different explanation of the fluorescence spectra and picosecond time scale spectral relaxation in weakly polar solvents has been favoured by other groups[4,5,13-18], who propose a model in which an equilibrium is established after photoexcitation between a neutral, excitonic state, E, and a dipolar, charge transfer state, CT. The fluorescence spectra are then deconvoluted into two (or more) components on the basis of comparative solvent studies or the early-time relaxation kinetics, and equilibrium contributions of the E and CT states are then estimated. The CT state is often taken to resemble the highly dipolar state formed in polar solvents, *i.e.* with a dipole moment of *ca.* 20 D. To date however no mechanism has been proposed which can adequately explain the symmetry breaking required for the formation of the CT state, particularly in alkane solvents.

3.3.2 Microwave measurements.

As mentioned in the experimental section, the sum of the TRMC transients monitored at the half-power frequencies, $\Sigma_{\pm}$, is proportional to the change in the dielectric loss of the solution on flash-photolysis, $\Delta\varepsilon''$. The observation of a transient change in ε'' is indicative of the formation of a dipolar excited state for which the time scale for dipole relaxation (*i.e.* randomization of the net dipole moment), Θ_*, is comparable to the reciprocal radian frequency, $1/\omega$, of the microwaves used; corresponding to *ca.* 15 ps for X-band microwaves.

Dielectric loss transients are shown in Figure 5 for bianthryl solutions in *n*-hexane, cyclohexane, benzene and dioxane. For comparison, transients are also shown for solutions of monomeric anthracene in *n*-hexane and dioxane. For the monomer solutions signals close to the noise level are observed indicating, as expected, a very small, if any, dipole moment of the S_1 state of anthracene alone. In contrast, all of the bianthryl solutions display a $\Delta\varepsilon''$ transient which is outside of the noise limits. While the signals for the alkane solvents are much lower than those for benzene and dioxane, they are nevertheless readily measurable. The present results therefore confirm those in a previous TRMC[10] study in which it was concluded that the relaxed S_1 state of AA has a dipolar character with a relaxation time on the order of at least picoseconds, even in completely non-polar solvents.

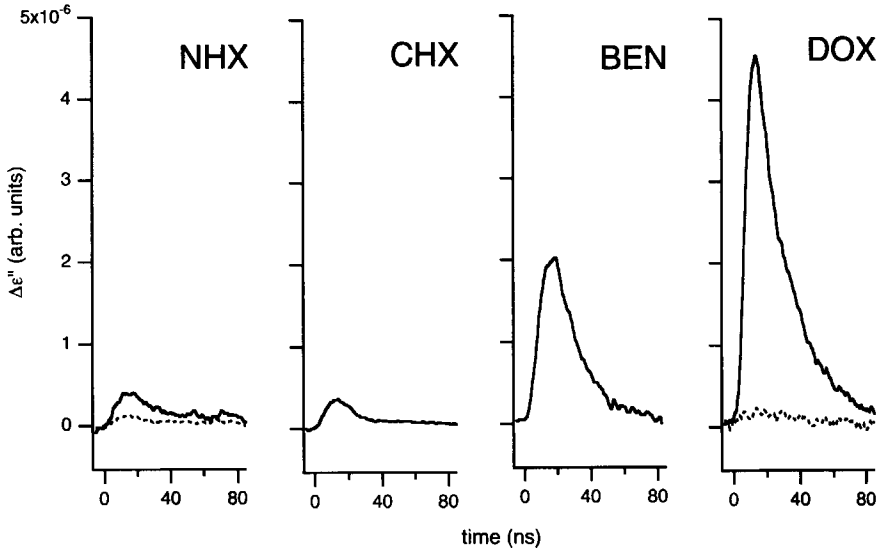

FIGURE 5: Transient changes in the dielectric loss, Δε", on flash-photolysis of solutions of 9,9'-bianthryl in (from left to right) n-hexane, cyclohexane, benzene and dioxane (solid line). The Δε" transients for anthracene solutions measured under similar conditions in n-hexane and dioxane are shown by the dashed lines.

The dicyano derivative, CAAC, was insufficiently soluble in the alkane solvents to carry out meaningful experiments. The Δε" transients for this compound in benzene and dioxane were however similar in magnitude to those for AA, indicating also a dipolar character of the relaxed S_1 state for this symmetrical derivative.

It is of interest to compare the Δε" transients for AA with those for the asymmetric compound CAA which are shown for *n*-hexane, benzene and dioxane solutions in Figure 6. Two aspects of such a qualitative comparison are worthy of comment. Firstly, the transient for CAA in *n*-hexane is more than an order of magnitude larger than that for AA. A much larger dielectric loss transient for CAA is however not particularly surprising since a larger excited state dipole moment might have been expected intuitively for the asymmetric derivative. In the case of dioxane however, the Δε" transient for CAA is seen to be substantially smaller than that for AA. An explanation for this, intuitively unexpected, result in terms of a larger dipole moment of the S_1 state of the symmetrical compound is considered to be extremely unlikely. Such an explanation would also be in contradiction with the fluorescence data, presented in the previous section and shown in Figures 3 and 4, which indicate a much larger dipolar character for CAA than for AA in benzene and dioxane. An explanation for this apparent anomaly can be found in the role that the dipole relaxation time plays in determining the magnitude of the dielectric loss transients. This is discussed below.

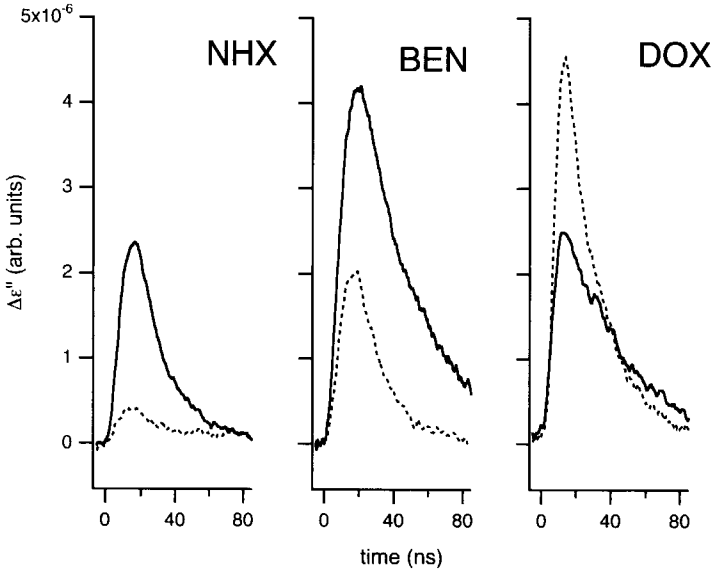

FIGURE 6: Transient changes in the dielectric loss on flash-photolysis of solutions of 10-cyano-9,9'-bianthryl in (from left to right) n-hexane, benzene and dioxane (solid lines). For comparison the transients of 9,9'-bianthryl are also included (dashed lines).

The formation of a concentration N_* of excited molecules with dipole moment μ_*, will result in a change in the dielectric loss given by equation (6):

$$\Delta\varepsilon'' = KN_*.\left[\frac{\omega\Theta_*}{1+(\omega\Theta_*)^2}\mu_*^2 - \frac{\omega\Theta_0}{1+(\omega\Theta_0)^2}\mu_0^2\right] = KN_*[\Delta\mathrm{Im}] \qquad (6)$$

with:

$$K = \frac{[\varepsilon(\infty)+2]^2}{27\varepsilon_0 k_B T} \qquad (7)$$

In equation (6), μ_0 and Θ_0 are the dipole moment and dipole relaxation time respectively of the ground state molecule. For AA and CAAC, $\mu_0 = 0$. For CAA μ_0 is expected to be close to the value of 4 D determined for 9-cyanoanthracene[32] so that the condition $\mu_0^2 \ll \mu_*^2$ will therefore be fulfilled for this compound if μ_* is as large as indicated by the solvatochromic shift measurements, *i.e.* 21 D. A good approximation for ΔIm for all of the solutes

TABLE II. Values of the parameters ΔIm (see equation (6)) and ΔRe (see equation (9)) derived from the transient change in the imaginary (dielectric loss) and real (dielectric constant) component of the complex permittivity of solutions of AA, CAA and CAAC in the solvents shown.

	ΔIm (10^{-60} C^2m^2)			ΔRe (10^{-60} C^2m^2)		
solvent	AA	CAA	CAAC	AA	CAA	CAAC
n-hexane	30.5	369	-(a	261	144	-(a
cyclohexane	32.1	-(a	-(a	269	-(a	-(a
benzene	202	264	165	429	99.2	526
1,4-dioxane	309	170	393	378	43.4	458

a) not measured

investigated is therefore:

$$\Delta \mathrm{Im} = \frac{\omega\Theta_*}{1+(\omega\Theta_*)^2}\mu_*^2 \tag{8}$$

The values of ΔIm derived from fitting the Δε" transients, using the known S_1 state lifetimes, are listed in Table II for all of the solute/solvent combinations studied.

As can be seen from (8), if $\omega\Theta_*$ is much larger than unity for CAA but is close to unity for AA and CAAC, then a much smaller Δε" transient would be obtained for the former compound even if the dipole moments were equal. We conclude therefore that the most probable explanation of the above mentioned anomaly is that dipole relaxation occurs much more rapidly for the relaxed S_1 state of the symmetrical compounds than for CAA.

A consequence of the occurrence of dipole relaxation on a time scale similar to or shorter than $1/\omega$ is that a substantial change in the real (dielectric constant) component of the complex permittivity, Δε', should also be observed. The dipolar contribution to Δε' is given by:

$$\Delta\varepsilon' = KN_*[\Delta \mathrm{Re}] \tag{9}$$

with:

$$\Delta \mathrm{Re} = \frac{1}{1+(\omega\Theta_*)^2}\mu_*^2 \tag{10}$$

For the condition that $\omega\Theta_*$ is much larger than unity, the change in ε' should be relatively small. Therefore, if the above explanation of the anomalously high dielectric loss transients is correct, a much smaller Δε' transient should be observed for CAA than for AA or CAAC.

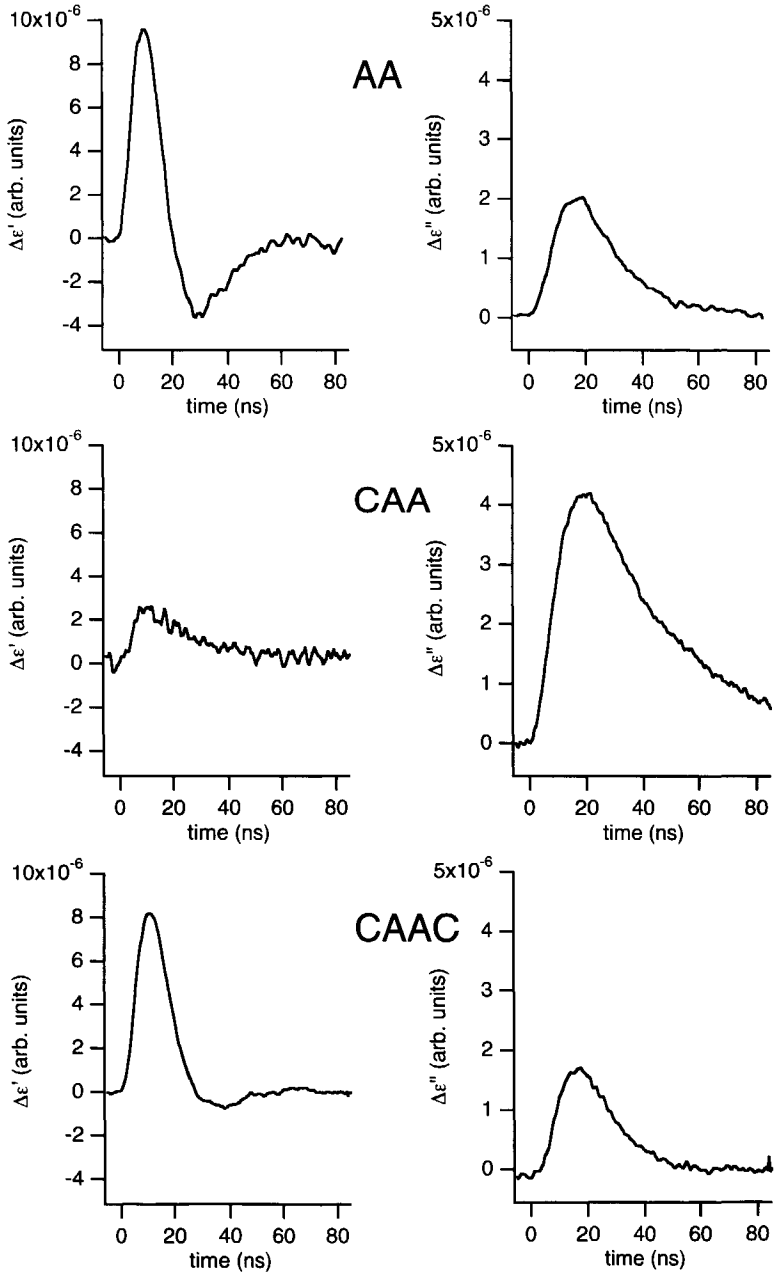

FIGURE 7. Transient changes in the real (dielectric constant, left) and imaginary (dielectric loss, right) components of the permittivity on flash-photolysis of benzene solutions of 9,9'-bianthryl (top), 10-cyano-9,9'-bianthryl (middle) and 10,10'-dicyano-9,9'-bianthryl (bottom).

Changes in ε' are reflected in the difference transients, $\Delta_{\pm}$, obtained by subtraction of the two TRMC transients monitored at the half-power frequencies. In Figure 7 both the sum, Δε", and difference, Δε', transients are shown for solutions of AA, CAA, and CAAC in benzene. The change in dielectric constant is in fact seen to be very much smaller for CAA than for AA or CAAC. As discussed above, this is an immediate, qualitative indication that the dipole relaxation time for the S_1 state of CAA is in fact considerably longer than for the symmetrical compounds. The values of ΔRe determined by fitting the Δε' transients are listed for all of the solute/solvent combinations studied in Table II.

As can be seen by comparing equations (8) and (10), the absolute value of the dipole relaxation time can be obtained from the relationship:

$$\Theta_* = \frac{1}{\omega}\frac{\Delta \mathrm{Im}}{\Delta \mathrm{Re}} \tag{11}$$

The values of Θ_* derived from the present experimental values of ΔIm and ΔRe are listed in Table III.

In using equation (11) to determine Θ_* the implicit assumption is made that the only contribution to ΔRe arises from out-of-phase dipolar motion. An additional contribution could however arise if the electronic polarizability of the molecules, α_e, increased substantially on photoexcitation. The change in ε' can in fact be discussed in terms of an overall change in the polarizability of the molecule, Δα, consisting of electronic and dipolar contributions, *i.e.* $\Delta\alpha = \Delta\alpha_e + \Delta\alpha_D$:

$$\Delta\varepsilon' = KN_*\left[3k_BT.\Delta\alpha\right] \tag{12}$$

From equations (9) and (12) the value of Δα is seen to be related to the measured value of ΔRe simply by:

$$\Delta\alpha = \frac{\Delta \mathrm{Re}}{3k_BT} \tag{13}$$

The values of the overall change in the polarizability obtained for AA and CAAC using equation (13) and the measured values of ΔRe are listed as the polarizability volumes, $\Delta\alpha' = \Delta\alpha/4\pi\varepsilon_0$, in Table III.

The values of Δα' of *ca.* 200 Å^3 or more for the relaxed S_1 state of the symmetrical compounds are an order of magnitude larger than the value of 17 Å^3 found for the vertical transition to the Franck-Condon state in electro-optical absorption measurements on anthracene or bianthryl[33,34]. They do however agree with the value of 220 Å^3 reported by Baumann *et al.* for the relaxed S_1 state of bianthryl in an electro-optical emission study[6,12].

TABLE III: The dipole relaxation time, Θ_*, effective dipole moment, μ_*, and excess polarisability volume, $\Delta\alpha'$, of the relaxed S_1 state of AA, CAA and CAAC for the solvents shown.

solvent	η^a (cP)	$\Theta_D{}^b$ (ps)	$\Theta_*{}^c$ (ps)			μ_* (D)			$\Delta\alpha'$ (Å^3)	
			AA	CAAC	CAA	AA	CAAC	CAA	AA	CAAC
NHX	0.31	66	1.8	-	(151)^d	4.9	-	18	190	-
CHX	1.02	225	1.9	-	-	4.9	-	-	196	-
BEN	0.65	139	7.9	5.3	316	6.9	7.2	(21)	313	383
DOX	1.41	312	14	14	485	7.5	8.4	(21)	276	334

a) Solvent viscosity.
b) Diffusional rotation time calculated from equation (14) assuming the molecule to occupy a compact sphere with a radius of 6 Å.
c) Determined for AA and CAAC from the ratio between ΔIm and ΔRe (equation (11)), and for CAA in benzene and dioxane from ΔIm assuming a dipole moment of 21 D (equation (8)).
d) Estimate based on the value of Θ_* for benzene and the ratio between the solvent viscosities.

On the basis of the much smaller values of $\Delta\alpha'$ found for anthracene alone and for CAA, we conclude that the major contribution to the excess polarizabilities found for the symmetrical dimers arises from dipole relaxation and hence that equation (11) can therefore be used to provide a reasonably good estimate of the dipole relaxation time. Any correction for an electronic contribution to the polarizability would tend to increase the value of Θ_* calculated. A further discussion of this aspect of the results will be given in the next section.

The values of Θ_* obtained for bianthryl in benzene and dioxane of 7.9 and 14 ps are similar to the values found for CAAC and are in reasonably good agreement with the values of 9.2 and 11.7 ps determined by Fessenden *et al.*[11]. In that work the authors directly measured the phase shift resulting from the change in dielectric constant using a experimental approach different from that used in the present work. They did, however, also make the assumption that the change in dielectric constant could be attributed entirely to dipole relaxation. For the non-polar alkanes, which could not be measured by Fessenden *et al.*, a considerably shorter relaxation time of *ca.* 2 ps is found.

The $\Delta\varepsilon'$ transients measured for CAA solutions are in general very small. Since, the $\Delta\varepsilon''$ transients measured for the same solutions are large, the observed amplitude of these $\Delta\varepsilon'$ transients will be determined to a large extend by the cross-talk contribution. The value of ΔRe of CAA given in Table II, which are derived from the cross-talk corrected $\Delta\varepsilon'$ transients, are therefore prone to a much larger error than the values determined for the symmetric compounds. As a result of this larger error in the values of ΔRe for CAA, the values of Θ_* calculated using equation (11) have to be considered as no more than very rough estimates. For this compound we have therefore used a different approach to estimate Θ_*. This is based on the observation that the bathochromic shifts of the fluorescence for CAA in benzene and dioxane are large and lie on the straight line drawn through all solvents in Figure 4. We make

the reasonable assumption therefore that the value of $\mu*$ for the S_1 state of CAA in these solvents is close to the value of 21 D determined from the combined fluorescence data. This value of $\mu*$ has then been substituted in equation (9) together with the experimental ΔIm values for the benzene and dioxane solutions to determine the corresponding values of $\Theta*$ which are listed in Table III.

The experimental values of $\Theta*$ are compared in Table III with estimated values of the rotational relaxation time, Θ_D, of the solute molecules in the different solvents. These values were calculated using the Stokes-Einstein relationship for a spherical molecular geometry with a molecular radius of 6 Å:

$$\Theta_D = \eta \frac{4\pi R^3}{3k_B T} \tag{14}$$

In equation (14), η is the microscopic coefficient of friction towards molecular rotation (taken to a first approximation to be equal to the viscosity) and R is the molecular radius.

For the symmetrical solutes, $\Theta*$ is much shorter than Θ_D and displays no correlation with the solvent viscosity. Dipole relaxation must therefore be occurring mainly via an intramolecular process of flip-flop dipole reversal as was suggested by Fessenden *et al.*[11]. In order to obtain the intramolecular relaxation time, Θ_I, from the measured $\Theta*$ values a correction should be applied for the contribution of Θ_D to the overall value of $\Theta*$:

$$\Theta_I = \frac{\Theta*}{\left(1 - \frac{\Theta*}{\Theta_D}\right)} \tag{15}$$

However, since the rotational relaxation times are in general more than an order of magnitude longer than the overall measured relaxation times for AA and CAAC, the correction will be small and Θ_I will in fact be close to the measured value of $\Theta*$.

The value of $\Theta*$ determined from the ΔIm/ΔRe ratio can be used together with the absolute values of ΔIm to determine the effective dipole moment of the dipolar state undergoing the intramolecular flip-flop process. These values are listed in Table III. Beginning with a value of approximately 5 D for the alkane solvents, $\Theta*$ increases slightly to approximately 7 D in benzene and 8 D in dioxane. These values are somewhat larger than the values determined by Fessenden *et al.* (3.9 D for benzene and 4.5 D for dioxane[11]) and by electrooptical emission measurements (*ca* 3 D for *n*-hexane and cyclohexane, and *ca.* 7 D for dioxane[12]). There is general agreement however that the effective dipole moment of the relaxed S_1 state in non-polar and weakly polar solvents is considerably lower than the *ca.* 20 D determined from fluorescence measurements for AA and CAAC in medium to highly polar solvents.

The values of Θ_* for CAA are seen to be larger than the values of Θ_D. This can be readily explained by the fact that the CAA molecules are in reality not perfect compact spheres. In fact taking the geometry to be closer to that of a prolate ellipsoid results in estimates of Θ_D which are approximately a factor of 2 larger than the values for a sphere and in quite good agreement with the values of Θ_* determined. The results for CAA in benzene and dioxane are therefore in accord with the formation of a relaxed S_1 state with a dipole moment close to 20 D for which dipole relaxation is controlled mainly by rotational diffusion of the molecules.

For CAA in *n*-hexane we have taken the rotational diffusion time to be approximately half of that for benzene on the basis of the difference in viscosity of the solvents, *i.e.* $\Theta_D \approx$ 151 ps. Combining this value with the value of ΔIm determined results in an estimate of 18 D for μ_*. Thus, even in this completely non-polar solvent, CAA appears to form a highly dipolar state on photoexcitation with a dipole relaxation time which is controlled mainly by rotational diffusion of the solute molecules. There is however evidence from the $\Delta\varepsilon'$ transients for CAA that, at least in *n*-hexane, dipole relaxation may be occurring to a certain extent via a flip-flop mechanism involving an equilibrium between the fully charge separated and locally excited states.

3.3.3 General discussion.

The present results demonstrate conclusively that the relaxed S_1 states of the symmetrical compounds AA and CAAC have a net dipolar character with flip-flop dipole reversal occurring on a time scale of picoseconds even in alkane solvents, in agreement with previous studies on AA using either microwave dielectric loss[10,11] or electro-optical emission[12] techniques. Since both the initial, locally excited state, LE, and the torsionally relaxed excitonic state, E, should be electrostatically neutral as a result of their underlying D_2 symmetry, a mechanism must exist whereby the molecular symmetry of the combined solute/solvent system is in some way broken in the excited state.

In the case of CAA the asymmetry of the molecule can clearly provide an energetic driving force for charge separation since the electron affinity of the CA moiety is larger by *ca.* 0.3 eV than that of unsubstituted anthracene[17]. In addition, the fact that CAA has a dipole moment in the ground state ensures that the surrounding solvent molecules have a prearranged orientation favorable for initiating full solvation of the zwitterionic state. That the energetic driving force is the major factor in ensuring complete charge separation for CAA is indicated by the very large dipole moment found for the S_1 state of this solute even in the apolar solvent *n*-hexane. It is worth noting that this result is in contradiction with the conclusion by Liptay *et al.* that "Neither the analysis of the fluorescence spectra nor the

evaluation of the fluorescence lifetime and quantum yield measurements yields any indication of a fluorescence from a CT state for CAAC and CAA in isopentane" [31].

Returning to the symmetric compounds: The optical absorption spectra leave no doubt that photoexcitation results initially in the formation of a locally excited anthryl moiety which is orthogonally oriented with respect to its ground-state partner. This has been further substantiated by electro-absorption (Stark effect) measurements[33] which show that the increase in polarizability of AA on vertical photoexcitation is relatively small (*ca* 20 Å^3) and close to that for excitation of anthracene alone. Since the anthryl moieties are electronically decoupled in their initial orthogonal conformation, the direct formation of a charge transfer state from the locally excited state, LE, is not possible even in a polar solvent.

The LE state can however subsequently undergo torsional relaxation and, for angular configurations other than 90°, electronic coupling between the two anthryl moieties becomes allowed. This results in the formation of a fully delocalised excitonic state, E, which is derived from a combination of the local ^1L_a type states of the aromatic moieties and charge resonance states, CR[3,13]. Because of the D_2 symmetry, the two mirror-image CR states are degenerate and do not therefore result in a net dipole moment of E. The intermixing of states is however expected to result in a large molecular polarizability. A slight asymmetry in the (di)electric environment of the molecule will then be sufficient to remove the degeneracy of the CR states and result in a net dipole moment[7].

The electronic coupling between two aromatic moieties, and hence the degree of stabilization of the excitonic state, should be maximum for a coplanar, *i.e.* zero degree, configuration. For bianthryl, however, there is a strong repulsive interaction between the hydrogen atoms at the 1,1' and 8,8' positions. The net result of the opposing electronic and steric interactions is the occurrence of potential minima for the excitonic state at angles of approximately 60 and 120 degrees[4,8,9,13,31,35]. The resulting central barrier to torsional relaxation is estimated to be only on the order of k_BT for AA and CAAC so that rapid equilibration of the angular distribution with maxima at the angles corresponding to the potential minima is expected to occur within a time scale on the order of a picosecond[8,9,31,35]. Within the ensemble of excited molecules at any given time there will therefore be those which are highly polarizable with torsional angles close to that corresponding to a potential minimum and those which are only weakly polarizable for angles close to 90°.

Ab initio calculations on the excited state of ethylene have shown that for this molecule a large increase in polarizability occurs at a torsional configuration between the planar and orthogonal geometries[36]. The calculations showed furthermore that while in this configuration even density (refractive index) fluctuations in an enviroment of non-polar molecules was capable of breaking the symmetry, thus removing the degeneracy of the CR states, and inducing a net dipole moment. The lifetime of such a density-fluctuation-induced

dipolar state, CT, is expected to be of the same order as the time taken for an acoustic wave to propagate over the dimensions of the solute/solvent system, *i.e. ca.* 1 nm. Since the velocity of sound in organic liquids is on the order of 1000 $m.s^{-1}$ this time scale will be on the order of a picosecond. The CT lifetime will, of course, also be influenced by the residence time of an excited molecule in the optimal, highly polarizable angular configuration. This is also expected to be on the order of picoseconds. In view of this we conclude that the transient dipolar state of AA and CAAC found in alkane solvents with a dipole relaxation time of *ca.* 2 ps results from solvent density fluctuations in the vicinity of those excited solute molecules which have a conformation close to that corresponding to a potential minimum.

In the case of polar solvents, density fluctuations will be accompanied by stochastic orientational fluctuations of the solvent dipoles (or quadrupoles) which can even more effectively break the symmetry of the overall solute/solvent system and induce a larger net dipole moment. This has also been shown by the theoretical calculations on ethylene[36]. The temporary induction of even a small, net dipole moment can, in this case, be followed by a snowball effect in which further dipole-induced solvent relaxation drives charge separation to completion, resulting in a fully charge separated state, CS. The tens of picoseconds fluorescence relaxation times found for AA in polar solvents do in fact agree quite well with the values expected for such a solvent relaxation mechanism[14-16,37,38]. The CS state can be further stabilised by torsional relaxation to an orthogonal configuration of the anthryl moieties. The lack of electronic coupling in this configuration would then retard intramolecular electron transfer and considerably slow down the return to the neutral excitonic state.

It is worth pointing out that in order to observe the full solvatochromic effect of a solvent on the fluorescence spectrum it is sufficient that dipole reversal occurs on a time scale considerably longer than the solvent relaxation time. Evidence that dipole reversal, *via* an intermediate neutral excitonic state, does in fact still take place in the case of AA and CAAC even in highly polar solvents is provided by the small, but readily observable shoulder in the fluorescence in the short wavelength region. This can be seen in Figure 3 even for acetonitrile. In addition, the transient optical absorptions observed on flash-photolysis of solutions of bianthryl in acetonitrile could not be explained completely in terms of the radical anion and radical cation spectra alone but required admixing of the spectrum of the non-polar excitonic state as found in *n*-hexane[39].

In weakly polar solvents the strength of the dipolar or quadrupolar (in the cases of benzene and dioxane) solvent interactions are apparently insufficient to drive charge separation to completion and prevent the rapid return to the neutral excitonic state on a time scale shorter than the time required for full solvent relaxation. The fact that a somewhat larger degree of stabilization of the charge transfer state occurs due to the quadrupolar nature of benzene and dioxane is however indicated by the slower intramolecular dipole relaxation

times and the somewhat higher transient dipole moments found in the present work for these solvents compared with alkanes.

Since the relaxed S_1 states in a molecular ensemble will contain some molecules with close to an orthogonal configuration and hence zero dipole moment and some with a configuration close to a potential minimum with an appreciable dipole moment, the question arises as to what the actual dipole moment of the "charge transfer" state is. This question is not easily answered since it requires a knowledge of the equilibrium angular distribution and the corresponding molecular polarizabilities. A provisional answer can however be obtained based on a frequently used, much simplified model in which the two possible CT states of dipole moment μ_{CT} are in thermal equilibrium with a non-dipolar excitonic state.

$$CT_{+/-} \underset{k_{CTE}}{\overset{k_{ECT}}{\longleftrightarrow}} E \underset{k_{CTE}}{\overset{k_{ECT}}{\longleftrightarrow}} CT_{-/+} \qquad (A)$$

In terms of the processes represented in scheme (A) the intramolecular dipole relaxation time is given by:

$$\Theta_I = \frac{1}{(k_{CTE} + 2k_{ECT})} \qquad (16)$$

Since the values of Θ_I for AA and CAAC in weakly polar solvents are much shorter than the eventual S_1 decay times of several nanoseconds, the processes in scheme (A) can be taken to be fully equilibrated in the present experiments. This being the case, the equilibrium fraction of excited molecules in a CT state, F(CT), will be:

$$F(CT) = \frac{[CT]_{eq}}{[CT]_{eq} + [E]_{eq}} \qquad (17)$$

$$= \frac{2k_{ECT}}{(k_{CTE} + 2k_{ECT})} \qquad (18)$$

$$= 2k_{ECT}\Theta_I \qquad (19)$$

For equilibrium conditions, the value of the CT state dipole moment can be derived from the measured effective dipole moment, μ_*, if F(CT) is known from:

$$\mu_{CT} = \frac{\mu_*}{\sqrt{F(CT)}} \qquad (20)$$

Estimates of F(CT) of 0.35, 0.70 and 0.74 for AA in the solvents *n*-hexane, benzene and dioxane respectively have been made by Barbara *et al.*[15] and Schütz and Schmidt[18] by analysing the fluorescence spectra on the basis of an equilibrium model. Using these values of F(CT) together with our measured $\mu*$ values results in estimates of 8.3, 7.8 and 8.7 D respectively for μ_{CT}. The values of the dipole moment of the CT state in weakly polar solvents obtained in this way are seen to be independent of solvent and less than half the value of the dipole moment of the CS state. If the dipole moment of the CT state was in fact as large as 20 D then this would require the CT content of S_1 to be only approximately 10%, which is much lower than the estimates based on the analysis of the fluorescence spectra. Those estimates have however been supported by an analysis of the picosecond fluorescence relaxation kinetics which also leads to an F(CT) value of approximately 0.7 for AA in toluene[17]. We emphasise that the two-state, equilibrium model used above to derive μ_{CT} values is much simplified and a fuller theoretical treatment is obviously required.

Support for a dipolar character of the CT state in weakly polar solvents much smaller than the CS state formed in polar solvents is provided by transient optical absorption measurements[39]. Thus in alkane solvents no trace is found of absorptions characteristic of the radical anion and cation of anthracene. Such absorptions would have been expected to be observable if CT was in fact a fully charge separated state present at a fractional concentration as high as 35% as derived from the fluorescence experiments.

A further aspect of the present results which can be related to fluorescence measurements is the relaxation time. According to scheme (A) the mean time to relax to the equilibrium situation starting from the neutral excitonic state should be equal to the value of $\Theta*$ measured in the present work. Zachariasse *et al.*[17] have monitored the spectral relaxation of the fluorescence from solutions of AA and CAAC in toluene and found initial relaxation times of 23 and 16 ps respectively. These values are to be compared with the $\Theta*$ values of 7.9 and 5.3 ps for AA and CAAC measured in the present work in benzene. The ratios of the relaxation times for the two solutes are seen to be closely similar. The fact that the relaxation times are longer in the fluorescence study can be ascribed to the lower temperature used in that work (-45°C). In fact if the values of $\Theta*$ for AA in benzene determined at 9°, 22° and 58° C by Fessenden *et al.*[11] are plotted in an Arrhenius fashion together with the value of Zachariasse *et al.*[17], a reasonably good linear relationship is found with a corresponding activation energy of 0.068 eV. Interestingly, this activation energy is quite close to the value of 0.058 eV estimated for the potential energy barrier for torsional motion for AA in benzene[9] indicating that torsional motions are probably the controlling factor in the rate of dipole reversal.

3.4 SUMMARY

We have confirmed that the relaxed S_1 state of bianthryl has a transient dipolar character in the weakly polar solvents benzene and dioxane and also in the non-polar solvents *n*-hexane and cyclohexane. Dipole relaxation, however, occurs on a picosecond time scale *via* an intramolecular, flip-flop mechanism involving an intermediate neutral, excitonic state. The relaxation times determined are 14, 7.9 and *ca.* 2 ps for 1,4-dioxane, benzene and the alkanes respectively. Similar relaxation times are found for the symmetrical 10,10'-dicyano derivative in 1,4-dioxane and benzene. The dipole moment of the charge transfer state is estimated to be *ca.* 8 D, *i.e.* much lower than the *ca.* 20 D found from the bathochromic shifts in the fluorescence in medium-to-high polarity solvents.

The results are in accordance with the following photophysical processes:
a) initial formation of a locally excited anthryl moiety in an orthogonal conformation with respect to its partner; b) torsional relaxation to the neutral excitonic state which has potential minima for angles of *ca.* 60° and 120. This state can be considered to contain contributions from charge resonance states and local excited states; c) a large increase in the exciton polarizability for conformations close to the potential minima; d) solvent-density-fluctuation-induced removal of the degeneracy of the charge resonance states and the development of a net dipole moment in the solute; e) rapid dipole relaxation due to fluctuations in the solvent environment and torsional motion about the central bond.

In the case of the asymmetrically substituted 10-cyano derivative the TRMC and fluorescence results show that a highly dipolar, *ca.* 20 D, charge separated state is formed even in *n*-hexane. In this case dipole relaxation occurs on a time scale of hundreds of picoseconds and is attributed to rotational diffusion of the solute molecules. Symmetry breaking for CAA is driven mainly by the *ca.* 0.3 eV difference in the electron affinities of the anthryl and cyano-anthryl moieties which results in close to complete charge separation in all solvents and probably the ultimate adoption of an electronically decoupled, orthogonal charge separated state.

ACKNOWLEDGEMENT

The authors express their thanks to Dr K. A. Zachariasse and Dr W. Kühnle (Max-Planck-Institute Göttingen) and Dr N. Detzer (University of Mainz) for providing the compounds investigated in this work. The present investigation was supported by the Netherlands Organisation for the Advancement of Research (NWO).

REFERENCES

[1] F. Schneider, E. Lippert: Ber. Bunsenges. Phys. Chem. 72 (1968), 1155-1160.
[2] F. Schneider, E. Lippert: Ber. Bunsenges. Phys. Chem. 74 (1970), 624-630.
[3] M. Zander, W. Rettig: Chem. Phys. Lett. 110 (1984), 602-610.
[4] S. Müller, J. Heinze: Chem. Phys. 157 (1991), 231-242.
[5] R. Fritz, W. Rettig, K. Nishiyama, T. Okada, U. Müller, K. Müllen: J. Phys. Chem. A 101 (1997), 2796-2802.
[6] K. Nishiyama, T. Honda, H. Reis, U. Müller, K. Müllen, W. Baumann, T. Okada: J. Phys. Chem. A 102 (1998), 2934-2943.
[7] K. Honma, K. Arita, K. Yamasaki, O. Kajimoto: J. Chem. Phys. 94 (1991), 3496-3503.
[8] R. Wortmann, K. Elich, S. Lebus, W. Liptay: J. Chem. Phys. 95 (1991), 6371-6381.
[9] R. Wortmann, S. Lebus, K. Elich, S. Assar, N. Detzer, W. Liptay: Chem. Phys. Lett. 198 (1992), 220-228.
[10] R.-J. Visser, P. C. M. Weisenborn, P. J. M. van Kan, B. H. Huizer, C. A. G. O. Varma, J. M. Warman, M. P. de Haas: J. Chem. Soc., Faraday Trans. 2 81 (1985), 689-704.
[11] D. B. Toublanc, R. W. Fessenden, A. Hitachi: J. Phys. Chem. 93 (1989), 2893-2896.
[12] W. Baumann, E. Spohr, H. Bischof, W. Liptay: J. Luminesc. 37 (1987), 227-233.
[13] W. Rettig, M. Zander: Ber. Bunsenges. Phys. Chem. 87 (1983), 1143-1149.
[14] M. A. Kahlow, T. J. Kang, P. F. Barbara: J. Phys. Chem. 91 (1987), 6452-6455.
[15] T. J. Kang, M. A. Kahlow, D. Giser, S. Swallen, V. Nagarajan, W. Jarzeba, P. F. Barbara: J. Phys. Chem. 92 (1988), 6800-6807.
[16] T. J. Kang, W. Jarzeba, P. F. Barbara, T. Fonseca: Chem. Phys. 149 (1990), 81-95.
[17] Th. von der Haar, A. Hebecker, Yu. Il'ichev, Y.-B. Jiang, W. Kühnle, K. A. Zachariasse: Recl. Trav. Chim. Pays-Bas 114 (1995), 430-442.
[18] M. Schütz, R. Schmidt: J. Phys. Chem. 100 (1996), 2012-2018.
[19] D. F. Eaton: Pure & Appl. Chem. 60 (1988), 107-1114.
[20] M. P. de Haas, J. M. Warman: Chem. Phys. 73 (1982), 35-53.
[21] W. Schuddeboom:"Photophysical Properties of Opto-Electric Molecules studied by Time-Resolved Microwave Conductivity", Ph.D. Thesis: Delft 1994, ISBN 90-73861-21-7.
[22] J. M. Warman, W. Schuddeboom, S. A. Jonker, M. P. de Haas, M. N. Paddon-Row, K. A. Zachariasse, J.-P. Launay: Chem. Phys. Lett. 210 (1993), 397-404.
[23] C. Reichardt: Chem. Rev. 94 (1994), 2319-2358.
[24] E. Lippert: Z. Naturforsch. 10a (1955), 541-545.
[25] N. Mataga, Y. Kaifu, M. Koizumi: Bull. Chem. Soc. Jpn 28 (1955), 690-691.
[26] H. Beens, A. Weller: Chem. Phys. Lett. 3 (1969), 666-668.
[27] G. F. Mes, B. de Jong, H. J. van Ramesdonk, J. W. Verhoeven, J. M. Warman, M. P. de Haas, L. E. W. Horsman-van den Dool: J. Am. Chem. Soc. 106 (1984), 6524-6528.
[28] K. Yamasaki, K. Arita, O. Kajimoto, K. Hara: Chem. Phys. Lett. 123 (1986), 277-281.
[29] O. Kajimoto, K. Yamasaki, K. Arita, K. Hara: Chem. Phys. Lett. 125 (1986), 184-188.
[30] L. R. Khundkar, A. H. Zewail: J. Chem. Phys. 84 (1986), 1302-1311.
[31] K. Elich, S. Lebus, R. Wortmann, F. Petzke, N. Detzer, W. Liptay: J. Phys. Chem. 97 (1993), 9947-9955.
[32] A.L. McClellan:"Tables of Experimantal Dipole Moments", Rahara Enterprises: El Cerrito 1989, Vol. 2, p 598.
[33] W. Liptay, G. Walz, W. Baumann, H.-J. Schlosser, H. Deckers, N. Detzer: Z. Naturforsch. 26a (1971), 2020-2038.
[34] R. Mathies, A.C. Albrecht: J. Chem. Phys. 60 (1974), 2500-2508.
[35] M. J. Smith, K. Krogh-Jespersen, R. M. Levy: Chem. Phys. 171 (1993), 97-106.
[36] R. W. J. Zijlstra, F. C. Grozema, M. Swart, B. L. Feringa, P. Th. van Duijnen: J. Phys. Chem A 105 (2001), 3583-3590.
[37] M. Jurczok, P. Plaza, W. Rettig, M. M. Martin: Chem. Phys. 256 (2000), 137-148.
[38] V. Nagarajan, A. M. Brearley, T.-J. Kang, P. F. Barbara: J. Chem. Phys. 86 (1987), 3183-3196.
[39] N. Mataga, H. Yao, T. Okada, W. Rettig: J. Phys. Chem. 93 (1989), 3383-3386.

4

THREE-FOLD SYMMETRY[‡]

4.1 INTRODUCTION

The properties of molecules or molecular complexes with a high degree of symmetry are of interest in a large number of research areas. Exciton migration *via* intramolecular excitation transfer[1] and trapping of the excited state upon incorporation of the chromophore in proteins and rigid matrixes[2] has been investigated in relation to the symmetry of these compounds, both theoretically[3,4], and experimentally using picosecond time-resolved polarized fluorescence[5,6] and transient absorption techniques[7]. Moreover, the octupolar

[‡] Chapter 4 has appeared previously as an article: W. Verbouwe, M. Van der Auweraer, F. C. De Schryver, J. J. Piet, J. M. Warman:"Excited state localization or delocalization in C_3-symmetric amino-substituted triphenylbenzene derivatives", J. Am. Chem. Soc. 120 (1998), 1319-1324.

contribution to the large hyperpolarizability, found for several symmetric compounds[8,9], has led to a surge of interest in the nature of the excited state of these symmetric compounds[10,11].

In particular symmetry breaking upon excitation in molecules with 2-fold or 3-fold symmetry, leading to a polar singlet excited state, has been studied. Biaryl compounds such as bianthryl, for instance, are characterized by a polar excited state although they do not carry a specific donor or acceptor subunit[12-17]. Also the excited states of symmetrical amino-substituted triphenyl-benzene derivatives (see Figure 1) and triphenylphosphines [18], are characterized by an increased charge separation with respect to the ground state. Although the large fluorescence rate constant observed for most amino-substituted triphenylbenzene derivatives suggests the formation of a conjugated intramolecular charge transfer state[19], the similarity of the photophysical properties and the solvent dependence of the triphenylbenzene compound, pEFTP, and its biphenyl model compound, pEFBP (Figure 1), suggests the formation of a polar excited state which is localized in one branch of the triphenylbenzene derivative[20]. The importance of geometrical changes to the excited-state deactivation of C_3-symmetric dyes has been demonstrated for triphenylmethane dyes[21-23]. For these compounds an increased planarity in the singlet excited state compared to the propeller-like structure in the ground state has been suggested to explain their photophysical properties[24].

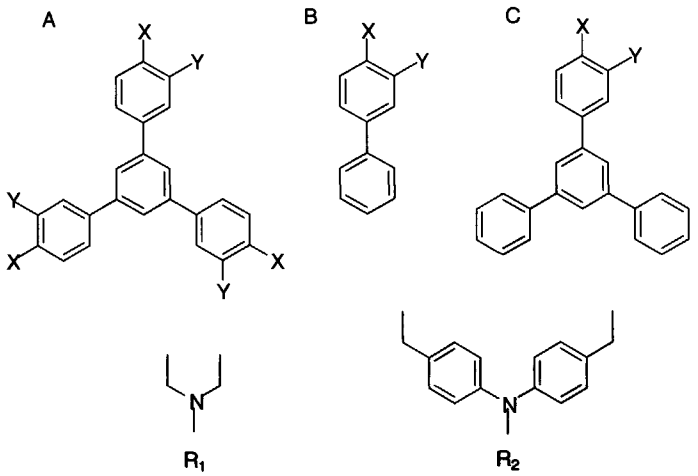

FIGURE 1: Structures of (a) the triphenylbenzene compounds pETP (X = R_1,Y = H), mETP (X = H, Y = R_1), pEFTP (X = R_2,Y = H), and mEFTP (X = H, Y = R_2); (b) the biphenyl model compounds mEBP (X = H, Y = R_1), pEFBP (X = R_2,Y = H), and mEFBP (X = H, Y = R_2); and (c) 1-pETP (X = R_1,Y = H).

In addition to this localization of the excited state, the interaction of the three different branches is expected to result in an intramolecular excitation transfer among the three spatially different branches. Using fluorescence depolarization it is possible to observe this intramolecular excitation transfer because the latter process will be accompanied by a reorientation of the transition dipole resulting in partial depolarization of the emission. The rate of this reorientation of the transition dipoles has been observed for ruthenium(II)

tris(bipyridine) complexes and proteins with a 3-fold symmetry by picosecond polarized transient absorption techniques[25]. If the transition dipoles are in the same plane as the central benzene ring and perpendicular to the symmetry axis, the law of additivity of polarization[26,27], yields a limiting anisotropy, r_0, of 0.1 in the absence of rotational diffusion around any axis in the molecular plane. This has been observed in triphenylene and mesitylene, where a completely delocalized excited state with D_{3h} symmetry is formed[28]. If the intramolecular excitation transfer is slow with respect to the depopulation of the excited state, the limiting anisotropy will rise above 0.1[29].

For pEFTP cyclic voltammetry and coulometry show a unique, reversible, oxidation wave corresponding to a three-electron process. During the partial oxidation of pEFTP, the absorption of near-IR radiation results in the site-to-site migration of the hole by intramolecular electron transfer[30]. It has been demonstrated that this intervalence transition depends only to a limited extent upon substitution in the *meta* position of the central phenyl group[31].

The use of time-resolved microwave conductivity (TRMC) to estimate the change of the dipole moment and the change of the polarizability upon excitation has been demonstrated for several donor-acceptor and other compounds[32-35]. In the analysis of the TRMC transients knowledge of the dipole relaxation time is required in order to obtain absolute values for the dipole moment. It has been shown that for symmetric compounds such as pETP and mETP, the dipole relaxation time involves, in addition to the rotational diffusion time, a relaxation time due to intramolecular excitation transfer[36].

In this contribution the similarity between the photophysical properties of the tri-amino-substituted triphenylbenzene derivatives and their monosubstituted biphenyl or triphenylbenzene model compounds, Figure 1, is used to study the intramolecular excitation transfer in these symmetric compounds. The latter process is described by means of stationary fluorescence depolarization in 1,2-propanediol glass and picosecond time-resolved fluorescence depolarization in benzene.

TRMC transients suggest large excited-state dipole moment and polarizability changes upon excitation of the C_3-symmetric compounds which are explained by the introduction of a picosecond intramolecular dipole relaxation path. The excited state properties of triphenylbenzenes and model compounds in combination with the TRMC transients are used consequently to estimate quantitatively the intramolecular excitation migration.

4.2 EXPERIMENTAL SECTION

See Supporting Information (Appendix A).

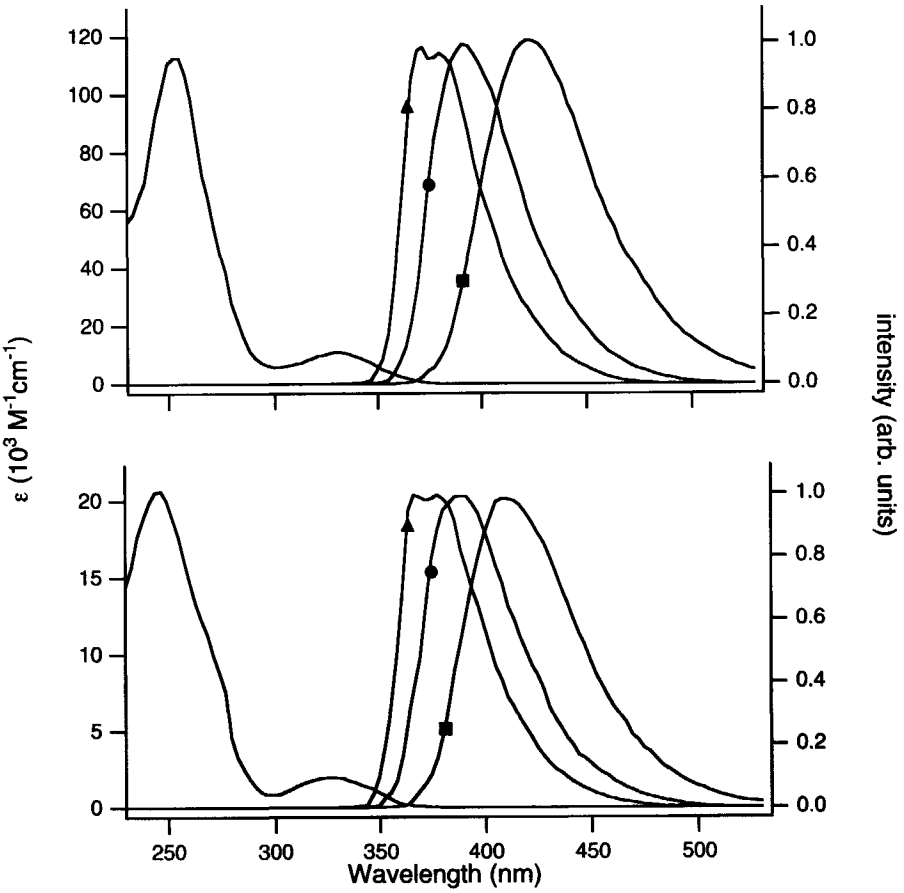

FIGURE 2: Absorption spectrum in acetonitrile and emission spectrum (λ_{ex} = 320 nm) in isooctane (triangle), diethyl ether (circle), and acetonitrile (square) of mETP (top) and mEBP (bottom).

4.3 RESULTS AND DISCUSSION

4.3.1 Photophysical properties of mETP and mEBP.

The absorption spectrum of mETP in acetonitrile at room temperature is characterized by maxima at 332 nm (10 600 $M^{-1}cm^{-1}$) and 256 nm (111 000 $M^{-1}cm^{-1}$). The solvent dependence of the emission maximum of mETP indicates that even in non-polar solvents the emission occurs from a state with a considerable dipole moment. The dipole moment has been estimated from the solvatochromic shift from diethyl ether to acetonitrile at 16.4 ± 1.5 D[19]. Using TRMC measurements, we obtained a value of 14.1 D in benzene[36]. The large Stokes shift which is still observed in apolar solvents is attributed to the difference in equilibrium

geometry between the excited state and the ground state. This effect was reported in detail for pEFTP and pEFBP[24].

More recently, a biphenyl model compound, mEBP, was synthesized. The photophysical properties of mEBP and its solvent dependence are similar to the properties of mETP (see Figure 2). The absorption spectrum at room temperature is not dependent on the solvent polarity and is characterized in acetonitrile by a strong absorption with a maximum at 247 nm (21 000 $M^{-1}cm^{-1}$) and a weak absorption at 330 nm (2400 $M^{-1}cm^{-1}$) which matches the absorption spectrum of mETP in the same solvent. This similarity between mETP and mEBP suggests that upon excitation, the 3-fold symmetry disappears and the Franck-Condon excited state will probably be localized in one branch of mETP. Moreover, the molar extinction coefficients of mEBP are approximately one-third of the value obtained for mETP. Despite the structural differences between mETP and mEBP, the emission occurs in a similar wavelength region and shows a similar solvent dependence. Upon excitation, charge transfer leads to a polar excited state which induces a solvatochromic shift of the emission. The substitution of two ethylanilino groups in the *meta* position of the central phenyl ring in mETP has only a marginal effect upon the emission.

4.3.2 Fluorescence depolarization of mETP and its biphenyl model compound mEBP in propanediol glass.

The polarization of the emission of the biphenyl model compound mEBP has been measured in 1,2-propanediol at -60 °C. At this temperature, at which the solvent forms a rigid glass, no depolarization of the emission occurs through rotational diffusion, and the anisotropy r, reaches the limiting anisotropy r_0. When excitation occurs in the S_0-S_1 absorption band (λ_{ex} = 340 nm), the anisotropy increases from 0.22 to 0.33 at 11 °C and -36 °C, respectively, and reaches 0.35 at -60 °C. The limiting anisotropy is almost 0.4, which means that the transition dipoles of absorption and emission are close to collinear. Moreover, the anisotropy of mEBP stays constant over the whole emission wavelength region which indicates that only one emission (S_1-S_0) contributes to the emission band. The minor difference between the anisotropy at -36 °C and -60 °C suggests that at temperatures below -36 °C the molecular rotational diffusion is slow with respect to the fluorescence lifetime.

The anisotropy of mETP (λ_{ex} = 350 nm), however, increases from 0.14 to 0.22 and to 0.28 when the temperature decreases from 0 °C to -27 °C to -60 °C, respectively, and stays constant over the whole emission wavelength region. Moreover, the anisotropy reaches no plateau value around -30 °C for mETP and is smaller than the model compound although the volume of mETP is larger than for mEBP and the lifetime of fluorescence is similar for both compounds (9.3 ns and 7.3 ns for mETP and mEBP in acetonitrile, respectively).

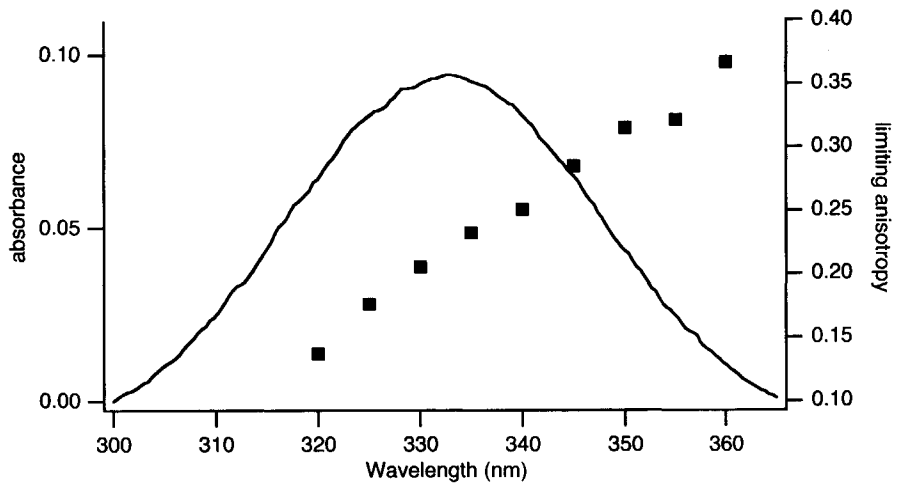

FIGURE 3: Increase of the limiting anisotropy of mETP in 1,2-propanediol at -60 °C upon excitation at the red edge of the S_0-S_1 absorption band (λ_{em} = 430 nm).

This indicates that in mETP depolarization occurs by another mechanism in addition to molecular rotation. This mechanism could be intramolecular excitation transfer which will rotate the transition dipole over 120°in a molecular plane. The limiting anisotropy r_0, however, should be equal to 0.1 for molecules with a 3-fold symmetry when intramolecular excitation transfer redistributes the excitation energy among the three spatially degenerate transition dipole moments[28]. This means that, in the present case, the intramolecular excitation transfer is slow with respect to the lifetime of the excited state. The latter process becomes relatively more important at lower temperatures where the rotation of the molecule is blocked.

In contrast to what was observed for mEBP, the limiting anisotropy increases when the excitation occurs at the red edge of the S_0-S_1 absorption spectrum of mETP (Figure 3). In this excitation region, the emission becomes more polarized and a limiting anisotropy close to the maximum value of 0.4 can be found.

This cannot be due to overlap with other transitions or to scattered light because the emission was monitored at 390 nm where no scattered light is observed. Also, when the excitation spectra were obtained at a longer emission wavelength the limiting anisotropy r_0 observed became larger. This increase of r_0 indicates that excitation transfer between the three branches becomes less efficient when excitation occurs at the red edge of the absorption spectrum. A possible explanation of this increase could be a reduction of the 3-fold symmetry of mETP in 1,2-propanediol at low temperatures. Under these conditions the solvent configuration around, as well as the phenyl-phenyl and amino-phenyl torsion angles in the three branches, could be slightly different. If this configuration persists for a time which is

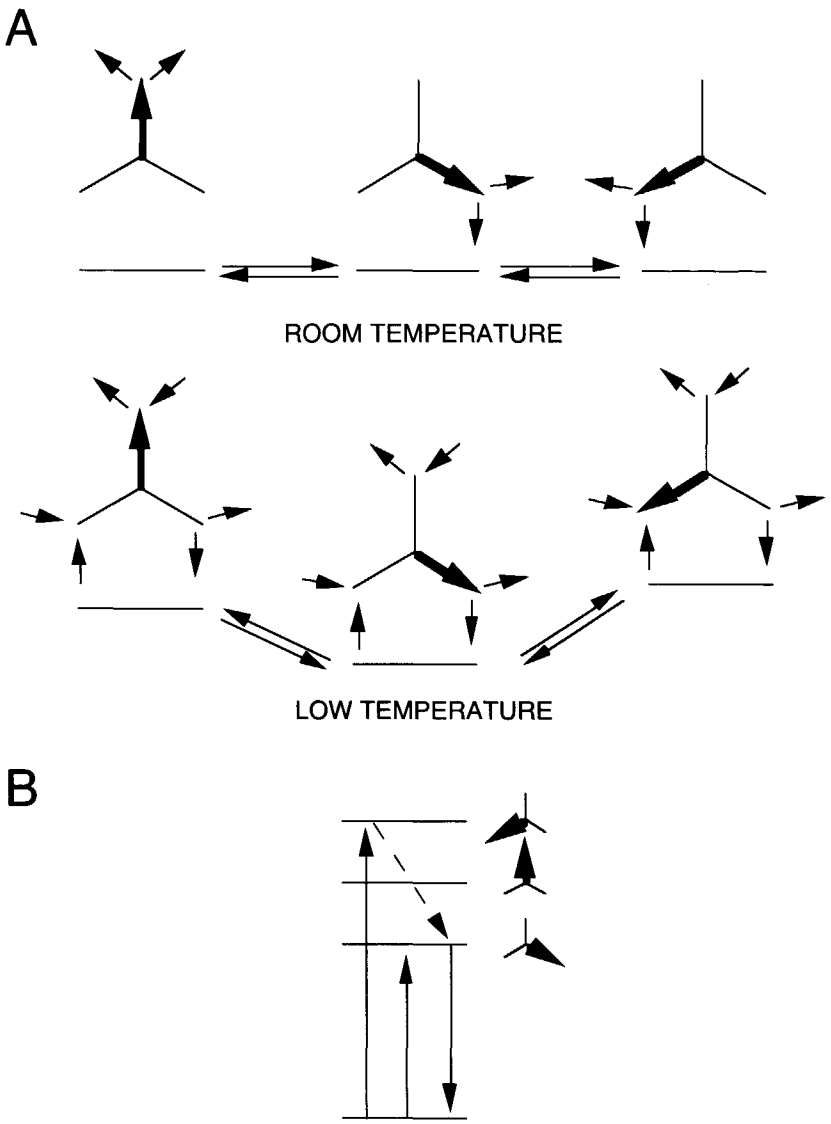

FIGURE 4: (A) Scheme of the transition dipole relaxation process of mETP at room temperature and at low temperature. The large and small arrows represent the orientation of the transition dipole and the solvent, respectively. (B) Relaxation of the transition dipole moment at low temperature upon excitation at short or long wavelengths.

long compared to the excited-state lifetime, the excited state of the three branches will be stabilized to a different extent by dipole-dipole interactions or hydrogen bonding on one hand, and because of geometrical interactions on the other hand (Figure 4A). Here we assume that solvation of the three branches of mETP is to a certain extent uncorrelated. At -60 °C, the

excitation migration will be determined by high-frequency vibrations of the solute and solvent matrix surrounding the polar excited state.

Under these conditions excitation at the red edge of the absorption band will excite that branch of mETP where the dipolar excited state has the largest stabilization. Hence excitation transfer to other branches will become endergonic. This will slow the rate of excitation transfer and will increase the anisotropy. On the other hand, excitation at shorter wavelengths will excite other branches where the dipolar excited state experiences a smaller solvent stabilization and hence excitation transfer to other branches will become exergonic. This will increase the rate of excitation transfer and decrease the anisotropy (Figure 4B).

4.3.3 Time-resolved fluorescence depolarization of pEFTP and its biphenyl model compound pEFBP in benzene.

The time-resolved depolarization of the fluorescence of pEFTP and pEFBP at room temperature in benzene was obtained and analyzed as described in the experimental section. The decays were obtained with a time increment of 3.7 ps per channel so that excited-state processes slower than 20 ps could be resolved. The fluorescence depolarization decay of the biphenyl pEFBP could be analyzed as a monoexponential fluorescence decay (τ = 1.068 ± 0.003 ns) and a single rotational relaxation time (Θ = 90 ± 8 ps) with good acceptable statistical parameters. The β value of 0.31 ± 0.02 corresponds to the limiting anisotropy. The latter property indicates a nearly parallel orientation of the absorption and emission transition dipole for the biphenyl compound pEFBP in benzene at room temperature, similar to that suggested for mEBP in propanediol glass at -60 °C.

The fluorescence depolarization decay of the C_3-symmetric pEFTP could be analyzed as a monoexponential fluorescence decay (τ = 1.059 ± 0.003 ns) with one rotational relaxation time Θ = 320 ± 40 ps. The small β-value of 0.077 ± 0.004, however, suggests an additional relaxation mechanism in the excited state through intramolecular excitation transfer. No improvement of the fit, however, is observed when a second relaxation time is introduced. Despite the picosecond resolution of the experimental setup, no direct measurement of the relaxation time associated with the latter process could be obtained. The relaxation time Θ can be assigned to the rotational diffusion out of plane of pEFTP in benzene at room temperature.

4.3.4 Time-resolved microwave conductivity.

On photoexcitation, a transient change of the permittivity was observed for all compounds in benzene solution (Figure 5). The transients measured at the resonance frequency, f_0, are proportional to the change in the dielectric loss, $\Delta\varepsilon''$, and are characterized by a rise, followed by a slow decay. Initially after excitation, mainly the singlet excited state

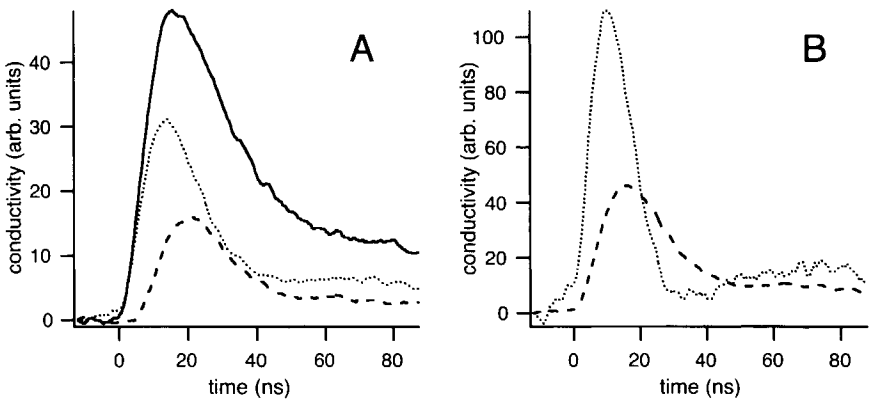

FIGURE 5: (A) Typical TRMC transients observed on flash photolysis of a solution of 1-pETP in benzene at the cavity resonance frequency f_0 (full line), and at the upper, f+ (dashed), and lower, f- (dotted), half-power frequency. (B) The sum $\Sigma\pm$ (dashed), and difference, $\Delta\pm$ (dotted), combinations of the transients monitored at the half-power frequencies for the traces in (A). $\Sigma\pm$ is proportional to $\Delta\varepsilon''$ and $\Delta\pm$ is a function of $\Delta\varepsilon'$.

contributes to the observed transient, whereas at longer times after the excitation, the signal is due to the triplet excited state. Lifetimes for the singlet and triplet state were obtained separately from the fluorescence decay, using the single-photon counting technique, and from the TRMC transients at long times after the laser pulse. The fast component of the TRMC signal corresponds to the singlet lifetime. This justifies the attribution of the dielectric loss to the dipolar character of both S_1 and T_1 and their amplitude can be used to calculate the charge separation in the excited state. The transient changes of the dielectric loss recorded for pEFTP, mEFTP, and mETP were compared to their biphenyl model compounds, pEFBP, mEFBP, and mEBP. The transients of pETP were compared to those of 1-pETP, the singlet properties of which are closer to those of pETP than to those of a biphenyl model derivative of pETP.

From the fits, μ_S^2/Θ can be determined, where μ_S is the dipole moment of S_1 and Θ is the dipole relaxation time (Table I). Normally the dipole relaxation time is determined by the rotational diffusion, and can be calculated using an empirical expression based on an assumed shape. Because of their comparable shape, Θ will not depend significantly on the substitution (*meta* or *para*) for isomeric compounds. The ratio of the dipole moments of the *meta* and *para* compounds will therefore be given to a good approximation, if $(\omega\Theta)^2$ (where ω is the

TABLE I: Decay time, dipole moment, rotational relaxation time and polarizability volume.

compound	τ_{FL} (ns)	μ_s^2/Θ (D^2/ps)	μ_s^2/a^3 ($D^2/Å^3$)[a]	Θ_R (ps)[b]	μ_s (D)[c]	$\Delta\alpha'$ ($Å^3$)[d]
pEFTP	1.3	1.58	1.00	244	19.7	583
pEFBP	1.2	0.54	0.96	94	7.2	186
mEFTP	4.2	0.39	1.01	244	9.7	103
mEFBP	4.1	0.33	0.95	94	5.7	87
pETP	9.7	0.42	0.54	130	7.5	370
1-pETP	10.7	0.75	0.84	94	8.5	130
mETP	6.2	0.79	1.03	130	10.2	176
mEBP	2.9	1.06	0.81	56	8.0	92

[a] Slope of the emission maximum versus the solvent polarity; a is the solvent cavity radius. [b] The calculated rotational relaxation time for a dipole oriented in the plane of a sphere-shaped molecule. [c] Singlet dipole moment based on $\Theta = \Theta_R$. [d] Overall polarizability volume.

reciprocal radian frequency of the microwaves ($1/\omega \approx 15$ ps) used) was larger than 1, by:

$$\frac{\mu_s^{para}}{\mu_s^{meta}} = \sqrt{\frac{\left(\frac{\mu_s^2}{\Theta}\right)_{para}}{\left(\frac{\mu_s^2}{\Theta}\right)_{meta}}} \qquad (1)$$

This ratio can also be derived from solvatochromism because the solvent cavity radius depends also only slightly on the position of the substitution. Although agreement between the TRMC and solvatochromism result is found for pEFBP versus mEFBP, this is not the case for pEFTP versus mEFTP. Although an almost equal dipole moment is suggested by solvatochromism, the ratio μ_s^{pEFTP} / μ_s^{mEFTP} in the TRMC experiment (Table I) is 2.02. On substituting for Θ the *a priori* calculated value of the rotational relaxation time of a sphere-shaped molecule[37], the dipole moment for the biphenyl model compounds calculated is close to that obtained from solvatochromism[19]. The use of a sphere to model the rotational relaxation is supported by the correspondence with the experimentally obtained relaxation times in benzene by time-resolved fluorescence depolarization. The dipole moments of the triphenylbenzene derivatives determined in the same way are, however, larger than those obtained from the solvatochromic data. This discrepancy can be resolved if the dipole relaxation time of the triphenylbenzene derivatives is in fact much shorter than the rotational relaxation time of these molecules. This will be the case if intramolecular excitation transfer between the three branches occurs. Hence the rotational (Θ_R) and intramolecular (Θ_I) dipole relaxation times will both contribute to the overall dipole relaxation time Θ:

$$\frac{1}{\Theta} = \frac{1}{\Theta_R} + \frac{1}{\Theta_I} \qquad (2)$$

From the sum, $\Sigma\pm$, of a pair of TRMC transients observed at the half-power frequencies f+ and f-, $\Delta\varepsilon''$ can also be obtained and yields results identical to the measurements at f_0. From the difference, $\Delta\pm$, of these transients the change of the real component of the permittivity, $\Delta\varepsilon'$, can be obtained. This change is related to the change of the polarizability, $\Delta\alpha$, upon excitation (for more details see reference 34) *via*:

$$\Delta\varepsilon' = N_* \frac{[\varepsilon(\infty)+2]^2}{9\varepsilon_0}\Delta\alpha \qquad (3)$$

In equation (3), N_* is the concentration of excited molecules, $\varepsilon(\infty)$ is the relative dielectric constant of the solvent at high frequency, which can be equated with the square of the refractive index, and ε_0 corresponds to the permittivity of vacuum. It is most convenient to discuss them in terms of the change of the polarizability volume, $\Delta\alpha'$, given by:

$$\Delta\alpha' = \frac{\Delta\alpha}{4\pi\varepsilon_0} \qquad (4)$$

The value of $\Delta\alpha'$ is a measure of the degree of delocalization of the electron wave function in the excited state. The polarizability volume changes of the triphenylbenzene and the model compounds are listed in Table I. The *para*-substituted compounds display a much larger $\Delta\alpha'$ compared to the corresponding *meta* compounds, which suggests that the electronic delocalization is affected by the position of the substitution. More suprising is the much larger polarizability of the symmetric triphenylbenzene derivates, compared to the model compounds, despite their similar photophysical properties. For instance, $\Delta\alpha'$ amounts to 186 $Å^3$ for pEFBP but is no less than 583 $Å^3$ for pEFTP. To explain this large discrepancy, we assume that for the model compounds the dipole relaxation process can only occur by relaxation of the whole molecule via tumbling, characterized by $\Theta = \Theta_R$. This value was used to calculate μ_s from the TRMC experiments and yielded values in agreement with those from the solvatochromism. However, as already discussed, this was not the case for the triphenylbenzene derivatives, the Θ of which must be much shorter than the Θ_R, indicating the occurrence of flip-flop intramolecular relaxation process.

Because of the fast dipole relaxation, $\Delta\varepsilon'$ has to be considered to consist not only of an electronic contribution, $\Delta\alpha'_e$, but also a dipole contribution, $\Delta\varepsilon'_D$. Thus:

$$\Delta\varepsilon' = \Delta\varepsilon'_e + \Delta\varepsilon'_D \qquad (5)$$

in which:

$$\Delta\varepsilon'_e = N_* \frac{[\varepsilon(\infty)+2]^2}{9\varepsilon_0} \Delta\alpha_e \tag{6}$$

$$\Delta\varepsilon'_D = N_* \frac{[\varepsilon(\infty)+2]^2}{27\varepsilon_0 k_b T} \left[\frac{\mu_*^2}{1+(\omega\Theta_*)^2} - \frac{\mu_0^2}{1+(\omega\Theta_0)^2} \right] \tag{7}$$

In equation (7), the subscripts 0 and * refer to the ground state and the excited state, respectively. If $\mu_0 = 0$, which is a realistic assumption for the triphenylbenzene compounds, equation (7) can be simplified, because the last term drops out. By using equations (3) and (4), $\Delta\alpha'_i$ can be expressed as $\Delta\varepsilon'_i$, in which the subscript i can be either e or D.

Normally, if $\Theta = \Theta_R$, the denominator in equation (7) is large and $\Delta\varepsilon'_D$ will be close to zero and can therefore be neglected. In the case of the biphenyl model compounds where Θ is indeed large (Table I), $\Delta\alpha'_e$ will be overestimated by no more than 5 $Å^3$, due to neglect of the dipolar contribution. This is within the experimental error. The large polarizability of the triphenylbenzene derivatives suggests that in addition to the electronic component (equation (6)), the dipolar term (equation (7)) contributes to the observed polarizability. To quantify this contribution, the similarity of the photophysical properties between the symmetric triphenylbenzene compounds (TP) and the related biphenyl compounds (BP) is used and it is assumed reasonable that both will have an equal electronic polarizability:

$$\Delta\alpha_e'^{TP} = \Delta\alpha_e'^{BP} \tag{8}$$

With this assumption and using equations (3) and (4) to calculate $\Delta\varepsilon'_D$ from $\Delta\alpha'_D$, $\Delta\varepsilon'_D{}^{TP}$ can be estimated from equation (5) for the triphenylbenzene derivatives. These results indicate an important difference between the *para*- and *meta*-substituted compounds. Whereas the polarizability has mainly an electronic origin for the *meta* compounds, the dipolar contribution is the main contribution for the *para* compounds. From the calculated $\Delta\varepsilon'_D{}^{TP}$, Θ can be estimated *via*:

$$\frac{\Delta\varepsilon''}{\Delta\varepsilon'_D} = \omega\Theta \tag{9}$$

The dipole relaxation is an order of magnitude faster than the rotational dipolar relaxation, Θ_R. Thus Θ must be almost completely determined by the intramolecular excitation transfer. The flip-flop mechanism occurs in the subnanosecond time regime with an intramolecular dipole relaxation time, Θ_I,of 10 ps for pEFTP and 73 ps for mEFTP. Using the

TABLE II: Calculated dipole moment, μ_S,and intramolecular dipole relaxation time Θ_I (Flip-Flop) for the triphenylbenzene derivatives assuming $\Delta\alpha'_D{}^{TP}=\Delta\alpha'^{TP}-\Delta\alpha'^{BP}$.

compound	$\Delta\alpha'^{BP}$ (Å^3)	$\Delta\alpha'^{TP}$ (Å^3)	μ_S (D)	Θ (ps)	Θ_I(ps)
pEFTP	186	397	7.9	9.3	9.7
mEFTP	87	16	4.9	56.3	73.1
pETP	130	240	5.5	4.2	4.3
mETP	92	84	5.3	22.4	27.1

same procedure to estimate Θ_I for pETP and mETP yields relaxation times of 4 and 27 ps, respectively. The difference between pEFTP and mEFTP or pETP and mETP is attributed to the smaller interaction between the three amino sites in the *meta*-substituted compounds, compared to the *para*-substituted compounds.

The dipole moment of the excited state can be obtained from the analysis of the TRMC transients at the resonance frequency, f_0, and the dipole relaxation time, which includes the molecular rotational diffusion and the flip-flop relaxation process and is given in Table II. These dipole moments are more plausible than those reported in Table I where only Θ_R was considered. The fast dipole relaxation has been suggested not only for mETP in propanediol at -60 °C but also for other triphenylbenzene derivatives in benzene at room temperature. For pEFTP, it has been demonstrated by time-resolved fluorescence depolarization that excitation transfer between the three branches occurs at times shorter than 20 ps.

4.4 CONCLUSION

The localized character of the polar excited state of amino-substituted triphenylbenzene derivatives with a 3-fold symmetry has been studied. The similar absorption and emission properties of the symmetric compounds and the model compounds indicate that the excited state reached immediately after excitation and vibrational relaxation is localized in one branch of the 3-fold symmetric compound. During the lifetime of the excited state, however, intramolecular excitation transfer occurs between three energetically degenerate excited states. This redistribution of transition dipoles will depolarize the emission to a certain extent. Hence the limiting anisotropy of mETP is smaller than 0.4 which has been observed for the model compound mEBP and indicates collinear transition dipoles for the latter compound. Because of this flip-flop mechanism, the relaxation of the dipole involves, in addition to the rotational diffusion, an intramolecular relaxation path. The importance of this process has been demonstrated in the analysis of the TRMC transients where it is necessary to obtain a similar excited-state dipole moment for the triphenylbenzene and its model compound consistent with the solvatochromic shift of the emission.

If the exciton was redistributed completely among the three sites during the lifetime of the excited state, the limiting anisotropy, however, would be 0.1. The larger value experimentally obtained for mETP suggests that the flip-flop between different sites in 1,2-propanediol at -60 °C is slow with respect to the other deactivation processes of S_1. This probably is due to a relatively small interaction between the three branches. Moreover, in a rigid glass matrix, the three sites will be stabilized to a different extent in the polar excited state so that the degeneracy disappears. This is translated in an increase of the limiting anisotropy when excitation occurs in the red edge of the absorption band. The exciton will be trapped in the most stable site from where emission mainly will occur. For pEFTP in benzene at room temperature the limiting anisotropy is close to 0.1 and suggests a fast intramolecular excitation transfer compared to the excited-state lifetime.

Upon excitation, a relatively large increase of the polarizability which consists of an electronic and dipolar contribution, is observed for all compounds. Although for the model compounds the dipolar contribution is negligible, the large dipolar contribution for the symmetric compounds indicates an intramolecular excitation transfer in the time range of the reciprocal radian frequency ω. The dipole relaxation time associated with the latter process has been estimated to be approximately 10, 73, 4, and 27 ps for pEFTP, mEFTP, pETP, and mETP, respectively. The *meta*- or *para*-substitution pattern, as well as the molecular geometry of the molecule and the solvent reorganization around the branches, influences the interaction between the three amino sites and hence determines the rate of intramolecular excitation transfer.

ACKNOWLEDGEMENT

W.V. acknowledges the IWT for a scholarship. M.V.d.A. is an Onderzoeksdirekteur of the FWO-Vlaanderen. The authors gratefully acknowledge the FKFO, the "Nationale Loterij", and the continuing support from DWTC (Belgium) through IUAP IV-11. This investigation is supported by the Dutch Foundation for Chemical Research (SON) with financial aid from the Dutch Organization for Scientific Research (NWO).

REFERENCES

[1] L. B. A. Johansson, P. Edman, P. O. Westlund: J. Chem. Phys. 105 (1996), 10896-10904.
[2] D. L'Espérance, E. L. Chronister: Chem. Phys. Lett. 222 (1994), 217-223.
[3] A. A. Demidov, D. L. J. Andrews: Photochem. Photobiol. 63 (1996), 39-52.
[4] A. A. Demidov: Appl. Opt. 33 (1994), 6303-6304.
[5] N. C. Maiti, S. Mazumdar, N. Periasamy: J. Phys. Chem. 99 (1995), 10708-10715.
[6] P. A. Lyle, ; W. S. Struve: Photochem. Photobiol. 53 (1991), 359-365.
[7] R. E. Riter, M. D. Edington, W. F. Beck: J. Phys. Chem. B. 101 (1997), 2366-2371.
[8] O. F. J. Noordman, N. F. van Hulst: Chem. Phys. Lett. 253 (1996), 145-150.
[9] T. Verbiest, K. Clays, C. Samyn, J. Wolff, D. Reinhoudt, A. Persoons: J. Am. Chem. Soc. 116 (1994), 9320-9323.

[10] J. Zyss, I. Ledoux: Chem. Rev. 94 (1994), 77-105.
[11] J. L. Brédas, F. Meyers, B. M. Pierce, J. Zyss: J. Am. Chem. Soc. 114 (1992), 4928-4929.
[12] F. Schneider, E. Lippert: Ber. Bunsenges. Phys. Chem. 72 (1968), 1155-1160;
[13] F. Schneider, E. Lippert: Ber. Bunsenges. Phys. Chem. 74 (1970), 624-630.
[14] H. Laguitton-Pasquier, R. Pansu, J. P. Chauvet, A. Collet, J. Faure, R. Lapouyade: Chem. Phys. 212 (1996), 437-455.
[15] R. J. Visser, P. C. M. Weisenborn, P. J. M. van Kan, B. H. Huizer, C. A. G. O. Varma, J. M. Warman, M. P. de Haas: J. Chem. Soc., Faraday Trans. 2 81 (1985), 689-704.
[16] D. B. Toublanc, R. W. Fessenden, A. Hitachi: J. Phys. Chem. 93 (1989), 2893-2896.
[17] J. Dobkowski, Z. R. Grabowski, B. Paeplow, W. Rettig, K. H. Koch, K. Müllen, R. Lapouyade: New J. Chem. 18 (1994), 525-533.
[18] M. Vogel, W. Rettig, P. Heimbach: J. Photochem. Photobiol., A Chem. 61 (1991), 65-75.
[19] G. Verbeek, S. Depaemelaere, M. Van der Auweraer, F. C. De Schryver, A. Vaes, D. Terrell, S. De Meutter: Chem. Phys. 176 (1993), 195-213.
[20] W. Verbouwe, M. Van der Auweraer, F. C. De Schryver, R. Pansu, J. Faure in "Proceedings AIP Conference on Fast Elementary Processes in Chemical and Biological Systems, Villeneuve d'Ascq 1995", A. Tramer Ed., Woodbury: New York 1996, p 429
[21] Th. Förster, G. Hoffman: Z. Phys. Chem., Neue Folge 75 (1971), 63-76.
[22] M. M. Martin, P. Plaza, Y. H. Meyer: J. Phys. Chem. 1991, 95, 9310-9314.
[23] M. Vogel, W. Rettig: Ber. Bunsenges. Phys. Chem. 89 (1985), 962-968.
[24] W. Verbouwe, L. Viaene, M. Van der Auweraer, F. C. De Schryver, H. Masuhara, R. Pansu, J. Faure: J. Phys. Chem. A 101 (1997), 8157-8165.
[25] L. F. Cooley, P. Bergquist, D. F. Kelley: J. Am. Chem. Soc. 112 (1990), 2612-2617.
[26] G. Weber: Biochem. J. 51 (1952), 145-155.
[27] H. Zimmermann, N. Joop: Z. Electrochem. 65 (1961), 61-65.
[28] R. D. Hall, B. Valeur, G. Weber: Chem. Phys. Lett. 116 (1985), 202-205.
[29] E. Leroy, H. Lami: Chem. Phys. Lett. 41 (1976), 373-377.
[30] J. Bonvoisin, J.-P. Launay, M. Van der Auweraer, F. C. De Schryver: J. Phys. Chem. 98 (1994), 5052-5057.
[31] J. Bonvoisin, J.-P. Launay, W. Verbouwe, M. Van der Auweraer, F. C. De Schryver: J. Phys. Chem. 100 (1996), 17079-17082.
[32] W. Schuddeboom, S. A. Jonker, J. M. Warman, U. Leinhos, W. Kühnle, K. A. Zachariasse: J. Phys. Chem. 96 (1992), 10809-10819.
[33] S. I. van Dijk, P. G. Wiering, C. P. Groen, A. M. Brouwer, J. W. Verhoeven, W. Schuddeboom, J. M. Warman: J. Chem. Soc. Faraday Trans. 91 (1995), 2107-2114.
[34] M. R. Roest, J. W. Verhoeven, W. Schuddeboom, J. M. Warman, J. M. Lawson, M. N. Paddon-Row: J. Am. Chem. Soc. 118 (1996), 1762-1768.
[35] J. M. Warman, W. Schuddeboom, S. A. Jonker, M. P. de Haas, M. N. Paddon-Row, K. A. Zachariasse, J.-P. Launay, Chem. Phys. Lett. 210 (1993), 397-404.
[36] W. Schuddeboom, J. M. Warman, M. Van der Auweraer, F. C. De Schryver, D. D. Declerq: Chem. Phys. Lett. 222 (1994), 586-591.
[37] W. Schuddeboom:"Photophysical Properties of Opto-Electric Molecules studied by Time-Resolved Microwave Conductivity", Ph.D. Thesis: Delft 1994, ISBN 90-73861-21-7, p 71-78.

APPENDIX A, Supporting Information.

The synthesis of the whole series of triphenylbenzene derivatives (TP) pETP, mETP, pEFTP, mEFTP has been described previously[a]. The biphenyl model compounds (BP) have been synthesized starting from nitrobiphenyl (Acros) using a similar procedure. 1-pETP has been synthesized from mono-amino triphenylbenzene, prepared earlier from tri-amino triphenylbenzene[b]. Absorption spectra were recorded with a Perkin Elmer Lambda 6 UV/VIS spectrometer. 1,2-Propanediol (Aldrich) was of analytical quality and checked for fluorescence before use. Benzene (Fluka) was of UV spectroscopic grade. The temperature, monitored inside the cuvette, is controlled by a methanol filled Dewar system to prevent condensation and a Lauda RUL 480 thermostat-cryostat using a RPt100 resistor.

Steady-state fluorescence spectra are measured with an SLM-8000C spectrofluorimeter in L-format. The depolarization of the emission spectra $\langle r(\lambda_{em})\rangle$ is obtained by passing the excitation and emission light through a Glan-Thompson polarizer, and correcting for the bias in the detection system, using:

$$\langle r(\lambda_{em})\rangle = \frac{I_{VV}(\lambda_{em}) - G(\lambda_{em})I_{VH}(\lambda_{em})}{I_{VV}(\lambda_{em}) + 2G(\lambda_{em})I_{VH}(\lambda_{em})} \qquad \text{(A.1)}$$

where G is an instrumental factor given by:

$$G(\lambda_{em}) = \frac{I_{HV}(\lambda_{em})}{I_{HH}(\lambda_{em})} \qquad \text{(A.2)}$$

In these equations, I stands for the fluorescence intensity, and the first and second subscript refer to the settings of the excitation and emission polarizer respectively (V for vertical and H for horizontal orientation). In order to eliminate the possibility of intermolecular energy transfer, the optical density of the sample was below 0.2 at the long wavelength absorption maximum which corresponds to a concentration of the order of 10^{-5} M.

The polarized emission decays are obtained by the single-photon counting technique. Pulses at 330 nm from a frequency-doubled "KITON red" dye laser, pumped by a beam-locked argon ion laser at 514 nm were used for excitation. The fluorescence photons are detected by a microchannel plate and the full width at half-maximum of the instument response function (IRF) is typically around 50 ps. The decays are collected at three different orientations of the emission polarizer θ (0°, 54.7° and 90°) with a time window of 3.7 ps/channel. The number of counts in the peak channel is around 10000. The decays are simultaneously analysed with the IRF as reference using a global analysis fitting program

according to:

$$i(\theta,t) = \left[\kappa(\theta)/3\right]\alpha\exp\left(-t/\tau\right)\left[1+\left(3\cos^2\theta-1\right)\right]\beta\exp\left(-t/\Theta\right) \qquad \text{(A.3)}$$

where τ represents the fluorescence decay time and Θ the rotational relaxation time. The quality of the fit to the experimental decay is expressed by the χ_g^2 value (<1.2)[c].

For the time-resolved microwave conductivity (TRMC) measurements dilute solutions ($\approx 10^{-4}$ M) were photoexcited using a 7 ns, 308 nm pulse from a Lumonics HyperEX-420 excimer laser. Intensities corrsponding to considerably less than one absorbed photon per solute molecule in the beam path were used for the data reported. Any change occuring in the complex permittivity of the solution, $\Delta\varepsilon^*$, on photo-excitation was monitored as described previously[d-f]. By measuring at the microwave cavity resonance frequency ($f_0 \approx 9.5$ GHz), only changes in the dielectric loss, $\Delta\varepsilon''$, resulting from changes in the dipole moment of the solute molecules are observed. Combined changes in $\Delta\varepsilon''$ and the real component of the permittivity, $\Delta\varepsilon'$, which also results from a change in the molecular polarizability, can be monitored by measuring at the half-resonance frequencies[d].

[a] M. Van der Auweraer, F. C. De Schryver, G. Verbeck, C. Geelen, D. Terrell, S. De Meutter: Eur. Pat. EPP 349034.

[b] J. Bonvoisin, J.-P. Launay, W. Verbouwe, M. Van der Auweraer, F. C. De Schryver: J. Phys. Chem. 97 (1993), 17079-17082.

[c] M. Crutzen, M. Ameloot, N. Boens, R. M. Negri, F. C. De Schryver: J. Phys. Chem. 97 (1993), 8133-8145.

[d] J. M. Warman, W. Schuddeboom, S. A. Jonker, M. P. de Haas, M. N. Paddon-Row, K. A. Zachariasse, J.-P. Launay, Chem. Phys. Lett. 210 (1993), 397-404.

[e] J. M. Warman, M. P. de Haas in "Pulse Radiolysis", Y. Tabata Ed., CRC Press, Boca Raton 1991, ch.6.

[f] M. P. de Haas, J. M. Warman: Chem. Phys. 73 (1982), 35-53.

5

SIX-FOLD SYMMETRY[‡]

5.1 INTRODUCTION

Since the discovery of circular chlorophyllic arrays within the photosynthetic machinery of certain light-harvesting bacteria[1,2] there has been intense interest in the mechanism of energy storage and rotary diffusion within such antenna complexes[3-9]. This interest arises from a curiosity in the workings of natural photosynthesis itself and from the possibility that similar molecular complexes could be synthesised in the laboratory and their unique properties utilised in man-made solar energy conversion devices. In the present work we have synthesised a simple model compound for such circular chromophoric arrays with

[‡] Chapter 5 has appeared previously as an article: J. J. Piet, H. A. M. Biemans, J. M. Warman, E. W. Meijer: "Rapid rotation of energy in the excited state of a circular hexa-carbazole array", Chem. Phys. Lett. 289 (1998), 13-18.

the intention of investigating whether its photophysical properties resemble those of the much more complex natural systems. We have found that this is in fact the case with rapid, rotary diffusion of energy occurring in a time of 3 picoseconds via a transient, dipolar excimer-like state. Our molecule consists of a circular array of six carbazole moieties arranged around a benzene core, in a propeller configuration as shown in Figure 1.

5.2 EXPERIMENTAL

Hexacarbazolylbenzene, HCB, was prepared by an adaptation of the synthetic procedure reported for hexapyrrolylbenzene[10], using the sodium anion of carbazole and hexafluorobenzene. Because of the poor solubility of HCB the dodeca-hexyl substituted derivative, DDH-HCB, was synthesised and was used in most of the measurements. Where comparison was possible the optical properties of HCB and DDH-HCB were found to be almost identical after correction for monomer impurity in the former, less soluble and more difficult to purify, compound. The substituted carbazole precursor of DDH-HCB was prepared by Friedel-Crafts acylation, followed by Clemmensen reduction. For a full description of the synthesis and the characterization of the products by ^{1}H-NMR, ^{13}C-NMR, elemental analysis and FD-MS see reference 11. The monomeric reference compound N-phenyl-carbazole, MCB, was purchased from Aldrich. The chemical structures of MCB, HCB and DDH-HCB are shown in figure 2. The solvents used were all UV spectroscopic grade.

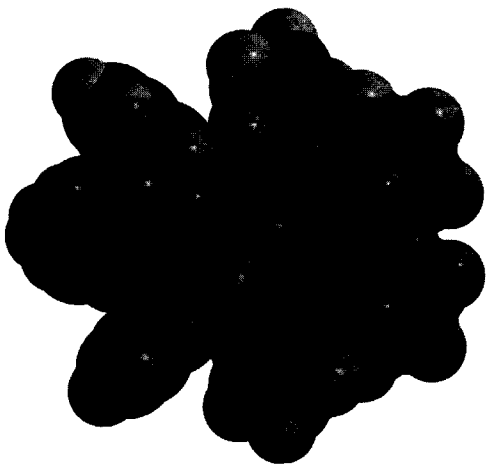

FIGURE 1: Space-filling model of HCB showing the propeller-like conformation of the carbazoles.

Optical absorption spectra were measured using a Kontron "Uvikon-940" UV/VIS spectrophotometer. Fluorescence excitation and emission spectra were measured using a PTI (Photon Technology International) "Quantamaster-1" spectrofluorimeter equipped with a double excitation and a single emission monochromator. Excitation spectra, monitored at the fluorescence maximum, were identical to the absorption spectra for MCB and DDH-HCB in all solvents. The fluorescence decay times given in Table I for benzene solutions were determined by flash-photolysis using a 0.8-ns pulse of 337-nm light from a Laser Photonics

"LN1000" nitrogen laser with a Jobin Yvon monochromator and a Photek "PMT-113-UHF" channel-plate photomultiplier as detector.

Changes in the real and imaginary components of the complex microwave conductivity on photoexcitation, using a 7-ns, 308-nm pulse from a Lumonics "HyperEX-420" excimer laser, were monitored using the time-resolved microwave conductivity technique (TRMC). The experimental methodology and data handling involved in the application of the TRMC technique has been fully described elsewhere[12-15].

5.3 RESULTS AND DISCUSSION

The optical absorption and emission spectra of the hexacarbazole derivative DDH-HCB and the reference monocarbazole compound MCB are shown in Figure 3. The most pronounced difference in optical properties between the two compounds is seen to be the shape and solvent-sensitivity of the fluorescence. Thus, the vibrationally structured and weakly solvent dependent emission of MCB, with a maximum at 343 nm in cyclohexane, is replaced for DDH-HCB by an emission with a maximum at 394 nm which is broad and quite strongly solvent dependent. Similar broad, strongly Stokes-shifted e mission bands have been found previously for 1,3-biscarbazolyl propane (BCBP)[16] and polyvinyl carbazole (PVCB)[17]. These have been attributed to the formation of sandwich-type excimers between carbazole units and this is most probably the underlying cause of the present observations. The fact that the emission for DDH-HCB is at a shorter wavelength than the 430 nm found for the excimer of BCBP in cyclohexane suggests that the "perfect" sandwich configuration of carbazole moieties allowed by the flexible trimethylene bridge in BCBP cannot be achieved in the more restricted HCB geometry.

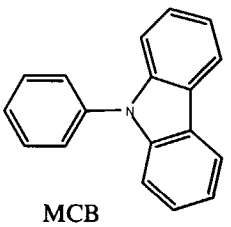

MCB

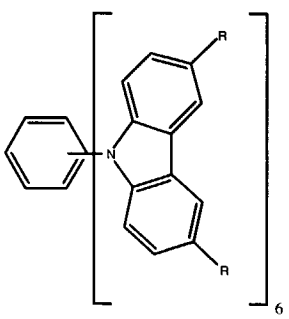

R = -H : HCB
R = -C_6H_{13} : DDH-HCB

FIGURE 2: Chemical structures of the compounds studied.

The absorption spectra of solutions of both BCBP and PVCB were found to be nearly identical to that of reference monomeric compounds[16,17], indicating the absence of intramolecular complex formation in the ground state. For the present hexacarbazolyl compounds however, a relatively strong, new absorption band appears to the red of the N-phenylcarbazole absorption. This band becomes weaker in more polar solvents and is hardly visible at all for

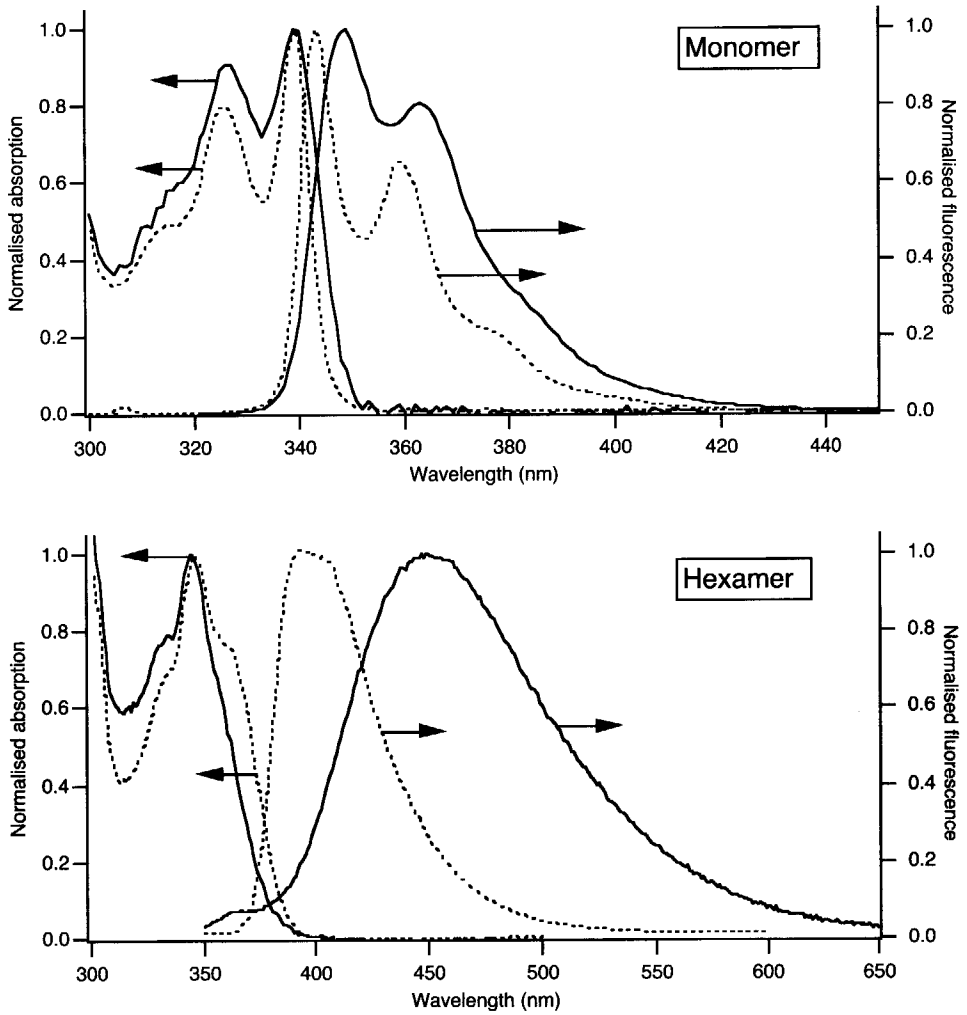

FIGURE 3: Absorption (left y-axis) and emission (right y-axis) spectra of a solution of the monomer, MCB (upper), and the hexamer, DDH-HCB (lower), in cyclohexane (dashed line) and acetonitrile (full line). All spectra are normalised to 1 at their maximum. The excitation spectra, monitored at the maximum of the emission, were almost identical to the absorption spectra.

acetonitrile, as shown in Figure 3. It would appear that intramolecular aggregation, possibly resulting in pairing of neighbouring carbazole units, occurs even in the ground state for low polarity solvents.

From the solvent dependence of the emission maximum of DDH-HCB (cyclohexane, 394 nm , diethylether, 415 nm , tetrahydrofuran, 423 nm , dichloromethane, 424 nm , acetone, 430 nm, acetonitrile, 450 nm) we have determined the parameter $\Delta\mu^2/\rho^3 = 0.93\ D^2/Å^3$, with $\Delta\mu^2$ the difference between the squares of the excited state and ground state dipole moments

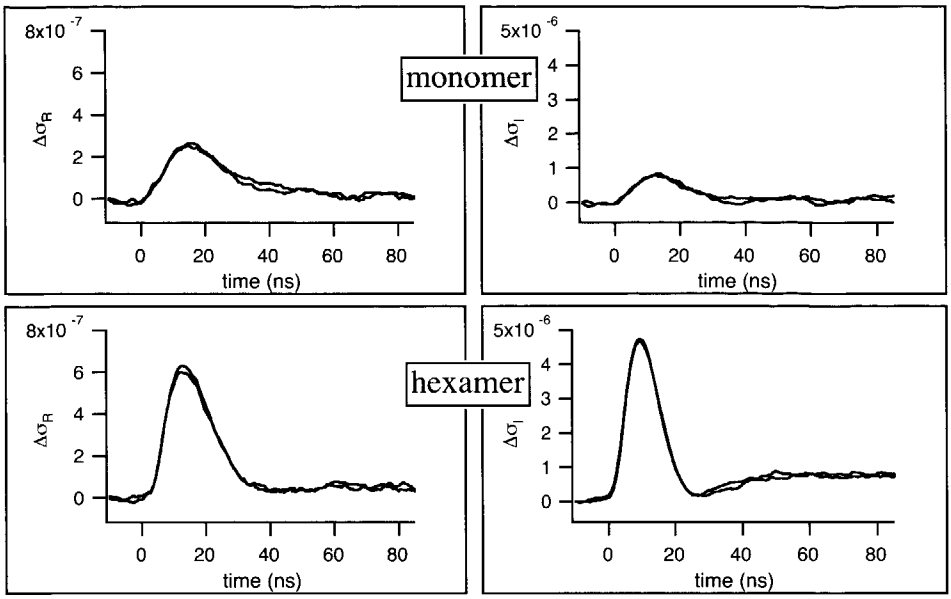

FIGURE 4: Transient changes in the real, $\Delta\sigma_R$, (left) and imaginary, $\Delta\sigma_I$, (right) components of the complex microwave conductivity on flash-photolysis of benzene solutions of MCB (upper) and DDH-HCB (lower). $\Delta\sigma_R$ and $\Delta\sigma_I$ are measures of the change in polarity and polarisability respectively of the solute molecules on photoexcitation.

and ρ the effective cavity radius of the dipolar excited state, from the slope of a Lippert-Mataga plot[18,19]. This value is to be compared with the much lower value of 0.17 $D^2/Å^3$ determined for MCB from the wavelength shift of only 6 nm in going from cyclohexane to acetonitrile. When this latter value for MCB is taken together with a ground state dipole moment of 1.7 D[20] and an excited state dipole moment of 3.5 D (see below), then the effective cavity volume, $4\pi\rho^3/3$, is calculated to be 230 $Å^3$. This is not unreasonable in view of the fact that the molecular volume of a carbazole moiety is 280 $Å^3$ based on a density of 1 g/cm^3.

Taking the above estimate of the cavity volume for MCB to represent the minimum possible value for the excited state of the hexamer, *i.e.* assuming in effect only local carbazole excitation, then a minimum value of the dipole moment of the excited state of DDH-HCB of 7.2 D is derived from the value of $\Delta\mu^2/\rho^3$ given above. The somewhat larger cavity volume which might be expected to be associated with an excimer-like complex would result in an upward revision of the dipole moment to as high as 10 D if the cavity volume were twice as large. This highly dipolar character shows that the underlying symmetry of the molecule is broken in the relaxed S_1 state by (temporary) formation of an excimer with considerable charge-transfer character between neighbouring carbazole moieties.

The transient changes in the real, $\Delta\sigma_R$, and imaginary, $\Delta\sigma_I$, components of the complex conductivity accompanying flash-photolysis of benzene solutions of MCB and DDH-HCB are shown in Figure 4. The much larger transient change in the real component of the microwave conductivity for DDH-HCB shown by the results in Figure 4 is qualitatively in agreement with the much larger dipolar character of S_1 of the hexamer as deduced on the basis of the larger solvatochromism. The very much larger $\Delta\sigma_I$ transient for DDH-HCB shows in addition that the polarisability of the hexamer S_1 state is considerably larger than that of the monomer.

$\Delta\sigma_R$ is related to the dipole moments of the ground and excited state, μ_0 and μ_* respectively, by

$$\Delta\sigma_R = N_* \frac{[\varepsilon+2]^2\omega}{27k_BT}\Delta\left[\mu^2 g(\omega\Theta)\right] \qquad (1)$$

In equation (1), N_* is the excited state concentration, ε the dielectric constant of the solution, ω the radian microwave frequency (5.9×10^{10} radians/s in the present work), k_B the Boltzmann constant, T the temperature and the term $\Delta[\mu^2 g(\omega\Theta)]$ is given by

$$\Delta\left[\mu^2 g(\omega\Theta)\right] = \frac{\omega\Theta_*}{1+(\omega\Theta_*)^2}\mu_*^2 - \frac{\omega\Theta_0}{1+(\omega\Theta_0)^2}\mu_0^2 \qquad (2)$$

In equation (2), Θ_0 and Θ_* are the dipole relaxation times of the ground and excited states respectively. The parameter $\Delta[\mu^2 g(\omega\Theta)]$ can be determined by quantitatively fitting the $\Delta\sigma_R$ transients[12,13] and is listed in Table I.

The change in the imaginary conductivity is related to the change in the molecular polarisability, $\Delta\alpha = \alpha_* - \alpha_0$, by

$$\Delta\sigma_I = N_* \frac{(\varepsilon+2)^2\omega}{9}\Delta\alpha \qquad (3)$$

From quantitative fits to the $\Delta\sigma_I$ transients[14,15] the values of $\Delta\alpha$ can be determined. These are listed in Table I as $\Delta V_p = \Delta\alpha/4\pi\varepsilon_0$, the "excess polarisability volume" with ε_0 the permittivity of vacuum.

For the monomer MCB it is reasonable to assume that dipole relaxation occurs by rotational diffusion of the whole molecule and that both Θ_0 and Θ_* will therefore be close to the rotational relaxation time of 61 ps calculated for a sphere of molecular weight 243 g/mol[13]. Taking this value of Θ, together with the known ground state dipole moment of 1.7 D[20], we calculate from the value of $\Delta[\mu^2 g(\omega\Theta)]$ given in Table I the dipole moment of S_1 of MCB to be 3.5 D. This is close to the value of 3.4 D determined previously by other

TABLE I: The lifetime, τ, rotational relaxation time, Θ_R , polarity parameter, $\Delta[\mu^2 g(\omega\Theta)]$, and excess polarisability volume, ΔV_P, of the relaxed S_1 excited states of the molecules studied.

Compound	τ (ns)	Θ_R (ps)[a]	$\Delta[\mu^2 g(\omega\Theta)]$ (D^2)	ΔV_P ($Å^3$)
MCB	9.7	61	2.4	29
HCB	5.5	268	10.3	446
DDH-HCB	3.5	520	9.5	477

a) calculated based on a spherical molecular geometry[16].

techniques[20] for the singlet excited state of unsubstitued carbazole. As shown in the previous section, this value leads to the derivation of a reasonable value for the cavity volume from the solvatochromism of MCB. If a disk-shaped geometry is taken for MCB then a longer relaxation time of 115 ps is calculated[13] which leads to a somewhat higher estimate of 4.5 D for the S_1 state dipole moment.

For the symmetrical, hexameric molecules it is reasonable to assume that the ground state has zero dipole moment and that therefore

$$\Delta\left[\mu^2 g(\omega\Theta)\right] = \frac{\omega\Theta_*}{1+(\omega\Theta_*)^2}\mu_*^2 \qquad (4)$$

The values of $\Delta[\mu^2 g(\omega\Theta)]$ for HCB and DDH-HCB are seen to be very similar despite the fact that the rotational relaxation time of the latter should be close to twice that of the former. If Θ_* is in fact taken to be equal to the rotational relaxation times given in Table I which were calculated on the basis of the molecular weight for a spherical geometry, then very large and significantly different values of 13 and 18 D respectively are found for μ_*. Taking a more realistic disk-shaped geometry for these compounds results in longer relaxation times which lead to even larger dipole moments and an even greater discrepancy between the μ_* values for the two hexamers. We conclude therefore that dipole relaxation in the hexamers is controlled not by molecular rotation but by a more rapid, intramolecular relaxation process within the HCB moiety itself.

Rapid, intramolecular dipole relaxation could also explain the very large values of the excess polarizability volume for the hexamers; values which are more than an order of magnitude larger than for MCB and equal to almost twice the volume of a single carbazole moiety. The overall change in the polarisability can consist of an electronic component, $\Delta\alpha_E$, and a dipolar contribution, $\Delta\alpha_D$,

$$\Delta\alpha = \Delta\alpha_E + \Delta\alpha_D \qquad (5)$$

with the latter given by

$$\Delta\alpha_D = \frac{\mu_*^2}{3k_BT\left[1+(\omega\Theta_*)^2\right]} \qquad (6)$$

If the electronic contribution to $\Delta\alpha$ is taken to be negligible, then according to equations (4) and (6) the values of $\Delta\alpha$ and $\Delta[\mu^2 g(\omega\Theta)]$ can be combined to provide an estimate of the relaxation time, Θ_*,

$$\Theta_* = \frac{3k_BT\Delta\alpha}{\Delta\left[\mu^2 g(\omega\Theta)\right]} \qquad (7)$$

The value found is 2.9 ps. Correction for an electronic polarisability contribution to $\Delta\alpha$ on the order of the polarisability change found for the monomer would increase the value of Θ_* calculated by at most 6% to 3.1 ps.

The value of $\Theta_* = 3$ ps can in turn be used to determine the transitory dipole moment of the excimeric state from the average value of 9.9 D^2 found for $\Delta[\mu^2 g(\omega\Theta)]$ for the hexamers. The value found is 7.6 D which is only slightly larger than the lower limit of 7.2 D estimated from the solvatochromism of DDH-HCB.

A fully consistent explanation of both the optical and microwave results for the hexacarbazole derivatives studied involves therefore the formation of a relaxed S_1 state in which the underlying 6-fold symmetry is temporarily broken by the formation of an excimer-like complex between neighbouring carbazole moieties. This transitory excimeric state has a dipole moment of *ca* 8 D, indicating a quite high degree of charge-transfer character. It undergoes rapid rotary diffusion within the circular array of carbazole moieties with a relaxation time of *ca* 3 ps, which corresponds to more than a thousand "round-trips" during its lifetime of a few nanoseconds. The hexa-carbazolylbenzene moiety may therefore be considered to be a simple model for the much more complex circular chlorophyllic arrays found in nature in so far as it performs a "storage-ring" function with only partial energy delocalization over the ring[4,5]. An exciton hopping mechanism of excitation energy transfer would appear to be operative rather than Förster transfer. The latter may however become more important at lower temperatures or in a rigid matrix where the freedom of movement of the individual chromophores is restricted. This could possibly result in even more rapid rotary energy migration than found in the present high-temperature, low-viscosity medium.

ACKNOWLEDGEMENT

The present investigation was supported by the Netherlands Organisation for the Advancement of Research (NWO).

REFERENCES

[1] G. McDermott, S. M. Prince, A. A. Freer, A. M. Hawthornthwaite-Lawless, M. Z. Papiz, R. J. Cogdell, N. W. Isaacs: Nature 374 (1995), 517-521.
[2] J. Koepke, X. Hu, C. Muenke, K. Schulten, H. Michel: Structure 4 (1996), 581-597.
[3] X. Hu, K. Schulten: Physics Today (1997), 28-34.
[4] T. Pullerits, M. Chachisvilis, V. Sundström: J. Phys. Chem. 100 (1996), 10787-10792.
[5] S. E. Bradforth, R. Jimenez, F. van Mourik, R. van Grondelle, G. R. Fleming: J. Phys. Chem. 99 (1995), 16179-16191.
[6] V. I. Novoderezhkin, A. P. Razjivin: FEBS Lett. 368 (1995), 370-372.
[7] H. M. Visser, O. J. G. Somsen, F. Mourik, S. Lin, I. H. M. van Stokkum, R. van Grondelle: Biophys. J. 69 (1995), 1083-1099.
[8] H. Fidder, J. Knoester, D. A. Wiersma: J. Chem. Phys. 95 (1991), 7880-7890.
[9] X. Hu, T. Ritz, A. Damjanovic, K. Schulten: J. Phys. Chem. B 101 (1997), 3854-3871.
[10] H. A. M. Biemans, C. Zhang, P. Smith, H. Kooijman, W. J. J. Smeets, A. L. Spek, E. W. Meijer: J. Org. Chem. 61 (1996), 9012-9015.
[11] H. A. M. Biemans:"Multi-chromophoric arrays in molecules of high symmetry", PhD Thesis, Technical University of Eindhoven: Eindhoven 1997; ISBN 90-386-0818-7.
[12] M. P. de Haas, J. M. Warman: Chem. Phys. 73 (1982), 35-53.
[13] W. Schuddeboom: "Photophysical Properties of Opto-electric Molecules Studied by Time- Resolved Microwave Conductivity"; PhD Thesis, Delft University of Technology 1994, ISBN 90-73861-21-7.
[14] J. M. Warman, W. Schuddeboom, S. A. Jonker, M. P. de Haas, M. N. Paddon-Row, K. A. Zachariasse, J.-P. Launay: Chem. Phys. Lett. 210 (1993), 397-404.
[15] J. M.Warman, G. H. Gelinck, J. J. Piet, J. W. A. Suykerbuyk, M. P. de Haas, B. M. W. Langeveld-Voss, R. A. J. Janssen, D.-H. Hwang, A. B. Holmes, M. Remmers, D. Neher, K. Müllen, P. Bäuerle, Proc. Int. Soc. Opt. Eng., SPIE, 3145 (1997), 142-149.
[16] W. Klöpffer: Chem. Phys. Lett. 4 (1969), 193-194.
[17] W. Klöpffer: J. Chem. Phys. 50 (1969), 2337-2343.
[18] E. Lippert: Z. Electrochem, Ber. Bunsenges. Physik. Chem. 61 (1957), 962-975.
[19] N. Mataga, Y. Kaifu, M. Koizumi: Bull. Chem. Soc. Jpn. 29 (1956), 465-471.
[20] A. L. McClellan:"Tables of Experimantal Dipole Moments", Rahara Enterprises: El Cerrito 1989, Vol. 3, p 692.

6

PORPHYRIN DIMERS[‡]

6.1 INTRODUCTION

Porphyrin derivatives are essential ingredients in all natural photosynthetic systems. In addition to being used as light-harvesting chromophores because of their broad range of optical absorption covering the entire visible spectrum, porphyrin derivatives play a key role in the processes that direct the absorbed solar energy from the initial antenna complex to the reaction center where they are also responsible for triggering the initial stages of transmembrane charge separation. These functions depend on collective interactions between two or more closely similar, or even identical, porphyrinic units juxtapositioned in organised

[‡] Chapter 6 has appeared previously as an article: J. J. Piet, P. N. Taylor, H. L. Anderson, A. Osuka, J. M. Warman: "Excitonic interactions in the singlet and triplet excited states of covalently-linked zinc porphyrin dimers", J. Am. Chem. Soc. 122 (2000), 1749-1757.

assemblies, as in the "storage ring" arrays of bacterial antenna systems[1] or in the "special-pair" of the reaction center[2]. In attempts to understand and reproduce these natural functions a large number of porphyrinic arrays have been synthesised[3-6].

The photophysical properties of an assembly of identical chromophores can be quite complex as a result of Coulombic and electronic interactions between neighboring monomeric units. Even in the absence of covalent bonding, pronounced differences in the optical absorption and emission spectra between the assembly and the corresponding monomer are often found. A qualitative explanation of such effects was first given by Kasha in terms of the Coulombic interaction between neighboring chromophores with isoenergetic electronic transitions[7,8]. Such dipolar exciton coupling can lead to the splitting of an energy level, generally referred to as "Davydov splitting", and is exemplified by either bathochromic or hypsochromic spectral shifts. The magnitude of the interaction, as measured by the excitonic splitting, δE, is related to the transition dipole moment, μ_{0n}, associated with a transition from the ground state, S_0, to an excited state, S_n, and to the distance between the chromophores, R_{cc}, according to,

$$\partial E = K\frac{|\mu_{0n}|^2}{R_{cc}^3} \qquad (1)$$

The parameter K in equation (1) is dependent on the geometrical relationship between the chromophores and the spectral overlap. Dipolar coupling is also the basis of the Förster mechanism of energy transfer between chromophores, the rate of which obeys an inverse 6^{th} power dependence on distance[9].

In the Kasha and Förster approaches to excitonic interactions no electronic overlap or electron exchange between the chromophores is taken into account. While this may be a reasonable approximation for through-space interactions since electronic overlap is expected to decrease exponentially with distance, it may break down for covalently bonded chromophores. In the latter case, through-bond interactions involving the σ,σ^* and π,π^* orbitals of the bridge can result in electronic interactions over much longer distances[3,10-12]. The resulting interchromophore coupling will then depend on the specific nature of the bridge and a simple monotonic decrease with distance may no longer be assumed. This is clearly shown to be the case in the present work where we have measured the extent of excitonic interactions in several zinc porphyrin dimers linked by a variety of covalent bridges and found that the electronic coupling can even *increase* with an increase in the length of the bridge.

In the past, evidence for excitonic interactions in molecular assemblies has been derived mainly from comparisons of the optical absorption and emission characteristics of

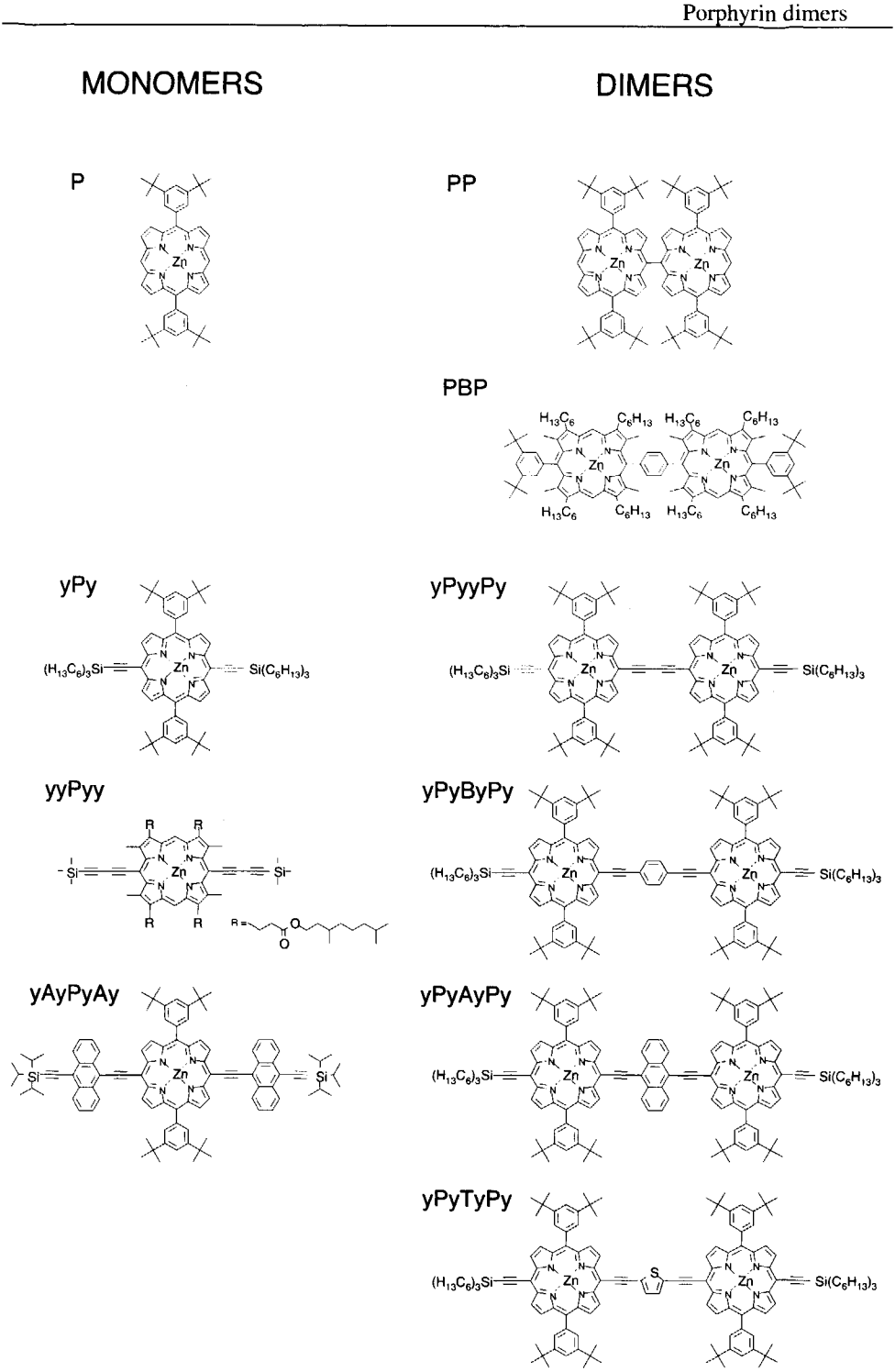

Figure 1: The structures of the molecules investigated and the pseudonyms used throughout the text.

assemblies with those of a model monomer molecule. In the present work we have used, in addition to optical methods, a modification of the flash-photolysis time-resolved microwave conductivity method (FP-TRMC)[13-15] to measure the increase in molecular polarizability on formation of the relaxed excited singlet and triplet states. The method, which provides a direct measure of the extent of electron delocalization, has previously been used to study excitonic interactions in other symmetrical multichromophoric assemblies[16-19] and, more recently, in conjugated polymers[15,20,21].

6.2 EXPERIMENTAL

The structures of the porphyrin dimers and corresponding model monomers studied in the present work are shown together with their pseudonyms in Figure 1. Their methods of synthesis and structural characterisation have been given in previous publications[22-25], which are listed in the last column of Table I. All measurements were carried out on dilute solutions in benzene (Merck, Uvasol) to which 1 wt% 1,4-diazabicyclo[2,2,2]octane, DABCO (Aldrich 98%), was added to prevent aggregation by complexation with the central zinc atoms.

Optical absorption spectra were recorded on a Kontron Uvikon 940 double-beam UV-Vis spectrophotometer. Emission spectra were recorded on a PTI "quantamaster 1" spectrofluorometer equipped with a double excitation and a single emission monochromator. All samples were excited at a wavelength close to the maximum of their B-band. The absorbance at the excitation wavelength never exceeded 0.2.

The fluorescence decay times of the compounds P, PP and PBP were determined from real-time transients using the 0.8-ns, 337-nm pulse of a Laser Photonics LN1000 nitrogen laser as excitation source and a Photek "PMT-113-UHF" channel-plate photomultiplier with a risetime of 150 ps as detector. For the remaining compounds the fluorescence decay time was determined by single photon counting using the 90-ps, 630-nm pulse from a cavity-dumped mode-locked dye laser synchronously pumped by the second harmonic of a continuous-wave, mode-locked Nd:YAG laser. The decay times thus obtained, which were used as the singlet excited state lifetime in the fitting procedure of the TRMC transients, are listed in Table I.

For the TRMC experiments the solutes were photoexcited using single 7-ns, 308-nm unfocused pulses from a Lumonics HyperEX-400 (HE 420) excimer laser. The molar absorption coefficients of the solutes were *ca.* 1×10^4 $M^{-1}cm^{-1}$ at the laser wavelength and the absorbance of the solutions varied from *ca.* 0.2 to 0.9 for a 1 cm path length. Prior to use, the solutions were purged with CO_2 to remove oxygen and scavenge any free electrons which might be generated in low yield by multi-photon events. A maximum of 16 pulses was used for signal averaging. The power output of the laser was monitored routinely using a Scientec 365 power meter and the actual fraction of photons entering the TRMC-cell was determined using a solution of 4-(N,N-dimethylamino)-4'-nitrostilbene (DMANS) in benzene as an

internal actinometer[13,14,26]. The average concentration of photons absorbed in the solutions was calculated to be *ca.* 10 μM per pulse for the absorbances used.

The solutions were contained in an X-band (8.2-12.4 GHz) resonant cavity. Transient changes in the power reflected by the cavity on flash-photolysis, ΔR, were monitored at the upper and lower half-power frequencies, f_+ and f_-, of the cavity resonance at *ca.* 9.4 GHz. By addition and subtraction of the two transients, signals related to the change in the real, Δε' (dielectric constant), and imaginary, Δε" (dielectric loss), components of the complex permittivity of the solutions were obtained[15,21]:

$$\Sigma_{\pm} = \left(\Delta R_{-} + \Delta R_{+}\right) = B\Delta\varepsilon'' \tag{2}$$

$$\Delta_{\pm} = \left(\Delta R_{-} - \Delta R_{+}\right) = C\Delta\varepsilon' + D\frac{d\Delta\varepsilon'}{dt} \tag{3}$$

Such "real" and "imaginary" transients are shown for all of the compounds investigated in Figure 2, 4 and 6.

The values of B and C in equations (2) and (3) can be calculated from the characteristics of the resonant cavity[14]. The differential term in equation (3) results from a non-dissipative change in the energy stored within the cavity as a result of the fluctuation in ε'. This leads to an oscillatory component in the $\Delta_{\pm}$ transients. The value of D was determined by fitting transients for the formation of the highly polarizable triplet state of Michler's ketone[27]. Knowing B, C, and D, the absolute magnitude of the change in ε' and ε" on flash-photolysis can be determined. The signals actually observed have a noise level which corresponds to a fluctuation in the relative dielectric constant of less than 1 ppm in the irradiated volume of the cell.

A change in the complex permittivity of a solution on photoexcitation of the solute, Δε, can result from a change in the electronic polarizability, Δα, or a change in the dipole moment, $\Delta\mu = \mu_* - \mu_0$, of the solute molecules. The overall change in permittivity is given by,

$$\Delta\varepsilon = \frac{(\varepsilon(\infty)+2)^2 N_*}{9\varepsilon_0}\left(\Delta\alpha + \frac{(\mu_*^2 - \mu_0^2)}{3k_B T(1 + j\omega\Theta)}\right) \tag{4}$$

$$= \Delta\varepsilon' - j\Delta\varepsilon'' \tag{5}$$

In equation (4), N_* is the concentration of the excited state, ε(∞) is the optical dielectric constant, k_B is the Boltzmann constant, T is the temperature, ω is the radian microwave frequency, Θ is the dipole relaxation time, ε_0 is the permittivity of vacuum, and j is $\sqrt{-1}$. In the present case of a non-polar solvent (ε(∞) = ε') and solute molecules with zero dipole moment

in the ground state, the individual changes in the real and imaginary components of ε are, from equation (4),

$$\Delta\varepsilon' = \frac{(\varepsilon'+2)^2 N_*}{9\varepsilon_0}\left(\Delta\alpha + \frac{\mu_*^2}{3k_BT(1+\omega^2\Theta^2)}\right) \tag{6}$$

and

$$\Delta\varepsilon'' = \frac{(\varepsilon'+2)^2 N_*}{27\varepsilon_0 k_B T}\left(\frac{\omega\Theta\mu_*^2}{(1+\omega^2\Theta^2)}\right) \tag{7}$$

A change in the electronic polarizability is seen to result only in a change in ε' whereas a dipole moment change results in a change in both ε' and ε". For the present molecules no measurable change in ε" could be observed, as can be seen from the results in Figure 2, 4 and 6, indicating that the excited states have no dipolar character, as might be expected on the basis of their symmetry. Therefore any changes in ε' which are observed can be attributed entirely to changes in the electronic polarizability on photoexcitation, *i.e.*:

$$\Delta\varepsilon' = \frac{(\varepsilon'+2)^2 N_*}{9\varepsilon_0}\Delta\alpha \tag{8}$$

As can be seen in Figures 4 and 6, the Δε' transients are characterised by a combination of a fast and a slow component, with the decay of the latter extending well into the microsecond regime. Since zinc porphyrins are known to undergo intersystem crossing with high efficiency, we ascribe the fast and slow components in the present measurements to the relaxed singlet and triplet states, S_1 and T_1, respectively. The data were therefore fitted using a convolution procedure with numerical calculation of the S_1 and T_1 concentrations during and after the pulse using the known laser pulse shape and intensity, the optical properties of the solution and the S_1 lifetime determined from the fluorescence measurements. From the fits, values of the excess polarizability of the excited singlet state, $\Delta\alpha(S_1)$, and the product of the quantum yield and the excess polarizability of the triplet state, $\phi_{isc}\Delta\alpha(T_1)$, could be determined. For convenience of discussion, these values are given in Table I as the excess polarizability volume $\Delta V_p = \Delta\alpha/4\pi\varepsilon_0$ in units of $Å^3$.

6.3 RESULTS AND DISCUSSION

As mentioned in the introduction, the photophysical properties of identical chromophores in close proximity can be influenced by mutual Coulombic or electronic interactions. The former results in Davydov splitting of the energy levels with the magnitude of the splitting being dependent on the relative orientation and distance between the chromophores, and the transition dipole moment associated with a particular transition as given in equation (1). In the case of porphyrins, the B-band in the 400—500-nm region is particularly sensitive to such effects because of the extremely large transition dipole moment associated with it. The Q-band of the porphyrins on the other hand, has a much lower transition dipole and is correspondingly much less sensitive to Coulombic interactions. Spectral changes in the B-band absorption spectrum can therefore in principle be used as an indication of the magnitude of Coulombic interporphyrin interactions. The effect of the Coulombic interaction alone can however be obscured by other effects. Additional substituents on the porphyrin macrocycles, for instance, can lift the degeneracy of the two orthogonal B-band transitions, which can also lead to a splitting of the B-band.

Electronic interactions, either *via* direct orbital overlap or *via* electron exchange, are expected to lead to a reduction in the gap between the highest occupied molecular orbital, the HOMO, and the lowest unoccupied molecular orbital, the LUMO. This should therefore be observed as a bathochromic shift of the lowest energy Q-band and the (0,0) band of the fluorescence. Of particular relevance to the present work are the delocalization of the electronic wavefunction and partial charge transfer character of the S_1 excited state, which are consequences of electron exchange. This should be observable as an increase in the electronic polarizability of the molecule on excitation, an effect which is ideally suited to study by the present TRMC technique.

Considering the above, we divide the present compounds into three groups based on their combined optical properties and excess polarizabilities: 1) the compounds P, PP and PBP which have extremely low excess polarizabilities but display B-band splitting in the dimeric compounds; 2) the monomer series P, yPy, yyPyy and yAyPyAy for which a gradual increase in excess polarizability is found with or without associated B-band splitting; and 3) the diethynyl bridged dimers, denoted generally by yPyXyPy, all of which have large values of $\Delta V_p(S_1)$ and complex B-band spectra. These groups will be discussed separately below.

In addition to information on the relaxed excited singlet states of the present compounds, the TRMC technique is capable of providing information on the excess polarizability, and hence degree of delocalization, in the triplet state. This will be discussed in a separate section after first considering the singlet state results.

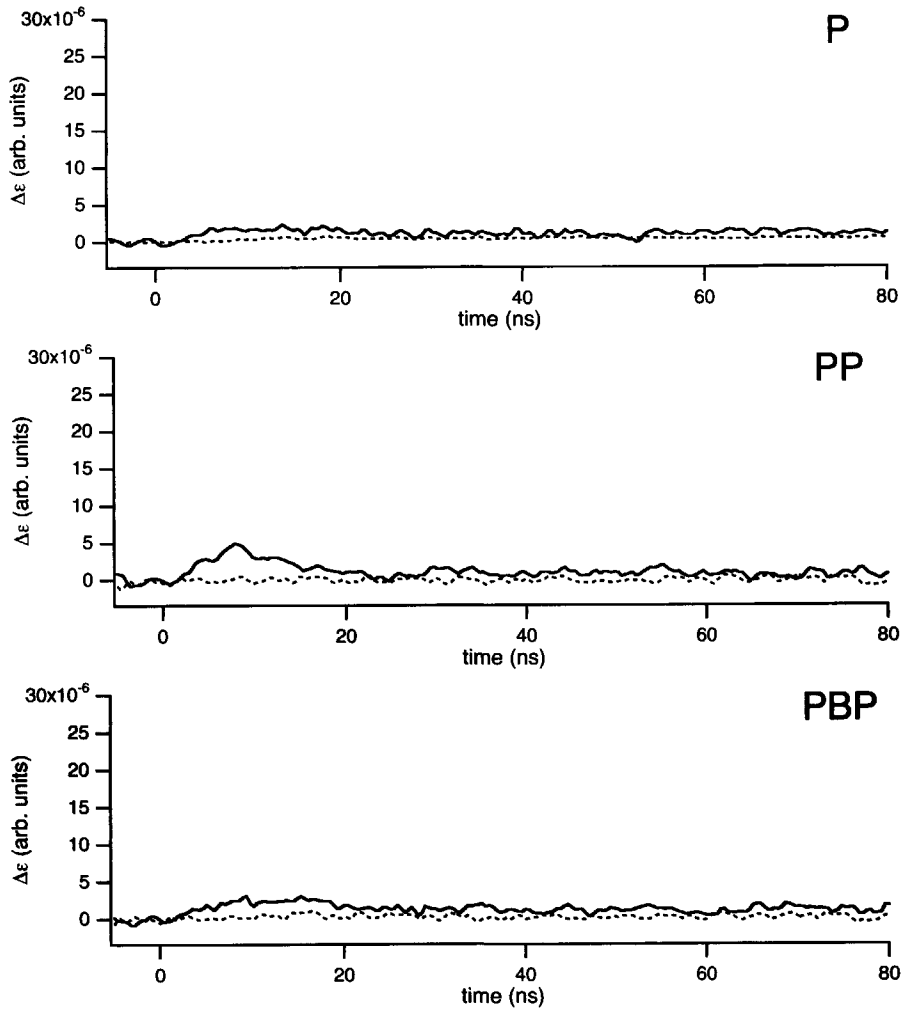

Figure 2: TRMC-transients corresponding to changes in the imaginary (dashed line) and real (full line) components of the complex permittivity of dilute solutions of P (top), PP (middle) and PBP (bottom) in benzene to which 1wt% of DABCO was added.

6.3.1 Singlet states of P, PP, PBP.

As can be seen in Figure 2, any change in ε' which may have occurred on photoexcitation of the monomer P was within the noise level of the measurements, which corresponds to a value of $\Delta V_p(S_1)$ of approximately 20 $Å^3$. From this we conclude that excitation of an electron from the HOMO to the LUMO occurs with very little change in the degree of delocalization of the electronic wavefunction. The monomer P therefore provides an ideal reference point for monitoring the influence of substituents since any measurable value

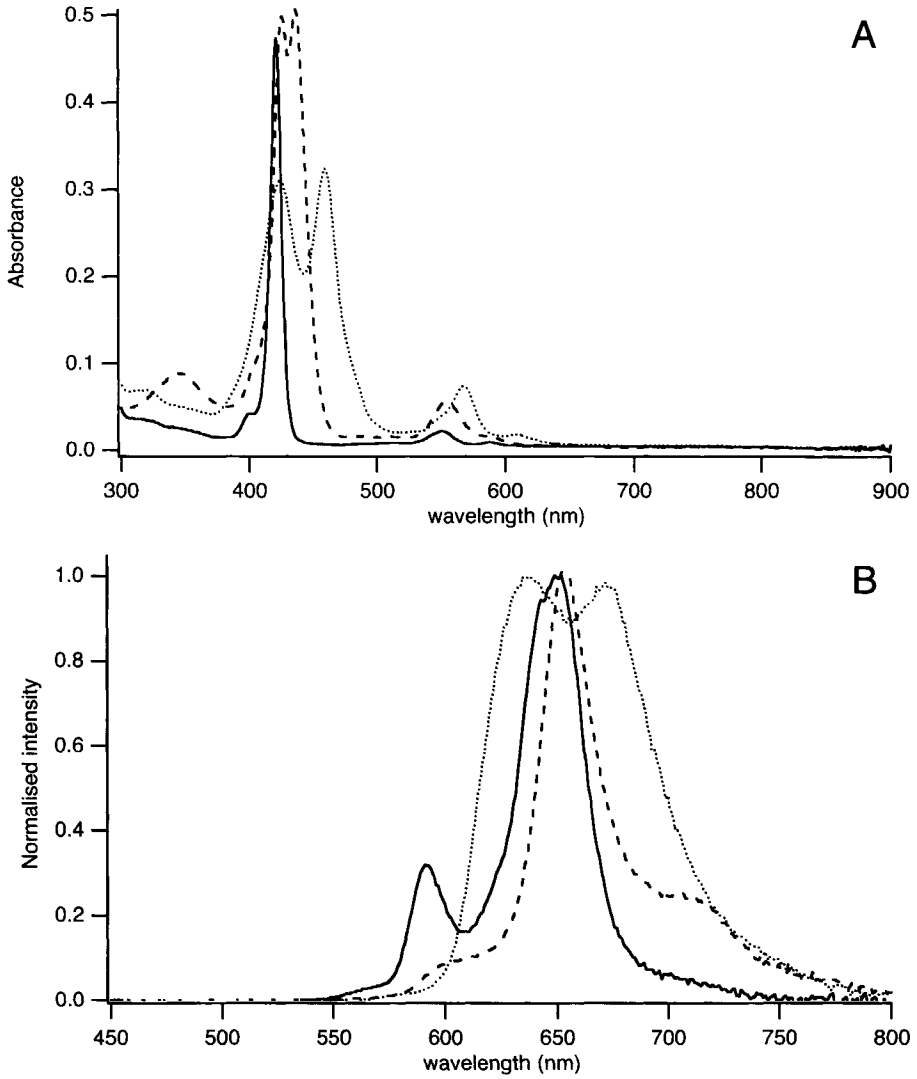

Figure 3: UV-Vis absorption spectra (A) and fluorescence spectra (B) of the compounds P (full line), PP (dotted line) and PBP (dashed line) in benzene with 1wt% of DABCO added.

of $\Delta V_p(S_1)$ must arise from electron delocalization involving the molecular orbitals of the substituent.

For the simplest, directly covalently linked dimer, PP, a TRMC transient slightly outside of the noise level is observed in Figure 2 which corresponds to $\Delta V_p(S_1) = 50$ Å^3. On the basis of this we conclude that there is a small but significant degree of electronic coupling between the two porphyrin moieties. This is also apparent in Figure 3 as a small bathochromic

shift of 0.15 eV in both the Q-band absorption and the emission. A much more pronounced effect is seen on the B-band absorption, which is split by 0.25 eV as observed previously[22,28]. We conclude therefore that for PP the interaction between the two chromophores is dominated by Coulombic effects with electronic coupling playing only a minor role. The weakness of the electronic interaction can be ascribed to the lack of coplanarity of the macrocycles induced by steric hindrance[22,29].

For the 1,4-phenylene bridged dimer, PBP, both the Coulombic and electronic coupling are found to be much smaller than for PP. The former effect is shown in Figure 3 by the considerably reduced (but still observable!) splitting of the B-band of only 0.09 eV[22,28]. The much reduced Kasha-type exciton coupling for PBP is to be expected on the basis of the increased distance between the porphyrin units as given by equation (1).

The lack of significant electronic interaction in PBP is indicated by the absence of a measurable $\Delta\varepsilon'$ transient in Figure 2 and the lack of a substantial red-shift in the fluorescence maximum compared with that for the monomeric compound, as shown in Figure 3. The fact that the porphyrin macrocycles can adopt a coplanar arrangement in PBP would appear to be insufficient to compensate for the negative effect on the electronic coupling of the larger interchromophore separation. The present results lead therefore to the conclusion that the excitation energy is almost completely localized on a single porphyrin unit in PBP. This is in agreement with resonance Raman measurements on a nickel analogue of PBP which indicated that hardly any electronic interaction is mediated *via* the intervening 1,4-phenylene bridge[30].

As mentioned in the introduction, distance cannot be used as the only criterion in discussing electronic coupling in bridged dimers since through-bond coupling can play an important role. In this regard one would tend to conclude from the present results for PBP that the 1,4-phenylene unit is in fact a very weak coupling agent. Previous experiments on phenylene-bridged porphyrins have also indicated that the coupling efficiency of the 1,4-phenylene unit is weak[31-33]. The lack of efficiency of the 1,4-phenylene bridge is attributed, at least in part, to the forced non-coplanarity between the phenylene and porphyrin ring systems caused by steric hindrance[23,31]. This reduces the orbital interactions between chromophore and bridge necessary for through-bond coupling. As will be shown below, a bridge consisting of a phenylene unit interposed between two ethynyl groups can act as an efficient coupling agent. In that case the phenylene ring *can* adopt a conformation in which it is coplanar with both porphyrins.

6.3.2 Singlet states of P, yPy, yyPyy, yAyPyAy.

In Figure 4 the TRMC transients for all of the monomeric porphyrin derivatives are compared. The magnitude of the transients and the corresponding $\Delta V_p(S_1)$ values given in Table I are seen to increase gradually with increasing complexity of the substituents at the

Table I: The fluorescent lifetime, $\tau(S_1)$, the excess polarisability volume of the singlet state, $\Delta V_p(S_1)$, the product of the intersystem crossing efficiency and the excess polarisability volume of the triplet state, $\phi_{isc}\Delta V_p(T_1)$, and the energy of the (0,0) transition of the fluorescence, E_{fl}.

compound	$\tau(S_1)$ (ns)	$\Delta V_p(S_1)$ (Å^3)	$\phi_{isc}\Delta V_p(T_1)$ (Å^3)	E_{fl} (eV)	Reference[b)]
P	2.9	<20[a)]	<5[a)]	2.10	22
PP	2.1	50±20	<5[a)]	1.95	22
PBP	1.3	<20[a)]	<5[a)]	2.06	23
yPy	1.6	30±20	<5[a)]	1.90	24
yyPyy	1.9	50±20	13±5	1.84	25
yAyPyAy	0.8	330±30	28±5	1.68	24
yPyyPy	1.3	400±40	30±5	1.64	24
yPyByPy	0.8	270±30	17±5	1.78	24
yPyTyPy	0.8	390±40	30±5	1.71	24
yPyAyPy	1.1	590±60	19±5	1.61	24

a) Upper limit corresponds to the noise level.
b) Reference to synthesis.

opposing *meso* positions up to a relatively large value of 330 Å^3 for yAyPyAy. As shown in Figure 5, the Q-band absorption and the (0,0) band of fluorescence undergo corresponding bathochromic shifts within the series. Clearly there is a substantial degree of electron delocalization from the porphyrin ring into the substituents in the S_1 state of the monomeric ethynyl-containing derivatives and in particular for the 9,10-diethynylanthracene substituent. These conclusions are in agreement with the results of Beljonne *et al.*[34] on compounds very similar to yPy and yyPyy and LeCours *et al.*[35] on *meso*-arylethynyl derivatives. These workers, together with Wang *et al.*[36], have also carried out theoretical calculations which substantiate the delocalization of the LUMO wavefunctions into the *meso* substituents. In particular, the low lying singlet states of the arylethynyl derivatives were found to be highly polarized which would explain the large polarizability found in the present work for yAyPyAy.

The bathochromic shift in the Q-bands and in the fluorescence of the ethynyl substituted monomers is accompanied by a considerable red-shift in the B-band, as shown in Figure 5. In addition, there is clear evidence of B-band splitting for yPy and yAyPyAy, whereas yyPyy displays only a single sharp band. These results for the monomeric compounds illustrate the care that must be taken in interpreting such B-band effects in terms of excitonic interactions alone. The splitting in the case of the first two compounds and its absence for yyPyy is possibly related to the fact that the former compounds have additional 3,5-di-*tert*-butylphenyl substituents at the 10,20-*meso* positions whereas yyPyy has none. A full discussion of these interesting differences is outside the scope of the present work.

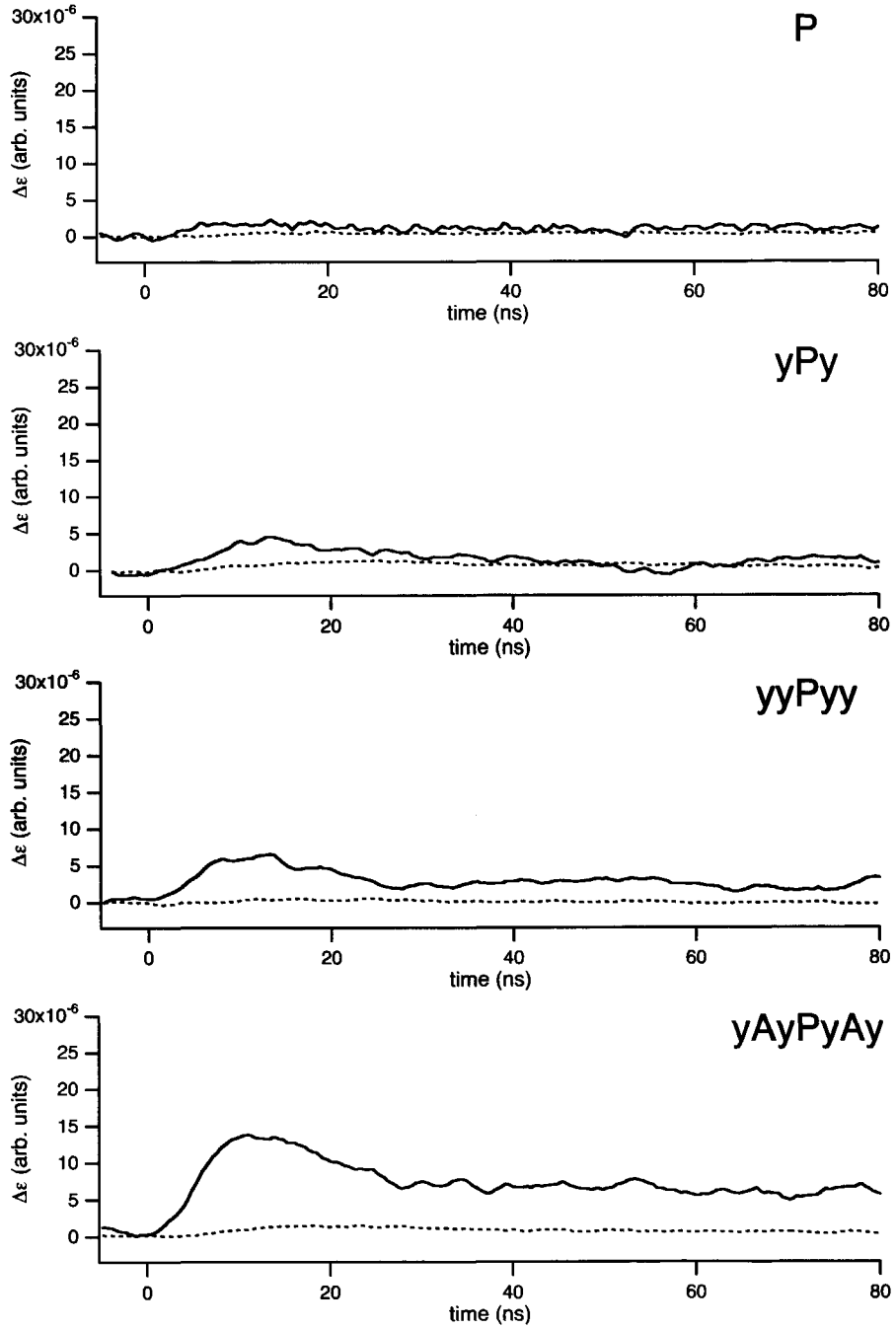

Figure 4: TRMC-transients corresponding to changes in the imaginary (dashed line) and real (full line) components of the complex permittivity of dilute solutions of the series of mono porphyrinic compounds in benzene to which 1wt% of DABCO was added. From top to bottom: P, yPy , yyPyy and yAyPyAy.

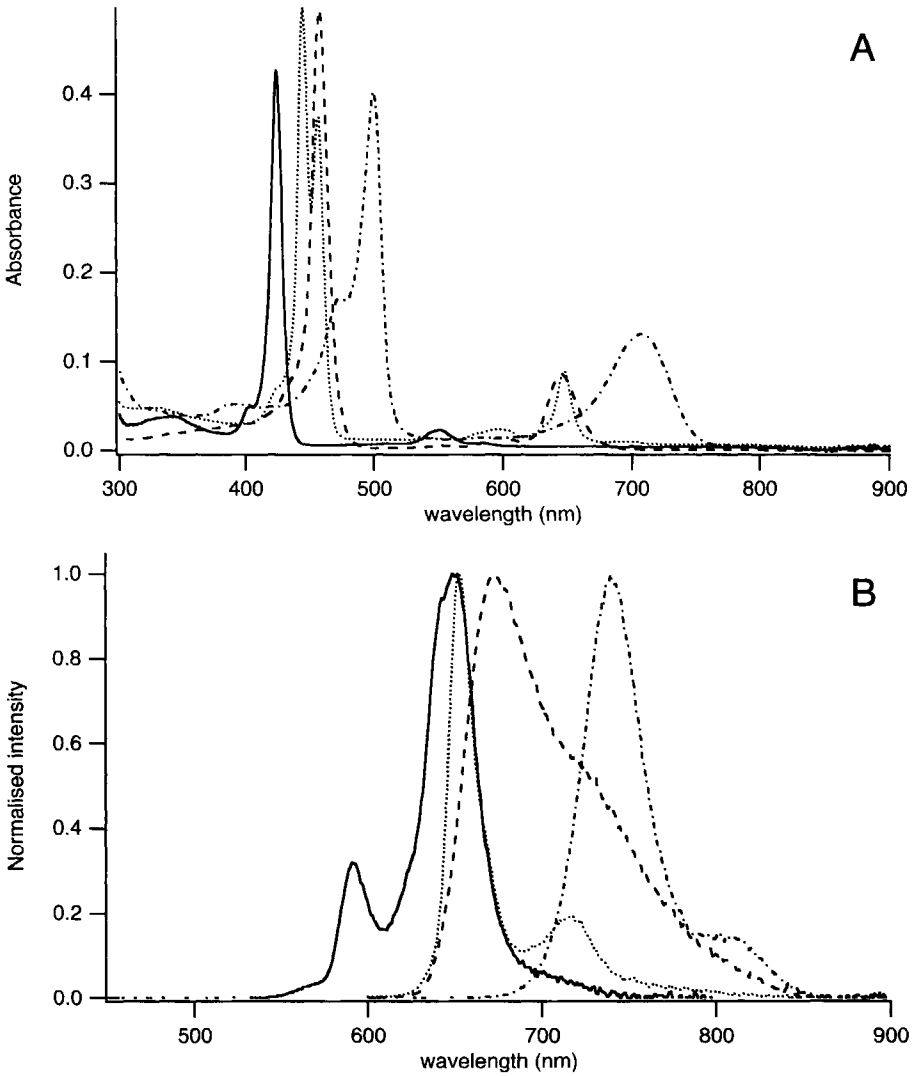

Figure 5: UV-Vis absorption spectra (A) and fluorescence spectra (B) of the compounds P (full line), yPy (dotted line), yyPyy (dashed line) and yAyPyAy (dotted-dashed line) in benzene with 1wt% of DABCO added.

6.3.3a Singlet state of yPyyPy.

The $\Delta V_p(S_1)$ value of 400 $Å^3$ for the butadiyne dimer, yPyyPy, derived from the $\Delta\varepsilon'$ transient displayed in figure 6, is much larger than the values of *ca* 30 $Å^3$ and 50 $Å^3$ found for the monomeric yPy and yyPyy compounds. This is direct evidence that strong electronic coupling between the two porphyrin moieties is mediated by the intervening butadiyne bridge. A large

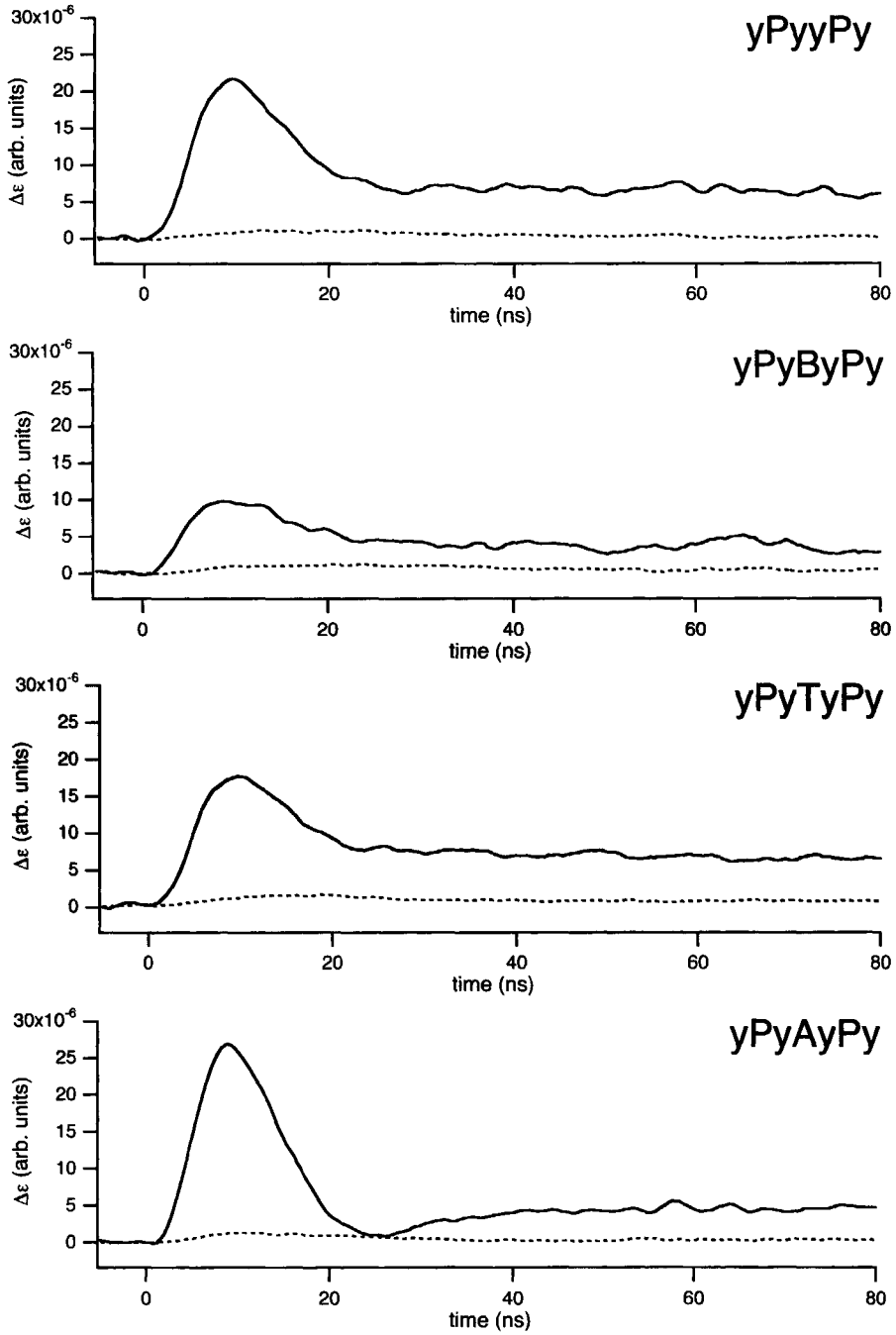

Figure 6: TRMC-transients corresponding to changes in the imaginary (dashed line) and real (full line) components of the complex permittivity of dilute solutions of the series of bis ethynylenic linked porphyrin dimers in benzene to which 1wt% of DABCO was added. From top to bottom: yPyyPy, yPyByPy, yPyTyPy, and yPyAyPy.

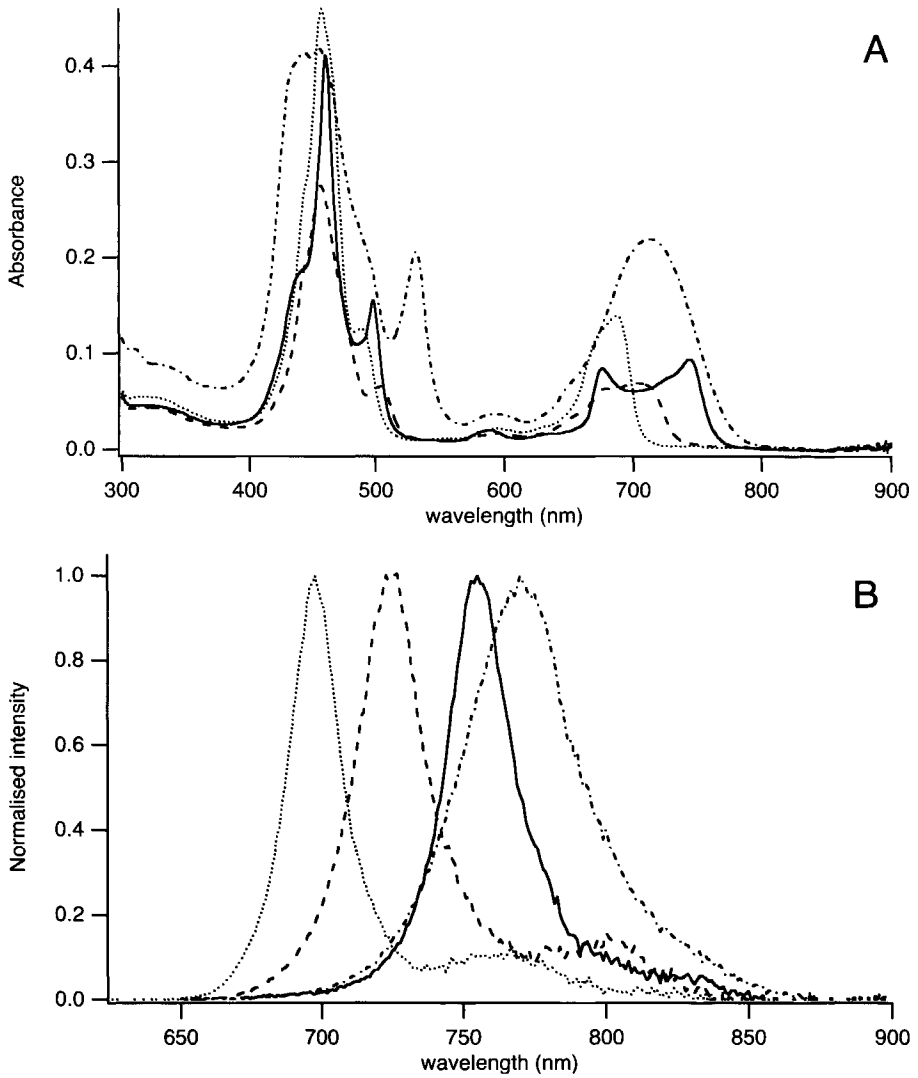

Figure 7: UV-Vis absorption spectra (A) and fluorescence spectra (B) of the compounds yPyyPy (full line), yPyByPy (dotted line), yPyTyPy (dashed line) and yPyAyPy (dotted-dashed line) in benzene with 1wt% of DABCO added.

degree of interchromophore interaction is also indicated by the pronounced bathochromic shift of the dimer fluorescence shown in Figure 7, which corresponds to a decrease in the HOMO-LUMO gap from 1.90 eV for the yPy monomer to 1.64 eV. The present results support the conclusion that a butadiyne bridging unit provides efficient interaction between porphyrin moieties, which was drawn previously on the basis of the optical properties of the closely related compound yyPyyPyy[34].

In addition to $\Delta V_p(S_1)$ for the yPyyPy dimer being much larger than for the model monomers, it is also very much larger than the values found for the PP and PBP dimers, despite the fact that the edge-to-edge distance between the porphyrin moieties in yPyyPy is larger. It could be argued that the larger excitonic interaction observed for yPyyPy than for PP is the result of the freedom of rotational motion of the chromophoric units provided by the butadiyne bridge, which allows the porphyrin macrocycles to adopt a coplanar arrangement. Conformational relaxation in S_1 to form a coplanar emitting state has been found to occur within *ca.* 30 ps for a PyP type dimer[37]. Coplanarity alone however cannot be the sole cause of the large coupling since this is also possible in the case of PBP for which no significant excess polarizability could be observed.

It has been suggested that the explanation of the highly efficient electronic coupling provided by oligoethynyl chains lies in the adoption, in the excited state, of a cumulenic structure[34,38], as illustrated in Figure 8. Theoretical calculations on 1,4-diphenylbutadiyne

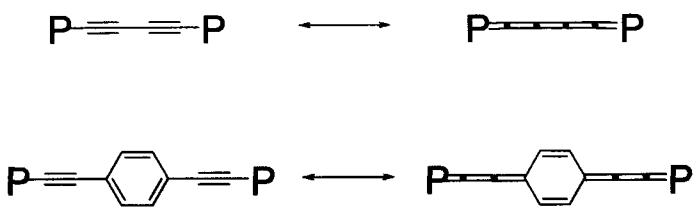

Figure 8: The ethynylenic and cumulenic resonance structures of the yy bridging unit (top) and aromatic-ethynylenic and quinoidal-cumulenic resonance structures of the yXy (X=B or A) bridging unit (bottom).

have shown that the degree of bond alternation in the butadiyne unit does in fact decrease considerably in the excited state[34]. Such cumulenic structures introduce the possibility of charge-transfer states which may lie close to the locally excited state. Strong electronic coupling between the local and charge-transfer states could explain the very large excess polarizability found for yPyyPy.

6.3.3b Singlet states of the yPyXyPy series.

Interposing a 1,4-phenylene moiety in the butadiyne bridge to give yPyByPy results in a decrease in the interaction between the chromophores, as shown by the considerable decrease in $\Delta V_p(S_1)$ from 400 to 270 $Å^3$ and the increase in the HOMO-LUMO gap from 1.64 to 1.78 eV. A substantial decrease in coupling efficiency would have been expected simply on the basis of the considerably increased interchromophore distance. On the basis of the weak coupling found for PBP, it is in fact surprising that the decrease is not even larger.

This can be explained, at least in part, by the removal of the steric hindrance to rotation of the phenylene ring by the presence of the intervening ethynylenic units. This allows the central aromatic ring to adopt a coplanar orientation with respect to the porphyrin moieties. In such a coplanar conformation, increased conjugation would be favoured by an increased contribution from a combined cumulenic-quinoidal resonance structure[24], as illustrated in Figure 8.

Evidence for the importance of a cumulenic-quinoidal resonance structure is provided by the results for yPyAyPy. Thus, even though the interporphyrin distance remains constant compared with yPyByPy, the value of $\Delta V_p(S_1)$ increases by almost a factor of 2. Since the energy difference between an aromatic and a quinoidal structure is considerably smaller for anthracene than for benzene, substitution of a 9,10-anthrylene unit for the 1,4-phenylene group should favour the formation of a cumulenic-quinoidal structure[39-41] and hence result in an increase in the coupling efficiency of the bridge as is observed. Not only is the excess polarizability for yPyAyPy larger than for yPyByPy, it is even larger than for the much shorter bridge compound yPyyPy! The 9,10-diethynylanthracene moiety appears therefore to be an exceptionally good agent for the electronic coupling of porphyrinic chromophores, as was previously concluded on the basis of the optical properties of these compounds[24]. The series PBP, yPyyPy, yPyAyPy provides therefore a good illustration of the inverse effect of an *increase* in electronic coupling accompanying an *increase* in interchromophore distance.

The optical properties of yPyAyPy are of themselves of interest. Thus, while the lowest energy absorption band of this compound is higher in energy than that for yPyyPy, its highest energy fluorescence band is lower in energy. The large Stokes shift for yPyAyPy, is further evidence that a substantial structural change occurs after photoexcitation. This is in agreement with the bond rearrangement required for the formation of the cumulenic-quinoidal structure in the relaxed S_1 state.

On the basis of the excess polarizability value of 390 $Å^3$ for yPyTyPy, the 2,5-diethynylthiophene bridge, yTy, is seen to have a coupling efficiency intermediate between those of yBy and yAy and close to that for the butadiyne group alone. This is in agreement with the ordering of the fluorescence emissions and the positions of the B- and Q-band absorptions shown in Figure 7. In the case of yPyTyPy a cumulenic-semiquinoidal structure may be taken to be responsible for the highly efficient coupling. It would appear that the bent nature of the yTy bridge does not have a significant negative influence on the electronic coupling efficiency.

The B-bands of the yPyXyPy compounds are seen in Figure 7 to be complex, with in all cases multiple splitting occurring as has been observed previously for similar ethynyl-bridged dimers[42,43]. Compared to the corresponding monomers described in the previous section, this splitting is much more pronounced and therefore cannot solely be attributed to the asymmetric substitution around the porphyrin macrocycle. For instance, from the spectrum of yPyyPy we estimate a splitting of *ca.* 0.2 eV, which is similar in magnitude to

that of the directly coupled dimer PP. This is a surprising result, since the Coulombic interactions responsible for the B-band splitting would be expected to be much weaker for the large interchromophore distance in yPyyPy. We are tempted to conclude that the strong electronic interaction between the porphyrin chromophores has the additonal effect of extending the range of the Coulombic coupling considerably in the yPyXyPy compounds[42].

Arnold and coworkers[43] recently put forward an alternative explanation for the complex B-band of covalently linked bis-porphyrinic compounds solely based on electronic interaction. The four orbital model of Gouterman[44,45] for a single porphyrin is the starting point of what they have called the eight-orbital model. This model evolves from the two set of four orbitals by a process best described as the linear combination of molecular orbitals (LCMO). Non-zero overlap between two iso-energetic orbitals of neighboring porphyrins generates a new pair of orbitals, consisting of a bonding and anti-bonding orbital with an energy difference dependent on the strength of the interporphyrin interaction. Notwithstanding its simplicity, this model succeeds amazingly well in describing the complex shape of the B-band and the red-shift of the Q-band in the electronic spectrum of covalently linked porphyrinic dimers such as PyyP as well as those of their mono- and di-anion, which is clearly related to the ethynylenic bridged dimers we have investigated.

Most important for this chapter is that whichever explanation is used, both lead to the same conclusion: the broadest B-band indicates the strongest electronic coupling between the porphyrin moieties. The trend in porphyrin-porphyrin interaction shown by the splitting of the B-band in the optical data is therefore in agreement with the outcome of the TRMC measurements.

6.3.4 Triplet states.

Zinc porphyrins are known from transient optical absorption and EPR experiments to have high efficiencies for intersystem crossing, ϕ_{isc}, to form relatively long-lived triplet states[46]. The value of ϕ_{isc} for a derivative very similar to yyPyy has for example been determined to be 0.8[47]. We therefore attribute the long-lived TRMC transients observed for some of the ethynyl derivatives in the present experiments to the formation of T_1 states with a polarizability larger than that of the ground state molecules. The values of $\phi_{isc}\Delta V_p(T_1)$ derived from the transients are listed in Table I. If we assume the intersystem crossing efficiency to be similar to that given above then the actual values of $\Delta V_p(T_1)$ would be only approximately 20% larger than the products given in Table I. A general qualitative conclusion that can immediately be drawn from the data is that the T_1 state has a considerably lower polarizability, by approximately an order of magnitude, than S_1. This indicates a much smaller degree of delocalization which is in agreement with EPR measurements on the triplet state of a series of ethynylic bridged multiporphyrin arrays by Angiolillo *et al.*[48]. By

comparing the results for monomeric porphyrins similar to P, yPy and yyPyy with oligomers of the type PyP, PyyP and PyPyP these authors concluded that the electron spins associated with T_1 were strongly localized on a single chromophore of the oligomer.

The absolute values of $\phi_{isc}\Delta V_p(T_1)$ for the diethynyl substituted compounds indicate that there may be some delocalization of the triplet wavefunction into the substituent groups. There is however no definite trend in the values similar to that found for the excited singlet states.

6.4 CONCLUSIONS

The interaction in the excited singlet state between two zinc porphyrin moieties joined together by a covalent bridge is strongly dependent on the nature of the bridging unit. For linkage *via* a single σ-bond or a 1,4-phenylene group the interaction is mainly Coulombic and is much weaker for the latter, as evidenced by the influence on the B-band absorption. Bridges containing ethynyl groups lead to strong electronic coupling between the porphyrins, as evidenced by a large polarizability change on photoexcitation, $\Delta V_p(S_1)$, and a large bathochromic shift in the Q-band absorption and fluorescent emission. The order of the strength of the electronic coupling for the different bridges (with $\Delta V_p(S_1)$ in parentheses) is the following: 1,4-phenylene (< 20 Å^3) < σ-bond (50 Å^3) < 1,4-diethynylbenzene (270 Å^3) < 2,5-diethynylthiophene (390 Å^3) ≈ butadiyne (400 Å^3) < 9,10-diethynylanthracene (590 Å^3). The strong electronic coupling for butadiyne and the ethynyl containing units is attributed to the contribution of cumulenic and cumulenic-quinoidal resonance structures in the excited state. Interestingly, the strong electronic coupling in these ethynylenic coupled dimers appears to extend the effective range of the Coulombic interaction. The relatively weak electronic coupling for the σ-bond and 1,4-phenylene linkages is attributed, at least in part, to steric hinderance, preventing coplanarity of the porphyrin macrocycles in the former case and the central phenylene ring in the latter case.

The excess polarizabilities associated with triplet state formation are approximately an order of magnitude less than for the S_1 state, indicating a much greater degree of localization for the former.

ACKNOWLEDGEMENT

We would like to thank Dr. Bas Wegewijs for the helpful discussions concerning the contents of the paper and Paul Miller, Melanie de Souza and Garry Rumbles for their help in carrying out the single photon fluorescence decay measurements at Imperial College, London, UK. The research was financially supported by The Netherlands Organisation for Scientific Research (NWO) and EPSRC, UK.

REFERENCES

[1] G. McDermott, S. M. Prince, A. A. Freer, A. M. Hawthornthwaite-Lawless, M. Z. Papiz, R. J. Cogdell, N. W. Isaacs: Nature 374 (1995), 517-521.

[2] J. Diesenhofer, H. Michel: Science 245 (1989), 1463-1473.

[3] M. R. Wasielewski: Chem. Rev. 92 (1992), 435-461.

[4] J. M. Tour: Chem. Rev. 96 (1996), 537-553.

[5] V. Balzani, F. Scandola:"Supramolecular Photochemistry", Ellis Horwood: New York 1991, ISBN 0-13-877531-1.

[6] H. L. Anderson: Chem. Commun. (1999), 2323-2330.

[7] M. Kasha: Rad. Res. 20 (1963), 55-71.

[8] M. Kasha, H. R. Rawls, M. A. El-Bayoumi: Pure Appl. Chem. 11 (1965), 371-392.

[9] Th. Förster: Disc. Farad. Soc. 27 (1959), 7-23.

[10] P. F. Barbara, T. J. Meyer, M. A. Ratner: J. Phys. Chem. 100 (1996), 13148-13168.

[11] M. J. Shephard, M. N. Paddon-Row, K. D. Jordan: Chem. Phys. 176 (1993), 289-304.

[12] W. B. Davis, W. A. Svec, M. A. Ratner, M. R. Wasielewski: Nature 396 (1998), 60-63

[13] M. P. de Haas, J. M. Warman: Chem. Phys. 73 (1982), 35-53.

[14] W. Schuddeboom:"Photophysical Properties of Opto-Electric Molecules studied by Time-Resolved Microwave Conductivity", Ph.D. Thesis: Delft 1994, ISBN 90-73861-21-7.

[15] J. M. Warman, G. H. Gelinck, J. J. Piet, J. W. A. Suykerbuyk, M. P. de Haas, B. M. W. Langeveld-Voss, R. A. J. Janssen, D.-H. Hwang, A. B. Holmes, M. Remmers, D. Neher, K. Müllen, P. Bäuerle: Proc. Int. Soc. Opt. Eng., SPIE 3145 (1997), 142-149.

[16] W. Verbouwe, M. Van der Auweraer, F. C. De Schryver, J. J. Piet, J. M. Warman: J. Am. Chem. Soc. 120 (1998), 1319-1324.

[17] S. A. Jonker, J. M. Warman: Chem. Phys. Lett. 185 (1991), 36-40.

[18] J. J. Piet, H. A. M. Biemans, J. M. Warman, E. W. Meijer: Chem. Phys. Lett. 289 (1998), 13-18.

[19] G. D. Scholes, G. O. Turner, K. P. Ghiggino, M. N. Paddon-Row, J. J. Piet, W. Schuddeboom, J. M. Warman: Chem. Phys. Lett. 292 (1998), 601-606.

[20] G. H. Gelinck, J. J. Piet, J. M. Warman: Synth. Met. 101 (1999), 553-554.

[21] G. H. Gelinck:"Excitons and Polarons in Luminescent Conjugated Polymers", Ph.D. Thesis, Delft University Press: Delft 1998, ISBN 90-407-1787-7.

[22] A. Osuka, H. Shimidzu: Angew. Chem. Int. Eng. Ed. 36 (1997), 135-137.

[23] A. Osuka, N. Tanabe, S. Nakajima, K. Maruyama: J. Chem. Soc. Perkin Trans. 2 (1995), 199-203.

[24] P. N. Taylor, A. P. Wylie, J. Huuskonen, H. L. Anderson: Angew. Chem. Int. Ed. 37 (1998), 986-989.

[25] H. L. Anderson: Inorg. Chem. 33 (1994), 972-981.

[26] W. Schuddeboom, S. A. Jonker, J. M. Warman, U. Leinhos, W. Kühnle, K. A. Zachariasse: J. Phys. Chem. 96 (1992), 10809-10819.

[27] J. M. Warman, W. Schuddeboom, S. A. Jonker, M. P. de Haas, M. N. Paddon-Row, K. A. Zachariasse, J.-P. Launay: Chem. Phys. Lett. 210 (1993), 397-404.

[28] T. Nagata, A. Osuka, K. Maruyama: J. Am. Chem. Soc. 112 (1990), 3054-3059.

[29] R. G. Khoury, L. Jaquinod, K. M. Smith: Chem. Commun (1997), 1057-1058.

[30] S. P. Greiner, J. Winzenburg, B. von Maltzan, C. J. Winscom, K. Möbius: Chem. Phys. Lett. 155 (1989), 93-98.

[31] R. W. Wagner, T. E. Johnson, J. S. Lindsey: J. Am. Chem. Soc. 118 (1996), 11166-11180.

[32] J.-S. Hsiao, B. P. Krueger, R. W. Wagner, T. E. Johnson, J. K. Delaney, D. C. Mauzerall, G. R. Fleming, J. S. Lindsey, D. F. Bocian, R. J. Donohoe: J. Am. Chem. Soc. 118 (1996), 11181-11193.

[33] J. Seth, V. Palaniappan, R. W. Wagner, T. E. Johnson, J. S. Lindsey, D. F. Bocian: J. Am. Chem. Soc. 118 (1996), 11194-11207.

[34] D. Beljonne, G. E. O'Keefe, P. J. Hamer, R. H. Friend, H. L. Anderson, J. L. Brédas: J. Chem. Phys. 106 (1997), 9439-9460.

[35] S. M. LeCours, S. G. DiMagno, M. J. Therien: J. Am. Chem. Soc. 118 (1996), 11854-11864.

[36] Z. Wang, P. N. Day, R. J. Pachter: Chem. Phys. 108 (1998), 2504-2510.

[37] R. Kumble, S. Palese, V. S.-Y. Lin, M. J. Therien, R. M. Hochstrasser: J. Am. Chem. Soc. 120 (1998), 11489-11498.

[38] V. S.-Y. Lin, S. G. DiMagno, M. J. Therien: Science 264 (1994), 1105-1111.

[39] U. Scherf, K. Müllen: Synthesis (1992), 23-38.
[40] A. Ohlemacher, R. Schenk, H. P. Weitzel, N. Tyutyulkov, M. Tasseva, K. Müllen: Makromol. Chem. 193 (1992), 81-93.
[41] R. Garay, H. Naarmann, K. Müllen: Macromolecules 27 (1994), 1922-1927.
[42] V. S.-Y. Lin, M. J. Therien: Chem. Eur. J. 1 (1995), 645-651.
[43] D. P. Arnold, G. A. Heath, D. A. James: J. Porphyrins Phthalocyanines 3 (1999), 5-31.
[44] M. Gouterman: J. Mol. Spectroscopy 6 (1961), 138-163.
[45] M. Gouterman, G. H. Wagnière, L. C. Snyder: J. Mol. Spectroscopy 11 (1963), 108-127.
[46] S. Gentemann, N. Y. Nelson, L. Jaquinod, D. J. Nurco, S. H. Leung, C. J. Medforth, K. M. Smith, J. Fajer, D. Holten: J. Phys. Chem. B 101 (1997), 1247-1254.
[47] G. E. O'Keefe, G. J. Denton, R. T. Phillips, R. H. Friend, H. L. Anderson: J. Chem. Phys. 104 (1996), 805-811.
[48] P. J. Angiolillo, V. S.-Y. Lin, J. M. Vanderkooi, M. J. Therien: J. Am. Chem. Soc. 117 (1995), 12514-12527.

7

PORPHYRIN OLIGOMERS[‡]

7.1 INTRODUCTION

Research on excitons in multi-porphyrinic arrays gained considerable momentum from the elucidation of the structure of the LH2 antenna complex of the photosynthetic purple bacterium *Rhodopseudomonas acidophila*[1]. Bacteriochlorophyll is the most abundant chromophore in LH2 and the circular arrangement of eighteen of these porphyrin derivatives has attracted special attention[2]. To elucidate the underlying structure-property relation of these subtly organized arrays of chromophores a large variety of covalently bound multi-porphyrinic arrays have been synthesized[3-5]. To fully understand the relation between the

[‡] Chapter 7 has appeared previously as an article: J. J. Piet, P. N. Taylor, B. R. Wegewijs, H. L. Anderson, A. Osuka, J. M. Warman "Photoexcitations of covalently bridged zinc porphyrin oligomers: Frenkel versus Wannier-Mott type excitons.", J. Phys. Chem. B 105 (2001), 97-104.

three-dimensional structure and the photophysical properties a more thorough knowledge is required of the dependence of the photophysics of a multi-chromophoric array on the two possible kinds of inter-chromophoric interactions: electrostatic and electronic[6].

The properties of photoexcitations of multi-chromophoric arrays are frequently discussed in terms of excitons by analogy with the theory of excitations in molecular crystals[7,8]. An exciton is a neutral, bound electron-hole pair which has properties that differ from those of the excited state of an isolated chromophore. These differences result from a combination of electrostatic and electron-exchange interactions with other identical chromophores in the vicinity.

If electron exchange between chromophores is inhibited, *i.e.* the exciton is localized almost exclusively on a single chromophore, then the inter-chromophoric interactions will be mainly electrostatic in origin. Such a tightly bound electron-hole pair is referred to as a Frenkel exciton[8,9]. Transfer of energy within a chromophoric array in this case occurs *via* the concerted recombination of the exciton on one chromophore and excitation of its neighbor, mediated via the transfer of a virtual photon. This mechanism of energy migration, which is commonly referred to as Förster transfer[10], can result in "photonic-wire" characteristics of one-dimensional arrays.

Electronic interaction, either by direct overlap of the π-orbitals of the chromophores or mediated by the orbitals of the intervening bridge, allows electron exchange between individual chromophores to occur. As a consequence, the hole and electron, forming the exciton, are not necessarily localized on the same chromophore at any given moment in time. In molecular crystal theory such a weakly bound electron-hole pair is referred to as a Wannier-Mott exciton[8,11,12]. The process of exchange of the electron and hole between chromophoric units offers an additional pathway for exciton migration which is not available to Frenkel excitons. If thermal energy suffices to overcome the Coulombic attraction between the electron-hole pair of a Wannier-Mott exciton, it can dissociate into separate mobile charge carriers.

The optical properties of Frenkel excitons only differ from those of an isolated chromophore by small red or blue shifts of absorption bands, which are the result of Davydov splitting[13,14]. The size and sign of this purely electrostatic effect depends on the magnitude of the transition dipole moment associated with the particular excitation and the relative orientation of the chromophores involved, as described by Kasha *et al.*[15]. Wannier-Mott excitons, on the other hand, can display relatively large shifts to lower energies of the lowest absorption and emission bands because of the increased conjugation length and the creation of new charge-transfer states. In this case the effects are independent of the transition dipole moment of the original excitation and they depend on the relative orientation only insofar as it affects the electronic coupling matrix element between chromophores.

In addition to such distinguishing differences in optical properties, it should in principle be possible to differentiate Frenkel and Wannier-Mott type excitons by their polarizabilities. Thus, the strongly bound electron-hole pair of the former should be only weakly polarizable, whereas the weak binding of the latter should be apparent as a relatively large polarizability. Measurement of the polarizability of photoexcitations has recently become possible using the flash-photolysis time-resolved microwave conductivity technique (FP-TRMC)[16,17] by which the changes in the real and imaginary components of the dielectric constant of a solution occurring on photoexcitation of the solute can be monitored. Changes in the molecular polarizability are observed as a change in the real part of the complex permittivity: the dielectric constant[18-21].

In the previous chapter[22] on covalently bridged porphyrin dimers it was shown that the type of interchromophoric interaction prevailing is strongly dependent on the nature of the intervening bridge. A 1,4-phenylene bridge, for example, allows only electrostatic interaction between the attached porphyrins because of steric hindrance, which forces the 1,4-phenylene unit out of co-planarity with the porphyrin rings[23,24] and prevents efficient π-orbital overlap. On the other hand, electronic interactions dominate when an 1,4–butadiynylene bridge is used. The efficient electronic coupling *via* ethynylenic bridges has been substantiated by theoretical calculations[25] and is ascribed to a cumulenic resonance structure of the bridging unit in the excited state[26,27]. In this chapter we have investigated the effect of increasing the number of porphyrin moieties in linear multi-porphyrinic arrays on the polarizability and optical properties of the singlet and triplet excited states in relation to the prevailing interchromophoric interaction.

7.2 EXPERIMENTAL SECTION

In Figure 1 the molecular structures of the pentamers of the two series of porphyrin oligomers investigated are given to illustrated the major differences. The methods of synthesis and structural characterization of the compounds under investigation have been given in other publications[28-30], which are indicated in the last column of Table I. The exact structures of the other oligomers investigated can be found in these references as well. Throughout this chapter the following pseudonyms are used: $(PB)_n$ for the 1,4-phenylene-bridged compounds and $(yPy)_n$ for the 1,4–butadiynylene-bridged compounds, where n equals the number of porphyrins in the oligomer.

All measurements were performed in benzene (Merck, Uvasol). The solute concentrations range between $10^{-5}-10^{-4}$ M. To prevent aggregation 1 wt% 1,4-diazabicyclo[2,2,2]octane, DABCO (Aldrich 98%), was added, which is equal to a concentration of *ca.* 10^{-1} M.

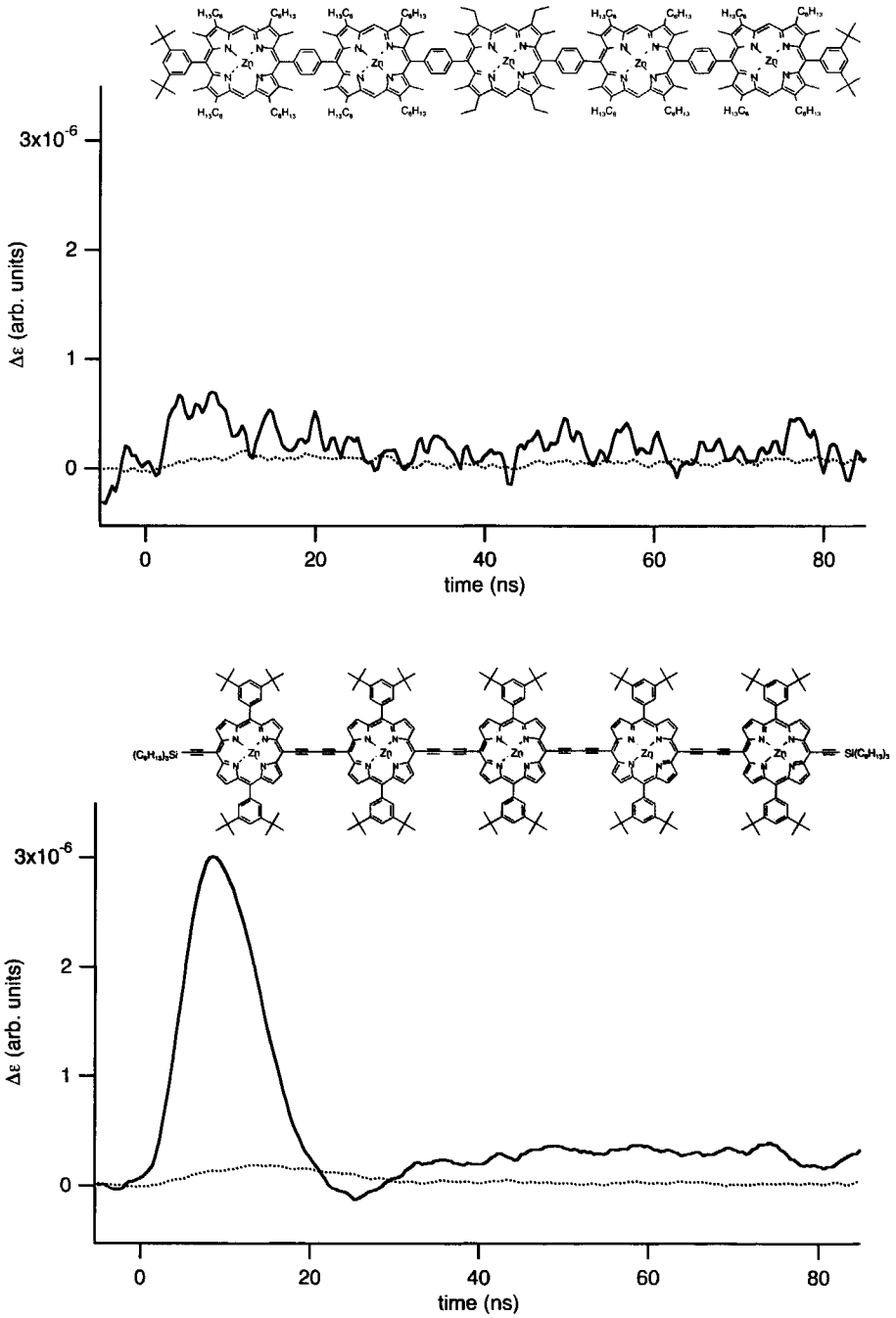

FIGURE 1: The molecular structure of $(PB)_5$ and $(yPy)_5$ shown together with their real (full line) and imaginary (dotted line) $\Delta\varepsilon$ transient measured on dilute solutions in benzene with 1% DABCO.

The large excess of DABCO ensures that only a negligible amount of solute molecules is present as ladders[28].

Optical absorption spectra were recorded on a Kontron Uvikon 940 spectrophotometer or a Perkin-Elmer Lambda 20 UV-Vis-NIR spectrophotometer. Emission spectra were recorded either on a PTI "quantamaster 1" spectrofluorimeter equipped with a double excitation and a single emission monochromator or on a FluoroMax-2 spectrofluorometer fitted with a red-sensitive R928P photomultiplier. All samples were excited at a wavelength close to the maximum of their B-band. The optical density at the excitation wavelength never exceeded 0.2.

The fluorescence lifetimes of the $(PB)_n$ series were determined from real-time transients using the 0.8-ns, 337-nm pulse of a Laser Photonics LN1000 nitrogen laser as excitation source and a Photek "PMT-113-UHF" channel-plate photomultiplier with a risetime of 150 ps as detector. For the $(yPy)_n$ series the fluorescence lifetime was determined with a time resolution of less than 100 ps using the 630-nm pulse from a cavity-dumped mode-locked dye laser synchronously pumped by the second harmonic of a continuous-wave, mode-locked Nd-YAG laser.

For the TRMC experiments the solutes were contained in an X-band (8.2-12.4 GHz) resonant cavity and were photo-excited at 308 nm using single unfocused 7-ns FWHM pulses from a Lumonics HyperEX-400 (HE 420) XeCl excimer laser. A maximum of 16 pulses was used for signal averaging. The optical densities of the solutions varied from *ca.* 0.3 to 0.9 for a 1-cm path length. Prior to use, the solutions were purged with CO_2 to remove oxygen. A pair of transients was recorded at the lower, f-, and upper, f+, half-power frequency. The real and imaginary contributions to the photo-induced changes of the complex dielectric constant, $\Delta\varepsilon'$ and $\Delta\varepsilon''$, can be obtained separately by subtraction and addition of the f- and f+ transients respectively. The procedure for the analysis of the data is given in previous publications[18,22].

7.3 RESULTS & DISCUSSION

7.3.1 TRMC results.

As mentioned in the previous section, changes in both the real and imaginary component of the complex permittivity, $\Delta\varepsilon = \Delta\varepsilon' - j\Delta\varepsilon''$, resulting from photoexcitation of the solute molecules can be measured separately with the FP-TRMC technique. A change in the imaginary component or dielectric loss, $\Delta\varepsilon''$, is related to the formation of mobile charges. This results from either translational motion of free charge carriers or rotational motion of dipolar excited states. Changes in the real component or the dielectric constant, $\Delta\varepsilon'$, indicate an increase in the polarizability of the solute molecules after excitation, $\Delta\alpha$. Out-of-phase motion of mobile charges can also contribute to $\Delta\varepsilon'$. Therefore, it is possible to determine $\Delta\alpha$

from $\Delta\varepsilon'$ only when an estimate of this contribution to $\Delta\varepsilon'$ can be made from a knowledge of $\Delta\varepsilon''$. For convenience of presentation the change in polarizability per excited molecule is expressed as the change in polarizability volume, ΔV_p ($= \Delta\alpha/4\pi\varepsilon_0$).

The $\Delta\varepsilon'$ and $\Delta\varepsilon''$ transients for the pentamers of each series, $(PB)_5$ and $(yPy)_5$, are shown in Figure 1. No significant $\Delta\varepsilon''$ transient is observed in either case. This is found for all of the oligomers investigated and shows unequivocally the absence of any contribution to $\Delta\varepsilon'$ from mobile charges or dipolar excited states. It can be concluded therefore that only neutral excitons are formed and ΔV_p can be derived from $\Delta\varepsilon'$ using equation (1)[22]:

$$\Delta V_p = \frac{9}{4\pi(\varepsilon'+2)^2 N_*}\Delta\varepsilon' \qquad (1)$$

In equation (1) N_* is the concentration of excited states and ε' is the dielectric constant of the solution.

Values of ΔV_p of the excited states formed were derived from fits to the $\Delta\varepsilon'$ transients. Because only neutral excited states are populated, only contributions from the lowest singlet, S_1, and the lowest triplet state, T_1, were taken into account. The lifetimes of the S_1 states used in the fitting procedure, were obtained from fluorescence decay measurements and are given in Table I. The lifetime of the T_1 state was not measured but, since no decay of the T_1 state is observed in the first 100 ns after excitation, it is expected to be at least several μs. In the fitting procedure it is sufficient to use an arbitrary lifetime of 1 μs for all molecules investigated. The use of longer T_1 lifetimes in the fitting procedure do not yield significantly different results. The value of $\Delta V_p(S_1)$ could be obtained directly from the fits, since the quantum yield for formation of S_1 may be assumed to be unity. For the triplet state however, only the product $\phi_{isc}\Delta V_p(T_1)$ could be obtained, with ϕ_{isc} the quantum efficiency for intersystem crossing. The values of $\Delta V_p(S_1)$ and $\phi_{isc}\Delta V_p(T_1)$ are given in Table I.

7.3.1.1 $(PB)_n$ series.

None of the $\Delta\varepsilon'$ transients of any member of the $(PB)_n$ series exceeded the noise-level. Because of this, only an upper limit of 20 Å^3 could be determined for $\Delta V_p(S_1)$. Therefore, we conclude that the excited singlet state of the $(PB)_n$ series is localized on a single chromophore and consists of a tightly bound electron-hole pair. This means that the S_1 excited state of the $(PB)_n$ series can be characterized as a Frenkel type exciton.

Similarly, for the product $\phi_{isc}\Delta V_p(T_1)$ only an upper limit of 5 Å^3 could be estimated. Since the quantum efficiency for intersystem crossing for zinc porphyrins is known to be very high, *i.e.* ϕ_{isc} is close to unity[31,32], $\Delta V_p(T_1)$ must be close to zero. This shows that the triplet state of the $(PB)_n$ oligomers is also highly localized on a single porphyrin moiety.

Table I: The fluorescent lifetime, $\tau(S_1)$, the excess polarisability volume of the singlet state, $\Delta V_p(S_1)$, the product of the intersystem crossing efficiency and the excess polarisability volume of the triplet state, $\phi_{isc}\Delta V_p(T_1)$, and the maximum of the fluorescence, $E_{fl,max}$.

compound	$\tau(S_1)$ (ns)	$\Delta V_p(S_1)$ (Å^3)	$\phi_{isc}\Delta V_p(T_1)$ (Å^3)	$E_{fl,max}$ (eV)	Reference[a)]
$(PB)_1$	1.30[b)]	<20[c)]	<5[c)]	1.91	29
$(PB)_2$	0.90[b)]	<20[c)]	<5[c)]	1.89	30
$(PB)_3$	0.75[b)]	<20[c)]	<5[c)]	1.90	30
$(PB)_5$	0.65[b)]	<20[c)]	<5[c)]	1.89	30
$(yPy)_1$	1.60	30±20	<5[c)]	1.90	28
$(yPy)_2$	1.25	400±40	30±5	1.64	28
$(yPy)_3$	1.08	690±70	20±5	1.55	28
$(yPy)_4$	0.89	920±90	16±5	1.51	28
$(yPy)_5$	0.82	830±80	12±5	1.50	28
$(yPy)_6$	0.86	960±100	10±5	1.49	28

a) Reference to synthesis.

b) Fastest component of a two component fit, in all cases a second component with a lifetime of *ca.* 5 ns was used.

c) Upper limit corresponding to the noise level.

7.3.1.2 $(yPy)_n$ series.

FP-TRMC measurements show a completely different behaviour of the $(yPy)_n$ series. Figure 1 displays the large $\Delta\varepsilon'$ transient observed for $(yPy)_5$. The transient consists of a short-lived component and a long-living tail, which is typical for a singlet and a triplet contribution respectively. Comparable transients are obtained for all other members of the $(yPy)_n$ series, except the monomer, $(yPy)_1$, whose triplet contribution fails to exceed the noise level. The values of $\Delta V_p(S_1)$ and $\phi_{isc}\Delta V_p(T_1)$ obtained from the fits to the transients are listed in Table I.

The dramatic increase in $\Delta V_p(S_1)$ from 30 Å^3 for the monomer, $(yPy)_1$, to 400 Å^3 for the dimer, $(yPy)_2$, has been reported previously[22]. As can be seen from the data in Table I, $\Delta V_p(S_1)$ increases further on increasing the length of the oligomers, up to a value of 960 Å^3 for the hexamer. This value is more than twice the 400 Å^3 of the dimer, indicating a delocalization of the exciton wave function over most of the available chromophores even in the longest oligomers. Therefore, the electron-hole pair on the $(yPy)_n$ oligomers is only weakly bound and the exciton must be of the Wannier-Mott type. Since electron exchange between the porphyrin chromophores occurs, the required electronic interaction has to be mediated by the intervening bridge. This apparent efficacy of the 1,4–butadiynylene bridge in promoting electronic interactions between porphyrins has been attributed previously to the participation of cumulenic resonance structures in the excited state[22,25-27,33]

The development of the optoelectronic properties of linear molecular arrays with increasing chain length is frequently discussed in terms of the delocalization or correlation length of the excitonic state. This is a rather ill-defined property however, which purports to give a measure of the physical extent of the excitonic wavefunction in terms of the number of monomer units. In the present case the values of the S_1 state polarizabilities, as given by $\Delta V_p(S_1)$ in Table I, appear to saturate for a chain lengths of 4 or longer. The effective exciton delocalization length for the present compounds may therefore be concluded to be 3 to 4 monomer units

Using perturbation theory, the exciton polarizability can be expressed in simple quantum mechanical terms, which relates the polarizability of the S_1 state to the coupling between S_1 and all other states in the singlet manifold according to

$$\alpha = \frac{2}{3}\sum_{n\neq 1}\frac{\mu_{n1}^2}{\Delta E_{n1}} \qquad (2)$$

with μ_{n1} the transition dipole matrix element and ΔE_{n1} (= $|E_n - E_1|$) the energy gap between S_1 and S_n. For the frequently made simplification of a three level system involving the ground state S_0, the first excited state, S_1 and a second state S_2, equation (2) becomes

$$\alpha = \frac{2}{3}\left(\frac{\mu_{21}^2}{\Delta E_{21}} - \frac{\mu_{01}^2}{\Delta E_{01}}\right) \qquad (3)$$

A large exciton polarizability will result therefore from strong coupling between S_1 and an upper state which lies close in energy. In the present case this is most probably a state with a high degree of charge transfer character.

It is interesting to compare our results on the polarizability of S_1 with the results from recent degenerate four wave mixing (DFWM) experiments on the same $(yPy)_n$ oligomers[34]. In the DFWM experiments, a dramatic increase in the second hyperpolarizability constant, γ, was found in going from the monomer to the dimer, 0.0063 to 0.48 in units of 10^{-45} m^5/V^2, followed by successive substantial increases with further increase in the chain length up to γ = 3.1 for the pentamer. The value of γ can also be described in terms of electronic coupling using a three state model which results in equation (4) for non-dipolar ground and excited states.

$$\gamma \propto \frac{\mu_{01}^2}{\Delta E_{01}^2}\left(\frac{\mu_{21}^2}{\Delta E_{02}} - \frac{\mu_{01}^2}{\Delta E_{01}}\right) \qquad (4)$$

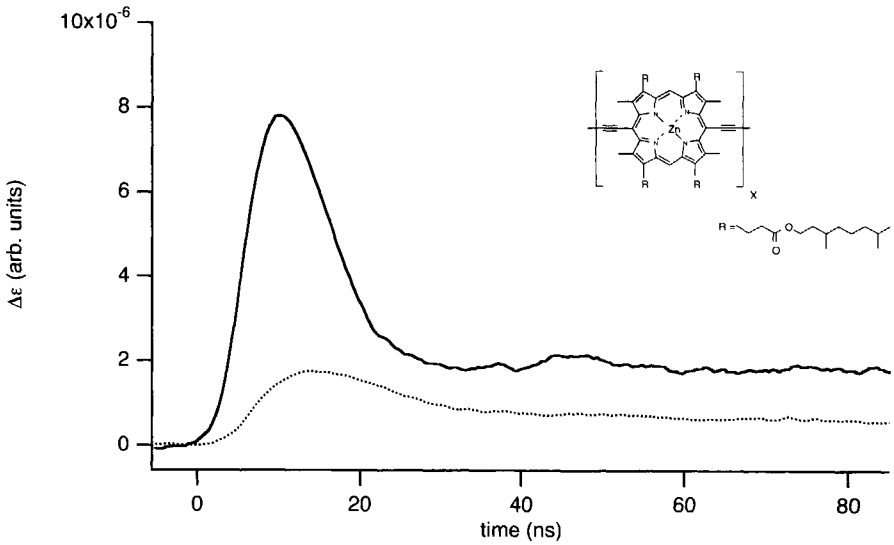

FIGURE 2: The real (full line) and imaginary (dotted line) $\Delta\varepsilon$ transient of the short polymer $(yPy)_x$ measured in benzene with 1% DABCO and as inset the molecular structure of $(yPy)_x$ (x > 10).

Both α and γ are seen to be large for large values of μ_{21} and to increase with decreasing energy difference between the states in the singlet manifold. The correlation between these two parameters is therefore to be expected for the present compounds for which the transition energies are found to decrease markedly with increasing chain length.

DFWM measurements on a related short polymer, $(yPy)_x$ with x between 10 and 15, showed again a very large increase in the third order polarizability in comparison to the longest oligomer[34,35]. In line with the above given parallel dependences of α and γ on chain length a very large $\Delta\varepsilon'$ transient is measured for $(yPy)_x$, which is shown in Figure 2. Unfortunately, a complication arises for $(yPy)_x$ that prevents the determination of $\Delta V_p(S_1)$ and $\phi_{isc}\Delta V_p(T_1)$ from the $\Delta\varepsilon'$ transient. In a previous publication we reported for $(yPy)_x$ a significant long-lived $\Delta\varepsilon''$ transient after excitation. This transient, which is also shown in Figure 2, was attributed to the formation of mobile charges by low-yield exciton dissociation[36]. This was substantiated by the non-exponential decay of the transient. Because the contribution of the mobile charge carriers to the $\Delta\varepsilon'$ transient is not known, equation (1) no longer holds and the value of $\Delta V_p(S_1)$ cannot be determined. However, from the large $\Delta\varepsilon'$ transient in Figure 2 it is clear that the primarily formed S_1 state is highly polarizable. A small amount of these Wannier-Mott like excitons must decay by exciton dissociation to explain the mobile charge carriers responsible for the $\Delta\varepsilon''$ transient.

In order to compare the polarizability volumes of the S_1 and T_1 states, a knowledge of the intersystem crossing is required to calculate $\Delta V_p(T_1)$ from $\phi_{isc}\Delta V_p(T_1)$. As mentioned in

the previous section, ϕ_{isc} for zinc porphyrin derivatives are in general large[31] and a value of 0.80 has been determined[32] for $(yPy)_2$. Using this value $\Delta V_p(T_1)$ is calculated to be 38 Å^3, which is an order of magnitude smaller than $\Delta V_p(S_1)$ of the same molecule. Therefore, the T_1 state must be much more localized than the S_1 state of $(yPy)_2$ or any other members of the $(yPy)_n$ series. Actually, the value is very close to the value of 30 Å^3 found for the S_1 state of the monomer, indicating that the T_1 state must be considered to be localized on a single porphyrin moiety. This is in agreement with EPR experiments on a related ethynylenic bridged porphyrin dimer and a trimer[37].

In view of this, it seems justifiable to conclude that $\Delta V_p(T_1)$ is independent of chain length and has a value close to the 38 Å^3 determined for $(yPy)_2$. Using this value to calculate ϕ_{isc} from $\phi_{isc}\Delta V_p(T_1)$, a steady decrease in ϕ_{isc} with increasing oligomer length is found: 0.52 for n=3, 0.42 for n=4, 0.32 for n=5 and eventually 0.26 for n=6. Thus, with increasing chain length intersystem crossing becomes increasingly less favourable as a decay pathway for the S_1 state.

7.3.2 Optical measurements.

The UV-Vis absorption spectra of monomeric zinc-porphyrins are characterized by two main features in the visible range: the Q-band (S_0-to-S_1 transition) and the B-band (S_0-to-S_2 transition). The B-band is an extremely intense and sharp absorption band in the 400—500 nm region of the spectrum. The Q-band is considerably weaker than the B-band. It also displays vibrational structure. The emission band of a monomeric zinc-porphyrin is usually a mirror image of the Q-band.

The extremely large transition dipole moment of the B-band can strongly interact electrostatically with other porphyrin B-band transition dipole moments in its vicinity. Because the B-band actually consists of two degenerate transitions which are orthogonal, their respective transition dipole moments can interact differently. If this occurs, the B-band will split. This phenomenon, first recognised as such by Kasha *et al.*, is an example of Davydov splitting[14,15] and is a clear indication of an electrostatic interaction. Because of the much weaker transition dipole moment of the Q-band, Davydov splitting has never been observed for this absorption band for porphyrin derivatives.

Electronic interactions between an orbital of a single chromophore and an orbital close in energy of, for instance, the intervening bridge or an identical chromophore in its neighborhood will replace these two localized orbitals by a pair of new and more extended orbitals. The energy difference between these new orbitals will be proportional to the magnitude of the interaction. If the interaction involves a pair of the highest occupied or lowest unoccupied orbitals the energy gap between the ground-state and the excited state will

be reduced. A bathochromic shift of the affected absorption band will result. Therefore, substantial changes in the position and shape of absorption bands with increasing chain-length suggest electronic interactions between at least some of the chromophores of an oligomer.

Considering the different effects to be expected for electrostatic and electronic inter-chromophoric interactions on the optical properties of multi-porphyrinic arrays, as outlined in the previous paragraphs, it was of interest to compare the FP-TRMC results with the concomitant changes in the optical absorption and emission spectra.

7.3.2.1 $(PB)_n$ series.

The optical absorption and emission spectra for the $(PB)_n$ series are shown in figure 3. As expected in the case of Frenkel excitons, the optical data show no indication of electronic interaction between the chromophores. Apart from the splitting of the B-band the spectra of the three oligomers strongly resemble each other, and even the spectrum of the monomer, $(PB)_1$. Importantly, the position and shape of the Q-band is completely unaffected by the successive addition of porphyrin subunits within the entire series. This shows that the lowest excited state is unaltered compared to an isolated zinc-porphyrin. This is corroborated further by comparison of the emission spectra displayed in figure 3b. The position of the maximum of the emission spectra, see also Table I, shows almost no dependence on the number of chromophores. Only a slight bathochromic shift of the maximum and a change in the shape of the spectrum is observed on going from $(PB)_1$ to $(PB)_2$. A further shift of the emission maximum with an additional increase in the number of monomer units is completely absent.

The splitting of the B-band, which is observed for all members of the $(PB)_n$ series except the monomer, increases with the number of porphyrin subunits in the chain. Similar behaviour has been observed for a closely related $(PB)_n$ series in 1,2-dichlorobenzene as solvent[38]. The splitting of the B-band of the oligomers results in two bands of almost identical magnitude and similar in width. The highest energy band has a maximum at 2.92 ± 0.01 eV, independent of the number of monomer units and equal to that found for the monomer itself. The lower energy band is shifted bathochromically with respect to the higher energy band by 0.07 eV, 0.11 eV and 0.15 eV for n=2, 3 and 5 respectively. This is characteristic for Davydov splitting. According to the Kasha treatment, the bathochromic shift indicates that the main electrostatic interaction involves the transition dipole in the oligomer chain direction. In agreement with this, the evolution of the shift with increasing monomer units is close to that expected, *i.e.* $\Delta E \propto (n-1)/n$, for in-line dipoles[39,40]. The lack of an appreciable blue shift of the higher energy band indicates that the electrostatic interaction between the transition dipole moments orthogonal to the chain direction is extremely weak.

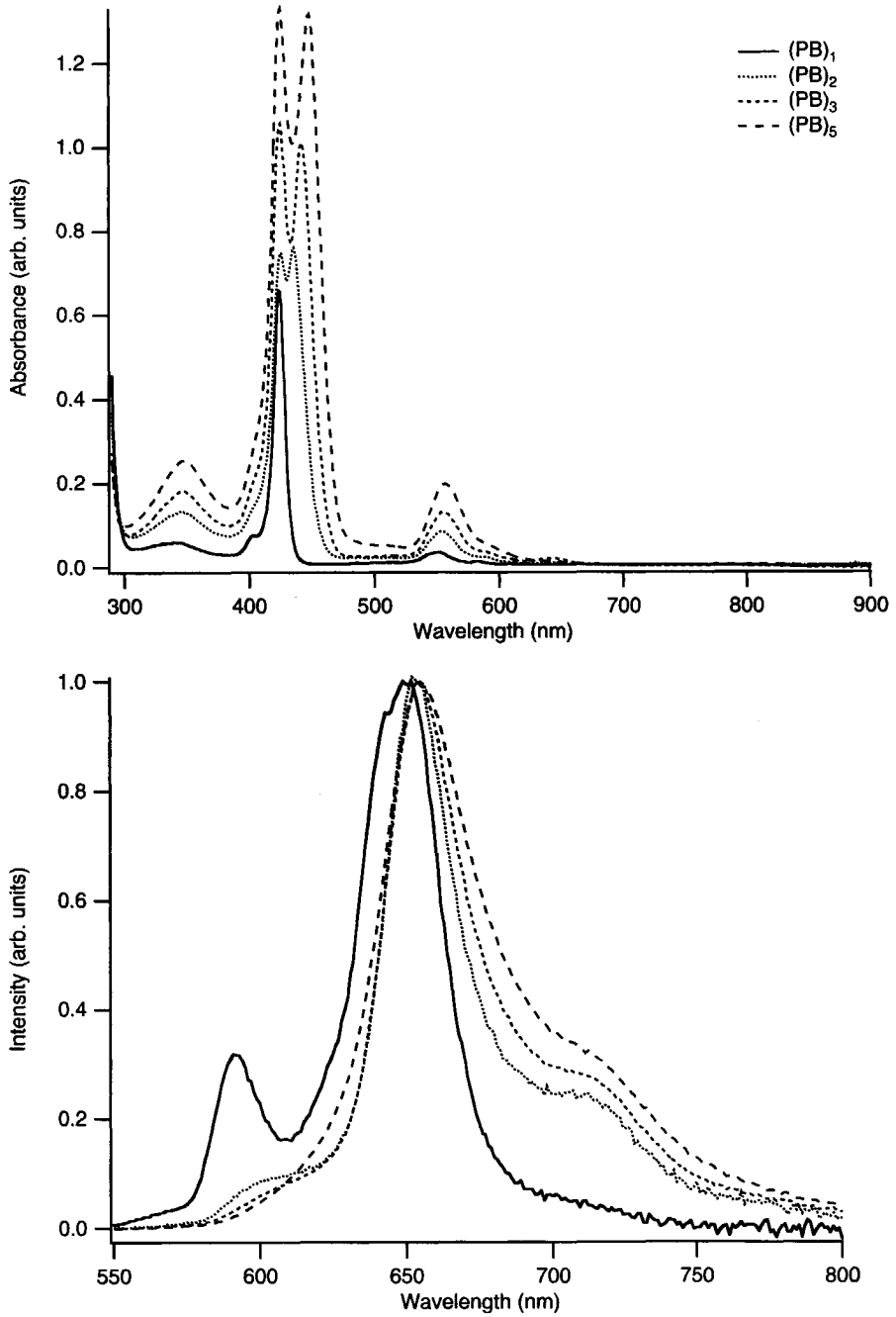

FIGURE 3: The UV-Vis absorption (top) and emission (bottom) spectra of the $(PB)_n$ series in benzene with 1% DABCO.

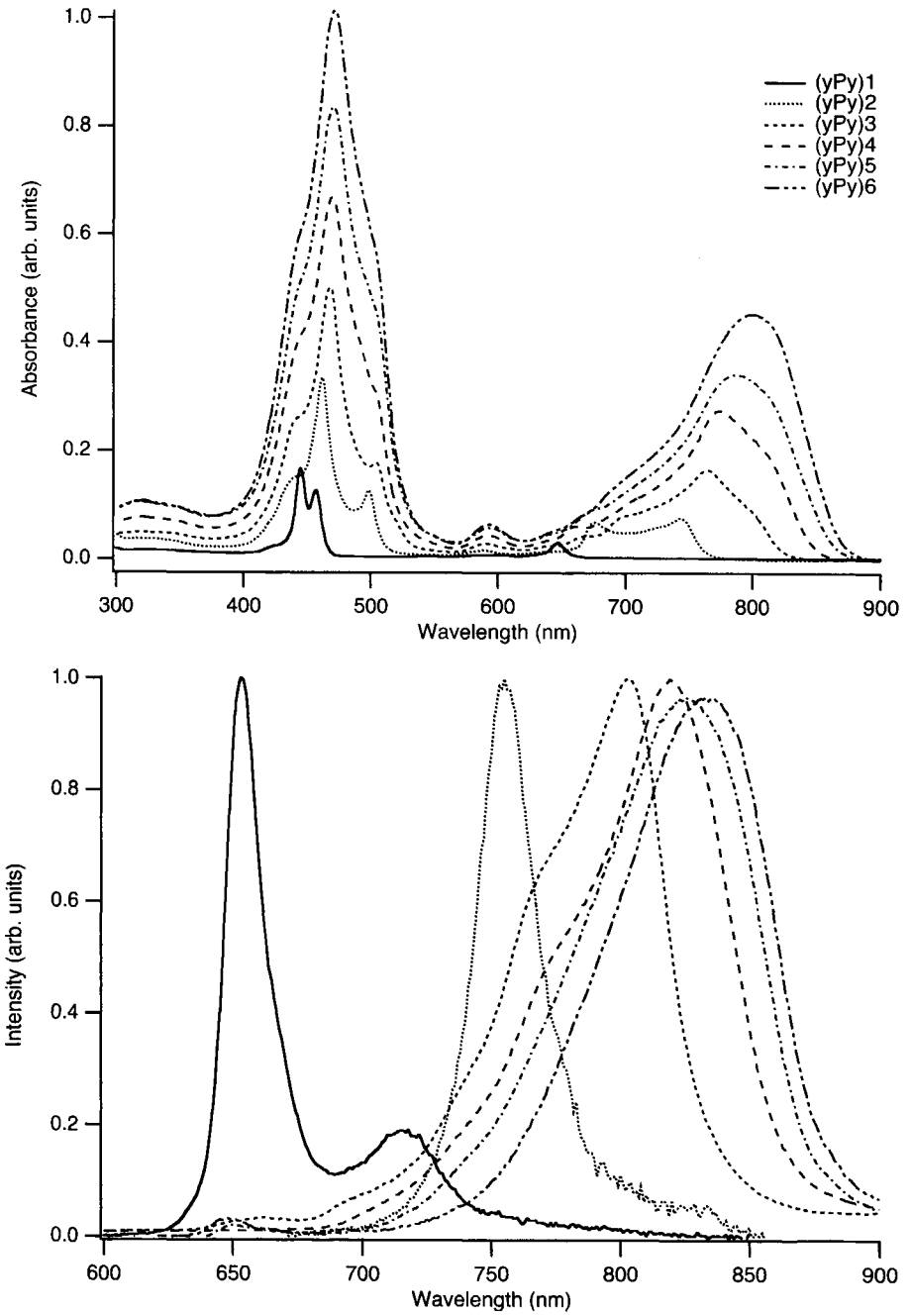

FIGURE 4: The UV-Vis absorption (top) and emission (bottom) spectra of the $(yPy)_n$ series in benzene with 1% DABCO.

7.3.2.2 $(yPy)_n$ series.

Evidence for strong electronic interactions in the $(yPy)_n$ series, as indicated by the polarizability measurements, is apparent from the marked dependence of the position of the Q-band on the length of the oligomer, as shown in figure 4a. In addition to the marked shift of the Q-band to lower energy, its shape is also altered considerably. The structured Q-band with its two maxima typical for a zinc-porphyrin is replaced by a broad band that consists of several gaussian subbands. The different bands can be readily observed as shoulders in the Q-band of the trimer and tetramer. In the longest oligomers they merge completely into a single broad and structureless band.

A pronounced bathochromic shift and broadening is also observed in figure 4b for the emission spectra of the $(yPy)_n$ series. Interestingly, the shift of the emission is more pronounced than that of the Q-band absorption. This means that the Stokes' shift increases with chain length. For two short *meso*-to-*meso* ethynylene bridged porphyrin oligomers, Kumble *et al.* showed that the Stokes' shift of these oligomers is considerably larger than that of a single porphyrin[33]. They put forward the hypothesis that the increase in Stokes' shift in these molecules could result from a relaxation process that forces the porphyrin rings of a single oligomer to adopt a co-planar geometry in the excited state. In this co-planar geometry the conjugation extends over all chromophores and a highly delocalized excited state results, which was expected to be highly polarizable. The hypothesis of Kumble *et al.* is corroborated by the present TRMC measurements, which unequivocally show this large excited state polarizability. Therefore, in line with this hypothesis, we think it is reasonable to relate the increase of the Stokes' shift with increasing chain length to the increase in the number of bridges which must adopt a partial cumulenic bond length pattern to allow the extensive delocalization typical for Wannier-Mott excitons.

In contrast to the Q-band, the position of the B-band is hardly affected by the number of repeat units in the oligomers. A marked change is observed however on going from the monomer to the dimer; there is a substantial shift of the maximum and a change in the splitting pattern. From the trimer onwards, only minor shifts of the maximum are observed with increased oligomer length and the shape of the band hardly alters between $(yPy)_2$ and the longest oligomer, $(yPy)_6$. Only a gradual broadening of the individual sub-bands appears to occur with increasing chain length.

The two maxima of the B-band of the monomer $(yPy)_1$ indicate that the two orthogonal B-band transitions are no longer degenerate in the $(yPy)_n$ series. It is tempting to simply attribute this to the unequal substitution at the two pairs of opposite *meso*-positions, but it is unclear if this is indeed the reason. The splitting pattern of the other members of the $(yPy)_n$ series can be understood from the spectrum of $(yPy)_1$ by assuming electrostatic interactions between neighboring chromophores.

In a recent article Arnold and co-workers introduced a model that seemed to explain the complex shape of the entire UV-Vis spectra of the neutral and the mono- and bis-anion of a butadiynylene-bridged porphyrin dimer from electronic interactions alone[41]. An important prediction of their "eight orbital model" is that pronounced changes in the Q-band should be accompanied by similar changes in the B-band. Figure 4a shows unequivocally that this is not the case for the longer oligomers. Therefore, in contrast to the Q-band of the $(yPy)_n$ series, the B-band is mainly affected by electrostatic interactions.

7.4 CONCLUSION

The photophysics of an array of porphyrins depends strongly on the type of interaction between the chromophores. The two series investigated in this chapter confirm that these properties are determined to a large extend by the nature of the bridge in linear covalently linked arrays.

The 1,4-phenylene bridging unit of the $(PB)_n$ series electronically isolates the porphyrin chromophores. The optical data of all oligomers investigated strongly resemble that of a single porphyrin. The only difference between the spectra is Davydov splitting of the B-band, which results from electrostatic interaction between porphyrins. On excitation only Frenkel excitons are formed. The strongly bound character of the electron-hole pair is shown by the FP-TRMC technique, *i.e.* on photoexcitation a negligible increase in polarizability is observed.

The 1,4–butadiynylene bridging unit of the $(yPy)_n$ series mediates electronic interaction between the porphyrin chromophores *via* a cumulenic resonance structure. A substantial bathochromic shift of the Q-band is observed with increasing number of porphyrin units in an oligomer. The FP-TRMC technique shows the formation of a neutral but highly polarizable excited state. This kind of behaviour is in agreement with the formation of a weakly bound electron-hole pair characteristic of a Wannier-Mott-like exciton. The delocalization of the exciton is seen to increase with increasing chain-length, even up to 6 porphyrin units. For a polymeric $(yPy)_x$ derivative with $x > 10$, evidence is found for dissociation of the Wannier-Mott type exciton into separate mobile charges.

For both oligomer series the T_1 state is found to be localized on a single porphyrin unit.

ACKNOWLEDGEMENT

We would like to thank Paul Miller, Melanie de Souza and Garry Rumbles for their help in carrying out the single photon fluorescence decay measurements at Imperial College,

London, UK. The research was financially supported by The Netherlands Organisation for Scientific Research (NWO) and EPSRC, UK.

REFERENCES

[1] G. McDermott, S. M. Prince, A. A. Freer, A. M. Hawthorntwaite-Lawless, M. Z. Papiz, R. J. Cogdell, N. W. Isaacs: Nature 374 (1995), 517-521.

[2] J. Phys. Chem. B. 101 (1997), 7197-7359 (Special issue on Light-Harvesting Physics Workshop).

[3] M. R. Wasielewski: Chem. Rev. 92 (1992), 435-461.

[4] J. M. Tour: Chem. Rev. 96 (1996), 537-553.

[5] H. L.Anderson: Chem. Commun. (1999), 2323-2330.

[6] V. S.-Y. Lin, M. J. Therien: Chem. Eur. J. 1 (1995), 645-651.

[7] M. A. Pope, C. E. Swenberg: "Electronic Processes in Organic Crystals and Polymers", Oxford University Press: New York 1999.

[8] A. S. Davydov:"Theory of Molecular Excitons", Plenum: New York 1971.

[9] J. Frenkel: Phys. Rev. 37 (1931), 1276-1294.

[10] Th. Förster: Ann. Phys. 2 (1948), 55-75.

[11] G. H. Wannier: Phys. Rev. 52 (1937), 191-197.

[12] N. F. Mott: Trans. Faraday Soc. 34 (1938), 500-506.

[13] A. S. Davydov:"Theory of Molecular Excitons", McGraw-Hill: New York 1962.

[14] M. Kasha: Rad. Res. 20 (19630, 55-71.

[15] M. Kasha, H. R. Rawls,M. A. El-Bayoumi: Pure Appl. Chem. 11 (1965), 371-392.

[16] M. P. de Haas, J. M. Warman: Chem. Phys. 73 (1982), 35-53.

[17] W. Schuddeboom:"Photophysical Properties of Opto-Electric Molecules studied by Time-Resolved Microwave Conductivity", Ph.D. Thesis: Delft 1994, ISBN 90-73861-21-7.

[18] J. M. Warman,G.H. Gelinck,J. J. Piet, J. W. A. Suykerbuyk, M. P. de Haas, B. M. W. Langeveld-Voss, R. A. J. Janssen, D.-H. Hwang, A. B. Holmes, M. Remmers, D. Neher, K. Müllen, P. Bäuerle: Proc. Int. Soc. Opt. Eng., SPIE 3145 (1997), 142-149.

[19] G. H. Gelinck:"Excitons and Polarons in Luminescent Conjugated Polymers", Ph.D. Thesis: Delft University Press: Delft 1998, ISBN 90-407-1787-7.

[20] G. H. Gelinck, J. J. Piet, J. M. Warman: Synth. Met. 101 (1999), 553-554.

[21] G. H. Gelinck, J. J. Piet, B. R. Wegewijs, K. Müllen, J. Wildeman, G. Hadziioannou, J. M. Warman: Phys. Rev. B. 62 (2000), 1489-1491.

[22] J. J. Piet, P. N. Taylor, H. L. Anderson, A. Osuka, J. M. Warman: J. Am. Chem. Soc. 122 (2000), 1749-1757.

[23] A. Osuka, N. Tanabe, S. Nakajima, K. Maruyama: J. Chem. Soc. Perkin Trans. 2 (1995), 199-203.

[24] R. W. Wagner, T. E. Johnson, J. S. Lindsey: J. Am. Chem. Soc. 118 (1996), 11166-11180.

[25] D. Beljonne, G. E. O'Keefe, P. J. Hamer, R. H. Friend, H. L. Anderson, J. L. Brédas: J. Chem. Phys. 106 (1997), 9439-9460.

[26] V. S.-Y. Lin, S. G. DiMagno, M. J. Therien: Science 264 (1994), 1105-1111.

[27] P. N. Taylor, A. P. Wylie, J. Huuskonen, H. L. Anderson: Angew. Chem. Int. Ed. 37 (1998), 986-989.

[28] P. N. Taylor, H. L. Anderson: J. Am. Chem. Soc. 121 (1999), 11538-11545.

[29] A. Osuka, H. Shimidzu: Angew. Chem. Int. Eng. Ed. 36 (1997), 135-137.

[30] A. Osuka, N. Tanabe, S. Nakajima, K. Maruyama: J. Chem. Soc. Perkin Trans. 2 (1995), 199-203.

[31] R. L. Brookfield, H. Ellul, A. Harriman: J. Chem. Soc., Faraday Trans. 2 81 (1985), 1837-1848.

[32] G. E. O'Keefe, G. J. Denton, R. T. Phillips, R. H. Friend, H. L. Anderson: J. Chem. Phys. 104 (1996), 805-811.

[33] R. Kumble, S. Palese, V. S.-Y. Lin, M. J. Therien, R. M. Hochstrasser: J. Am. Chem. Soc. 120 (1998), 11489-11498.

[34] J. R. G. Thorne, S. M. Kuebler, R. G. Denning, I. M. Blake, P. N. Taylor, H. L. Anderson: Chem. Phys. 248 (1999), 181-193.

[35] S. M. Kuebler, R. G. Denning, H. L. Anderson: J. Am. Chem. Soc. 122 (2000), 339-347.

[36] J. J. Piet, J. M. Warman, H. L. Anderson: Chem. Phys. Lett. 266 (1997), 70-74.

[37] P. J. Angiolillo, V. S.-Y. Lin, J. M. Vanderkooi, M. J. Therien: J. Am. Chem. Soc. 117 (1995),

12514-12527.
[38] T. Nagata, A. Osuka, K. Maruyama: J. Am. Chem. Soc. 112 (1990), 3054-3059.
[39] E. G. McRae, M. J. Kasha: Chem. Phys. 28 (1958), 721-722.
[40] E. S. Emerson, M. A. Conlin, A. E. Rosenoff, K. S. Norland, H. Rodriguez, D. Chin, G. R. Bird: J. Phys. Chem. 71 (1967), 2396-2403.
[41] D. P. Arnold, G. A. Heath, D. A. James: J. Porphyrins Phthalocyanines 3 (1999), 5-31

8

PORPHYRIN POLYMER[‡]

8.1 INTRODUCTION

Charge and energy migration within organised assemblies of porphyrinic macrocycles forms the basis of natural photosynthesis and of many of the artificial systems proposed for solar energy conversion.[1-3] Because of this, a large international research effort has been focused on obtaining a fundamental understanding of the factors which control the electronic coupling between porphyrin units. This involves the effects of variables such as the relative geometrical configuration of macrocycles within self-assembling multiple arrays, the presence of peripheral or central substituents, and the incorporation of conjugated or sigma-bonded bridges between like or unlike chromophoric units. The efforts of synthetic chemists have

[‡] Chapter 8 has appeared previously as an article: J. J. Piet, J. M. Warman, H. L. Anderson: "Photo-induced Charge Separation on Conjugated Porphyrin Chains", Chem. Phys. Lett. 266 (1997), 70-74.

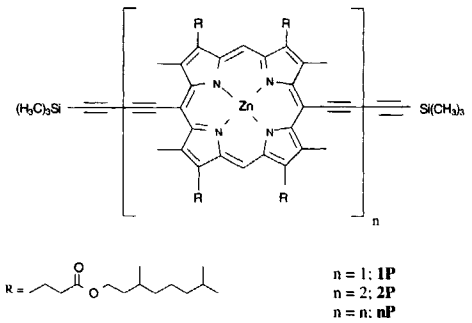

FIGURE 1: The molecular structures of the compounds studied in the present work with the abbreviations used in the text. The value of n for the "polymer" has been determined to be 7 < n < 15 (reference 14).

provided a wealth of porphyrin containing structures with which to test the influence of such variables.[1-4] Many different physical measurement techniques have been applied to interrogate the optoelectronic properties of these fascinating molecular assemblies.

In our own work we have applied microwave conductivity techniques to the study of charge migration within self-organised columnar stacks of porphyrin macrocycles[5] as well as to photo-induced charge separation in individual, sigma-bond-separated porphyrin-quinone dyads[6] and other model systems for photosynthesis.[7,8] The method requires no electrical contacts and can therefore be applied to the study of charge separation within isolated molecules dissolved in non-polar solvents.[9]

With the advent of alkyl-functionalised, conjugated polymers it has recently been demonstrated that the technique can be used to study photo-induced charge separation on isolated polymer chains.[10] In the present work we describe results on a dilute solution of a functionalised, conjugated porphyrin polymer[11] which show that long-lived mobile charge carriers are formed on the polymer chains subsequent to photoexcitation.

8.2 EXPERIMENTAL

The structures of the molecules studied in the present work are shown in Figure 1 together with their pseudonyms. Their synthesis and structural characterisation have been presented in previous publications.[11,12] The degree of polymerisation of nP has been estimated to lie in the range 7 < n < 15. The compounds were dissolved in benzene (Merck, Uvasol) to which up to 1 wt% 1,4-diazabicyclo[2,2,2]octane (DABCO) was added to retard aggregation by complexing with the central zinc atoms. At the laser wavelength of 308 nm the decadic extinction coefficients are *ca* 1×10^4 $M^{-1}cm^{-1}$ per monomer unit[11], and the optical densities were 0.5 (1P), 0.4 (2P) and 0.2 (nP). The solutions were deaerated by purging with CO_2 or N_2.

The solutes were photoexcited using single, 7 ns, 308 nm unfocused pulses from a Lumonics HyperEX-420 excimer laser. A maximum of 16 pulses were used for signal

averaging. The integrated full intensity per pulse at the cell was 6 mJ/cm^2 (9×10^{15} photons/cm^2) which corresponds to a total effective average concentration of absorbed photons within the solutions of *ca* 8×10^{-6} M for the optical densities used.

The formation of mobile charges was monitored as an increase in the microwave conductivity of the solution using the time-resolved microwave conductivity (TRMC) technique at 10 GHz as has been fully described previously.[9,13] Only measurements at the microwave cavity resonance frequency are presented in this report. These measurements are sensitive only to changes in the real component of the conductivity, *i.e.* the dielectric loss component of the permittivity, $\Delta\varepsilon''$. A fuller report of changes in both $\Delta\varepsilon''$ and the real component of the permittivity, $\Delta\varepsilon'$, which results from a change in the molecular polarisability on photoexcitation, will be given in a future publication.

Fluorescence spectra and decay times were measured by flash photolysis of *ca* 0.2 cm^{-1} absorbance solutions using a 0.8 ns, 337 nm pulse from a PRA LN1000 N_2 laser. After passage through a Jobin-Yvon monochromator the emitted light was detected using a Photek PMT-113-UHF channel-plate photomultiplier with a risetime of 150 ps.

8.3 RESULTS AND DISCUSSION

Figure 2 shows microwave conductivity traces for flash-photolysed solutions of 1P, 2P and nP. For the monomer there is a complete absence of any indication of the formation of mobile charges either during or after the pulse. The dimer displays a slight indication of the formation of a short-lived dipolar intermediate but the signal is close to the noise level. In contrast, flash-photolysis of the polymer results in a large and long-lived transient change in the microwave conductivity (dielectric loss) of the solution. The magnitude of the signal is found to be linearly dependent on the light intensity when this is varied by up to an order of magnitude.

The growth of the signal for the polymer solution follows closely the integrated laser pulse convoluted with the time response of the microwave cavity, *i.e.* there is no evidence for delayed formation of the transient species responsible. Since diffusional approach of the individual solute molecules would occur on a timescale of many microseconds for the concentrations used, we can exclude diffusional intermolecular interactions as a source of the signal observed. In addition, while more concentrated solutions of the polymer were found to be unstable with respect to coagulation, the solution used with an absorbance of 0.2 cm^{-1} was found to be stable even after standing in a refrigerator at *ca*. 5 °C for several weeks.

We conclude that the conductivity change observed results from the formation of a charge-separated, ion-pair state on isolated polymer chains. Because of the large size of the molecular entities, the conductivity cannot be attributed to the rapid rotational diffusion of a fixed dipole, as is the case for the charge-separated states of much smaller molecules such as

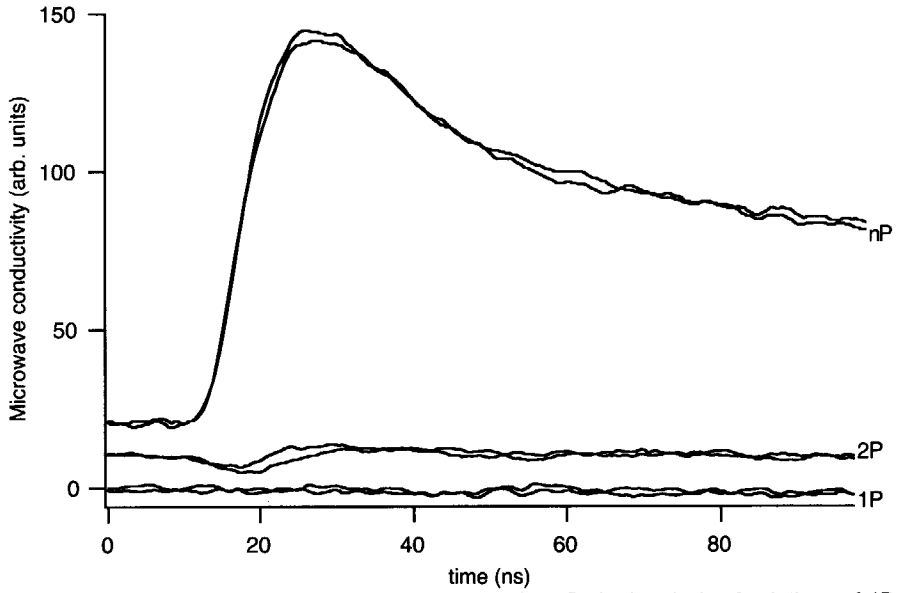

FIGURE 2: Microwave conductivity transients observed on flash-photolysis of solutions of 1P, 2P and nP in benzene (plus up to 1 wt% DABCO). The zinc porphyrin unit concentration was in all cases close to $3x10^{-5}$ M. Two traces are shown for each compound to indicate the reproducibilty. The base lines have been displaced by 10 units for clarity

bianthryl or simple donor-acceptor assemblies.[13] The charge centres must therefore be free to move along the polymer chain. The fact that a change in the real conductivity (or dielectric loss) is observed means however that there must be a frictional force associated with the motion which results in an in-phase component of the motion in the microwave electric field. As will be reported in a future publication, the change in the real component of the conductivity is accompanied by a large change in the imaginary component. This indicates that the charge centres are in fact highly delocalised over the polymer chain.

The decay of the conductivity signal is very disperse as shown by the close to linear behaviour in the double-logarithmic representation in figure 3. At long times the decay can be described quite well by an inverse 0.5 power dependence. The long times involved and the non-monoexponential decay kinetics show that the transient can certainly not be associated with the relaxed S_1 state. For 1P and 2P, S_1 lifetimes of 2.0 and 1.5 ns have been determined from the decay of the fluorescence at 660 nm (1.88 eV) and 750 nm (1.65 eV) respectively. The latter value is in reasonably good agreement with the estimate of 1.25 ns for the S_1 to S_0 transition of 2P from a photobleaching study of ground state recovery.[14] Fluorescence from the polymer, if it occurs at all, would be expected, on the basis of the absorption spectrum,[11,14,15] to appear at *ca* 900 nm which is outside the wavelength range of our detection equipment. Photobleaching experiments have suggested that at least 75% of S_1

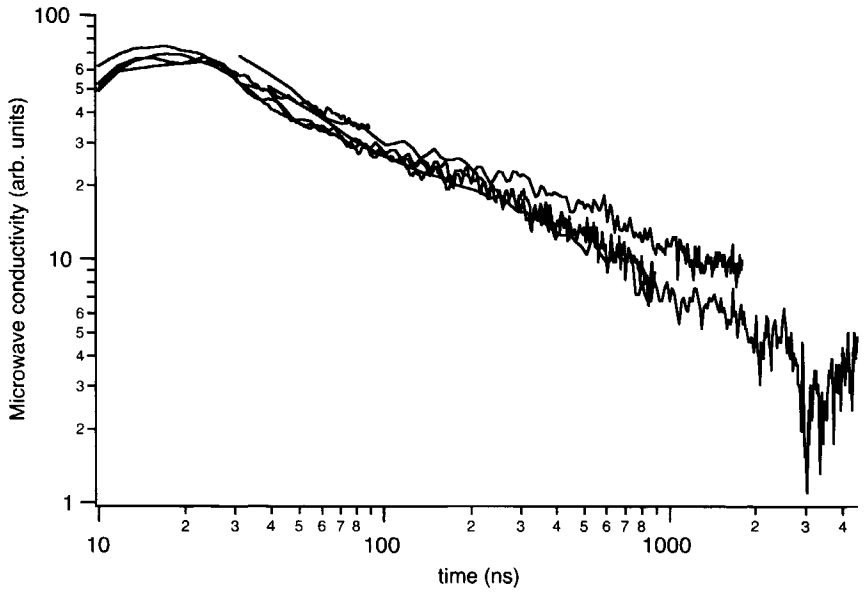

FIGURE 3: The decay of the microwave conductivity subsequent to flash-photolysis of a benzene with 1% DABCO solution of the polymer, nP. Several traces are shown taken on different, linear timescales.

excitons on the polymer relax back to the ground state within 2 ps with a subsequent slower relaxation process occurring on a timescale of approximately 200 ps.[14]

At the maximum beam intensity the total number of photons absorbed corresponds to excitation of 1 in 3 porphyrin-diacetylene units. However because of the much shorter exciton lifetime compared with the 7 ns pulse length, the number of excitations per monomer unit at any given time during the pulse will be at least an order of magnitude lower than 1/3. This consideration, together with the linear dependence of the signal down to a factor of 10 lower intensity, suggests that the mobile charge centres observed do, in fact, result from single-exciton heterolytic-dissociation events.

The efficiency of intersystem crossing in zinc porpyrins is known to be high[16] and the triplet state yield for the 2P compound has been estimated to be 0.8 in a photoabsorption study.[14] No evidence could be found however in the same study for a transient absorption in the infrared corresponding to a T_1 to T_2 transition for the polymer. Also, low temperature emission experiments on nP films have been unable to detect any evidence for phosphorescence.[15] The lack of observation of normal triplet state characteristics could be explained if the charge separated state, CS, observed in the present study lies below that of T_1. The long lifetime of CS may then be due to it having a triplet radical ion pair character.

Field-induced dissociation of excitons within aggregates of nP in a PMMA matrix has been found to occur readily[17] and thin films of pure nP have been found to be photo-

conductive.[15] In the latter study a value of *ca* 1×10^{-11} m^2/Vs was estimated for the major charge carrier (hole) mobility. It was pointed out however that this was almost certainly a lower limit with charge transport being limited by barriers to interchain transport presented by the intervening saturated hydrocarbon side-chains.

If we analyse the present TRMC transient for nP in the same way as was recently carried out for similar results on dilute solutions of polyphenylenevinylene (PPV) derivatives,[10] we can determine a value for the product of the quantum yield of charge carrier formation and the sum of the one-dimensional intrachain mobilities of $\phi\Sigma\mu_{1D} = 6\times10^{-8}$ m^2/Vs. This is an order of magnitude larger than that found for isolated fully-conjugated PPV chains.[10]

Since ϕ is always less than unity $\phi\Sigma\mu_{1D}$ represents a lower limit to the actual value of $\Sigma\mu_{1D}$. In view of the limited length of the nP molecules of between 100 and 200 Å, the use of a bulk parameter such as mobility may be considered to be somewhat dubious. The present value should therefore be considered as an "effective" molecular mobility which, hypothetically, could be observed if a DC conductivity experiment could be carried out on a single polymer chain of macroscopic length. The value obtained is in fact similar in magnitude to values on the order of 10^{-7} m^2/Vs estimated for the mobility of charge carriers in other conjugated polymers.[10,18-23]

ACKNOWLEDGEMENT

The present investigation was supported by the Netherlands Organisation for the Advancement of Research (NWO) and the EPSRC (UK).

REFERENCES

[1] M. R. Wasielewski: Chem. Rev. 92 (1992), 435-461.
[2] M. Grätzel in "Photoinduced Electron Transfer", M. A. Fox, M. Chanon Eds., Elsevier: Amsterdam 1988, vol. D, p 394.
[3] M. A. Fox, W. E. Jones Jr. D. M. Watkins: C&E News 71 (1993), 38-48.
[4] J. M. Tour: Chem. Rev. 96 (1996), 537-553.
[5] P. G. Schouten, J. M. Warman, M. P. de Haas, M. A. Fox, H.-L. Pan: Nature, 353 (1991), 736-737.
[6] M. Antolovich, P. Keyte, A. M. Oliver, M. N. Paddon-Row, J. Kroon, J. W. Verhoeven, S. A. Jonker, J. M. Warman: J. Phys. Chem. 95 (1991), 1933-1941.
[7] J. M. Warman, M. P. de Haas, M. N. Paddon-Row, E. Cotsaris, N. S. Hush, H. Oevering, J.W. Verhoeven: Nature 320 (1986), 615-616.
[8] J. M. Lawson, M. N. Paddon-Row, W. Schuddeboom, J. M. Warman, A. H. A. Clayton, K. P. Ghiggino: J. Phys. Chem. 97 (1993), 13099-13106.
[9] M. P. de Haas and J. M. Warman: Chem. Phys. 73 (1982), 35-53.
[10] G. H. Gelinck, J. M. Warman, E. G. J. Staring: J. Phys. Chem. 100 (1996), 5485-5491.
[11] H. L. Anderson, S. J. Martin, D. D. C. Bradley: Angew. Chem. Int. Ed. Engl. 33 (1994), 655-657.
[12] H. L. Anderson, Inorg. Chem. 33 (1994) 972-981.
[13] W. Schuddeboom: "Photophysical Properties of Opto-electric Molecules Studied by Time-Resolved Microwave Conductivity"; PhD Thesis, Delft University of Technology 1994, ISBN 90-73861-21-7.
[14] G. E. O'Keefe, G. J. Denton, E. J. Harvey, R. T. Philips, R. H. Friend, H. L. Anderson:

J. Chem. Phys. 104 (1996), 805-811.
[15] K. Pichler, H. L. Anderson, D. D. C. Bradley, R. H. Friend, P. J. Hamer, M. G. Harrison, C. P. Jarret, S. J. Martin J. A. Stephens: Mol. Cryst. Liq. Cryst. 256 (1994), 415-422.
[16] J. H. Brannon and D. Magde: J. Amer. Chem. Soc. 102 (1980), 62-65.
[17] G. E. O'Keefe, J. J. M. Halls, C. A. Walsh, G. J. Denton, R. H. Friend, H. L. Anderson: Chem. Phys. Lett. 276 (1997), 78-83.
[18] D. D. C. Bradley, Y. Q. Shen, H. Bleier and S. Roth: J. Phys. C: Sol. State 21 (1988), L515-L522.
[19] Y. Q. Shen, H. Lindenberger, H. Bleier, S. Roth in "Electronic Properties of Conjugated Polymers III", H. Kuzmany, M. Mehring, S. Roth Eds., Springer-Verlag: Berlin 1989, p 96.
[20] C. H. Lee, G. Yu, A. J. Heeger: Phys. Rev. B 47 (1993), 15543-15553.
[21] C. H. Lee, G. Yu, D. Moses, A. J. Heeger: Phys. Rev. B 49 (1994), 2396-2407.
[22] C. H. Lee, G. Yu, N. S. Sacriftci, A. J. Heeger: Synth. Met. 75 (1995), 127-131.
[23] G. H. Gelinck, J. M. Warman: J. Phys. Chem. 100 (1996), 20035-20042.

EXCITONIC INTERACTIONS IN MULTICHROMOPHORIC ARRAYS (SUMMARY)

The fundamental interest in exciton migration, delocalisation and dissociation evolved from the interest in the process of natural photosynthesis. The successive elucidation of the 3-dimensional structure of the photosynthetic reaction centre and the light harvesting complex LH2 showed the actual arrangement of the chromophores in these complexes. Initially, most of the interest was focused on the reaction centre itself. However, as knowledge on the reaction centre has increased, the interest has shifted towards the 18-membered ring of LH2. Research on LH2 itself yields hypotheses on the processes occurring in these circular multi-chromophoric arrays. Research on synthetic model compounds is performed to test specific aspects of these hypotheses. All of the work described in this thesis has been carried out on different model compounds with the overall aim of increasing our understanding of the photophysical properties of multichromophoric arrays. In chapters 3 to 8 different aspects of the photophysics of multichromophoric arrays are investigated using different model compounds.

The main technique used in this thesis to investigate the photophysical properties of multichromophoric arrays is the flash-photolysis time-resolved microwave conductivity (FP-TRMC) technique. In this technique microwaves are used to probe the change in the complex conductivity (or permittivity) of a medium following excitation with a laser pulse. The media investigated are solutions containing the multichromophoric arrays in low concentration. The solvents used are optically fully transparent at the excitation wavelength, hence only the solute molecules are excited, and are non-polar. On excitation, changes can occur in the complex permittivity. Using the approach described in **Chapter 2** changes in the real and imaginary components of complex permittivity can be obtained separately. The observed changes can be related to changes in the photoexcited arrays: changes in the imaginary permittivity (dielectric loss) indicate either the generation of mobile charge carriers or the formation of a highly dipolar excited state, while changes in the real permittivity (dielectric constant) are the result of an increase in the polarisability. The latter can be taken to be indicative of the formation of a highly delocalised excited state in which the electron and hole, the photo-generated electron vacancy, are only weakly coupled.

The TRMC results given in the six articles which form the remaining part of this thesis, *i.e.* the chapters 3 to 8, is, if possible, supported by additional information obtained from optical experiments, both steady-state and time-resolved.

In the research described in **Chapter 3**, the FP-TRMC technique has been used to investigate the nature of the relaxed S_1 state of 9,9'-bianthryl (AA), 10-cyano-9,9'-bianthryl (CAA) and 10,10'-dicyano-9,9'-bianthryl (CAAC). Changes in both the real,

$\Delta\varepsilon'$ (dielectric constant), and imaginary, $\Delta\varepsilon''$ (dielectric loss), components of the complex permittivity have been measured. The dielectric loss transients conclusively demonstrate the dipolar nature of S_1 for all three compounds in the pseudo-polar solvents benzene and 1,4-dioxane, and even in the non-polar solvents n-hexane and cyclohexane. The required symmetry breaking is considered to result from density and structural fluctuations in the solvent environment. The dipole relaxation times for AA (CAAC) are *ca* 2 ps for the alkanes and 7.9 (5.3) ps and 14 (14) ps for benzene and dioxane respectively. The timescale of dipole relaxation for the symmetrical compounds is much shorter than that for rotational diffusion and is attributed to intramolecular, flip-flop dipole reversal *via* a neutral excitonic state. The dipole moment of the transient dipolar state is estimated to be *ca* 8 D, *i.e.* much lower than the value of *ca* 20 D determined from the solvatochromic shifts in the fluorescence in intermediate to highly polar solvents which corresponds to close to complete charge separation. For the asymmetric compound, CAA, a dipole moment close to 20 D is found in all solvents, including n-hexane. Dipole relaxation in this case occurs on a timescale of several hundred picoseconds and is controlled mainly by diffusional rotation of the molecules. The mechanism and kinetics of formation of the dipolar excited states are discussed in the light of these results.

In **Chapter 4**, the site-to-site intramolecular excitation transfer and excitation trapping on one site in amino-substituted triphenylbenzene derivatives, which are characterised by a 3-fold symmetry, have been studied by fluorescence spectroscopy and TRMC. The importance of dipole relaxation due to intramolecular energy transfer has been demonstrated in the interpretation of the limiting anisotropy on one hand and the change of the dipole moment and polarisability upon excitation on the other hand. The interpretation of the experimental results is based on the comparison of the molecules with C_3-symmetry with biphenyl model compounds.

In **Chapter 5**, hexacarbazolylbenzene, a symmetrical propeller array of six carbazole units, has been investigated. The relaxed S_1 excited state has transient broken symmetry and a dipole moment of 8 debye caused by an excimer-like interaction between neighbouring carbazole units. The excimeric distortion undergoes rapid rotary diffusion within the array resulting in more than 1000 "round-trips" during the course of the *ca* 5 ns lifetime of the photoexcitation, thus mimicking the "storage-ring" function of the chlorophyllic arrays in light-harvesting bacteria.

In **Chapter 6**, the excess polarisability volumes, ΔV_p, of the relaxed S_1 and T_1 excited states of several covalently-bridged zinc porphyrin dimers and their corresponding monomers have been measured using the flash-photolysis time-resolved microwave conductivity technique. $\Delta V_p(S_1)$ increases from close to zero for a di-aryl substituted monomer up to a maximum value of 590 $Å^3$ for a dimer coupled by a 9,10-

diethynylanthracene bridge, yPyAyPy. The particularly large excess polarisability of yPyAyPy is attributed to strong electronic coupling between the porphyrin moieties resulting from stabilisation of the cumulenic-quinoidal resonance structure of the bridge. The strength of the electronic interaction, as indicated by the magnitude of $\Delta V_p(S_1)$, increases in the following order of bridging units: 1,4-phenylene < single σ-bond < 1,4-diethynylbenzene < 2,5-diethynylthiophene ≈ butadiyne < 9,10-diethynylanthracene. The results provide an example of an inverse distance effect whereby the electronic interaction between porphyrin moieties actually increases with increasing length of the intervening bridge. The product of the intersystem crossing efficiency and the excess polarisability volume of the triplet state, $\phi_{isc}\Delta V_p(T_1)$, is more than an order of magnitude less than $\Delta V_p(S_1)$, indicating a much smaller degree of exciton delocalisation in T_1 than in S_1. The microwave results are compared with results on the optical absorption and emission spectra which provide additional information on both the electronic and coulombic excitonic interactions.

In **Chapter 7**, the effect has been investigated of increasing chain-length on the excited state properties of two series of covalently-linked zinc porphyrin oligomers: one with a 1,4-phenylene bridge, $(PB)_n$ with n = 1, 2, 3 and 5, and the other with a 1,4–butadiynylene bridge, $(yPy)_n$ with n = 1 to 6. The two series differ dramatically in the nature of the porphyrin-porphyrin interaction. FP-TRMC measurements show that the excited singlet state (S_1) of the $(PB)_n$ oligomers has a very small excess polarisability (< 20 $Å^3$) which is characteristic of a tightly bound, Frenkel type exciton. In agreement with this, the optical absorption and emission spectra indicate that only electrostatic interactions occur between the transition dipoles of the porphyrin moieties. In contrast, very large excess polarisabilities are found for the S_1 state of the $(yPy)_n$ series indicating that a high degree of electron exchange occurs between the porphyrin moieties. This is confirmed by the marked changes also observed in the optical absorption and emission spectra. The polarisability increases with increasing length of the oligomers up to a maximum of 960 $Å^3$ indicative of a loosely-bound, Wannier-Mott type exciton. In contrast, the triplet excited state of the $(yPy)_n$ series has an excess polarisability less than 50 $Å^3$, indicating it to be much more localised than the S_1 state.

In **Chapter 8**, it is shown that photoexcitation of isolated conjugated chains of butadiyne-linked porphyrins ($[\text{-P-}\equiv\text{-}\equiv\text{-}]_n$ with n ≈ 10) in dilute solution in benzene is followed by intrachain charge separation. The product of the quantum-yield and the effective one-dimensional mobility of the ion-pair state formed, $\phi\Sigma\mu_{1D}$, is 6×10^{-8} m^2/Vs and the first half-life is *ca* 100 ns.

When taken together, the results in this thesis, carried out on a large variety of symmetrical molecular arrays, illustrate the great complexity of excitonic interactions. The extend of energy delocalisation is shown to be extremely sensitive; not only to the

nature of the bonding between the individual chromophoric units, but also to their relative orientations and even, in some cases, to density and structural fluctuations in the surrounding medium. The extensive results on linear porphyrinic arrays show how energy can be either highly localised on a single monomeric unit or highly delocalised over several units depending on the nature of the covalent bridging unit. For sufficiently long, strongly-coupled arrays heterolytic dissociation of excitons into separate positive and negative charges can even occur. The results are directly relevant to an understanding of energy delocalisation and migration in complex molecular systems such as for example discotic liquid crystals and photosynthetic antenna complexes. With regard to the latter, future experiments on non-covalently-bonded arrays, which are formed by self-aggregation of monomeric units, should prove to be of great interest. The results may also provide guidelines for the synthesis of organic molecular materials for application in man-made photovoltaic devices for solar energy conversion.

Job Piet

EXCITONISCHE INTERACTIES IN GEORDENDE SYSTEMEN DIE BESTAAN UIT MEERDERE CHROMOFOREN
(SAMENVATTING)

De interesse in fundamentele processen zoals migratie, delocalisatie en dissociatie van excitonen is voortgekomen uit de interesse in de fysische processen die plaatsvinden in de biologische fotosynthese. De opheldering met behulp van röntgendiffractie van de 3-dimensionale structuur van achtereenvolgens het fotosynthetisch reactiecentrum en het antenne complex LH2 toonde de exacte rangschikking van al de chromoforen die aanwezig zijn in deze eiwitcomplexen. In eerste instantie was vrijwel alle aandacht gericht op het fotosynthetisch reactiecentrum. Gaanderweg, als de kennis over de werking van het fotosynthetisch reactiecentrum toenam, verschoof de interesse steeds meer naar LH2, en in het bijzonder naar de cirkelvormige rangschikking van 18 identieke chromoforen (B850). Uit het onderzoek aan LH2 komen hypothesen naar voren met betrekking tot de excitonische processen die in deze cirkelvormige multi-chromofore systemen plaatsvinden. De specifieke aspecten van deze hypothesen kunnen worden onderzocht met behulp van synthetische modelverbindingen. Al het onderzoek dat in dit proefschrift beschreven staat is aan dergelijke modelverbindingen uitgevoerd. Doel was steeds weer om de bestaande kennis op het gebied van geordende multi-chromofore systemen te testen en verder uit te breiden. Met dit doel voor ogen, zijn een aantal uiteenlopende aspecten van de fotofysica van geordende multi-chromophore systemen onderzocht door gebruik te maken van een aantal verschillende series modelverbindingen. De resultaten van dit onderzoek worden beschreven in de hoofdstukken 3 tot en met 8.

De belangrijkste meettechniek die is toegepast in het onderzoek beschreven in dit proefschrift is de techniek van de lasergepulste tijdsopgeloste microgolfgeleiding, op basis van het acronym van zijn engelse naam aangeduidt als de FP-TRMC techniek. De FP-TRMC techniek maakt gebruik van microgolven om de verandering in de complexe dielektrische eigenschappen van een monster te meten nadat deze met behulp van een korte laser pulse in de aangeslagen toestand is gebracht. De monsters, die voor dit proefschrift onderzocht zijn, zijn sterk verdunde oplossingen van interessant geachte modelverbindingen in een niet polair oplosmidel. Een tweede eis die aan het oplosmiddel gesteld wordt is dat het oplosmiddel volledig transparant is voor de kleur licht van de gebruikte laser, zodat alleen de modelverbindingen worden aangeslagen tijdens een experiment. Wanneer de dielektrische eigenschappen van de modelverbindingen in de aangeslagen toestand anders zijn dan in de grondtoestand zal dit de microgolfgeleiding beïnvloeden. Met de methode beschreven in **Hoofdstuk 2** is het mogelijk om de verandering in de dielektrische eigenschappen te meten en de

bijdrage van de verandering in het reële en het imaginaire deel van elkaar te scheiden. Dit laatste is essentieel omdat uit deze twee delen geheel verschillende informatie kan worden verkregen met betrekking tot de veranderde eigenschappen van de modelverbinding. Een verandering van de imaginaire bijdrage (ookwel aangeduid met de term dielektrisch verlies) duidt of wel op het de aanwezigheid van mobiele ladings dragers of wel op de vorming van een dipolaire aangeslagen toestand. Een verandering van de reële bijdrage (de dielektrische konstante) is het gevolg van een toename van de polariseerbaarheid, hetgeen duidt op de vorming van een sterk gedelocaliseerde aangeslagen toestand. In een dergelijke toestand zijn het gat en het daaruit afkomstige electron nog slechts zeer zwak aan elkaar gekoppeld.

De TRMC resultaten, die worden beschreven in de zes wetenschappelijke artikelen die de hoofdstukken 3 tot en met 8 van dit proefschrift vormen, worden veelal aangevuld met resultaten van zowel statische als tijdsopgeloste optische experimenten.

In **Hoofdstuk 3**, is de FP-TRMC techniek gebruikt om de kenmerken van de gerelaxeerde S_1 toestand van 9,9'-bianthryl (AA), 10-cyano-9,9'-bianthryl (CAA) en 10,10'-dicyano-9,9'-bianthryl (CAAC) te onderzoeken. Hiervoor zijn, de veranderingen in het reële, $\Delta\varepsilon'$, en imaginaire deel, $\Delta\varepsilon''$, van de dielectrische eigenschappen van alle drie de modelverbindingen gemeten in een viertal oplosmiddelen. Ter vergelijking zijn dezelfde metingen ook vericht aan anthracene zelf, de kale chromofoor. De TRMC metingen leveren het onomstotelijke bewijs dat de S_1 aangeslagen toestand van de drie onderzochte bichromoforen een dipolair karakter bezit; niet alleen in de pseudo-polaire oplosmiddelen benzene en 1,4-dioxane maar zelfs in niet-polaire oplosmiddelen zoals n-hexane en cyclohexane. Dit is alleen mogelijk als de symmetry verbroken wordt hetgeen waarschijnlijk veroorzaakt wordt door structuur van de omringende oplosmiddel moleculen en dichtheidsfluctuaties in de omringende oplosmiddel mantel. Uit de interpretatie van de metingen is voor dipoolrelaxatietijd van AA (CAAC) een waarde van om-en-nabij de 2 ps bepaald in de alkanen en 7.9 (5.3) ps en 14 (14) ps in respectievelijk benzeen en dioxaan. De dipoolrelaxatietijden van de symmetrische verbindingen zijn veel korter dan men zou verwachten voor een molecuul van deze grootte, hetgeen alleen verklaard kan worden indien men aanneemt dat dipoolrelaxatie in deze moleculen plaatsvindt door middel van een met flip-floppen aangeduid proces in plaats van rotatiebewegingen van het gehele molecuul. In een flip-flop proces gaan de twee tegenovergesteld georienteerde dipolaire toestanden in elkaar over, hoogst waarschijnlijk via een neutrale aangeslagen toestand. Het dipoolmoment van de flip-floppende dipolaire toestand is geschat op 8 D, hetgeen veel kleiner is dan de waarde van 20 D die kan worden bepaald uit de kleurverandering van de emissie met toenemende polariteit van het oplosmiddel, (solvatochromie) in sterk polaire oplosmiddelen. De waarde van 20 D is ook de waarde die men zou verwachten indien

volledige landingsscheiding zou optreden in deze bichromophoren. Voor de asymetrische bichromofoor, CAA, wordt deze waarde wel gevonden in alle onderzochte oplosmiddelen, tot en met het zeer apolaire n-hexane toe. De dipoolrelaxatietijden die voor CAA worden gevonden zijn in de orde van grootte van honderden picoseconden. Dit zijn waarden zoals men die verwacht indien dipoolrelaxatie plaatsvindt middels rotatie van het gehele molecuul. Op basis van de overeenkomsten tussen AA en CAAC en de verschillen en overeenkomsten met CAA wordt stilgestaan bij de kinetiek en het mechanisme van de vorming van ladingsgescheiden toestanden in symmetrische bichromoforen.

In **Hoofdstuk 4** is de intramoleculaire exciton overdracht tussen de verschillende identieke lokaties en het vastpinnen van het exciton op één van deze lokaties onderzocht met behulp van fluorescentie spectroscopy en TRMC. De gebruikte modelverbindingen zijn amino gesubstitueerde trifenylbenzenen en bezitten een 3-voudige rotationele symmetrie. Daarnaast zijn ook een aantal bifenyl verbindingen onderzocht, die wat betreft substitutie en structuur zo goed mogelijk overeenkomen met een enkele arm van één van de onderzochte C_3 symmetrische moleculen. De resultaten verkregen van de metingen aan de C_3 symmetrische modelverbindingen zijn vervolgens vergeleken met resultaten verkregen uit de metingen aan de bifenyl verbindingen. In tegenstelling tot in de monochromoforen (bifenyl derivaten), is de geinduceerde anisotropy van de emissie slechts tijdelijk in de trichromoforen (triphenylbenzene derivaten) bij kamertemperatuur. De TRMC metingen tonen aan dat zowel de mono- als trichromoforen een dipolaire laagste aangeslagen toestand hebben, echter de toename van de polariseerbaarheid van de trichromophoren is aanzienlijk groter. Dit laatste verschil toont aan dat in de trichromoforen de aangeslagen toestand, gezien zijn dipolaire karakter, zich weliswaar steeds op slechts één van de drie armen van het molecuul bevindt, maar gezien de hoge polariseerbaar niet op deze ene arm blijft maar juist snel tussen de armen wordt uitgewisseld. De snel verdwijnende anisotropie van de emissie by kamertemperatuur is met bovenstaande verklaring in overeenstemming.

In **Hoofdstuk 5** is hexacarbazoolbenzeen onderzocht, een molecuul wiens stuctuur het best beschreven kan worden als een zesbladige scheepsschroef. De aangeslagen toestand van dit molecuul heeft een dipoolmoment van ongeveer 8 D, hetgeen erop duidt dat de zesvoudige symmetrie van de grondtoestand in de aangeslagen toestand is verbroken. Vermoedelijk vormen twee carbazolen samen een ladingsgescheiden excimeerachtig complex. Echter omdat er ook een hoge polariseerbaarheid gemeten wordt, blijft de aangeslagen toestand niet op één en hetzelfde paar zitten maar loopt hij rond. Op basis van onze metingen waarschijnlijk zelf enkele 1000 malen gedurende de 5 ns levensduur van de aangeslagen toestand. Dit

soort gedrag lijkt sterk op het veronderstelde gedrag van een exciton op de "opslag ring" van antenne complexen zoals LH1 en LH2.

Hoofdstuk 6 bevat de resultaten van een uitgebreide serie modelverbindingen met zink porfyrines als chromofoor. De serie bestond uit bichromoforen, waarvan de chromoforen covalent zijn gekoppeld met verschillende tussenstukken en een aantal sterk verwante monochromoforen. Met behulp van de FP-TRMC techniek is de verandering in het polariseerbaarheidsvolume, ΔV_p, van de gerelaxeerde S_1 en T_1 aangeslagen toestanden ten opzichte van de grondtoestand van deze moleculen bepaald. Binnen de onderzochte serie verandert $\Delta V_p(S_1)$ van nagenoeg niets zoals gevonden voor de di-aryl gesubstitueerde monochromofoor, P, naar een maximum waarde van 590 $Å^3$ voor de bichromofoor met het 9,10-di-ethynylanthracene tussenstuk, yPyAyPy. De grote waarde gevonden voor yPyAyPy duidt op een sterke elektronische interactie tussen de twee chromoforen via het tussenstuk. De electronische interactie is zo hoog in het geval van yPyAyPy omdat het tussenstuk middels cumuleen-chinon-achtige resonantie structure in staat is de elektronische interactie te stabiliseren. Op basis van de grootte van $\Delta Vp(S_1)$ zijn de onderzochte tussenstukken als volgt te rangschikken: : 1,4-fenylene (B) < direct via één σ-binding < 1,4-diethynylbenzeen (yBy) < 2,5-diethynylthiofeen (yTy) ≈ butadiyn (yy) < 9,10-diethynylanthraceen (yAy). Dit resultaat lijkt vreemd omdat de electronische interactie toeneemt hoewel de afstand tussen de chromoforen ook toeneemt, echter alleen als men de tussenstukken louter een passieve rol toedicht. De eveneens uitgevoerde optische metingen leveren interessant informatie op over de belangrijkste twee vormen van electronische en electrostatische interakties tussen chromoforen en de mate waarin deze optreden in de onderzochte modelverbinding. De uitkomsten van de optische metingen laten zich goed vergelijken met de resultaten uit de TRMC metingen. Zelfs de grootste gemeten verandering in het produkt van de efficientie van de intersysteem overgang en de verandering in het polariseerbaarheidsvolume van de triplet toestand, $\phi_{isc}\Delta V_p(T_1)$, is meer dan een orde van grootte kleiner dan $\Delta V_p(S_1)$. Aangezien de efficientie van de intersysteem overgang in een zink porfyrine hoog is, meestal ongeveer 80% ($\phi_{isc} = 0.8$), duidt dit erop dat de triplet toestand, in tegenstelling tot de singlet toestand, veel minder gedelocaliseerd is.

In **Hoofdstuk 7** zijn twee series oligomeren onderzocht die beide porfyrinen als belangrijkste chromofoor hebben maar verschillen in het soort tussenstuk. De ene serie heeft 1,4-fenyleen eenheden als tussenstuk tussen de chromoforen aangeduidt met $(PB)_n$ waarin n = 1, 2, 3 of 5, en de andere serie heeft 1,4–butadiynylene tussenstukken en wordt aangeduidt met $(yPy)_n$ waarin n een waarde kan hebben van 1 tot en met 6. Ten gevolge van de verschillende tussenstukken is het karakter van de interakties tussen de porfyrine chromoforen in de twee series geheel anders. De FP-TRMC techniek laat zien dat de bezetting van de singlet aangeslagen toestand van de $(PB)_n$ serie nauwlijks een

toename van het polariseerbaarheidsvolume ten gevolg heeft, $\Delta V_p < 20$Å, hetgeen aantoont dat het gevormde exciton van het Frenkel type is. Optische metingen laten inderdaad zien dat er alleen sprake is van electrostatische interacties tussen de chromoforen van de leden van de $(PB)_n$ serie. De FP-TRMC metingen aan de moleculen van de $(yPy)_n$ serie daarentegen laten een sterke toename van de polariseerbaar zien voor de singlet aangeslagen toestand. Binnen de serie neemt de polariseerbaarheid toe met toenemende ketenlengte van de oligomeren tot een maximale waarde van 960 Å^3. Dit duidt erop dat het gevormde exciton op een molecuul van de $(yPy)_n$ serie van het Wannier-Mott type is. De optische metingen aan de oligomeren van de (yPy)n serie laten ook zien dat elektronische interakties tusen de chromoforen optreden. De toename van de polariseerbaarheid van de triplet toestand daarentegen, ook in het geval van de langste oligomeer uit de $(yPy)_n$ serie, is nooit groter dan 50 Å^3, hetgeen laat zien dat de T_1 toestand veel sterker gelocaliseerd is dan de S_1 toestand van hetzelfde molecuul.

Het onderzoek beschreven in **Hoofdstuk 8** laat zien dat na foto-excitatie van een polymeer, bestaande uit porfyrine chromoforen en butadiyn tussenstukken, een deel van de excitonen dissocieert in mobiele ladingsdragers. Omdat de efficientie van dit proces niet bekend is kan er alleen een ondergrens gegeven worden voor de som van de mobiliteiten van de gevormde ladingsdragers; deze bedraagt 6×10^{-8} m^2/Vs. Recombinatie van deze ladingsdragers is een niet-exponentieel proces waarvan de eerste halfwaardetijd ongeveer 100 ns bedraagt.

De resultaten van de onderzoeken aan verschillende series modelverbindingen zoals gepresenteerd in de hoofdstukken 3 tot en met 8 laten de complexiteit zien van de excitonische interacties in multichromofore systemen. Uit de verschillende onderzoeken komt naar voren dat de mate waarin een exciton gedelocaliseerd is afhangt van intrinsieke eigenschappen van het complex zoals koppeling van de chromoforen, welke sterk afhangt van de binding tussen beide, en hun onderlinge orientatie. Echter, daarnaast blijken ook veranderingen in de omgeving, denk aan veranderingen in de structuur en fluctuaties in de dichtheid van de omringende oplosmiddelschil, van invloed te kunnen zijn op de eigenschappen van een excitonische toestand. De resultaten van de metingen aan systemen die bestaan uit gekoppelde porfyrine chromoforen laat zien dat afhankelijk van de soort koppeling tussen de chromoforen, electrostatisch of electronisch, het exciton gelocaliseerd kan zijn op een enkele chromofore eenheid, een Frenkel exciton, of juist gedelocaliseerd over verschillende eenheden, een Wannier-Mott exciton. Voor deze laatste soort exitonen is aangetoond dat als keten voldoende lang het exciton uiteen kan vallen in twee beweegelijke ladingsdragers. Al deze resultaten zijn van belang voor een goed begrip van processen zoals energie migratie en de vorming en migratie van ladingsdragers in complexe

moleculaire sytemen zoals discotische vloeibaar kristallijne materialen en photosynthetische antenne complexen. Toekomstig onderzoek op dit gebied zou dan ook moeten worden uitgevoerd aan niet-covalent gebonden complexen die uit zichzelf vormen door aggregatie. Daarnaast is er de hoop dat deze resultaten en inzichten synthetisch chemici zullen inspireren om nieuwe en betere materialen te ontwikkelen, bijvoorbeeld voor organische zonnecellen.

Job Piet.

ACKNOWLEDGEMENT / DANKWOORD

Measurements on modelsystems was the central part of my PhD research. Since no synthesis is done within our department, I was fully dependent for my supply of model compounds on the generous gifts of synthetic chemist who were willing to share their precious molecules with me. For that reason, I like to thank: Prof. Dr. A. Osuka and co-workers from Kyoto University, Dr. Toine Biemans and Prof. Dr. Bert Meijer from Eindhoven University of Technology, Dr. K. A. Zachariasse and co-workers from Max Planck Göttingen, Prof. Dr. K. Müllen and co-workers from Max Planck Mainz, Prof G. Hadziioannou and co-workers from the University of Groningen and Prof. Dr. M. N. Paddon-Row and co-workers from the University of New South Wales.
and I do fear that I might have forgotten some people for which I sincerely apologise.

I have appreciated it even more, when people accompagnied their molecules and visited us at the insitute to help with the measurements on their molecules and discuss the results afterwards. For that reason, I would like to thank: Dr. Peter Taylor and Dr. Harry Anderson of the University of Oxford; Dr. Wouter Verbouwe, Prof Dr. Marc van der Auweraer and Prof Dr. Frans De Schryver of the University of Leuven; Dr. Jos Nijhof and Prof. Dick Stufkens of the University of Amsterdam; Drs Richard van Delden and Prof Dr. Ben Feringa of the University of Groningen and af course the long living and still continuing collaboration with the University of Amsterdam: Dr. Mattijs Koeberg, Dr. Xavier Lauteslager, Dr. Robert Willemse, Dr. Fred Brouwer and Prof. Dr. Jan Verhoeven.

Nu verder in het Nederlands. Ook op het IRI zelf zijn er mensen die ik niet onvermeld kan laten:

Ad Verkooijen wil ik bedanken dat hij als mijn promotor wilde optreden en daarmee alle onzekerheid met betrekking tot de formaliteiten, die in de toch al moeizame eindfase de kop dreigden op te steken, in de kiem gesmoord heeft.

John Warman, die als mijn begeleider het meest direct betrokken is geweest bij de totstandkomming van dit proefschrift. John, achteraf terugkijkend denk ik dat we elkaars kwaliteiten te laat op waarde hebben weten te schatten, maar gezien de resultaten hebben we de schade beperkt weten te houden. Bovendien moet ik eerlijk toegeven dat ik toch steeds meer waardering heb gekregen voor je gevoel voor details en je streven naar kwaliteit en leesbaarheid, dingen die me tijdens het schrijfproces zelf meer dan eens tot wanhoop hebben gedreven, vooral door tijdgebrek.

En tevens al de mensen van de afdeling stralingschemie. De leden van de vaste staf: Ruben Abellon (Voor de soms zinvolle, maar vaak ook grappige discussies die je steeds weer op gang wist te brengen), Thijs de Haas (Naast microgolfvraagbaak, ook

nog freelance en onbezoldigd P&O-functionaris), Marinus Hom (Organisator van veel en Ikea-kenner), Leny Horsman, Lee Luthjens, Cecilia Quick (Onmisbaar voor de sociale gebeurtenissen), Paul Rijkers (Met name voor je hulp in de eindfase van dit proefschrift wanneer ik weer eens de weg was kwijt geraakt in de wonderbaarlijke wereld van Microsoft Word (Alice in Wonderland ?)), Tom Savenije (Je weet op meer vragen een antwoord dan je zelf lijkt te beseffen), Laurens Siebbeles, John Suykerbuyk (De fitprogrammatuur) en Martien Vermeulen (Het onderhoud van de laser TRMC opstelling). En ook al de AIO's, OIO's en post-docs gedurende mijn verblijf op het IRI: Marion van Brederode, Luis Candeias, Anick van de Craats, Gary Dicker, Marc Frahn, Gerwin Gelinck (Als mijn belangrijkste klankboord voor de polariseerbaarheids-metingen, kwam jouw promotie voor mij eigenlijk te vroeg), Ferdinand Grozema (Bedankt voor alle discussies, zowel degene die hebben geleid tot publicaties als, en misschien wel vooral, degene die tot niets leiden), Romano Hoofman (Gezellig ouwehoeren en samen klagen), Jessica Kroeze, Ger van der Laan, Bas Wegewijs (Vooral je interesse voor boeken, films en ook nog een beetje muziek) en de Spaanse maffia: Alfonso Alba-Garcia en Jorge Piris (Bedankt ? Waarvoor ? Voor het ons steeds maar weer confronteren met het feit dat Spanje een echte eetcultuur heeft en Nederland niet ?).

CURRICULUM VITÆ

The author of this thesis was born in Eindhoven on 28 Februari 1970. He attended secondary school at "het Eindhovens Protestants Lyceum" were he obtained the diploma Atheneum B in June 1988. In September of the same year he started the to study chemistry at the Rijks Universiteit Utrecht and obtained his propadeuse in June 1990. He continued his studies at the same university who was renamed during that time into the Universiteit Utrecht. During his specialisation he worked on research in the following topics: Solid State Chemistry under supervision of Prof. Dr. G. Blasse on "Luminescence of Hafniumoxide X-ray storage phosphors", Farmacology, an internship at the R.I.V.M. under supervision of Dr. J. G. C. van Amsterdam on "Determination of the concentration of nitric oxide metabolites in body fluids" and Physical Organic Chemistry under supervision of Prof. Dr. L. W. Jenneskens on "Synthesis and characterisation of new molecules for intra-molecular long-range electron transfer: donor and acceptor substituted oligocyclo-hexylidenes. On the latter subject he graduated in August 1995. From October 1995 until December 1999, he was appointed "Onderzoeker in opleiding" on an NWO (Initially NWO-SON, later after the reorganisation NWO-CW) grant at the Interfaculty Reactor Institute, were he carried out post-graduated research on "Charge and energy migration in rigid bridged molecules and organised molecular materials." in the Radiation Chemistry Department of Prof. Dr. A. Hummel under supervision of Dr. J. M. Warman. In this thesis part of the research from this period is presented. The author works since July 2001 as fixed income analyst at Rabobank International in Utrecht.

LIST OF PUBLICATIONS

W. J. Schipper, J. J. Piet, H. J. de Jager, G. Blasse: "On the luminescence of Hafnium compounds."; *Mater. Res. Bull.* 29 (**1994**), 23-30.

C. van den Berg, J. G. C. van Amsterdam, A. Bisschop, J. J. Piet, J. Wemer, D. J. de Wildt: "Septic shock: no correlation between plasma levels of nitric oxide metabolites and hypotension or lethality."; *Eur. J. Pharmacol.* 270 (**1994**), 379-382.

J. J. Piet, J. M. Warman, H. L. Anderson: "Photo-induced charge separation on conjugated porphyrin chains."; *Chem. Phys. Lett.* 266 (**1997**), 70-74.

J. M. Warman, G. H. Gelinck, J. J. Piet, J. W. A. Suykerbuyk, M. P. de Haas, B. M. W. Langeveld-Vos, R. A. J. Janssen, D.-H. Hwang, A. B. Holmes, M. Remmers, D. Neher, K. Müllen, P. Bäuerle: "Time-resolved microwave measurements of the polarizability of photoexcitations on conjugated polymer chains."; *SPIE* 3145 (**1997**), 142-149.

W. Verbouwe, M. van der Auweraer, F. C. De Schryver, J. J. Piet, J. M. Warman: "Excited state localisation or delocalisation in C_3-symmetric aminosubstituted triphenylbenzene derivatives."; *J. Am. Chem. Soc.* 120 (**1998**), 1319-1324.

X. Y. Lauteslager, M. J. Bartels, J. J. Piet, J. M. Warman, J. W. Verhoeven, A. M. Brouwer: "Exploring the limits of the electrostatically induced conformational folding process in charge-separated excited states: retarding effect of long alkyl tails attached to the chromophores."; *Eur. J. Org. Chem.* (**1998**), 2467-2481.

J. J. Piet, H. A. M. Biemans, J. M. Warman, E. W. Meijer: "Rapid rotation of energy in the excited state of a circular hexa-carbazole array."; *Chem. Phys. Lett.* 287 (**1998**), 13-18.

G. D. Scholes, G. O. Turner, K. P. Ghiggino, M. N. Paddon-Row, J. J. Piet, W. Schuddeboom, J. M. Warman: "Electronic interactions in rigidly linked naphthalene dimers."; *Chem. Phys. Lett.* 292 (**1998**), 601-606.

J. Nijhoff, F. Hartl, D. J. Stufkens, J. J. Piet, J. M. Warman: "Charge separation in a triosmium cluster zwitterion revealed by time-resolved microwave conductivity: first application of TRMC in organometallic chemistry."; *Chem. Commun.* (**1999**), 991-992.

G. H. Gelinck, J. J. Piet, J. M. Warman: "The polarizability of triplet excitons on oligothiophene chains."; *Synth. Met.* 101 (**1999**), 553-554.

J. J. Piet, P. N. Taylor, H. L. Anderson, A. Osuka, J. M. Warman: "Excitonic interactions in the singlet and triplet excited states of covalently linked porphyrin dimers."; *J. Am. Chem. Soc.* 122 (**2000**), 1749-1757.

R. J. Willemse, J. J. Piet, J. M. Warman, F. Hartl, J. W. Verhoeven, A. M. Brouwer: "Stepwise versus direct long-range charge separation in molecular triads."; *J. Am. Chem. Soc.* 122 (**2000**), 3721-3730.

G. H. Gelinck, J. J. Piet, B. R, Wegewijs, K. Müllen, J. Wildeman, G. Hadziioannou, J. M. Warman: "Measuring the size of excitons on isolated phenylene-vinylene chains: from dimers to polymers."; *Phys. Rev. B.* 62 (**2000**), 1489-1491.

F. J. Hoogesteger, C. A. van Walree, L. W. Jenneskens, M. R. Roest, J. W. Verhoeven, W. Schuddeboom, J. J. Piet, J. M. Warman: "Photoinduced intramolecular charge separation in Donor/Acceptor-substituted bicyclohexylidene and bicyclohexyl."; *Chem. Eur. J.* 6 (**2000**), 2948-2959.

J. J. Piet, P. N. Taylor, B. R. Wegewijs, H. L. Anderson, A. Osuka, J. M. Warman: "Photoexcitations of covalently bridged zinc porphyrin oligomers: Frenkel versus Wannier-Mott type excitons."; *J. Phys. Chem. B.* 105 (**2001**), 97-104.

L. P. Candeias, G. H. Gelinck, J. J. Piet, J. Piris, B. Wegewijs, E. Peeters, J. Wildeman, G. Hadziioannou, K. Müllen: "Substituent effects on the excited states of phenyl-capped phenylene vinylene tetramers."; *Synth. Met.* 119 (**2001**), 339-340.

J. J. Piet, W. Schuddeboom, B. R. Wegewijs, F. C. Grozema, J. M. Warman: "Symmetry breaking in the relaxed S_1 excited state of bianthryl derivatives in weakly polar solvents."; *J. Am. Chem. Soc.* 123 (**2001**), 5337-5347.

J. J. Piet, J. M. Warman, U. Müller, K. Müllen: "The dipolar excitonic states of oligo-anthrylenes.", submitted.